

**Archimedes Screw Generators and Hydropower Plants:
A Design Guideline and Analytical Models**

by

Arash YoosefDoost

A Thesis
presented to
The University of Guelph

In partial fulfilment of requirements
for the degree of
Doctor of Philosophy
In
Engineering

Guelph, Ontario, Canada

© Arash YoosefDoost, May, 2022

ABSTRACT

ARCHIMEDES SCREW GENERATORS AND HYDROPOWER PLANTS: A DESIGN GUIDELINE AND ANALYTICAL MODELS

Arash YoosefDoost
University of Guelph, 2022

Advisor:
William David Lubitz

The Archimedes/Archimedean screw generator (ASG) is a new form of small hydroelectric powerplant technology that can operate under a wide range of flow heads and flow rates. ASGs have low impacts on wildlife, especially fish, and can generate power from almost any flow, even wastewater. Simplicity, low maintenance requirements and moderate costs make ASGs suitable even for remote or developing regions. However, there are few analytical methods for designing ASGs and almost no general and easy-to-use guidelines to design Archimedes screw power plants. This has been a major unanswered problem for about three decades. Therefore, the overall goal of this study was to develop design tools and guidelines to facilitate and support the design and operation of Archimedean screw hydropower plants. This goal was achieved by developing analytical equations and models to design Archimedes screw generators, estimate the volume of flow passing through the ASGs, and a guideline for designing Archimedes screw powerplants. In addition, methods for developing rapid estimation models were studied to facilitate initial studies of ASG hydropower projects, such as determining and evaluating suitable sites. Experimental measurements of a grid-connected ASG and five laboratory screws led to characterizing the phenomena of supply flow into ASGs and developing new equations for estimating the volumetric

flow entering ASGs as a function of the screw geometry, rotation speed, and inlet depth. At most ASG installations, water is supplied by an inlet channel and controlled using sluice gates. Five analytical models were evaluated using laboratory experiments. New equations and methods are proposed to facilitate the design, calibration, modelling and operation of sluice gates. Studying worldwide currently operating Archimedes screw power plants led to characterizing the important design aspects of ASGs and developing empirical screw sizing equations. An analytical equation was developed to estimate Archimedes screw geometry based on the common design characteristics of ASGs. These achievements led to the development of a design guideline for ASG hydropower plants. This work also helps remediate one of the biggest burdens when designing small hydropower projects, the unscalable initial investigation costs, by enabling the evaluation of site-specific possibilities of green and renewable Archimedes screw hydropower generation.

DEDICATION

To you! And future generations, who may live in peace, harmony and sustainability with other species that generously shared this planet with us. Also, whoever contributes to making a peaceful and sustainable future and improves the public welfare, which I believe is the opposite of injustice! And to my amazing family! None of these were possible without your love, patience and support during my academic journey.

ACKNOWLEDGEMENTS

I would like to express my greatest thanks to my family and all who supported me throughout this research as well as all researchers whose work is the foundation of this study. Thanks to my advisor, Professor William David Lubitz, for providing this opportunity. Thank you very much, David. None of this research would be possible without your support and guidance. Thank you very much to my advisory committee, Professor Andrew Binns and Professor Shohel Mahmud, for all support and guidance provided throughout my graduate studies.

I would like to thank Tony Bouk and Brian Weber of Greenbug Energy Inc. for all opportunities provided for this project. Also, thanks to my teammates in Archimedes screw lab, Scott Simmons and Murray Lyons, for all their work on this research. It was joyful to work with you. Thank you, Scott Simmons, Murray Lyons, Andrew Kozyn, Kathleen Songin, and Max Fisher, for your support with collecting the lab data used in this study and for all your investigations in this amazing research team that helped this project.

Thank you very much, Professor Andrew Gadsden and Mitra Kaviani, for all your support and help in our estimation theory project that became part of this thesis. Andrew, thanks for providing this opportunity for us. I learnt so many things while I was working with you and such an amazing team. Mitra, thanks for all your support, constructive comments and collaborations in our projects and all the new things I learned from you about data analysis techniques.

Last but definitely not least, thank you! And all audiences who utilize the outcome of this study in future studies and sustainable developments to make the planet that the other species generously

shared with us, and we borrowed from our future generations, a better place for all living beings.

Aspects of the presented study were financially supported by the Natural Science and Engineering Research Council (NSERC) of Canada, the Collaborative Research and Development (CRD) program (grant CRDPJ 513923-17) and Greenbug Energy Inc. (Delhi, Ontario, Canada).

TABLE OF CONTENTS

Abstract.....	ii
Dedication.....	iv
Acknowledgements.....	v
Table of Contents.....	vii
List of Tables.....	xiii
List of Figures.....	xv
1 Outline.....	1
1.1 Introduction.....	1
1.2 Introduction, Literature Review, Potentials and Problem Definition.....	4
1.3 Estimation of the Available Volumetric Flow Rate.....	4
1.4 Control and Management of the Flow Using Sluice Gates.....	6
1.5 Estimating the Volume of Flow Passing through the Archimedes Screws.....	6
1.6 Determination of the Archimedes Screw Geometry.....	7
1.7 A Guideline to Design the Archimedes Screw Hydropower Plants.....	8
1.8 Conclusion and Future Works.....	8
1.9 Summary.....	9
2 Introduction and Literature Review.....	10
2.1 Introduction.....	10
2.1.1 Sustainable Development.....	10
2.1.2 Renewable Energy.....	11
2.1.3 Hydropower.....	12
2.1.4 Archimedes Screw.....	14

2.2	Advantages of Archimedes Screw Generators.....	17
2.2.1	Technical Advantages.....	17
2.2.2	Economic Advantages	21
2.2.3	Environmental and Social Advantages	22
2.2.4	Disadvantages of Archimedes Screw Generators	24
2.3	Archimedes Screw Generators and Sustainable Development Approaches	26
2.3.1	Site Considerations	27
2.3.2	Reducing Erosion and Disturbance of Natural Sedimentation Processes.....	30
2.3.3	Power Generation from Unconventional Water Resources	30
2.3.4	Upgrade or Retrofit and Power Generation as an Added Value.....	32
2.3.5	Future Sustainability	36
2.4	Principles of Archimedes Screw Hydro Powerplants Design.....	39
2.4.1	Archimedes Screw Hydropower Plants Configurations	39
2.4.2	Components of Archimedes Screw Hydro Powerplants.....	43
2.4.3	Design of Archimedes Screws	44
2.4.4	Estimating the Generated Power of the Archimedes Screws.....	47
2.4.5	Archimedes Screw Power Loss Models	55
2.5	Conclusions	56
2.6	Nomenclature	59
3	Artificial Neural Networks and Extended Kalman Filter for Easy-to-Implement Runoff Estimation Models	61
3.1	Introduction	61
3.1.1	Artificial Neural Networks	63
3.1.2	Extended Kalman Filter & ANNs.....	65

3.1.3	ANN- EKF Based Runoff Estimation Model	67
3.2	Materials & Methods.....	72
3.2.1	Multilayer Perceptrons.....	72
3.2.2	Learning Algorithms.....	75
3.2.3	Gradient Descent.....	75
3.2.4	Study Area and Parameters.....	79
3.3	Model Structure.....	83
3.3.1	Approach 1: Single Dataset	84
3.3.2	Approach 2: Single, Randomized Dataset in Case of No Improvement.....	84
3.3.3	Approach 3: Randomized Dataset for Each Training.....	84
3.4	Results and Analysis	85
3.5	Conclusions	90
3.6	Nomenclature	90
4	Sluice Gates Design and Calibration: Simplified models to Distinguish Flow Conditions, Estimate Discharge Coefficient and Flow Rate	92
4.1	Introduction	92
4.2	Methods and Materials.....	100
4.2.1	Hydraulic Background.....	100
4.2.2	Sluice Gate Models.....	103
4.2.3	Laboratory Flume and Experiment.....	111
4.3	Results	114
4.3.1	Flow Regimes' Distinguishing Conditions.....	114
4.3.2	Discharge Coefficient and Flow Rate.....	114
4.4	Discussion	116

4.4.1	Flow Regimes' Distinguishing Conditions.....	116
4.4.2	Discharge Coefficient and Flow Rate.....	116
4.4.3	New Analytical Equations and Methods for Design Purposes.....	118
4.5	Conclusion.....	122
4.6	Nomenclature.....	124
5	Development of an Equation for the Volume of Flow Passing through an Archimedes Screw Generator.....	126
5.1	Introduction.....	126
5.2	Methodology.....	128
5.2.1	Genetic Algorithm.....	128
5.2.2	Principle Component Analysis.....	128
5.2.3	Base Model.....	129
5.2.4	Experimental Data.....	132
5.2.5	Evaluation of the Base Equation.....	133
5.2.6	Development of the Extended Equation.....	134
5.3	Results and Discussion.....	137
5.3.1	Error Analysis.....	138
5.3.2	Application of the Principle Component Analysis.....	139
5.3.3	Modified Extended Equation.....	142
5.4	Conclusions.....	145
6	Archimedes Screw Design: An Analytical Model for Rapid Estimation of Archimedes Screw Geometry.....	148
6.1	Introduction.....	148
6.2	Materials and Methods.....	150
6.2.1	Theoretical Basis.....	150

6.2.2	Case studies.....	157
6.3	Results and Analysis	158
6.4	Analytical Method for Designing Archimedes Screws.....	161
6.5	Conclusions	163
6.6	Nomenclature	164
7	Design Guideline for Hydropower Plants Using One or Multiple Archimedes Screws....	166
7.1	Introduction	166
7.2	Methods and Materials	168
7.2.1	Design Parameters of Archimedes Screws	168
7.2.2	Archimedes Screws Configurations in Hydropower Plants.....	169
7.2.3	Case Studies	171
7.3	Results and Discussion.....	171
7.3.1	Volumetric Flow Rate and Diameter of Archimedes Screws.....	171
7.3.2	Power and Diameter of Archimedes Screws	173
7.3.3	Analytical Equation	176
7.3.4	Evaluation of the Developed Equations.....	179
7.4	A Quick Design Guideline for Archimedes Screw Power Plants	181
7.4.1	Design Assessments of Archimedes Screw Hydro Powerplants	182
7.4.2	Determination of the ASG Configuration.....	184
7.4.3	Estimation of Archimedes Screws Design Properties	185
7.5	Conclusions	190
7.6	Nomenclature	191
8	Conclusion	193
	References.....	201

Appendices..... 228

A. Evaluation Criteria..... 228

LIST OF TABLES

Table 2.1: Operating conditions of common hydropower technologies.....	18
Table 2.2: Archimedes screws' geometry and operating variables.	45
Table 3.1: Specifications of stations in the upstream basin of Taleghan [200]–[202], [223].....	81
Table 3.2: The Minimum Epoch of the Best Among All Models.	89
Table 3.3: The Best, Optimum and MEB Optimum Models Specifications.	89
Table 4.1: HEC-RAS distinguishing range for sluice gate flow regimes [233]	110
Table 4.2: The range of target flow rates, sluice gate openings, and weir heights tested in the experiments	112
Table 4.3: The evaluation criteria for estimated flow rates.	115
Table 4.4: The estimated C_d for HEC-RAS and the evaluation criteria for estimated flow rates	120
Table 4.5: Evaluation of models in estimating the flow rate in the full sluice gate operation range	122
Table 5.1: Operating Details of the Archimedes screws studied in this experiment	133
Table 5.2: Investigated dimensionless groups	135
Table 5.3: Optimum native constants for each individual screw in Eq. (5-11)	136
Table 5.4: The Pearson correlation of dimensionless variables and each equation error	139
Table 5.5: The correlation matrix of the PCA results	140
Table 5.6: The Pearson correlation of dimensionless variables and prediction error using each equation.....	143
Table 5.7: Comparison of the MPE (%) of developed equations with optimum global constants for each ASG	144
Table 5.8: Comparison of the MAPE (%) of developed equations with optimum global constants for each ASG.....	144
Table 6.1: Details of Archimedes screw hydropower plants used for model evaluation.	157

Table 7.1: Hydropower plants using several parallel Archimedes screw generators. All screws at a plant are identical unless otherwise noted. Power and flow values are for a single screw at the plant: multiply by the number of screws for total plant flow and power..... 170

Table 7.2: Evaluation of equations based on the evaluation criteria. 179

LIST OF FIGURES

Figure 1.1: Overview of Archimedes screw power plant investigation needs.	2
Figure 2.1: Sustainable development as the confluence of three constituent parts. Adapted from [14]......	11
Figure 2.2: Classification of hydropower plants based on the installation capacity.....	13
Figure 2.3: Archimedes screw pump (left) and an Archimedes screw hydropower plant (right). 14	
Figure 2.4: Horizontally and (b) Vertically Oriented Water Wheels. (b-1) Undershot, (b-2) Overshot (b-3) Centershot From [51]	17
Figure 2.5: An example of commercial Archimedes Screws operating range [66], [67].	19
Figure 2.6: The range of head and flow rate corresponding to the generated power of different turbines (Adapted from [55])......	20
Figure 2.7: Cragside Archimedes Screw Generator (ASG), Northumberland, UK (modified from [87], [88])......	28
Figure 2.8: (a) A theoretical chain of small hydropower plants (b) Application of a chain of small ASGs in an irrigation channel to power street lights in Japan [86].	29
Figure 2.9: Yorkshire Water’s Esholt wastewater treatment ASG hydropower plant [89]......	31
Figure 2.10: Sediment shock load released from Manjil Dam, Iran, during the storage restoration process in 1982-1983, which caused an ecological disaster and a massive extinction of aquatic life downstream.	34
Figure 2.11: (a) Current Hydroelectric Plants in Ontario, Canada (Blue); (b) Sites with Hydropower Generation Potential (Red), ASG Suitable Sites (Green) [96].	36
Figure 2.12: Ultra-small all-in-one Archimedes screw generator (PicoPica 10): (a) PicoPica 10’s system Schematic [86]; (b) operational test in Myanmar [127]; (c) power Generation from unconventional water resources [128]; (d) Multi-ASG (two units) running since 2012 in Ibi-Cho, Gifu, Japan, to supply electricity for the security lights and the electric fence [129]; (e) a multi-ASG application for shallow water resources [130].	38
Figure 2.13: Small commercial all-in-one ASG generator (PicoPica 500), Nikko City, Japan [64], [126]......	38
Figure 2.14: The map of ASG powerplants across the world [97].	40

Figure 2.15: Multi-ASG hydropower plants in the UK: (a) Monmouth New Hydro Scheme, Osbaston [133]; (b) Radyr weir hydro, Radyr [136]; (c) Linton Falls Hydroelectric Power Station, Threshfield [137].	41
Figure 2.16: Solvay multi-ASG powerplant project at a glance [138].	42
Figure 2.17: Linton Lock multi-ASG powerplant.	42
Figure 2.18: Marengo multi-ASG hydropower plant in Goito, Italy [139].	43
Figure 2.19: Horizontally A Simple Model of an ASG-based Run-of-River (ROR) System.	44
Figure 2.20: Required parameters to define Archimedes screw geometry [1], [6].....	45
Figure 2.21: The relationship between the angular and radial positions within the screw in the Lubitz et al. (2014) Archimedes Screw model coordinate system.	49
Figure 2.22: Lubitz et al. gap leakage flow model parameters. From [49].....	53
Figure 3.1: A Perceptron Neuron.....	73
Figure 3.2:A Single Layer MLP.	74
Figure 3.3: Taleghan Upper Basin Location [200]–[202], [223].....	80
Figure 3.4: The Climatological and Hydrometric Stations in the Upstream Basin of Taleghan [200]–[202], [223].....	80
Figure 3.5: The Long-Term Average Precipitation in Each Station and Whole of the Basin [200]–[202], [223].	81
Figure 3.6: Long-term Average Temperature [200]–[202], [223].....	82
Figure 3.7: Long-term Average Runoff [200]–[202], [223].	83
Figure 3.8: R^2 of the Best Models.....	86
Figure 3.9: MAE of the Best Models.....	86
Figure 3.10: RMSE of the Best Models.....	86
Figure 3.11: EB of the Best Models.....	86
Figure 3.12:MEB Among All Models.	87
Figure 3.13: R^2 of the Models with MEB.	87

Figure 3.14: MAE of the Models with MEB.	87
Figure 3.15: RMSE of the Models with MEB.	87
Figure 4.1: Free Hydraulic Jump	93
Figure 4.2: Henry's 1950 nomograph for the range of C_d for free and submerged flow regimes in sluice gates [241].	94
Figure 4.3: Submerged (drowned) hydraulic jump	105
Figure 4.4: Schematic of the lab experiment configuration (not to scale).....	112
Figure 4.5: Lab experiment results (markers) categorized by observed flow regime, compared with predicted flow regimes by each model (lines).	114
Figure 4.6: The estimated volumetric flow rate of methods for free and submerged flows.....	115
Figure 4.7: The estimated volumetric flow rate of methods to estimate C_d for HEC-RAS.....	119
Figure 4.8: The estimated volumetric flow rate of all models compared to corresponding measured flow rates.....	121
Figure 5.1: Dimensionless effective inlet area (A_E/A_{Max}) as a function of dimensionless effective inlet depth (h_E/D_o) for different D_i/D_o ratios.	131
Figure 5.2: Predicted flow from Equation (5-3) versus measured flow for all ASG sizes	134
Figure 5.3: Estimations of Eq. (5-11) for all ASG sizes with native optimum constants.....	136
Figure 5.4: Non-dimensional results of estimations using Eq. (5-11) with general coefficients for all ASG sizes ($a = 0.839$, $b = 0.09$ and $c = -0.306$).....	136
Figure 5.5: Analysis of the relationship between dimensionless variables vs. equations' errors for predictions using the base equation (Eq. (5-3)) (top) and using the extended equation (Eq. (5-11)) (bottom).....	138
Figure 5.6: Principal component analysis of dimensionless groups.....	140
Figure 5.7: Non-dimensional results of Eq. (5-13)'s estimations with general coefficients for all ASG sizes.....	143
Figure 6.1: Required parameters to define the effective area.	153
Figure 6.2: Comparison of Eq. (6-14) results for $\delta = 0.5$ and different σ values.	156

Figure 6.3: Results of Eq. (6-16) for the whole range of the dimensionless inlet depth of the screw (Ξ) values in comparison with the currently installed ASG designs of Table 6.1.....	159
Figure 6.4: Comparison of Eq. (6-16) results with Dragomirescu [276] and the other Archimedes screw installations (Table 6.1).	160
Figure 6.5: The analytical method for designing Archimedes screws.....	162
Figure 7.1: Comparison of the volumetric flow rate and diameter of installed screws in hydropower plants listed in Table 7.1. All values above are for a single screw.	172
Figure 7.2: The theoretical available power vs. the power of installed screws published by manufacturers in current Archimedes screws hydropower plants represented in Table 7.1.	174
Figure 7.3: Comparison of the estimated power of each screw vs. the power of each installed screws in ASG hydropower plants.....	175
Figure 7.4: The theoretical available power vs. the diameter and number of installed screws in current hydropower plants represented in Table 7.1.....	176
Figure 7.5: The corresponding Θ of different δ and σ for a full range of Ξ	178
Figure 7.6: Graphical comparison of Eq. (7-2), Eq. (7-6) and Eq. (7-10) estimations vs. actual overall diameter of ASG installations.....	179
Figure 7.7: The guideline for quick estimations of Archimedes screw power plants design.	189

1 Outline

1.1 Introduction

This presented thesis outlines the analytical and experimental research that led to introducing new equations, models, and a guideline to support the design or operation of Archimedean screws and hydropower plants using one or more Archimedes screw generators (ASGs), which had been a major unsolved problem for about three decades. In addition, it outlines the process of developing new models for estimating the volume of flow passing through the Archimedes screw generators. In addition, it presents new equations and methods to facilitate the design, calibration and modelling of other ASG hydropower plants' components, such as sluice gates and studies of easy-to-implement ANN rapid estimation models.

The majority of the materials presented in this thesis are adapted from several published peer-reviewed journal papers, a published peer-reviewed book chapter, and an accepted peer-reviewed conference paper. The original publications were modified for this thesis to maintain the best continuity as a series of chapters by selectively shortening, updating, or moving some material, as well as removing redundancies. References for all chapters are listed in one common reference section at the end of the thesis.

The Archimedes/Archimedean screw generator (ASG) is a new form of small hydroelectric powerplant technology that can operate under a wide range of flow heads and flow rates. ASGs have low impacts on wildlife, especially fish, and can generate power from almost any flow, even wastewater. Simplicity, low maintenance requirements and moderate costs make ASGs suitable even for remote or developing areas. However, there are few general and easy-to-use analytical

methods for designing ASGs and no such guidelines for designing Archimedes screw hydropower plants. This drawback not only affects the feasibility of this technology but also makes ASG hydro powerplant designs highly dependent on the experience of the engineer who designs them.

As a result, the overall goal of this study was to develop design tools and guidelines to facilitate and support the design and operation of Archimedean screw hydropower plants. The power output of an Archimedes screw hydropower plant depends on the flow of water entering the screw, which is generally supplied by an upstream channel, modulated using a sluice gate and affected by losses at the screw inlet (Fig. 1.1). The screw must be sized and specified to utilize this available water.

To model an ASG hydropower plant for a specific site, at least four questions need to be addressed:

- 1) How much volumetric flow rate of water is available?
- 2) What is the possible geometry of the Archimedes screw(s) to utilize this flow?
- 3) How much flow passes through the ASG(s) in different scenarios?
- 4) How to manage and control this flow?

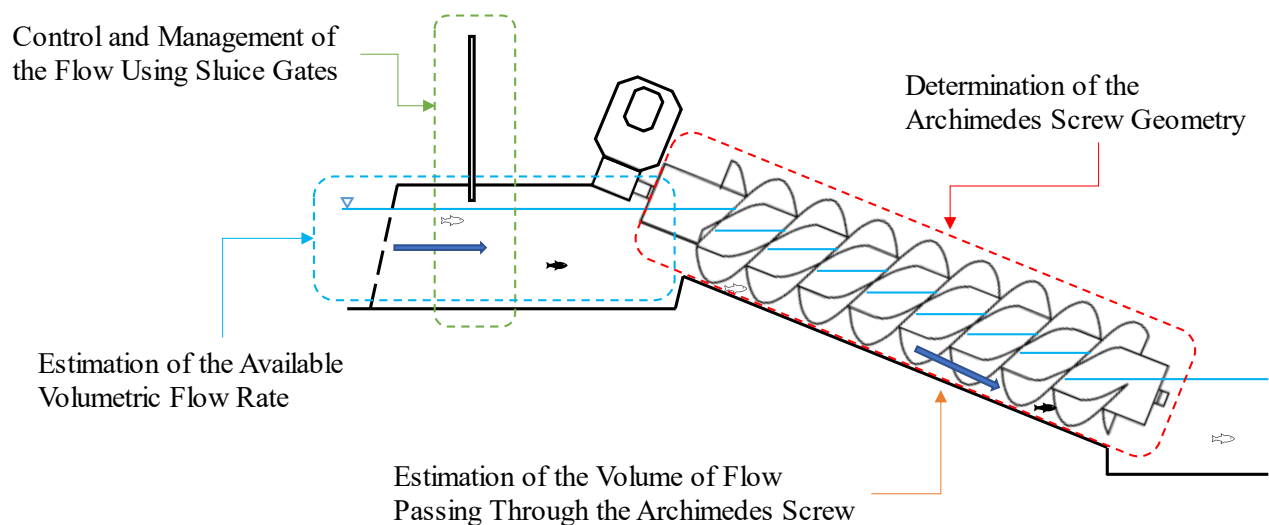


Figure 1.1: Overview of Archimedes screw power plant investigation needs.

These questions were addressed in this thesis through multiple related studies subsequently published in several peer-reviewed papers. The available volumetric flow rate is site-specific. Estimations of site-specific volume flow rate could be determined using the river's historical records to develop results such as flow duration curve. In addition, an estimation method is studied in Chapter 3 that could be practical for rapid estimations when traditional models and methods are limited or infeasible due to the data availability. This method is studied in the context of solving a runoff estimation problem using the minimum number and the most general of available parameters. Chapter 4 outlines the study of sluice gate depth and flow models as essential components for controlling and managing the flow in water delivery channels of Archimedes screws in ASG hydropower plants. Chapter 5 documents studies on developing an analytical equation to estimate the volume of flow rate passing through the Archimedes screws and calibration of this equation for several screws in different scales. Chapter 6 outlines the development of an analytical equation and methods to rapidly estimate the design of Archimedes screws which was an unsolved problem for about three decades. Finally, a guideline for designing Archimedes screw hydropower plants is represented in Chapter 7, which addresses the unsolved problem that was identified as one of the biggest disadvantages of ASGs for about three decades.

Note that in the modeling or optimization of systems, non-iterative and fast analytical calculations for each component are essential to maintain the overall efficiency of the multi-component system design and initial optimization. Therefore, in this study, models or equations that offer the remarkable advantage of low computational costs are referred to as "simple." In contrast, models or equations with the disadvantage of high computational costs (typically from needs for numerical or iterative solution methods), which decrease the overall efficiency of models by increasing the

processing requirements, and as a result the time and costs, are referred to as “complex.”

1.2 Introduction, Literature Review, Potentials and Problem Definition

The second thesis chapter outlines the Archimedes screw generator and provides a comprehensive literature review on this topic. This review outlines the characteristics of ASGs, then discusses and analyzes how they could benefit the sustainability of hydropower development. This chapter is adapted from a peer-reviewed journal paper published in the journal of Sustainability [1]. Some of the presented materials were adopted or updated from a peer-reviewed journal paper published in the journal of Energies [2] and a peer-reviewed journal paper published in the journal of Processes [3].

1.3 Estimation of the Available Volumetric Flow Rate

A realistic and reliable estimation of the available volumetric flow rate is essential for designing Archimedes screw hydropower plants. Historical data such as flow duration curves are great tools for the initial estimation of available volumetric flow rate for each site and the initial designs of Archimedes screw hydropower plants. Then comprehensive studies should be undertaken to evaluate different scenarios, such as the climate change effects on the available volume of flow. Such deep investigations on flow is a water resources engineering topic that is not in the scope of this study. However, developing general and easy-to-implement methods and tools to support such studies could improve the feasibility of initial studies on remote, hard-to-access or developing regions.

Analytical solutions and conceptual models are preferable where the required data is available.

However, solving complex problems with a few available variables could be almost impossible by many traditional models. In fact, the lack of enough data may make many studies infeasible for remote, hard to access or developing regions. Furthermore, studying new problems or even new cases usually requires a systematic approach that could be costly or time-consuming. A black box could be defined as a general or multi-purpose model that maps the inputs of a system to its output without the need for knowing the governing rules and phenomena in the system, or details such as the dynamics of, or interactions between, the system's components. Based on this definition, developing a multi-purpose black box such as an ANN could be beneficial to speed up studies or make them feasible where enough samples are available for training the network, but the number of available variables is not enough and utilizing traditional methods is hard, expensive, time-consuming, or technically infeasible.

The third chapter provides an easy-to-implement method to develop ANN-based estimation models that could assist in finding or evaluating potential sites for ASG hydropower plants. The non-scalable initial investigation costs are one of the biggest burdens of small projects. Moreover, solving a complex problem with a few parameters is almost impossible by many traditional models, and the lack of data may make many studies infeasible for remote, hard to access or developing areas. Artificial neural networks (ANNs) could help reduce investigations costs and make many projects feasible to study by acting as input-output mapping algorithms. This extra study provides an easy to understand and implement method to develop fast ANN-based estimation models using the multilayer perceptron (MLP) neural network and Extended Kalman Filter (EKF) or Gradient Descent (GD) as the training algorithm. Also, three approaches to feeding training data to the models were studied. This method is applied for solving a runoff estimating problem using

the minimum number of input parameters, precipitation and temperature, that are easy to measure and widely available. This chapter is adapted from a peer-reviewed paper that was submitted to the CSCE 2022 annual conference [4].

1.4 Control and Management of the Flow Using Sluice Gates

Sluice gates are essential components in the water delivery channels of Archimedes screw Hydropower plants since at most ASG installations water is supplied by an inlet channel that is controlled using sluice gates. Generally, each power generation unit could be considered as a system of a sluice gate and Archimedes screw installed in a channel: Water enters the delivery channel from a small pondage or a water diversion system, passes through a trash rack and is controlled and managed using a sluice gate for each ASG. Therefore, it is essential to develop or determine fast, reliable and efficient models for modeling sluice gates as a component of the ASG hydropower plants.

As a result, the fourth chapter outlines the study on sluice gates and several common models. A laboratory experiment was conducted that led to introducing new data applied for studying several sluice gate models. Also, new equations and methods are proposed to facilitate the design, calibration and operation of sluice gates as one of the most important water delivery components in ASG power plants. This chapter is adapted from a peer-reviewed journal paper that is published in the journal of Water [5].

1.5 Estimating the Volume of Flow Passing through the Archimedes Screws

Measuring the volume of flow passing through the ASGs is incredibly hard for large operating

screws and requires a small team. Moreover, simple equations to estimate the volume of flow rate passing through the screws are essential for studies on hydropower plants, the development of models, and management and operation plans. The fifth chapter outlines the conducted research on the estimation of the volume of water that can pass through the Archimedes screws, which is essential in designing Archimedes screws and ASG hydropower plants as well as for operating ASGs and making operation plans. In ASGs, water flows through a helical array of blades wrapped around a central cylinder while there is a small gap between the trough and screw in a free-flow condition. Screw geometry and rotation speed are two other important factors that intensify the scaling difficulties. In this study, experimental measurements of a grid-connected ASG and five lab screws at the University of Guelph were used to characterize the phenomena of supply flow into ASGs and led to developing a new equation to estimate the volumetric flow rate entering ASGs as a function of the governing factors including screw geometry, rotation speed and inlet depth. This chapter is adapted from a peer-reviewed book chapter that is published by Springer publication [6].

1.6 Determination of the Archimedes Screw Geometry

Chapter six outlines the research on the design aspects of ASGs by studying the worldwide currently operating ASGs in Archimedes screw power plants designed and installed by different manufacturers. The important design aspects of ASGs were studied and categorized, and empirical equations were developed. This chapter also outlines the analytical research that led to the development of an analytical equation to design Archimedes screws. In designing Archimedes screws, determination of the geometry is among the fundamental questions that may affect many

aspects of the Archimedes screw powerplant. Most plants are run-of-river and highly depend on local flow duration curves that vary from river to river. The ability to rapidly produce realistic estimations for the initial design of a site-specific Archimedes screw plant helps to facilitate and accelerate the design and optimization of the powerplant. The proposed analytical method dramatically facilitates and accelerates estimating the design aspects of Archimedes screws' geometry based on the accepted, proved or reported common designs' characteristics. This chapter is adapted from a peer-reviewed journal paper published in the journal of Energies [2]. Some of the presented materials were adopted from the peer-reviewed journal paper published in the journal of Processes [3].

1.7 A Guideline to Design the Archimedes Screw Hydropower Plants

The seventh chapter provides a design guideline for Archimedes screw hydropower plants using one or multiple Archimedean screw generators based on the results and achievements of this research. This guideline remediates one of the biggest burdens when designing small projects, the unscalable initial investigation costs, by offering a simple method to evaluate the site-specific possibilities of green and renewable Archimedes screw hydropower generation. This chapter is adapted from a peer-reviewed journal paper published in the journal of Processes [3]. Some of the presented materials were adopted from the peer-reviewed journal paper published in the journal of Sustainability [1] and the peer-reviewed journal paper published in the journal of Energies [2].

1.8 Conclusion and Future Works

Chapter eight concludes the results and outcome of the entire research represented in this thesis

and provides recommendations for further studies on Archimedes screws.

1.9 Summary

This chapter outlined the overall objective and framing of this thesis. Due to the “thesis by paper” nature of this study, each chapter is a published peer-reviewed paper. Therefore, this chapter outlined the necessity and relationships between each chapter to ensure that the audience can easily understand the importance and coherency of the study.

2 Introduction and Literature Review

Adapted from:

A. YoosefDoost and W. D. Lubitz, “Archimedes screw turbines: A sustainable development solution for green and renewable energy generation-a review of potential and design procedures,” *Sustain.*, vol. 12, no. 18, p. 7352, Sep. 2020, doi: 10.3390/SU12187352.

Thesis Author’s Contribution:

This article is an original literature review on Archimedes screw generators that was written by Arash YoosefDoost [1]. Some parts were adopted or updated from original research articles that were written by Arash YoosefDoost [2], [3]. The figures are all original, or from explicitly referenced sources.

2.1 Introduction

This chapter outlines the characteristics of ASGs, then discusses and analyzes how they could benefit the sustainability of hydropower development.

2.1.1 Sustainable Development

Sustainable development is described as “the organizing principle for the achievement of human development objectives while at the same time preserving the capacity of natural systems to provide the natural resources and ecological services on which the economy and community rely” [7]. Sustainable development often implies “a development that addresses current needs without influencing potential generations’ capacity to fulfill their own needs” [8], [9].

In 1979 René Passet proposed a three-sphere framework for sustainable development projects [10] (Figure 2.1). According to this framework, a development can be considered sustainable only if it simultaneously has positive social, environmental, and economic impacts. If a project satisfies the economic and social aspects but fails to satisfy the environmental aspects, it is categorized as equitable. If a development project can satisfy the environmental aspects but fails one of the social or economic aspects, the development could still be bearable or viable, respectively. If a development cannot satisfy at least two of the three mentioned aspects, it cannot be categorized anywhere in this definition. Some authors consider a fourth sustainability pillar of culture, institutions, or governance [11], or reconfigure the four domains to be social-ecology, economics, politics, and culture [12]. Overall, the focus of the modern sustainable development concept is simultaneous economic development, social progress, and environmental protection for current and future generations [13].

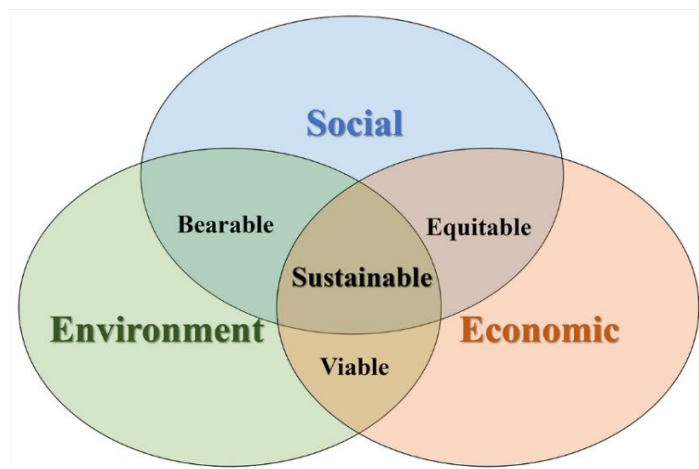


Figure 2.1: Sustainable development as the confluence of three constituent parts. Adapted from [14].

2.1.2 Renewable Energy

Renewable energy is defined as energy that is obtained from resources that are fully replenished

on a human time scale. [15]. According to REN21's year 2019 report, renewable resources provided 2378 GW of power capacity, which is more than 33% of the world's total electrical generating capacity. In this list, hydropower capacity (excluding pure pumped storage capacity) is 1132 GW, which is about half of total renewable energy. In 2018, annual new investment in hydropower grew 11% in comparison to the previous year [16]. The majority of hydropower investment is in large dams and associated generating stations that inherently include complex networks of social, economic, and ecological effects, maybe more than any other large infrastructure project [17].

2.1.3 Hydropower

Hydropower is one of the most efficient and reliable sources of renewable energy [18] and offers significant value for a sustainable future [19]. By the end of 1999, around 2650 Terawatt hours (TWh) (19%) of the world's total electricity relied on hydropower [20]. It rose to about 3100 TWh by 2009, and it was estimated that it would reach 3606 TWh in 2020 [21]. Dams are essential tools for controlling, storing, managing, and operating water for humankind. Large dams serve various specific purposes for our civilization, including water supply, flood control, navigation, sedimentation control, and hydropower [22]. However, they also come with disadvantages, including flooding large areas of land, impeding fish migration, and affecting the physical characteristics of the dam's downstream river [23]. Construction of large dams needs significant capital, so many large dam projects are national (or even international) in scope. Currently, most new large dams are being constructed to provide combinations of energy, irrigation, and flood control in developing countries. At the same time, dam decommissioning is an increasing trend in developed countries because of environmental impacts and the economic costs of maintaining

aging structures [17].

Hydropower plants can be classified based on the electrical generating capacity, as in Figure 2.2 [24]. Typical categories and associated capacities are: large hydro (> 10 MW), small hydro (< 10 MW), mini-hydro (< 1 MW), micro-hydro (< 100 kW), and pico-hydro (< 5 kW) [24]. It is estimated that about 10% of global hydropower is generated from powerplants with less than 10 MW of capacity [24].



Figure 2.2: Classification of hydropower plants based on the installation capacity.

In a run-of-river (ROR) configuration, hydropower plants utilize the natural flow of water [25] and usually have little or no controlled water storage, meaning that ROR typically has small or no reservoirs. The lack of a large, actively controlled reservoir formed by a dam, or significant control of river flow, avoids or minimizes the disadvantages associated with large reservoirs, at the cost of more variable or poorly timed power generation. It minimizes flooding land and soil destruction, greenhouse gas emissions, as well as environmental [26] and social impacts [1]. However, the resulting reduction in control of river flow can result in more variable or poorly timed power generation [1].

Micro hydropower plants can often be considered a sustainable development option for generating electricity in both developing and developed countries. There is often no need to build expensive

dams and flood massive areas for the reservoir. This minimizes land and soil destruction, threats to wildlife, climate change effects, and other environmental impacts, especially on ecosystems [26], as well as the social impacts of large hydropower plants. New ROR hydropower technologies such as Archimedes Screws Turbines (ASGs) can be particularly advantageous in these regards.

2.1.4 Archimedes Screw

The Archimedes screw (also known as an Archimedean or hydrodynamic screw) is considered to be one of the earliest hydraulic machines [27]. It is composed of one or more helical arrays of blades wrapped around a central cylinder, like a woodscrew [28]. This screw is supported within a surrounding fixed trough. There is a small gap between the trough and screw that allows the screw to rotate freely while allowing only a small amount of water to leak past the blade edges. It is believed that the Archimedes screw was invented by Archimedes of Syracuse (circa 287-212 BCE), the Greek physicist, mathematician, and inventor [29]. However, there is evidence suggesting the invention and use of the screw technology may date back to over three centuries before Archimedes under the reign of King Sennacherib (704-681 BCE) in the 7th century BCE in the Assyrian Empire [30].

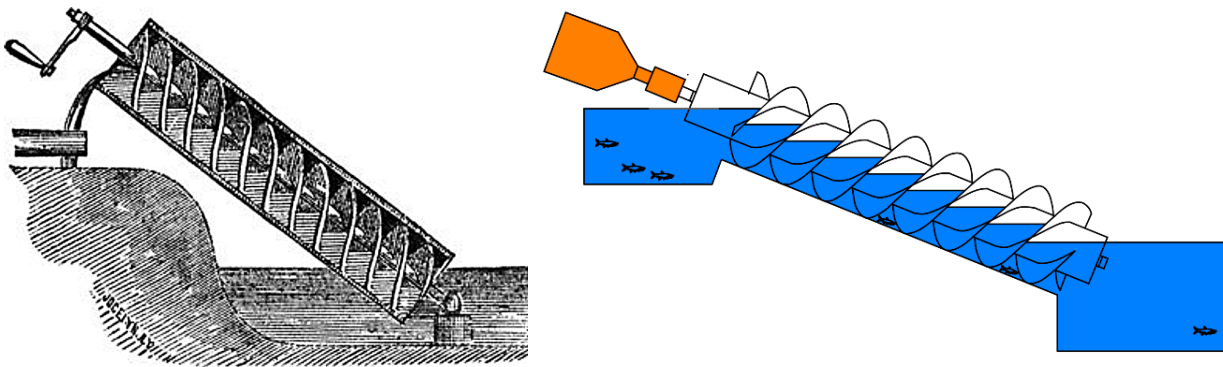


Figure 2.3: Archimedes screw pump (left) and an Archimedes screw hydropower plant (right).

2.1.4.1 Archimedes Screw Pump

Archimedes screws have been used as water pumps for irrigation and de-watering for a long time [29], especially for irrigation and dewatering purposes. For example, over 300 Archimedes screws were used as drainage pumps in the Netherlands in the early 20th century [31]. Some historical sources claim that Archimedes used the device to launch a ship [29]. Archimedes screws are commonly used today as high-volume pumps and are particularly adapted to wastewater treatment facilities since debris and obstructions in the water usually have minimal or no effect on the operating screw [32]. Today Archimedes screws pumps (ASPs) are widely used in wastewater treatment plants, for dewatering low-lying regions, irrigation systems, fish conveyors, etc. [33]. Figure 2.3 shows that the Archimedes screw can be configured as either a pump or a generator [34].

2.1.4.2 Archimedes Screw Generator

Archimedes screws can also be used to produce power if they are driven by flowing fluid instead of lifting fluid. Water transiting the screw from high to low elevation generates torque on the helical plane surfaces, causing the screw to rotate. This mechanical rotation can be used to produce electricity by attaching a generator [35]. In this way, the ASG is a variation of the ancient Archimedes screw pump for generating power [36]. ASGs offer a clean and renewable source of energy and can be safer than other types of hydroelectric turbines for wildlife and especially fish [37]–[44]. The Archimedes screw is theoretically a reversible hydraulic machine, and there are several examples of Archimedes screw installations where the screw can operate at different times as either pump or generator, depending on needs for power and watercourse flow [45].

In 1862, Ruhlmann categorized Archimedes screw as a kind of water wheel and proposed to use it to generate mechanical power [46]. However, it was not until 1992 that the Archimedes screw generator was implemented and patented by Radlik [47]. The earliest patent involving using a screw in hydro power plants dates back to 1922 [48], but examples of application of Archimedes screw generator (ASG) technology date back only to the 1990s [36].

The first ASG was installed in the 1990s [32]. Since 1993, at least 400 ASG hydropower plants have been installed in Europe [36]. However, there are just two ASG power plants in North America [49]. There are only two operational ASGs connected to the grid in North America, the first of which was installed near Waterford, Ontario, Canada, in 2013 [49].

Generally, modern hydropower turbines could be categorized as impulse turbines and reaction turbines. However, work is done by ASGs due to pressure differences across the blades created by the weight of the water, so they do not categorize as using either an impulse or reaction mechanism. ASGs constitute a third category of hydropower converter that is driven by the weight of water, which would also include water wheels. These machines can be considered quasi-static pressure machines.

A water wheel is generally a circular rotor with some form of buckets around the circumference. Most turn about a horizontal axis, but there are several different configurations (Figure 2.4). Water at a higher elevation fills buckets, which empty at a lower point as the wheel turns [50]. Horizontal waterwheels have a vertical rotation axis, and vertical ones have horizontal rotation axes [50].

The energy transfer mechanism in an Archimedes screw is similar to a water wheel, although the configuration is different. In an ASG, a water bucket is defined as the volume of water entrapped

between two adjacent helical plane surfaces.

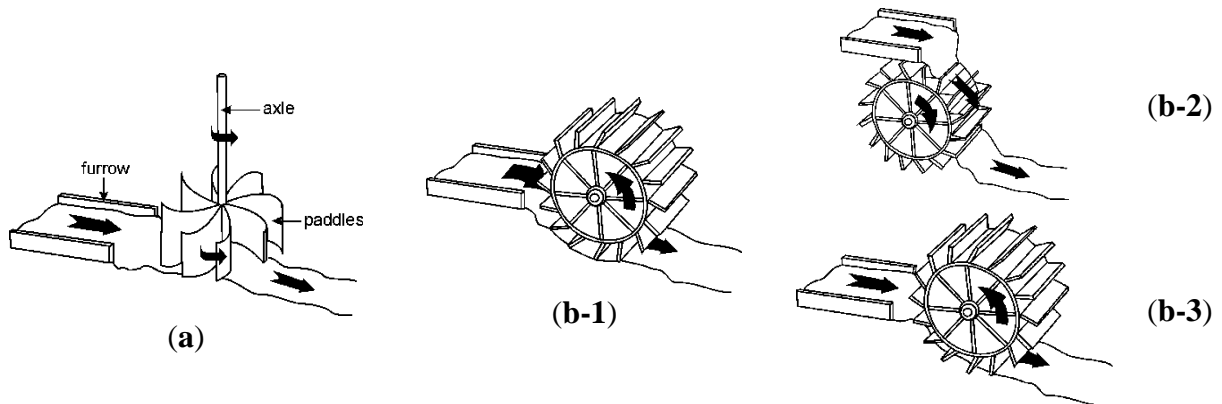


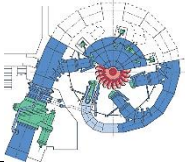
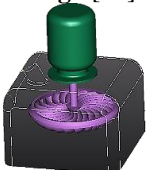
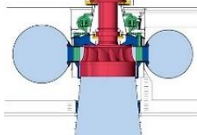
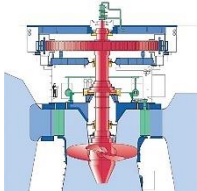
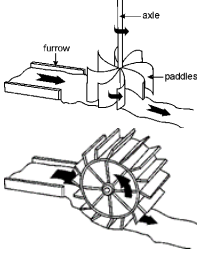
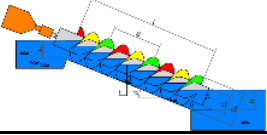
Figure 2.4: Horizontally and (b) Vertically Oriented Water Wheels. (b-1) Undershot, (b-2) Overshot (b-3) Centershot From [51]

2.2 Advantages of Archimedes Screw Generators

2.2.1 Technical Advantages

The typical river-to-wire efficiency (the theoretically available hydraulic power to the electrical power delivers to the grid) of ASGs is as high as 60% to 80% [52]. Depending on the screw design, installation, operation condition, as well as the fill height of the screw, its minimum and maximum efficiency may differ or happen in different conditions (i.e., fill heights and/or rotation speeds) for different designs. For example, measurements of several ASGs indicate hydraulic efficiencies (the theoretically available hydraulic power to the exploited shaft power) higher than 80% full-load and as high as 94% in partial-load conditions [53]. Table 2.1 compares the operating conditions for the most common energy converters used in hydropower generation. These materials indicate that efficient electricity generation with just a few meters of water head and a wide range of supported flow rates is a particular advantage of ASGs [28] that could increase the number of potentially suitable sites available for micro hydropower development.

Table 2.1: Operating conditions of common hydropower technologies.

Type	Turbine	Head (m)	Flow Rate (m ³ /s)	Notes
Impulse	Pelton [54] 	50 *– 1000 [18]	<50 [55]	A high-pressure jet of water is directed at bucket-shaped blades, and nearly all of the flow energy is converted to rotational mechanical energy [56].
	Turgo [57] 	50 **– 250 [58]	<10 [59]	A modification of a Pelton, in which the incoming water jet is directed at an angle of 20 degrees to the buckets. A larger jet stream of water relative to the turbine diameter for the same flow and head produces more power or can be constructed smaller [58].
Reaction	Francis [60] 	40–600 [58]	0.2–1000 [55] (Specific Flow)	Flow enters the turbine radially, then is redirected in a direction along the axial length of the turbine. The pressure difference across the blades is accomplished by changing flow direction and can be 90% to 95% efficient [56]. Efficiency reduces dramatically in flow rates below 75% of the design flow [56]
	Kaplan [61] 	<50 [62]	0.5–1000 [55]	Flowing water pushing past the propeller blades creates a pressure difference [56]. Best suited for heads less than impulse and Francis turbines for the same flow, and for flow rates higher than Francis and Pelton turbines for the same head. The propeller angle can vary to optimize energy extraction.
Quasi-static Pressure	Water wheel [51] 	<10	<5	Vertical axis Water Wheels rotate due to the force exerted on the paddles by the momentum of the flow. Horizontal axis Water Wheels rotate because of the momentum of the water, as well as the weight of water on the small water buckets formed between the paddles. So, they are a bit more efficient than conventional horizontal ones [50]. The efficiency of well-constructed WWs is 50%–70% [50]. The hydraulic efficiency of Vertical Water Wheels is reported to be up to 85% [63].
	Archimedes Screw 	<10 [52], [59]	<10 [52], [64]	Efficiency range between 60% and 80% and remains high even as available head approaches zero. Produce up to 355 kW [65] of power [36]. Practical even in combined low head and low flow

Notes:

* A Pelton turbine with a flow of 50 m³/s is a very extreme case.

** Micro-hydro impulse turbines sometimes operate with less than 50 m of the head.

To decide about the best option depending on the site properties, there are charts for each turbine operation condition. Most of them, even those in general literature, ultimately are made based on companies which usually mark the areas of their products. For example, Figure 2.5 represents the related water head and flow rate for different power ranges of ASGs made by the ANDRITZ company. To deal with this issue, several charts could be combined, such as Figure 2.6 [55], which represents the range of head and flow rate corresponding to the generated power of a Pelton, Francis, Cross-flow, and Kaplan as well as Water wheels and Archimedes Screws. It is important to note that for ASGs, this chart only includes industrial sizes. As mentioned, recently, there have been many investigations to utilize ASGs in micro and even pico scales. This includes ASGs such as PicoPica 10 and PicoPica500, which change the operation flow rate and head of ASGs from 0.01 to 10 m³/s and 0.1 to 10 m, respectively.

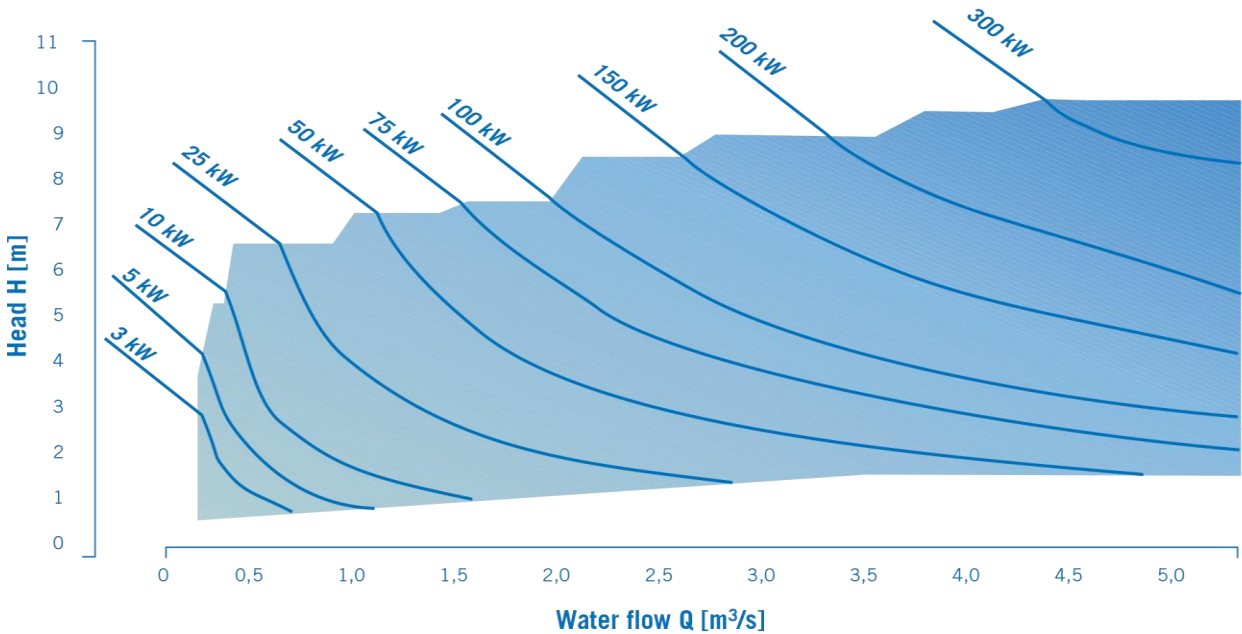


Figure 2.5: An example of commercial Archimedes Screws operating range [66], [67].

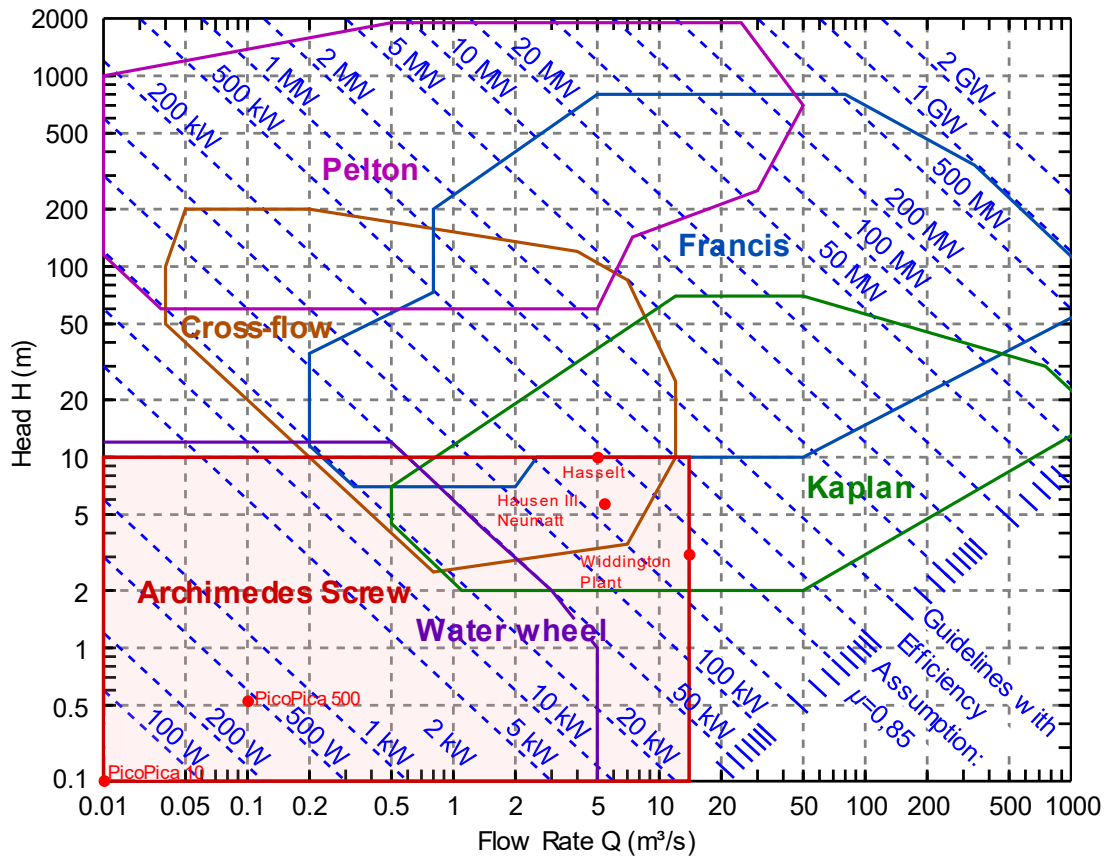


Figure 2.6: The range of head and flow rate corresponding to the generated power of different turbines (Adapted from [55]).

In the last decade of the 20th century, initial experimental investigations for using Archimedes screws as generators showed that a rather small screw has an efficiency of more than 80% in converting hydraulic energy into mechanical energy [33], and even higher efficiencies could be obtained by larger screws [68]. It was stated that the largest outer diameter of ASGs usually does not exceed 4 m because of technical limitations, especially for fatigue cracking of the flights' weld to the central cylinder [69]. However, the largest screw diameter known to the author at the time of publication is 5 m, as in the “Widdington Plant” [1]. In terms of length, the Hasselt hybrid (pump and turbine) screws are claimed as the largest hybrid Archimedean screws in the world

[70]. In terms of power, manufacturers have announced single screws that can pass flow rates as high as 15 m³/s and generate up to 800 kW of power [53]. In terms of the largest number of installed parallel screw generators, currently, the largest known number is six parallel Archimedes screws in hydropower plants such as Marengo (in Goito, Italy) [1], Rosko (in Rosko, Poland) and Steinsau (in Alsace, France) which are all listed in Table 6.1.

2.2.2 Economic Advantages

2.2.2.1 Capital Costs

Depending on site specifications, an Archimedes screw may offer cost advantages, especially in terms of capital costs. For example, a case study for a specific site in Yorkshire, UK, found that the ASG cost would be about 10% less than a Kaplan turbine, while the generated energy was estimated to be about 15% more. For this case, in terms of capital cost per MWh per year, the ASG was projected to be 22% cheaper than a Kaplan turbine [71].

2.2.2.2 Operational and Maintenance Costs

Overall operation and maintenance costs of ASGs are expected to be lower than other turbines [72]. Regular ASG maintenance includes checking fluid levels and replacing grease cartridges at the upper bearing and gearbox. The bottom bearings are usually designed to operate without any maintenance until replacement [73]. ASGs have few wear points, and their operational speed is low, reducing wear and scouring issues. The common types of physical and chemical erosion occur only in trough and blade flights. Major maintenance of an ASG is typically required after 20 to 30

years for the lower bearing [74]. The screw flights would typically be refurbished when the lower bearing and the trough are replaced [72].

Since maintenance and operating costs of ASGs are lower than other micro-hydro turbines [75], they can be considered one of the best options for undeveloped regions and areas with no easy access, such as high elevations of mountains or small communities that are far from facilities and infrastructure. This is an important advantage for small communities where connecting to central grids is not easy nor cost-effective.

2.2.3 Environmental and Social Advantages

Dams block the natural connection of a river between upstream and downstream regions. Therefore, river ecosystems may lose their access which causes negative environmental impacts such as wide-ranging species extinctions. This has been documented in the temperate areas of the Americas due to large hydropower dams [76]. For example, the extinction of 38 species and the near-extinction of other 71 species occurred due to dams in the Mobile River basin, Alabama, USA [77]. It is important to note that negative effects on ecosystems are not limited only to large dams. Any disturbance in natural processes, including the construction of hydraulic structures, such as small weirs or diversions, can also have side effects. Studies indicate that even low-head hydropower facilities are not risk-free, especially for fish that migrate downstream [38].

A novel study was conducted by Boys et al. [38] on the physical stresses that would be experienced by fish species passing through a very low head (VLH) turbine, Archimedes screw, and horizontal Kaplan turbines. A novel fish-simulating sensor package called Sensor Fish was passed through operating turbines and recorded conditions in order to assess potential injury mechanisms reported

in studies on live fish [38]. This study found that rapid decompression is not significant in VLH and ASGs. However, in the low-head horizontal Kaplan turbine, it was so serious that impacts on fish could be expected to be comparable to high-head vertical axis Kaplan turbines. It was also mentioned that physical strikes are a potential fish injury source in all turbine types. The authors suggested that minimizing structures near the tailrace of screw generators and operating VLH turbines at higher powers with greater runner blade openings could reduce the possibility of strikes [38].

Several studies have found that using ASGs could limit impacts on wildlife and aquatic species. Archimedes screws are even used as pumps to move fish between holding pens in some fish farms, with between 98% and 99% of fish unharmed during passage [39]. The results could be similar in ASGs since both systems have slow rotational speeds and large openings that allow the safe passage of small objects.

A British study [40] showed that eels and juvenile salmon passed through an ASG safely with a low mortality rate. Further investigations found that applying a rubber bumper to the leading edge of the screw blades further reduced injury potential: with this intervention, no salmon sustained injuries of any sort, and just minor recoverable damage was reported for less than 1% of eels [40]. Another study indicates that fish lighter than 1 kg can safely pass through an ASG that is rotating at typical operating speeds [41]. Applying rubber bumpers on the leading edges can increase this mass up to 4 kg without being harmed [41]. According to the UK Environment Agency Hydropower Good Practice Guidelines, using the compressible rubber bumps is recommended for ASGs with a typical speed higher than 3.5 m/s. This guideline also suggests using trash-racks to screen larger debris before entering the turbine for a range of ASG diameters in order to block the

passage of fish and debris that are larger than the ASG's buckets and diverting them into a spillway or parallel stream with no harm [42].

A two-year study on the possibility of second-order effects of ASGs tried to answer additional questions about fish behaviour alternation before and after passage as well as long-term survival and fitness after-effects [43]. Movement patterns and behaviour analysis indicated that adult eels could descend the ASG. However, under high flows, they preferred the faster passage of the parallel overshot weir. Passing through the screw caused no immediate eel mortality and no effect on their migration behaviour. This study mentioned that adult eels milled about at the entrance to the screw outlet and then rejected it as a migration path. Other fish exhibited a startle response to the turbine start-up. However, ASGs can be considered a potential downstream passage route for both eels and Potadromous species [43].

It is also notable that compared to other turbine types, ASGs allow greater downstream passage of sediment, floating debris, and other material. This capacity to pass larger materials means that trash racks and upstream screens can be coarser and therefore less expensive, with less head loss, than those necessary for other turbine types.

2.2.4 Disadvantages of Archimedes Screw Generators

2.2.4.1 Relatively New Technology

Looking back to the history of using Archimedes screws as generators shows that this is a relatively new technology, and there are many not well-known things about ASGs in comparison to other hydropower technologies. Fortunately, ASGs have become increasingly popular in Europe during

the past decade because of their robustness, simplicity, and fish friendliness [33], and there is an increasing rate of research interest in these machines.

2.2.4.2 Insufficient General Design Guideline

The lack of general standards or guidelines makes the hydraulic design of the Archimedes screws and ASG hydropower plants highly dependent on the experience of the designers[33]. Reviewing the literature indicates that there are not sufficient English guidelines for designing ASGs for different sites and flow conditions [49]. Presently, the Rorres [34] and Nuernbergk and Rorres [33] are well-known studies for the optimum design of ASGs. However, they are not easy to understand and implement. Even the non-English literature, including Brada (1996) [78], Aigner (2008) [79], Schmalz (2010) [80], Lashofer et al. (2011) [81], and the new version of “Hydro-power screws - Calculation and Design of Archimedes Screws” [82], which is available only in the German language, do not provide a comprehensive physics-based design model for ASGs [36], [49].

2.2.4.3 Technical Limitations

For very high flow rates or water heads, a single screw may not take advantage of all available potential due to material, structural, technical, and physical limitations: bending could be a serious issue for very long structures. Increasing the inner diameter of the screw could help to increase the ASG length with the cost of making the screw larger or reducing the effective area. However, because of the weight of the screw, the bearing limitations is one of the most critical technical constraints. The idea of multi-ASG powerplants (parallel or in series) could be considered as a solution. However, according to Table 2.1, there are other turbines developed to take advantage of such conditions.

Archimedes screws operate at low rotation speeds relative to other hydropower turbines. This provides environmental advantages such as good ecological behaviour and reduced noise. However, a gearbox is required to convert this rotation speed to the required speed of the generator, and the losses in the gearbox, as well as in the generator, affect the overall efficiency of the system. Muysken proposed a maximum recommended rotation speed (ω_M) for Archimedes screws as follows [83]:

$$\omega_M = \frac{5\pi}{3D_o^{2/3}} \quad (2-1)$$

It is possible to run an ASG with flow rates less or more than the optimal design volume flow rate. Studies show that ASGs can handle flow rates even of up to 20% more than optimal filling without a significant loss in efficiency [78]. However, running screws in non-optimal conditions such as high filling heights or rotation speeds higher than the Muysken maximum rotation speed (Eq. (2-1)) may lead to significant losses due to physical and hydraulic limitations. Fortunately, there are some solutions to deal with some of these limitations: when the conditions are not perfect for a single screw, utilizing variable-speed ASGs, or installing more than one screw to potentially better utilize available flow at a wider range of sites, including those with high seasonal variability.

2.3 Archimedes Screw Generators and Sustainable Development Approaches

Based on the discussed advantages of ASGs, they could provide a wide range of opportunities and options for developments. In terms of sustainable development, ASGs offer economic, social, and environmental advantages and could address or compensate for some of the sustainable development components in some of the current water industry developments. This section will

propose and analyze some of the ASGs applications that could improve the sustainability of water industry developments.

2.3.1 Site Considerations

While large dam sites require very special conditions to construct, this is less of an issue in site selection for ASG-based run-of-river (ROR) hydropower plants. Even for ROR plants with a reservoir, the size of the reservoir is much smaller than traditional hydropower plants. By utilizing ASGs, ROR hydropower plants could utilize relatively small heads and flows.

The size of an ASG can be scaled based on the available volume of flow and site specifications. Conventional ASGs can operate with heads between 1 m and 6 m, and flow rates between 0.1 m³/s and 6 m³/s, producing 1 kW [36] to 300 kW [66], [67] of power generation. However, recent development shifted this range dramatically. Currently, there are pico ASGs that can generate around 10 watts of power with 0.01 m³/s of flow rate and 0.1 m of water head [64]. The largest installed ASG could generate up to 355 kW of power with 3 m of water head and has 14.5 m³/s of flow rate capacity [65]. According to Table 2.1, currently ASGs are suitable for sites with head up to 10 m [59], [64], [84] and flow rates up to 10 m³/s [52], [55], [64]. Recently, manufacturers have announced larger screws that can pass flow rates as high as 15 m³/s and generate up to 800 kW of power [53]. Surveying operating ASGs, the length of the operating ASGs varies from about 1 m to 17 m. Figure 2.7 shows Cragside (UK) screw, which is a uniquely 17 m long and steep screw plant that generated about 21 MWh in 2019 [85]. Figure 2.8 shows several pico hydro-scale ASGs in series, each about 1 m long, being used in Japan [86].



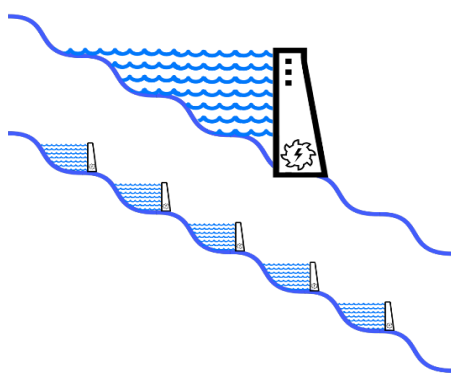
Figure 2.7: Cragside Archimedes Screw Generator (ASG), Northumberland, UK (modified from [87], [88]).

ASGs can operate efficiently even at very low heads and flows [36]. Therefore, ASGs could help to generate electricity for hard to access or undeveloped regions where connecting them to the electricity network is difficult, expensive, or even impossible. Ideally, ASGs could make hydropower generation possible almost everywhere flowing rivers are available. In areas of low flow but the higher head, this idea could be expanded to a theoretical chain of hydropower plants such as what is proposed in Figure 2.8-a. Figure 2.8-b shows an implementation of such a chain of ASGs in a roadside irrigation channel. The power output was used to power adjacent street lights in Japan [86]. The Yorkshire Water's Esholt wastewater treatment (in Section 2.3.3) could be considered as another example of using several ASGs in series to take advantage of available water head alongside a relatively long (here around 30 m) pathway [89].

The idea of installing ASGs in series in chains of small hydropower plants could further increase the potential of green and renewable hydroelectricity generation in locations where the flow is low, and the head is somewhat higher than would be appropriate for a single ASG. In remote areas, the modular nature of multiple small ASGs could be a logistical advantage. In appropriate locations,

installing chains of ASGs in series could offer several advantages in addition to reducing fossil fuels usage and greenhouse gas (GHG) emissions by:

- Allowing hydroelectricity generation in regions where the construction of large dams is not reasonable or feasible. For example, in relatively smooth plains where suitable conditions do not exist to support the construction of large dams.
- Maximizing the hydroelectricity generation even in regions where a large dam exists by extracting energy alongside the river downstream.
- Reducing the electricity power loss alongside the distribution network by generating power near where it is required and consumed, which could reduce the length and cost of the distribution network (as illustrated in Figure 2.8-b).
- Generating baseload power with small hydropower plants. Currently, in many locations, the majority of electricity baseload is mainly generated by fossil fuel, and nuclear power plants and hydropower is used to meet peak demands. However, the proposed theoretical chain of ROR powerplants could generate a baseload since most of the ROR plants do not store water.



(a)



(b)

Figure 2.8: (a) A theoretical chain of small hydropower plants (b) Application of a chain of small ASGs in an irrigation channel to power street lights in Japan [86].

2.3.2 Reducing Erosion and Disturbance of Natural Sedimentation Processes

Suspended sediments can cause damage passing through traditional turbines, e.g., by eroding the component surfaces, especially when sediments are composed of hard materials like quartz and feldspar [90]. To prevent sediment-related problems in small hydropower plants, the construction of settling basins to remove sediments is possible [91], but it is often uneconomical [92]. In addition, even if construction and operating costs are ignored, there is no guarantee of complete removal of suspended sediment before the water enters the plant [92]. Unlike many traditional turbines, suspended sediments could pass through ASGs with minimal effect because of their lack of tight tolerances and their low operational speeds [72]. Letting the sediments pass a hydropower plant instead of depositing upstream in reservoirs or settling basins could offer environmental advantages by reducing the disturbance of the natural erosion/sedimentation process while also reducing operating costs associated with settling basin maintenance. Passing sediment could lead to erosion prevention and soil conservation since according to Lane's law, water transporting sediment has less capacity for eroding banks and natural features [93]. Passing sediment through the plant could also offer economic advantages since reduced upstream sediment deposition increases the effective service life of reservoirs and dams.

2.3.3 Power Generation from Unconventional Water Resources

Since Archimedes screw generators run in open channel flow, theoretically, small hydropower could be considered as an alternative to the energy dissipator hydraulic structures [94] to make use of the flow energy and offer the added value of power generation. Since large living organisms such as fish can pass through ASGs, there is no surprise that sediment and small debris can pass

through ASGs as well. This advantage enables ASGs to generate power from almost any flow, even unconventional sources such as wastewater that are often not appropriate for conventional hydro turbines [1], [89], [95], [96]. A recent study on micro hydropower plants using sewage water flows indicates that a single ASG with a sewage line with a flow rate of about $0.24 \text{ m}^3/\text{s}$ and 1.5 m of the head could generate up to 1963 watts of power [95]. This experiment was physically implemented at the sewage treatment plant for municipal wastewater of Hayatabad Peshawar, Pakistan. It was found that in the worst scenario, a coarse screen can be added to prevent the garbage from entering the screw. Increasing the number of screws, flow rate, and head leads to a linear increase in generated power [95]. Moreover, theoretically, sediments could be released continuously from reservoirs while this flow is used for power generation by ASGs.



Figure 2.9: Yorkshire Water's Esholt wastewater treatment ASG hydropower plant [89].

Another example is the Yorkshire Water's Esholt wastewater treatment upgrade in 2007 that enables it to generate hydropower from untreated sewage by installing two Archimedean screw generators installed in series (Figure 2.9) between the inlet works and the new primary settlement

tanks [97]. This hydropower plant has been switched on since 2009 [89] and could utilize about 10 m of the head and up to 3.24 m³/s of wastewater passing through a 1.8 m diameter pipe when it flows sequentially through the two screws [97]. The diameter and length of each screw are 2.6 m and 14 m, respectively [89]. This upgrade could provide more than 180 kW of treatment process' required power [97] for the UK's first energy self-sufficient (neutral) urban sewage plant [98].

2.3.4 Upgrade or Retrofit and Power Generation as an Added Value

ASGs could offer a considerable value add-on for some big projects whose main purpose is not power generation [97] for improvement or conservation of current resources. The Yorkshire Water's Esholt wastewater treatment upgrade, which is mentioned in Section 2.3.3, is one of the examples. In addition, the wide range of ASG operating feasibility makes it possible to use them as an upgrade or retrofitting solution at existing dams. Since the civil work associated with the dam already exists, this can reduce the capital costs of installing an ASG hydropower plant. Many ASGs have been installed at sites with existing dams.

Dams and weirs may leave unattended or completely abandoned after ending their service period due to removal costs or other reasons. Leaving such obsolete hydraulic structures unattended can become a social and environmental hazard since they can threaten public safety. Just in the United States, there are over 87,000 registered dams, and some estimations increase this number to about two million dams that many of them are no longer used and are considered unsafe [99]. In some cases, the repair costs of a dam could be three times higher than dam removal. Therefore, dam deconstruction may be economically more reasonable because of maintenance and renovation costs [100]. However, dam removal expenses are usually too high to be covered just by one

financer [101]. In addition, many existing dams have been in place for a very long time, and it is not easy to balance the ecosystem and cultural-historical values of such old and historically important structures in communities [102]. The ecosystem and social changes resulting from dam construction usually lead to a new balance over several decades of dam operation [103]. In addition, the deconstruction of old dams provides a large area of stored sediment that is highly suitable to plant colonization. So, native species may fail to survive in competition with aggressive plant colonists [104]–[106].

Few investigations have focused on the dam deconstruction effects on contaminant distribution, especially in the case of small dams with heights of less than 2 m [107]. However, some studies about the evaluation of the extent and magnitude of biological and chemical changes caused by dam removal documented potential changes, especially in contaminant inventories [108]. As an example, after the Ft. Edwards dam removal in 1973, analysis of the displaced sediment downstream during 1977–1978 indicated highly contaminated polychlorinated biphenyls (PCBs) [109]. Therefore, sometimes the deconstruction of old dams may not be the most effective solution. Each dam deconstruction should be evaluated for the potential sedimentary contaminant redistribution [108] and other possible consequences. Figure 2.10 is an example of the shock load of releasing sediments deposited in a reservoir during the storage restoration process of Manjil Dam, Iran, in 1982–1983. This sediment shock load caused massive extinction of aquatic life downstream.

Installing an ASG at an existing dam or weir can offer economic and environmental benefits by generating renewable hydroelectricity at a previously unutilized site with a minimum of changes to the overall site [35]. An ASG installation can also provide a reason for performing deferred and

ongoing maintenance on an otherwise neglected dam, improving the structural stability of dam infrastructure [35]. Considering ASGs as a retrofit option could offer environmental advantages, especially if the deconstruction of an old dam may threaten aquatic life and wildlife of the downstream. Moreover, as detailed in Section 3.2, such upgrades could help reduce the disturbance of sediment transport processes and realize environmental and economic advantages by implementing renewable hydroelectricity generation.



Figure 2.10: Sediment shock load released from Manjil Dam, Iran, during the storage restoration process in 1982-1983, which caused an ecological disaster and a massive extinction of aquatic life downstream.

Many sites, such as small weirs or dams without existing hydropower plants, are suitable for installing or using ASGs as an upgrade. At existing sites, the dam construction has already been completed, the return on investment has been satisfied, and the environmental impacts have been incurred for many years [74]. The minimum construction requirements of ASGs and their small scale make the environmental impacts and GHG emissions of this upgrade very low [110]. Additionally, such upgrades provide green electricity, which could help to reduce fossil fuel usage and continuous greenhouse gas emissions. Therefore, upgrading dams for hydroelectricity can not

only be a reasonable economic decision but also could partly remediate some prior environmental or social impacts.

For example, within the province of Ontario, Canada, there are approximately 2600, mostly small, dams [111] that were primarily constructed for flood control and milling. About 70% of these dams were constructed prior to 1970. Since the expected service life of a typical small dam ranges between 50 and 70 years, many of these dams will require major restorations or structural repairs within 10 to 15 years because of safety and structural quality concerns [112]. Additionally, in the United States, the Army Corps of Engineers national inventory estimates there are 18,140 dams with heights under 4.6 m that are in need of structural repair due to improper or deferred maintenance [113].

It is also worth mentioning that in the province of Ontario, Canada, nearly one-quarter of all energy production is provided through hydro resources, which are about 90% of all the province's renewable energy supplies [114]. This represents about 8100 MW of hydroelectricity capacity from 240 dam sites across 24 river systems [115]. Since the focus of increases in hydropower is largely on sites with generating capacity greater than 1 MW [116], sites under 1 MW power generating potential were ignored in this study. However, ASGs could be considered a reasonable solution for the utilization of these sub-1 MW sites [35].

According to Ontario Hydro and the Ministry of Natural Resources Water Potential Site database, there are approximately 280 sites within Ontario (Figure 2.11) with less than 200 kW power generating capacity and heads less than 5 m [117]. Considering these statistics and typical ASG efficiency, the total power generating capacity of ASGs just within Ontario is approximately 16

MW [96]. Therefore, such a retrofitting and upgrade approach could be considered a development with low impacts that can provide a considerable amount of energy, especially at the local community level [35].

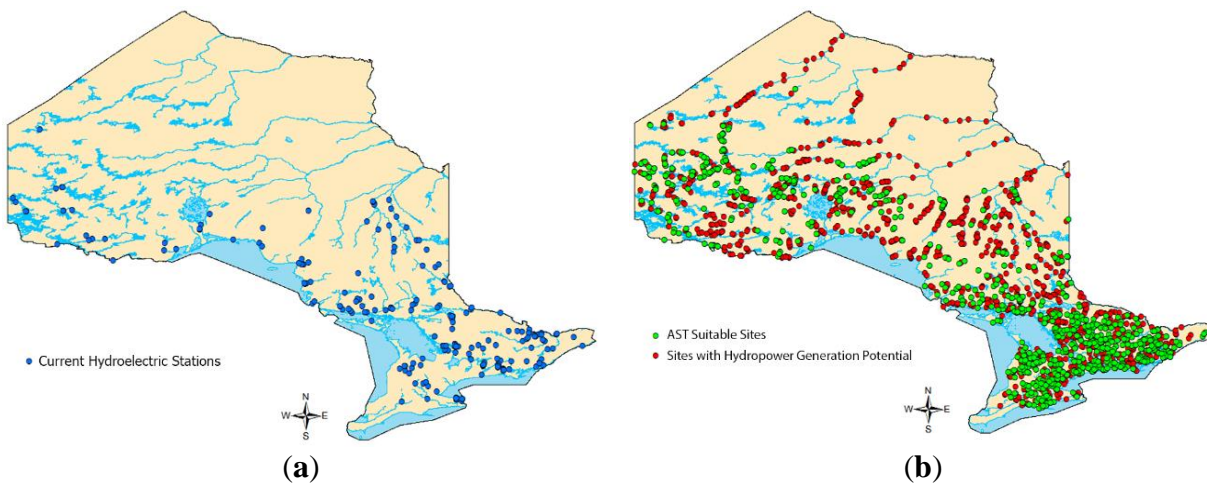


Figure 2.11: (a) Current Hydroelectric Plants in Ontario, Canada (Blue); (b) Sites with Hydropower Generation Potential (Red), ASG Suitable Sites (Green) [96].

2.3.5 Future Sustainability

According to the United Nations Development Program (UNDP), 1.4 billion individuals had no access to electricity in the past decade [118], especially in poor regions of developing countries [119]. Geographical limitations [120] and uneven population distribution are two important issues that affect the effectiveness of the electrical distribution infrastructure [121]. The structural simplicity, low operational demands, and modest costs make ASGs an environment-friendly and sustainable solution, especially in developing countries. ASGs could be used to generate electricity even with unconventional water resources, such as the about 2 kW ASG powerplant that runs by sewage water in Hayatabad Peshawar, Pakistan [95]. There have been several investigations proposing pico-hydro ASGs as an electrification solution [122], [123] for the 2519 villages in

Indonesia that do not have access to electricity because of inaccessible locations [123]. However, only around 1.8% of micro-hydro potential (out of 400 MW potential capacity) is currently exploited in Indonesia as a developing country [124]. Recent studies have examined applying ASGs in small, micro, and even pico scales and also considered methods to simplify the application of these ASGs. A recent study in Aceh, Indonesia, found that even a very simple ASG with just one blade ($N = 1$) with $D_o = S = 0.26$ m, $D_i = 0.14$ m, $L = 1$ m and $\beta = 30^\circ$ could generate about 116 Watts of power with 1 m of head at a flowrate of $0.02 \text{ m}^3/\text{s}$ and 24.75 rad/s rotation speed [125]. A commercial version of this idea has been developed: currently, the smallest all-in-one portable ASG generator from this project weighs just 17.5 kg, and is approximately 1 m long and 0.28 m wide [86]. It could be installed in very shallow waters and can generate around 10 watts of power in a flow of $0.01 \text{ m}^3/\text{s}$ and a head of 0.1 m [64]. Figure 2.12-a shows a diagram of this all-in-one ASG generator. This generator could be installed easily, and a 0.15 m tall metal plate helps to provide enough water head to generate power from even a very shallow water. It provides a wide range of new suitable sites to generate electricity. The turbines have been tested in undeveloped regions of Myanmar (Figure 2.12-b) and in urban flows (Figure 2.12-c). The generated power of each unit is very low in comparison to larger plants; however, units could be used in series (Figure 2.8-b) or in parallel (Figure 2.12-d,e) configured as a multi-ASG powerplant almost everywhere alongside any flow.

Figure 2.13 represents the fixed and larger version of this small commercial ASG that has been installed in Nikko City, Japan, since 2017 [126]. It can generate about 500 W with a flow of $0.1 \text{ m}^3/\text{s}$ and 0.7 m of head [64]. This ASG has a net weight of 250 kg, and it could generate enough power for nighttime lighting, refrigerators for preserving food and medicine, and

telecommunication equipment such as cellular phones, laptops and televisions [64]. Pico-scale ASGs present a flexible and reasonably practical option for improving local economies and welfare in remote, developing communities.

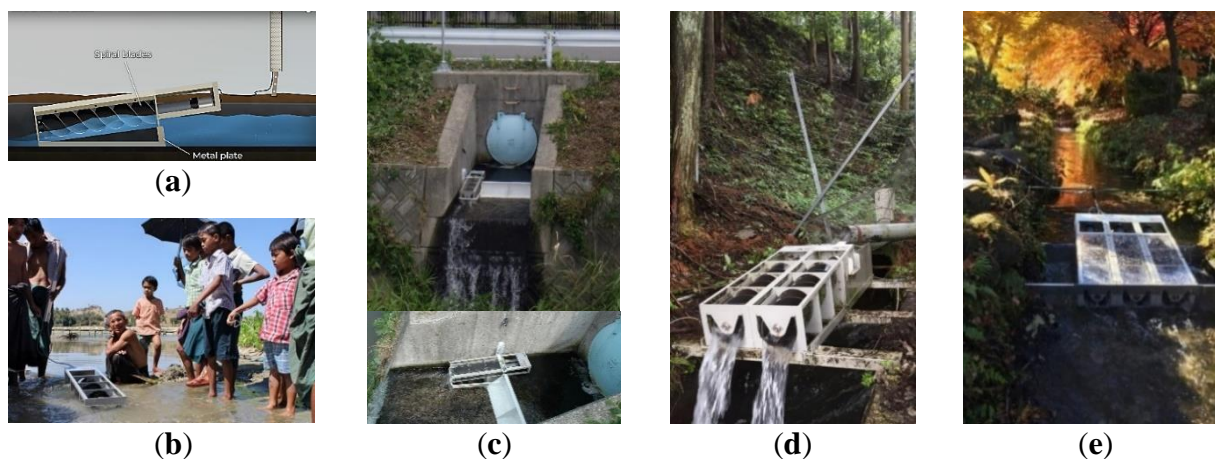


Figure 2.12: Ultra-small all-in-one Archimedes screw generator (PicoPica 10): (a) PicoPica 10's system Schematic [86]; (b) operational test in Myanmar [127]; (c) power Generation from unconventional water resources [128]; (d) Multi-ASG (two units) running since 2012 in Ibi-Cho, Gifu, Japan, to supply electricity for the security lights and the electric fence [129]; (e) a multi-ASG application for shallow water resources [130].



Figure 2.13: Small commercial all-in-one ASG generator (PicoPica 500), Nikko City, Japan [64], [126].

2.4 Principles of Archimedes Screw Hydro Powerplants Design

2.4.1 Archimedes Screw Hydropower Plants Configurations

Most early ASGs were designed to operate at one fixed rotation speed. However, variable speed operation is also possible by adding additional electrical equipment and accepting an efficiency reduction. Variable-speed ASGs are a practical solution to deal with large seasonal flow fluctuations. Increasing the ASG rotation speed increases the volume of flow that can pass through the ASG. However, ASG efficiency is reduced when rotation speeds exceed the maximum rotation speed suggested by Muysken's relationship (Eq. (2-1)) [83]. In addition, noise becomes a more significant issue at higher rotation speeds. When the volume of flow in a river is so high that an excessively large diameter (exceeding 5 m) or high rotation speed ASG (exceeding Eq. (2-1)) would be required to utilize the available flow, a multiple screw powerplant can be considered. In such cases, two or more ASGs can be installed (typically side by side) instead of a single big screw. When flow at the site is large, all ASGs could be turned on to generate power in their most efficient condition. The extra ASG(s) could be turned off at times when the flow is reduced, allowing the remaining ASG(s) to operate closer to optimum conditions.

Therefore, at sites where a considerable fluctuation in river flow is anticipated, plant designers may consider variable-speed ASGs and multi-ASG plants in order to effectively utilize available flow at both low flow and high conditions. Using two or more ASGs in a single site could also provide other benefits, including easier maintenance, more flexible operation plans, and even some savings in major costs. Currently, ASG design is usually based on the site specifications, regulatory limitations, and characteristics of available flow. One possibility is that multi-ASG powerplants

could lead to significant capital cost savings by allowing mass production of highly optimized ASGs in several specific sizes.

Figure 2.14 shows a crowd-sourced map maintained by Alois Lashofer of the locations of many ASG powerplants across the world [131] as of July 2020. The majority of the mapped ASG powerplants are single screw plants. However, there are several plants that benefit from more than one screw installation. While most multi-screw installations are in a parallel configuration, there are examples of installations of two or more ASGs in series to take advantage of the higher head [97], such as the Yorkshire Water’s Esholt wastewater treatment multi-ASG hydropower plant.

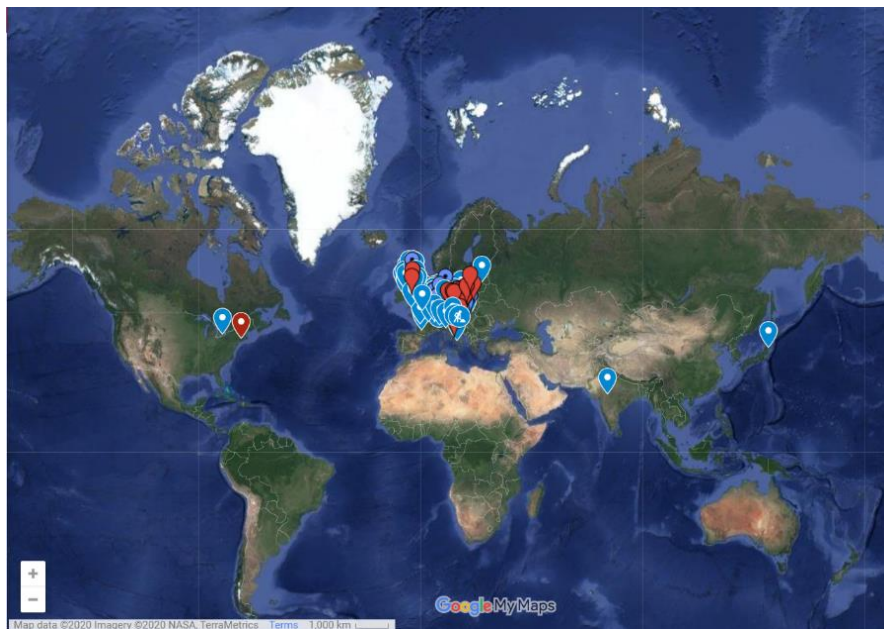


Figure 2.14: The map of ASG powerplants across the world [97].

Figure 2.15 shows some representative multi-ASG powerplants in the United Kingdom. Monmouth New Hydro (Figure 2.15-a) is constructed on the site of the Old Monmouth Hydro Station, which operated from 1899 to 1953. The new hydro scheme uses two ASGs and has been

operating since 2009 [132]. This multi-ASG powerplant on River Monnow could generate 75 kilowatts of power by each screw, which rotates at only 20 RPM and utilizes 3.4 m of water head [133]. Radyr Hydro Scheme (Figure 2.15-b) applies two 200 kW ASGs with a 3.5 m outer diameter and 10 m length in order to utilize a site on the River Taff with 3.5 m head and a mean flow of 22 m³/s. This powerplant can generate 1.8 million kWh of energy annually, which reduces 785 tons of CO₂ emission [134]. Linton Falls Hydro powerplant (Figure 2.15-c) operated from 1909 to 1948. Since 2012 it has been retrofitted with two ASGs with a diameter of 2.4 m. With the available 2.7 m of head and up to 4.5 m³/s of flow rate [97], each screw can pass 2.6 m³/s, which results in a combined 100kW of output power at their full capacity [135]. With an annual production of about 500 MWh, this powerplant could save more than 210 tons of CO₂ emissions per year [135].



(a)



(b)



(c)

Figure 2.15: Multi-ASG hydropower plants in the UK: (a) Monmouth New Hydro Scheme, Osbaston [133]; (b) Radyr weir hydro, Radyr [136]; (c) Linton Falls Hydroelectric Power Station, Threshfield [137].

One of the most recent multi-ASG powerplants (Q2, 2019) is the Solvay industrial plant, which is installed as a retrofit/upgrade on the small existing weir in Torrevieja, Spain (Figure 2.16). The entire project was constructed in just 4 months. This plant diverts part of the Saja River and applies two parallel ASGs that are able to produce a total of 70 kW of power (35 kW each) with 2 m of water head and 5 m³/s of flow rate for both turbines. The generated energy will be sold to the

electrical grid, and the return on investment will be recovered about 7 to 8 years after its start-up date [138].



Figure 2.16: Solvay multi-ASG powerplant project at a glance [138].

Even current ASG powerplants could upgrade to multi-ASG hydropower. Linton Lock powerplant is one of the pioneers in such an approach that benefits from two different sizes screws. Figure 2.17 shows this powerplant. The bigger screw is called “Widdington Plant,” and the smaller one is called the “Linton Plant.” The first screw was installed in 2012 with a diameter and length of 3 m and 8.5 m, respectively. With 3.2 m of water head and 4.5 m³/s capacity, this screw could offer 101 kW of power output. In 2017, the second screw with a 5 m of diameter was installed beside it. In terms of flow rate, utilizing up to 14.5 m³/s of flow makes “Widdington Plant” the largest screw. With 3 m of the head, this screw could provide 355 kW of power output [65].



Figure 2.17: Linton Lock multi-ASG powerplant.

Considering the number of installed screws, the Marengo powerplant in Goito, Italy, could be considered one of the multi-ASG hydropower's world records since it utilizes six parallel ASGs. Figure 2.18 shows this powerplant which is installed on the Mincio River through the Pozzolo-Maglio drain channel and has an average potential of 222.7 kW (up to 306 kW [139]) with 1.6 m of water head and 1.4 and 22.2 m³/s average and maximum flow rates, respectively [140]. Each screw is 3 m in diameter and can pass 3.7 m³/s of flow to generate up to 54 kW of power [139].



Figure 2.18: Marengo multi-ASG hydropower plant in Goito, Italy [139].

2.4.2 Components of Archimedes Screw Hydro Powerplants

Figure 2.19 shows the relationships between ASG and the other parts of a simplified ASG-based ROR hydropower system. This figure indicates that an Archimedes Screw generator (ASG) run-of-river (ROR) hydroelectricity powerplant can be considered as a system with three major components: a reservoir, a weir, and the ASG (which is connected to the system by a control gate and trash rack). At most real ASG locations, the incoming flow must be divided between the ASG

and a parallel weir. Typically, a minimum flow over the weir is mandated for the protection of the local environment. Therefore, other outlets, as well as a fish ladder, could be considered as the other components of this system. Therefore, in an ASG hydropower plant system, incoming river flow is the input, and the weir overflow, ASG outlet flow, and other outlets (i.e., fish ladder flow) are the outputs.

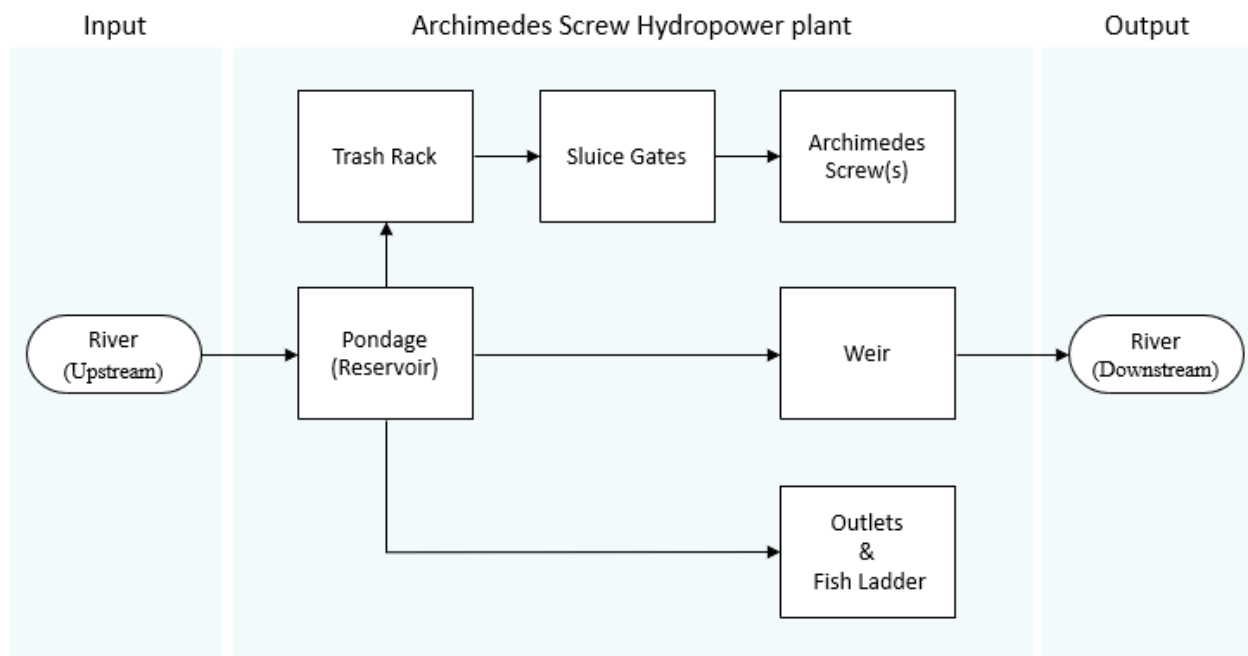


Figure 2.19: Horizontally A Simple Model of an ASG-based Run-of-River (ROR) System.

2.4.3 Design of Archimedes Screws

The Archimedes screw itself is a central component in an Archimedes Screw Hydropower Plant. Figure 2.20 shows a typical Archimedes screw configured as a hydropower plant and the most important dimensions and parameters required to define the Archimedes screw. These are:

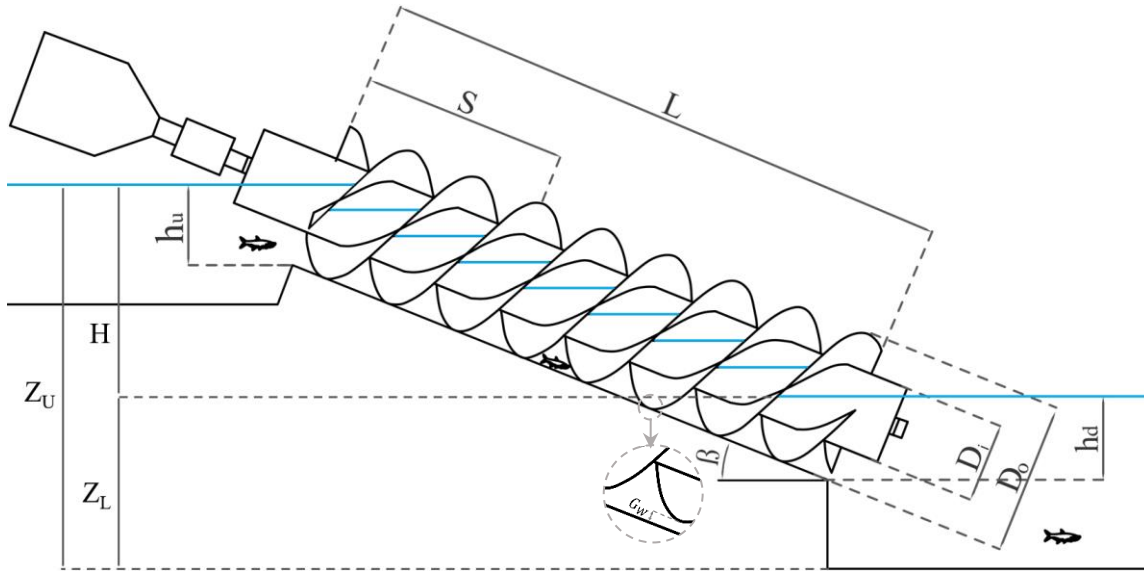


Figure 2.20: Required parameters to define Archimedes screw geometry [1], [6].

Table 2.2: Archimedes screws' geometry and operating variables.

Parameter	Description	Unit	Variable	Description	Unit
L	Length of the screw	(m)	ω	Rotation speed of screw *	(rad/s)
D_o	Outer diameter of the screw	(m)	h_u	Upper (inlet) water level	(m)
D_i	Inner diameter of the screw	(m)	h_L	Lower (outlet) water level	(m)
S	Screw's pitch or period [34] (The distance along the screw axis for one complete helical plane turn)	(m)	Q	Volumetric flow rate passing through the screw	(m ³ /s)
N	Number of helical planed surfaces (also called blades, flights or starts [34])	(1)	δ	Inner to outer diameter ratio $\delta = D_i/D_o$	(1)
β	Inclination Angle of the Screw	(rad)	σ	Pitch to outer diameter ratio $\sigma = S/D_o$	(1)
G_w	The gap between the trough and screw.	(m)	Ξ	Dimensionless inlet depth $\Xi = h_u/D_o \cos \beta$	(1)

* Note: In the fixed speed Archimedes screws rotation speed is a constant.

The geometry of an Archimedes screw is determined by external (D_o , L , and β) and internal (D_i , N , and S) parameters. The external parameters are generally determined based on the location of the screw and the passing flow rate. The internal parameters could be selected in a way that optimizes the performance of the screw [34]. Typically, the screw manufacturer should be involved

in detailed design. The following process may be useful for the initial planning and preliminary design of an ASG site:

First, determine the overall size and inclination angle of the screw. The inclination angle should be determined based on the site slope. If there are minimal constraints on the angle (and installation space), a value of $\beta = 22^\circ$ could be considered since many current ASG powerplants are installed at a similar inclination angle unless a steeper slope is required. Be careful if considering β values in excess of about 30° , since screw capacity will decrease markedly, or less than about 20° due to longer screw length. Determine the length (L) of the screw based on site specifications and technical limitations. Use information from existing plants and Equations (10) or Equations (11) to select an overall diameter D_o to accommodate the available flow.

Check L/D_o and if it is less than about 2, expect efficiency to be somewhat reduced. If L/D_o is less than about 1.25, the screw will likely be too short for its diameter. Consider two or more screws with a smaller diameter, particularly as L/D_o gets smaller. Use Equation (10) for screw rotation speed ω , let pitch $S = D_o$ and use $D_i = D_o/2$. These values could be reasonable for preliminary planning but may not be optimum values for the final design.

After determination of the geometry of the screw, the algorithm presented by Nuernbergk and Rorres [33] can be used to determine the inlet water head required for optimal operation of the screw to fill it to its optimum volume capacity without occurring overflow. This is needed to vertically position the screw relative to the dam crest or expected reservoir level. The screw must be low enough to ensure it fills completely, but not so low that the available head is not utilized. The Archimedes screw power generation model that is introduced in Section 5.3 could be used to

estimate the generated power of the designed powerplant. Finally, the net generated power of the Archimedes screw is the difference between the estimated generated power and the power losses introduced in Section 2.4.5.

Note that the process above and in the following two sections should only be used to check the feasibility of an ASG at a site. Additional design work will be needed to properly optimize the screw plant for a site.

2.4.4 Estimating the Generated Power of the Archimedes Screws

Despite the literature on Archimedes screws as pumps, currently, there is little English documentation on using them for extracting energy from flow, and a significant portion of it is about the case studies of installations, many of which are qualitative [49]. Several researchers have worked on developing mathematical models to predict the power output of an Archimedes screw. Early ASG power models assumed that the screw was driven by the weight of the water enclosed by the screw blades [32], [141]. Essentially, water contained within the buckets of the rotating screw produces a static pressure distribution on all submerged surfaces, and this distribution of pressures results in a net force in the direction of rotation.

Müller and Senior (2009) offered a model based on the hydrostatic pressure difference across the screw surfaces. To consider the effect of gap leakage, they used Nagel's (1968) empirical equation. However, their model simplifies the screw geometry to a level that they concluded that, by ignoring the bearing and friction losses, theoretically, there is no dependency between the rotation speed and the efficiency of an ASG [27], [49].

The main assumption for almost all Archimedes screws models is that the water level in each bucket is the highest level at which no water flows to the next bucket over the top of the inner cylinder. There is little theory or data for when ASGs run at partially full conditions [49]. Lubitz et al. [49] proposed a model to estimate the efficiency of screws for all ranges of possible fill levels. Based on the idea of analyzing a single water bucket, Lubitz et al. [49] proposed several mathematical models to estimate the flow and power of an ideal screw in a steady flow regime. This quasi-static model calculates the volumes of water buckets and the resulting torque on the screw by assuming the screw is not rotating and experiencing no internal water flows [49].

For an ideal screw operating under steady-state conditions (steady flow, constant rotational speed), all the buckets will have the same shape and volumetric size. The shape and size of a bucket are determined by the geometry of the screw, the screw rotation speed ω , and the volume flow rate of water through the screw Q [49]. The model determines the forces and flows operating within a single bucket for an idealized infinitely long screw. It is assumed that all buckets within the screw effectively function identically to this idealized bucket. Then, the forces, torques, and power can be scaled up based on the total length of the screw (L) to calculate total screw power [49].

2.4.4.1 Bucket Volume Theory

The Lubitz et al. [49] model requires defining the general positions on the helical plane surfaces in cylindrical coordinates (Figure 2.21). A 'w' axis is aligned with the rotational axis of the central cylindrical shaft, and a vertically oriented Cartesian axis 'z' is also defined with positive z vertically upwards. This vertical axis is used to calculate local water depths by projecting physical locations on the helical plane surfaces onto the vertical axis. It is assumed that the first leading

helical plane edge is vertically oriented at the top of the screw. So, for any position along the w axis, the radial positions ($r(\omega)$) and angular positions ($\theta(\omega)$) on the leading plane are described by the geometry of a helicoid of pitch length S . For any given position along the ‘ w ’ axis [49]:

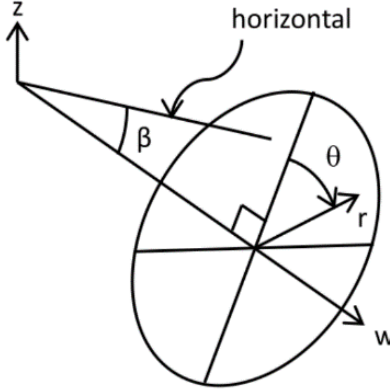


Figure 2.21: The relationship between the angular and radial positions within the screw in the Lubitz et al. (2014) Archimedes Screw model coordinate system.

$$r(w) = r \quad (2-2)$$

$$\theta(w) = 2\pi \frac{W}{S} \quad (2-3)$$

where r is the radial position, and θ is the angular position (Figure 2.21). For a screw with the number of blades N , the vertical position on the leading helical plane surface (Z_1) and the upstream helical plane (Z_2) at any point like $X(r, \theta)$ could be defined by [49]:

$$Z_1 = r \cos(\theta) \cos(\beta) - \frac{S\theta}{2\pi} \sin(\beta) \quad (2-4)$$

$$Z_2 = r \cos(\theta) \cos(\beta) - \left(\frac{S\theta}{2\pi} - \frac{S}{N} \right) \sin(\beta) \quad (2-5)$$

The minimum fill height can be approximated to occur at $\theta = \pi$, $r = D_o/2$ and the maximum (100%) fill height occurs at approximately $\theta = 2\pi$ and $r = D_i/2$. Therefore, the minimum bucket

water depth Z_{min} , maximum bucket depth without overflowing Z_{Max} and the actual water depth within the bucket Z_{wl} can be defined and related to the nondimensional water fill height (f):

$$Z_{min} = -\frac{D_o}{2} \cos(\beta) - \frac{S}{2} \sin(\beta) \quad (2-6)$$

$$Z_{Max} = \frac{D_i}{2} \cos(\beta) - S \sin(\beta) \quad (2-7)$$

$$Z_{wl} = Z_{min} + \frac{Z_{wl} - Z_{min}}{Z_{max} - Z_{min}} (Z_{Max} - Z_{min}) = Z_{min} + f \cdot (Z_{Max} - Z_{min}) \quad (2-8)$$

An infinitesimal, cylindrical volume element (dV) can be defined parallel to the ‘w’ axis connecting adjacent points of the helical planes on upstream and downstream of the bucket. If only the portion of this elemental volume that is submerged below the water line is considered part of the overall water bucket volume, the overall volume of a bucket V can be determined as [49]:

$$dV = \begin{cases} 0 & Z_l > Z_{wl} \text{ and } Z_{wl} < Z_2 \\ \frac{Z_{wl} - Z_1}{Z_2 - Z_1} \frac{S}{N} r dr d\theta & Z_1 \leq Z_2 \text{ and } Z_{wl} \leq Z_2 \\ \frac{S}{N} r dr d\theta & Z_l < Z_{wl} \text{ and } Z_{wl} > Z_2 \end{cases} \quad (2-9)$$

$$V = \int_{r=\frac{D_i}{2}}^{r=\frac{D_o}{2}} \int_{\theta=0}^{\theta=2\pi} dV \quad (2-10)$$

2.4.4.2 Flow Rate and Leakage Models

The amount of power generated by an ASG is proportional to the volume flow rate of water through it. The total flow (Q) of an ASG can be divided into the following five components: (1)

Main flow that is contained with the buckets and causes torque generation (Q_M), (2) Gap leakage flow (Q_G), (3) Overfilling flow leakage (Q_O), when water levels within a bucket are so high that some water spills over the top of the central cylinder, (4) Friction-leakage (Q_F), when water adheres to the flights and is flung out of the screw, and (5) No guiding plate leakage (Q_P), which occurs when water levels are high enough that water spills out of the top edge of the trough [33].

Total flow Q is the sum of all five of these flow components:

$$Q = Q_M + Q_G + Q_P + Q_O + Q_F \quad (2-11)$$

A relationship to estimate the overall volume of flow passing through the ASGs is developed in chapter 4. It can be assumed that generally, only Q_M contributes to meaningful power generation, while the other flow components do not contribute useful power and so are ideally minimized or eliminated. In modern screws, Q_P is usually eliminated by using a guiding plate to extend the trough to enclose more of the rotating screw. For screws running up to the optimal flow rate, Q_O is zero since overflow only happens above the optimum flow rates. Finally, the effect of Q_F is usually negligible in ASGs [33].

The gap flow (Q_G) is of particular interest since it is necessary to include a gap between the blades and trough, and so it is not possible to eliminate this component of lost flow. Nagel [142] presented an empirical equation for gap leakage flow in Archimedes screw pumps (not turbines) for the case of full buckets ($f = 1$) at normal rotational speeds:

$$Q_G = 2.5 G_W D_o^{1.5} \quad (2-12)$$

where the G_W gap width (in meters) and the diameter (D_O) must be entered in meters to get a resulting Q_G in m^3/s . The gap width is not easy to measure in full-scale screws. Nagel also provided an empirical relation to estimate G_W based on the size of the screw:

$$G_W = 0.0045\sqrt{D_O} \quad (2-13)$$

Nagel's model is necessarily an estimate only, as all physical and dynamic properties of the actual flow regime, rotational mechanics of the screw, and the fluid mechanics of the flow are neglected [142]. Neurnbergk and Rorres proposed a more complex equation attributed to Muysken to estimate gap flow leakage by including some additional parameters [33]:

$$Q_G = \mu_A G_W \frac{D_O}{2} \left(1 + \frac{G_W}{D_O}\right) \sqrt{1 + \left(\frac{S}{\pi D_O}\right)^2} \left(\frac{2}{3}(\alpha_3 + \alpha_5) + \alpha_4\right) \sqrt{2g\Delta h} \quad (2-14)$$

where μ_A is the contraction discharge coefficient, which is dependent on the edge of the blade's shape and typically is between 0.65 and 1 for the minimum and maximum leakage, respectively. The head difference $\Delta h = (S/N)\sin\beta$ and α_3 , α_4 , and α_5 are wetted angles around the gap (in radians) that can be determined from the algorithm proposed in Rorres (2000) [33], [34].

Lubitz et al. [49] presented an equation for Q_G that is functionally equivalent to the Muysken (1932) [83] and Nuernbergk and Rorres [33] leakage models, but cast in different geometric variables. It assumed that the entire gap leakage is driven by the static pressure difference across the gap, which is the result of the water height difference between adjacent buckets.

$$Q_G = C G_W \left(l_w + \frac{l_e}{1.5}\right) \sqrt{\frac{2gS}{N} \sin \beta} \quad (2-15)$$

where C is a minor loss coefficient that is less than or equal to 1 and previously taken to be 0.89; g is the gravitational constant (9.81 m/s^2); and l_w and l_e are wetted lengths along with a single turn of one flight, with l_w being the length of the gap that is submerged on both sides, and l_e being the length of the gap that is submerged on one side and exposed to air on the other (Figure 2.22).

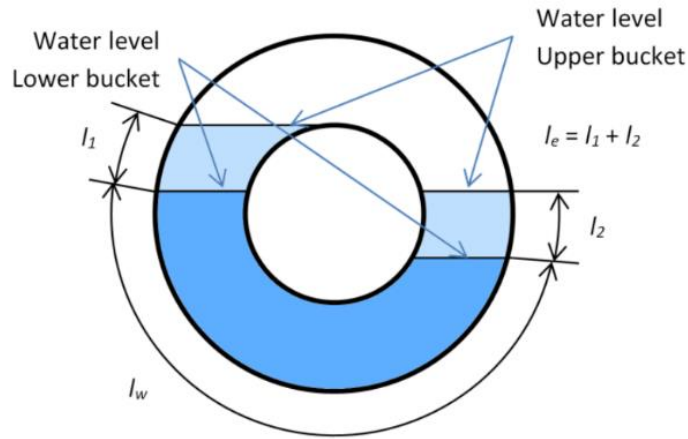


Figure 2.22: Lubitz et al. gap leakage flow model parameters. From [49].

When the bucket fill level exceeds 100% ($f > 1$), rising the water above the center cylinder causes a secondary flow that lets the water pour over the top of the center cylinder into the downstream bucket. Aigner [33] presented a leakage model based on assuming that the overflow could be approximated as weir flow through a triangular spillway [79]. The weir is approximated as a simple angled, V-notch weir since this is approximately the shape that the central shaft and the planes make at the overflow point [35].

$$Q_o = \frac{4}{15} \mu \sqrt{2g} \left(\tan \beta + \frac{1}{\tan \beta} \right) \sqrt{h_{ue}^5} \quad (2-16)$$

where μ is a loss coefficient and h_{ue} is the overflow head, calculated as [35]

$$h_{ue} = Z_{wl} - Z_{max} \quad Z_{wl} > Z_{max} \quad (2-17)$$

At optimum fill height and below, no spill occurs across the central tube, and h_{ue} and also Q_o will be zero.

2.4.4.3 Torque and Power Models

The torque on the screw is the result of water pressure on the helical planes. The Lubitz et al. model determines the hydrostatic pressure p at any point on the plane surfaces at a depth z below the water level by assuming static conditions within the buckets [49]:

$$p = \begin{cases} \rho g(Z_{wl} - Z) & Z < Z_{wl} \\ 0 & Z \geq Z_{wl} \end{cases} \quad (2-18)$$

The net pressure on the helical plane surfaces is the difference between the pressure on the up and downstream surfaces of the blade. Therefore, if p_1 and p_2 are assumed as the pressures on each side of the plane surface, the net torque on each element area of the helical plane surface (dT) and the total torque from a single bucket (T) can be calculated by integrating torque over the entirety of the submerged surfaces:

$$dT = (p_1 - p_2) \frac{S\theta}{2\pi} r dr d\theta \quad (2-19)$$

$$T = \int_{r=\frac{D_i}{2}}^{r=\frac{D_o}{2}} \int_{\theta=0}^{\theta=2\pi} dT \quad (2-20)$$

The total torque for the full length of screw is related to the total number of buckets and can be calculated by:

$$T_{Total} = T \left(\frac{NL}{S} \right) \quad (2-21)$$

Then, the total power will be:

$$P_{out} = T_{Total} \omega \quad (2-22)$$

2.4.5 Archimedes Screw Power Loss Models

The discussion above has described the performance of an ideal screw, in which many loss mechanisms are neglected. While overflow and gap leakage flow reduce the overall efficiency of an ASG [34], [143] and power output can be limited by the amount of water that can enter the screw inlet [33], a complete ASG power loss model should consider all possible known head losses [35], which include:

- Inlet losses due to head loss through the screw entrance
- Internal hydraulic friction between water and moving screw surfaces
- Outlet losses due to exit effects, geometric head losses, and additional drag torque
- Friction of bearings
- Additional mechanical and electrical losses in gearboxes, generators, and electrical controls

The screw is supported at both ends by a bearing. Friction losses in bearings reduce torque available at the ASG shaft. The magnitude of these losses depends on the mechanical properties of the bearing, which may vary from one ASG installation to another, and because bearing losses are both relatively low in full-scale ASGs and difficult to predict a priori, there is little guidance in the literature on this loss mechanism. While there are equations in the literature for predicting inlet and hydraulic frictional power losses, most of the outlet power loss calculation attempts are

based on adapting equations from related problems [144], [145], such as the Borda-Carnot equation for culvert outlet exit power losses. Notably, Nuernbergk presents equations for non-optimal outlet water level loss [36], and Kozyn and Lubitz developed an empirical equation for outlet drag torque power loss [146]. Methods of accurately calculating all of these power losses are a current area of ASG research.

2.5 Conclusions

Archimedes Screws Turbines (ASGs) are a new form of turbines for small hydroelectric powerplants that could be applied even in low head sites. ASGs offer a clean and renewable source of energy. They are safer for wildlife and especially fish. The low rotation speed of ASGs reduces negative impacts on aquatic life and fish.

It is important to note that ASGs are not the general solution for all energy generation demands and problems. ASGs have their own drawbacks, just like any other technologies: using Archimedes screws as generators is a relatively new technology, and in comparison with other hydropower technologies, many aspects of ASGs are not well recognized yet. Currently, there are no standards for the design of ASGs, and ASG hydro powerplant designs are highly dependent on the experience of the engineer who designs them. For very high flow rates or water heads, a single screw may not take advantage of all available potential due to material, structural, technical, and physical limitations. However, the increasing interest in ASGs, new advancements, and ideas such as multi-ASG powerplants offer some solutions to extend ASG usability.

ASGs provide a range of practical advantages for generating electrical energy at suitable locations.

For supporting sustainable development, ASGs offer economic, social, and environmental advantages. Considering the flexibility and advantages of ASGs, they could be considered one of the most practical options for a more sustainable electricity generation:

1. To increase the number of suitable sites for power generation, even in sites with very low flow rates and/or water heads. ASGs can be designed to operate in a wide range of flow rates (currently from 0.01–10 m³/s) and water heads (currently from 0.1–10 m), including at sites where other types of turbines may not be feasible. This increases the number of potentially suitable sites for hydropower.
2. To maximize hydropower generation even in rivers with high flow rate fluctuations. ASGs can handle flow rates even of up to 20% more than optimal filling without a significant loss in efficiency [78]. Even when the conditions are not perfect for a single screw, installing more than one screw, and utilizing variable-speed ASGs, allows developers to fully utilize available flow at a wider range of sites, including those with high seasonal variability.
3. To retrofit old dams or upgrade current dams or mills to make them economically (power generation) and environmentally (renewable energy) reasonable. Using ASGs as an upgrade for retrofitting old dams or upgrading operational dams makes it possible to add electrical generation with extremely low incremental environmental impact, at reasonable costs and with good potential for low social impacts while providing an incentive to maintain aging dams and infrastructure. ASGs utilized in this manner could help to reduce fossil fuel usage and greenhouse gas emissions by displacing electricity generated by more polluting methods.
4. To reduce the hydroelectricity major operational and/or maintenance costs: In addition to the

advantages of retrofitting/upgrading current dams, the capital costs of ASG hydropower can be less than other hydropower technologies at appropriate sites. The overall maintenance demands and costs of ASGs are often lower than other turbines. Major maintenance is required after 20 to 30 years.

5. To reduce the disturbance of natural erosion and sedimentation processes which could lead to soil and land conservation.
6. To make hydropower generation safer for aquatic wildlife, especially for fish.
7. To generate electricity for small communities or regions that are hard to access or connect to the power grid, especially because of the low operation and maintenance demands and costs of ASGs. These characteristics make ASGs a potential candidate for providing electrical power in undeveloped, remote, and small communities that currently lack energy infrastructure.
8. To improve the welfare of the developing countries and regions with limited access to the power grid or other infrastructures. Despite many other technologies, ASGs do not require high manufacturing capabilities and hi-tech technologies to design, implement, operate, or maintain. Simplicity, low operational demands, and moderate costs make ASGs a practical, environment-friendly and sustainable solution for supplying energy, especially in developing countries. At remote locations with a low head water supply, ASGs may provide a possible means of providing electricity that would otherwise be impractical in developing communities. Improving the economy and welfare of such communities is a win-win futuristic sustainable development approach that could be facilitated by using ASG hydroelectric plants.

2.6 Nomenclature

A_E	: Effective cross-sectional water area at the screw's inlet	(m ²)
A_{Max}	: Maximum cross-sectional water area at the screw's inlet	(m ²)
a	: Coefficient of dimensionless flow rate	(-)
b	: Coefficient of dimensionless area constant	(-)
c	: Coefficient of dimensionless rotation speed constant	(-)
D_i	: The inner diameter of the Archimedes screw	(m)
D_o	: The outer diameter of the Archimedes screw	(m)
f	: Fill height of water in a bucket of screw	(-)
g	: Gravitational constant	(9.81 m/s ²)
h_u	: Upper (inlet) water level of the screw	(m)
h_L	: Lower (outlet) water level of the screw	(m)
G_w	: Gap width (The gap between the trough and screw)	(m)
h_{ue}	: Overflow head	(m)
L	: The total length of the screw	(m)
l_e	: The wetted gap length along with a single turn of one flight that is submerged on one side and exposed to air on the other	(m)
l_w	: The wetted gap length along with a single turn of one flight that is submerged on both sides	(m)
N	: Number of helical plane surfaces	(-)
p	: The hydrostatic pressure at any point on the plane surfaces at a depth z below the water level	(Pa)
P_{Out}	: Output power/shaft power of screw	(W)
Q	: Total flow rate passing through the screw	(m ³ /s)
Q_F	: Friction-leakage	(m ³ /s)
Q_G	: Gap leakage flow	(m ³ /s)
Q_M	: The main flow that is contained with the buckets and causes torque generation	(m ³ /s)
Q_{Max}	: The maximum flow rate that could pass through a screw when $\omega = \omega_M$ and $A_E = A_{Max}$	(m ³ /s)
Q_O	: Overfilling flow leakage	(m ³ /s)
Q_P	: No guiding plate leakage	(m ³ /s)
r	: Radial position	(m)
S	: Pitch of the screw (Distance along the screw axis for one complete helical plane turn)	(m)
T	: The torque of a single bucket	(Nm)
V	: The overall volume of a bucket	(m ³)
V_T	: Axial transport velocity	(m/s)
T_{Total}	: Total torque of the entire screw	(Nm)
w	: The location along the screw centerline	(m)
z	: Vertical location	(m)

Z_{min}	:	Minimum bucket water depth of the screw	(m)
Z_{Max}	:	Maximum bucket depth of screw without overflowing	(m)
Z_{wl}	:	The actual water depth within the bucket	(m)
$\alpha_3,$:		
$\alpha_4,$:	Wetted angles around the gap	(rad)
α_5	:		
β	:	The inclination angle of the screw	(rad)
Δh	:	The head difference	(m)
θ	:	Angular position	(rad)
μ	:	Coefficient of the loss	
μ_A	:	Contraction discharge coefficient	
ρ	:	Density of water	(1,000 kg/m ³)
ω	:	The rotation speed of the screw	(rad/s)
ω_M	:	The maximum rotation speed of the screw (Muysken limit)	(rad/s)

Subscripts

i	:	inner
min	:	minimum
Max	:	Maximum
O	:	Outer
$Total$:	Total
wl	:	Water surface level
1	:	Surface 1 (downstream side of bucket)
2	:	Surface 2 (upstream side of bucket)

3 Artificial Neural Networks and Extended Kalman Filter for Easy-to-Implement Runoff Estimation Models

Adapted from:

A. Yoosefdoost, S. M. Tahsien, S. A. Gadsden, W. D. Lubitz, and M. Kaviani, “Artificial Neural Networks and Extended Kalman Filter for Easy-to-Implement Runoff Estimation Models,” 2022.

Thesis Author’s Contribution:

Arash YoosefDoost’s contributions were in conceptualization, development of methodology, investigation, visualization, writing, reviewing, and editing. S. M. Tahsien’s contributions were in investigation, software, validation and writing. Professor S. A. Gadsden’s contributions were in conceptualization, project administration, supervision, reviewing, and editing. Professor W. D. Lubitz’s and M. Kaviani’s contributions was in reviewing and editing [4]. The figures are all original, or from explicitly referenced sources.

3.1 Introduction

A realistic and reliable estimation of the available volumetric flow rate is essential for designing Archimedes screw hydropower plants. Historical data such as flow duration curves are great tools for the initial estimation of available volumetric flow rate for each site and the initial designs of Archimedes screw hydropower plants. Then comprehensive studies should be undertaken to evaluate different scenarios, such as the climate change effects on the available volume of flow. Such deep investigations on flow are water resources engineering topic that is not in the scope of this study. However, developing general and easy-to-implement methods and tools to support such studies could improve the feasibility of initial studies on remote, hard to access or developing regions.

Analytical solutions and conceptual models are preferable where the required data is available. However, solving complex problems with a few available variables could be almost impossible by many traditional models. In fact, the lack of enough data may make many studies infeasible for remote, hard to access or developing regions. Furthermore, studying new problems or even new cases usually requires a systematic approach that could be costly or time-consuming.

A black box could be defined as a general or multi-purpose model that maps the inputs of a system to its output without the need for knowing the governing rules and phenomena in the system or details such as the dynamics of, or interactions between, the system's components. Based on this definition, developing a multi-purpose black box such as an ANN could be beneficial to speed up studies or make them feasible where enough samples are available for training the network, but the number of available variables is not enough and utilizing traditional methods is hard, expensive, time-consuming, or technically infeasible.

In the modern world, widely applicable black box models could offer new, faster, or more effective solutions or assist in solving complex problems where it is not possible using traditional models. For example, ANNs are widely applied for solving complex problems in areas that there are a few or no alternatives for them, such as problems such as image processing, natural language processing etc.

Generally, using more samples for training the ANNs could improve the results. For example, a long-term dataset of effective variables in the precipitation-runoff phenomenon is required to train ANN-based runoff estimation models to achieve reasonable results. However, more training data comes at the cost of more training time, particularly for large neural networks. Therefore,

optimizing the size of neural networks is very important. In addition, efficient training algorithms are essential to reduce the training time of ANNs. Such algorithms could also benefit the computational costs by reducing the size of the ANN.

The non-scalable initial investigation costs are one of the biggest burdens of small projects. Artificial neural networks (ANNs) could help reduce investigations costs and make many projects feasible to study by acting as input-output mapping algorithms. Due to the proven applicability of ANNs in many areas in modern investigations, this study investigates an easy-to-implement and understand ANN-based method to develop estimation models when the minimum number of the available variables limits the feasibility of the application of traditional models. For this purpose, the effects of using the Extended Kalman Filter (EKF) as the training algorithm for MLP neural networks were evaluated by solving a runoff estimation problem and comparing the developed models with MLP networks using Gradient Descent (GD) as the training algorithm. This method is applied for solving a runoff estimating problem using the minimum number of input parameters, precipitation and temperature, that are easy to measure and widely available. This easy-to-implement method to develop ANN-based estimation models could assist in finding or evaluating potential sites for ASG hydropower plants.

3.1.1 Artificial Neural Networks

Artificial intelligence (AI) is the intelligence exhibited by machines taught by humans. This term is applied when a machine mirrors cognitive functions such as learning and problem-solving [147]. AI research has been divided into subfields [148] that include reasoning, planning, and learning

[147], [149]–[151]. Machine learning investigates the study and development of algorithms to learn from and make predictions on data [152]. Machine learning can accelerate and improve investigations by building a model from example inputs to make data-driven predictions instead of time-consuming and intensive deterministic analytical or computational approaches. Therefore, the quality of data is critical to the success of most AI-based or machine learning models.

Artificial neural networks (ANN) are biologically inspired neural networks used to estimate or approximate functions that can depend on a large number of inputs, which are generally unknown. ANNs usually make a correlation between inputs and outputs in a system, effectively acting as an input-output mapping algorithm with largely unknown properties [153]. Artificial neural networks (ANNs) date back to the idea of threshold logic by Warren McCulloch and Walter Pitts in 1943 [154], which is a generalization of the logic gates that work by comparing the inputs to a threshold [155]. In the 1940s, Hebb developed the so-called 'Hebbian learning,' a learning hypothesis based on the mechanism of neural plasticity [156]. Hebbian learning was applied to computational models with Turing's B-type machines in 1948. In 1954, Farley and Clark simulated a Hebbian network in computational machines [157]. In 1958, Rosenblatt developed the concept of Perceptron as a pattern recognition algorithm [158]. Group Method of Data Handling is the first functional network with many layers, which Litvinenko and Lapa introduced in 1965 [159]–[161]. However, publishing the Minsky and Papert research result in 1969 caused stagnation in ANN research [162]. The backpropagation algorithm introduced by Werbos in 1975 effectively solved the 'exclusive or' problem by making the training of multilayer networks feasible and efficient. It distributed the error term back through the layers and modified the weights at each node [163]. The resilient backpropagation (Rprop) algorithm introduced by Riedmiller and Braun in 1993 is

an effective learning algorithm for multilayer feedforward networks [164]. Today, many other algorithms and new approaches are developed for the optimization of the training process or outputs of ANNs.

3.1.2 Extended Kalman Filter & ANNs

In signal processing, the Kalman filter is known as the most popular method used to estimate the states of a linear system in the presence of white noise [165]. Different versions of the KF have been developed for nonlinear systems and measurements, and the most popular include the extended Kalman filter (EKF) and the unscented Kalman filter (UKF) [166]. The EKF estimation method has been found to be a fast training technique [167].

Many investigations studied the effectiveness of utilizing the recursive least squares technique (RLS) [168], [169] and EKFs [170], [171] in neural networks. In the 1990s, several studies autonomously used an EKF in training a multilayer perceptron and demonstrated that it performs better than utilizing a traditional backpropagation training approach [172]–[175]. In 1992, Ruck et al. studied the utilization of the EKF and backpropagation techniques as training algorithms [176]. In 1994, Puskorius & Feldkamp expanded the idea of training the neural network by applying an extended Kalman filter for trained recurrent networks in nonlinear dynamical systems [177]. In 1995 Plumer used Kalman filtering techniques to train multilayer perceptron neural networks (MLPs). Results demonstrated that the sequential-dual extended Kalman filter (DEKF) and batch-DEKF have fundamentally the same convergence properties and lead to a similar performance of the trained networks [178]. In 1998, Pui-Fai SUM [179] studied the possibility of applying the EKF in combination with pruning to speed up the learning process and specify the size of a trained

neural network. In 1999, Wan & Nelson proposed a dual Kalman filtering strategy for feedforward neural network training [180].

Williams [181] and Suykens [182] used the EKF to train a recurrent neural network as a state estimation problem. In 2002, Puskorius & Feldkamp proposed a decoupled strategy for the EKF to accelerate the training rates [183]. Also, in 2002, Leung Chi and Chan Lai studied using a dual-EKF method in recurrent neural networks to improve the detection and identification of an aerospace problem [184]. In 2003, they proposed using a dual-EKF strategy in recurrent neural networks. The simulation results demonstrated that the proposed approach is an effective joint-learning-pruning method for RNNs under online operation [185].

Pietruszkiewicz (2010) studied the application of nonlinear Kalman filtering to feedforward neural networks as the learning algorithm. This study showed that these filters have a high learning ability in the presence of noisy measurements when applied to a popular backpropagation neural network. A comparison of results showed that nonlinear Kalman Filters outperformed the classical error backpropagation learning algorithm [186]. In 2013, Kurylyak et al. reported that blood pressure could be evaluated accurately by combining Kalman filtering and ANNs [187]. The authors proposed a regulated KF approach to overcome the drawback of non-stationary impacts of breathing and measurement noise. The additional filtering was applied to remove low and high-frequency noise and accurate blood pressure estimates [187]. Krok (2013) applied KF for ANN learning. This study demonstrated that implementing a KF reduced the calculation time by using fewer parameters for learning the network [188]. In 2019, Jondhale proposed a KF framework based on real-time target tracking in wireless sensor networks (WSN) in an application with generalized regression neural networks (GRNNs). The experimental results demonstrated that the

proposed GRNN-UKF approach outperformed all other strategies for target tracking [189].

3.1.3 ANN- EKF Based Runoff Estimation Model

Ahmat Ruslan et al. (2013) studied developing flood prediction models for the Sungai Kelang basin by comparing a Back Propagation (BPNN) and Elman (ENN) neural networks that use the Extended Kalman Filter (EKF). The rainfall at flood location and water level at three upstream rivers were defined as model inputs, and the flood location at the downstream river is defined as outputs. This study's dataset resolution is for four days with 10 minutes time intervals, leading to 493 data points for training and validation. The developed networks had a single hidden layer and applied Gradient Descent (GD) or EKF with tangent sigmoid as a transfer function in the hidden and output layers and evaluated for a maximum of 1000 epochs of training. This study stated that using GD leads to reasonable results for the BPNN and ENN models with 10 and 15 neurons in the hidden layer, respectively. The researchers reported that using EKF in BPNN led to some improvements in tracking and filtering the nonlinearity of the BPN output that helped in reducing the RMSE. They also stated that using EKF led to further improvement in ENN and smoother flood water level prediction results by filtering out the nonlinearity of output data [190].

De Vos (2013) compared a variety of ANNs for forecasting twelve river basins in the Eastern United States. This study used time series of daily precipitation, potential evaporation, discharge, and the 20-day simple moving average of the precipitation time series as the inputs to the ANN models. EKF was applied to three ANNs of Elman recurrent ANN (EL), Williams–Zipser fully recurrent ANN (WZ) and Williams–Zipser fully recurrent and fully feedforward ANN (WZFF) as training methods. This study indicated that for the EKF models, four neurons in the hidden layer

were optimal. It also stated that the EKF training algorithm shows better performance on most basins [191].

Ahmat Ruslan et al. (2017) studied developing flood prediction models for Klang River using Neural Network Autoregressive with Exogenous Input (NNARX) and EKF. In these models, rainfall and water level were the inputs, and the water level was the output: 120, 78 and 170 data samples for training, validation and testing of developed models, respectively. This study does not provide information about the details of the models' neural networks. The NNARX converged at 83 training epochs. The authors stated that cascading the NNARX outputs to EKF helps filter the nonlinearity of the output data that led to improvements in the performance of NNARX. The author noted that the performance of the NNARX-EKF model is much better [192].

Karunasingha et al. (2018) incorporated ANN models in EKF to enhance the prediction of chaotic flow river time series. The proposed model was applied to the Lorenz and Mackey Glass series's benchmark time series and to the five daily flow time series of the rivers Mississippi river, Wabash river, Ciliwung river at Katulampa, Ciliwung river at Ratujaya and Ciliwung river at Sugutamu [193]. The ANN model used in this study was previously described in [194]. This single layer MLP was used to develop models of up to 100 neurons and 50 training epochs with five sets of initial weights. Nguyen–Widrow initialization algorithm was applied to initialize weights and biases. The logistic sigmoid transfer function was used for all hidden neurons. Levenberg–Marquardt optimization method was used as the training algorithm to update weights and biases. This study adopted the ANN models as the state-space models in EKF to time delays different from 1 unit. The researchers reported that EKF produces an improved prediction for the benchmark time series, and for the river flow time series of Ciliwung with low average flows, however,

prediction for three other flow series with large average flows did not improve [193].

Hosseini et al. (2020) compared the Extended Kalman Filter-based Neural Network (EKFNN) and the Gene Expression Programming (GEP) in estimating the runoff of the Malayer basin. The dataset used for this study had a daily resolution for runoff and rainfall from 2001 to 2013. This study does not provide information about the type, structure and topology of the developed EKFNNs. This study stated that the EKFNN model was superior to GEP for this case study [195].

A well-designed neural network can learn and break down complex relationships with adequate training [196]. However, designing an efficient ANN is challenging. A faster and/or smaller ANN with acceptable accuracy can reduce both the length and costs of scientific investigations. Therefore, the training algorithm, the number of neurons in each layer, and the type of topology are some of the most important design parameters. Finding the optimal size of a neural network for a particular problem is an important concern in neural networks. If this size is too small, it may not be possible to train the neural network well to solve the problem. Likewise, overfitting may occur if it is too large [197], which may waste resources. Pruning is an approach used to determine the optimal size of a neural network [198]. Great generalization capacity and quick training speed are two other essential criteria for evaluating the performance of the learning techniques in ANNs [179]. Model accuracy and computational costs are two important factors in model development.

Many different parameters may be included in real phenomena, which increases the complexity of the problem. Using traditional methods could be expensive or technically infeasible. Solving a complex problem with a few parameters is almost impossible by many common models. The lack of data may make many studies infeasible, particularly for remote, hard to access or developing

regions. To deal with such limitations, Artificial neural networks (ANNs) could be used as a black box that relates the system inputs to the output(s). This approach could help in reducing costs and making many projects feasible to study. ANNs have been utilized to solve a wide range of problems that are challenging in traditional programming [199]. However, ANNs sometimes treated as tools rather than modern, flexible mathematical models. This study provides an easy to understand and implement method to develop ANN-based estimation models using the multilayer perceptron (MLP) neural network and Extended Kalman Filter (EKF) or Gradient Descent (GD) as the training algorithms. Moreover, three methods to feed training data to the models were evaluated. Then the feasibility of this method is evaluated by solving a runoff estimation problem that uses the minimum number of input parameters.

The basin used in this study was formerly studied using different ANNs ([200]–[202]). Applying a different method for the same case study is a contribution to any study. The value of additional studies is to provide additional materials for future works. Moreover, it helps to compare this study's method with the previous methods. Previous studies on this basin used advanced temporal neural networks such as focused time-delay neural networks (FTDNNs) and FGam [200]–[202]. This study aims to develop an easy to implement and fast method to estimate runoff with a minimized, simple yet effective model using a minimum number of effective parameters: precipitation and temperature. These parameters are easy-to-measure and so basic that they are widely available in nearly all climatology or hydrology stations as well as other records. In this study, it is assumed that the developed models could estimate runoff efficiently if they could be trained well. EKF and GD are applied as the training algorithms, and three approaches are used to feed the training data to models.

In this study, an artificial neural network (ANNs) is used to model the basin as a BlackBox that relates the system inputs (temperature & precipitation) to its output (runoff). The study area information is used for training and testing the developed MLP-based models that apply EKF or GD as training algorithms. The results are compared using several evaluation criteria to measure the performance of each model and approach. This study also investigates the effects of three approaches to feed the training data to the developed ANN-based models. Finally, the results of the most efficient and effective models have been summarized as well as the models with a minimum requirement for training.

The ANNs and methods used in former studies in this basin ([200]–[202]) were difficult to understand and implement due to their complex structures. Additionally, advanced data mining techniques were applied to achieve effective results. Moreover, the developed models were highly dependent on the time-series continuity as inputs which is a strict assumption for reliable results [200]–[202]. The proposed approach in this study is much easier to understand and implement, and it does not need data mining techniques or complex temporal ANNs such as FTDNN or FGam to solve the same problem. In addition, the final model is not dependent on a continuous long-term time series and estimates the runoff with the current data.

In this study, the developed runoff estimation models use a minimum number of required parameters: precipitation and temperature, i.e., just two easy-to-measure and the most accessible parameters in nearly all climatology or hydrology stations. Estimating the runoff is among the most important and challenging issues in water resources management/engineering, not only for development plans but also for operation plans. There are many effective factors in this phenomenon, and the lack of adequate data makes many common models impractical. The non-

scalable initial investigation costs are one of the small projects' biggest burdens [2], [3]. This study helps to reduce costs and make it possible to study possible developments in many new potential sites in remote, hard to access or developing regions.

3.2 Materials & Methods

3.2.1 Multilayer Perceptrons

The Perceptron is a simplified model of a biological neuron and is a linear model that can mimic some behaviour seen in real neurons [203], [204]. This artificial neuron uses the Heaviside step function as the activation function. The single-layer Perceptron is a linear classifier and the simplest feedforward neural network. It is a binary classifier learning algorithm known as the threshold (unit step) function. This function maps a vector of inputs (x) to an output with a single binary value (Γ). A simple perceptron is defined as [205], [206]:

$$\Sigma = \sum_{n=1}^m w_n x_n + b \quad (3-1)$$

$$\Gamma = \begin{cases} 1 & \Sigma \geq 0 \\ 0 & \Sigma < 0 \end{cases} \quad (3-2)$$

Where x , Γ and w have real values, m is the number of inputs, b is the bias, and w is the vector of weights. The bias does not depend on input values and allows for shifting the sigma function Σ (decision boundary) up or down [205]. The weights could describe the effectiveness of each node (here input).

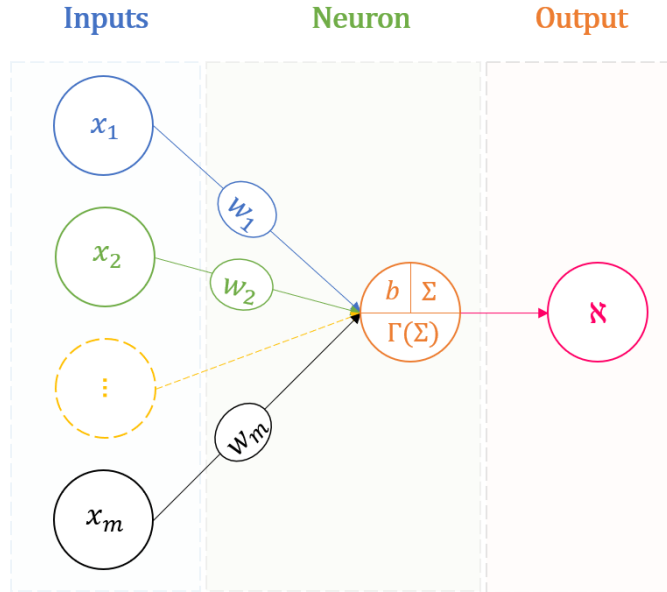


Figure 3.1: A Perceptron Neuron.

The Perceptron is a linear classifier and cannot distinguish data that is not linearly separable [207]; however, a multilayer perceptron (MLP) is able to do this [208]. The MLP is a feedforward ANN that consists of at least three layers of nodes: an input layer, a hidden layer, and an output layer. Except for the input nodes, each node is a neuron that uses an activation function [209], [210]. An MLP is distinguished from a linear perceptron by the multiple layers as well as a nonlinear activation function [208]. In Perceptron, Γ is an activation (transfer) function called the ‘hard-limit’ or ‘unit step’ function that maps the Σ values into desired values (here 0 or 1). By replacing Γ with other activation functions, $f(\Sigma)$ can map the neuron’s output into desired ranges. Therefore, in general form, the output of a neuron (\aleph) with any activation function f could be calculated as:

$$\aleph = f(\Sigma) = f\left(\sum_{n=1}^m w_n x_n + b\right) \quad (3-3)$$

Figure 3.2 shows the topology of a simple MLP. In this figure, x_m , $w_{m,n}^L$, b_n^L , Σ_n^L and f are the

input, weight, bias, sigma function, and activation function, respectively; n is the number of the current neuron, and m is the number of the neuron connected to the neuron n , and L is the number of layers.

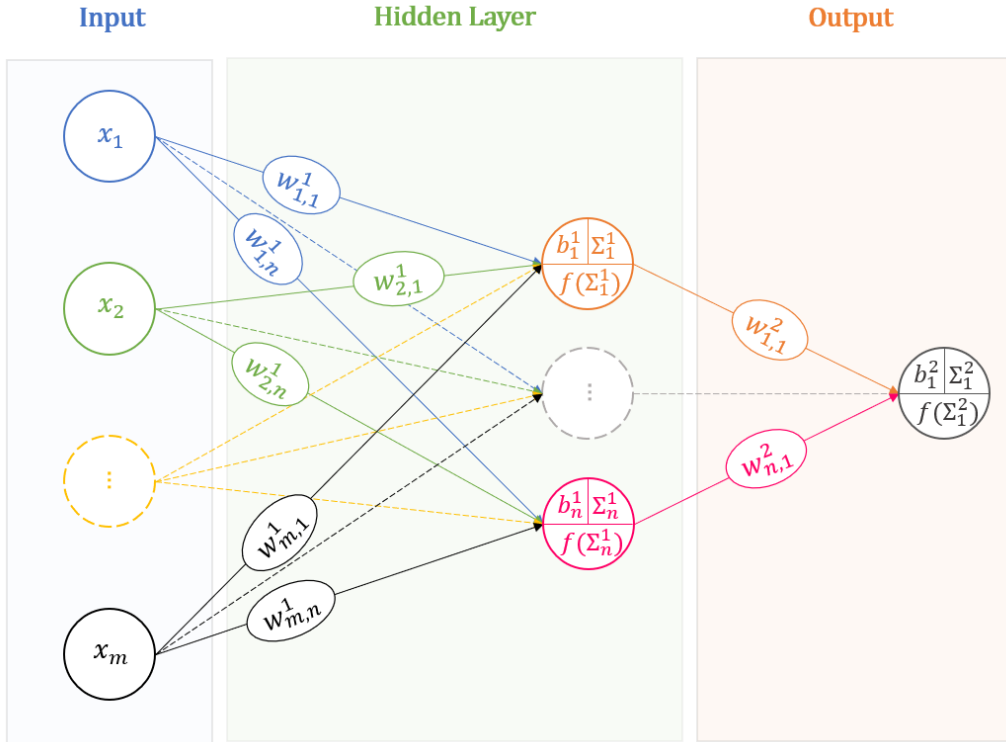


Figure 3.2:A Single Layer MLP.

Figure 3.2 could be described mathematically in the matrix form if for layer L , the matrixes of inputs (X^0), weights (W^L), biases (B^L), sigma function (Σ^L), and the neuron's output (\mathfrak{N}^L) are defined as:

$$X^0 = [x_1 \quad x_2 \quad \cdots \quad x_m] \quad (3-4)$$

$$W^L = \begin{bmatrix} w_{1,1}^L & w_{1,2}^L & \cdots & w_{1,n}^L \\ w_{2,1}^L & w_{2,2}^L & \cdots & w_{2,n}^L \\ \vdots & \vdots & \ddots & \vdots \\ w_{m,1}^L & w_{m,2}^L & \cdots & w_{m,n}^L \end{bmatrix} \quad (3-5)$$

$$B^L = \begin{bmatrix} b_1^L \\ b_2^L \\ \vdots \\ b_n^L \end{bmatrix} \quad (3-6)$$

$$\Sigma^L = X^L \cdot W^L + B^L \quad (3-7)$$

$$\aleph^L = f(\Sigma^L) \quad (3-8)$$

In a feedforward neural network, the output of each layer is the input of the next layer. Therefore, for layers after the first hidden layer, the neuron outputs of the former layer will be the input and:

$$X^{L+1} = (\aleph^L)' \quad (3-9)$$

3.2.2 Learning Algorithms

For the neural network's output Ψ_i and the desired output D_i , the learning algorithm could be defined as a method for optimizing the weights in order to make $\Psi_i \approx D_i$. A supervised learning process of MLPs occurs by changing the connection weights after each training epoch. This is typically based on the output error (the difference between the output and the desired result).

3.2.3 Gradient Descent

In machine learning, backpropagation (backprop, BP) is a popular algorithm for supervised learning widely used to train feedforward neural networks [164], [211]. The basic concept behind this approach is to use the chain rule repeatedly to calculate the effect of each weight in the network on an arbitrary error function E [212].

$$\frac{\partial E}{\partial w_{m,n}} = \frac{\partial E}{\partial \kappa_n} \frac{\partial \kappa_n}{\partial w_{m,n}} = \frac{\partial E}{\partial \kappa_n} \frac{\partial \kappa_n}{\partial \Sigma_n} \frac{\partial \Sigma_n}{\partial w_{m,n}} \quad (3-10)$$

By knowing the partial derivative for each weight, E could be minimized by using gradient descent [164], [213].

$$(w_{m,n})_{t+1} = (w_{m,n})_t - \eta \left(\frac{\partial E}{\partial w_{m,n}} \right)_t \quad (3-11)$$

Where η is the learning rate, which scales the derivative and is an important factor in the required time for the convergence and needs to be determined reasonably: too large η values may prevent the error from falling below a certain value, and too small ϵ leads to too many iterations to reach to acceptable results [212]. It can be shown that:

$$\frac{\partial E}{\partial w_{m,n}} = -(D_n - \Psi_n) f'(\Sigma_n) x_n \quad (3-12)$$

Combining Eq. (3-12) and Eq.(3-13) lead to a special form of the backpropagation algorithm called the Delta Rule, which is a Gradient Descent (GD) learning algorithm (rule) [214] for updating the weights:

$$(w_{m,n})_{t+1} = (w_{m,n})_t + \eta (D_n - \Psi_n) f'(\Sigma_n) x_n \quad (3-13)$$

For linear activation functions, the derivative is equal to one, and it makes the delta rule similar to the Perceptron's update rule (The delta rule cannot be used directly for the Perceptron since its activation function's (Heaviside step function) derivative does not exist at zero, and is equal to zero elsewhere.) [215], [216]:

$$(w_{m,n})_{t+1} = (w_{m,n})_t + \eta (D_n - \Psi_n) x_n \quad (3-14)$$

3.2.3.1 Extended Kalman Filter

Filters are a type of estimation strategy that is used to accurately extract knowledge of the states in the presence of noisy measurements and modelling uncertainties [217]. Kalman-based filters are the most well-known filters in estimation theory [218] [219] [220]. The Kalman Filter (KF) is applicable for linear systems and yields the optimal estimation solution in the presence of known systems and white noise [218] [221]. The extended Kalman Filter (EKF) is formulated the same as the KF, except that first-order Taylor series expansions (Jacobian matrices) are used to linearize the nonlinearities. The state function f and measurement function h are linearized to approximate the state and measurement error covariance matrices. Equations (3-15) and (3-16) are used to approximate the nonlinear systems [219].

$$F_k = \left. \frac{\partial f(x)}{\partial x} \right|_{x=\hat{x}_{k|k}, u_k} \quad (3-15)$$

$$H_{k+1} = \left. \frac{\partial h(x)}{\partial x} \right|_{x=\hat{x}_{k+1|k}} \quad (3-16)$$

Eq. (3-17) and Eq. (3-18) are used to predict the state estimates and state error covariances, respectively [165]. The state error covariance found in Eq. (3-18) is used to calculate the innovation covariance in Eq. (3-19) and calculate the corresponding EKF gain in Eq. (3-20). The predicted state estimates in Eq. (3-17) are used in conjunction with the EKF gain found in Eq. (3-20) to update the state estimates as per Eq. (3-21). Note that the measurement error is also used in Eq. (3-21). Finally, the state error covariance matrix is updated as per Eq. (3-22).

$$\hat{x}_{k+1|k} = f(\hat{x}_{k|k}, u_k) \quad (3-17)$$

$$P_{k+1|k} = F_k P_{k|k} F_k^T + Q_k \quad (3-18)$$

$$S_{k+1} = H_{k+1} P_{k+1|k} H_{k+1}^T + R_{k+1} \quad (3-19)$$

$$K_{k+1} = P_{k+1|k} H_{k+1}^T S_{k+1}^{-1} \quad (3-20)$$

$$\hat{x}_{k+1|k+1} = \hat{x}_{k+1|k} + K_{k+1} \left(z_{k+1} - h(\hat{x}_{k+1|k}) \right) \quad (3-21)$$

$$P_{k+1|k+1} = (I - K_{k+1} H_{k+1}) P_{k+1|k} (I - K_{k+1} H_{k+1})^T + K_{k+1} R_{k+1} K_{k+1}^T \quad (3-22)$$

Eq. (3-15) through Eq. (3-22) represent the EKF estimation process. The process is iterative, meaning that the values found in Eq. (3-21) and Eq. (3-22) are used again in Eq. (3-17) and Eq. (3-18). Note that other nonlinear KF variants have been developed, such as the unscented Kalman filter (UKF). However, the EKF was found to provide accurate results for this case study [165].

In order to use EKF as the training algorithm of the neural network, it is needed to define the system's dynamic relationships in the form of state-space by defining the weights as system states and the neuron output as the system output as:

$$(w_{m,n})_{t+1} = (w_{m,n})_t + N(0, Q) \quad (3-23)$$

$$\mathfrak{N}_{t+1} = \mathfrak{N}(x_{t+1}, w_{t+1}) + N(0, R) = f(y)|_{y=\Sigma_{t+1}} + N(0, R) \quad (3-24)$$

Where $N(0, Q)$ is the process noise with the covariance of Q and $N(0, R)$ is the measurement noise with the covariance of R . The weights could be updated by knowing the Kalman gain:

$$K_{t+1} = P_t H' (H P_t H' + R)^{-1} \quad (3-25)$$

Where P and H are the covariance matrix and Jacobian vector, respectively, and:

$$P_{t+1} = P_t (I - K_{t+1} H') + Q_t \quad (3-26)$$

Where I is the identity matrix and elements of vector H could be calculated as:

$$(H_n)_{t+1} = f(y) \frac{\partial f(y)}{\partial y} \Big|_{y=\mathcal{E}_{t+1}} \quad (3-27)$$

Therefore, the weights could be updated by the following equation:

$$(w_{m,n})_{t+1} = (w_{m,n})_t + K_{t+1} (D_n - \Psi_n) \quad (3-28)$$

3.2.4 Study Area and Parameters

According to the water master plan of Iran, the great SefidRood (White River) basin is divided into 17 sub-basins. The Taleghan upper basin is located in the center of the Alborz Mountains and the east of the SefidRood basin. Figure 3.3 shows the Taleghan upper basin location. The basin's area is 960 Km², representing 2.5% of this basin [202], [222]. The most important feature of this basin is the high altitude and steep slope. The slope of about half of this basin is greater than 40%, and its general direction is east-west. Its maximum and minimum heights are 4,300 m and 1,390 m above sea level, respectively. The average elevation is 2,665 m [202], [223]. The length of the Taleghan River is about 180 km [202], [224]. Table 3.1 represents the longitude and latitude of the Taleghan basin. The Taleghan earth dam is located at the end with a capacity of 420 CMC and an area of 12 km² [202], [225], [226].

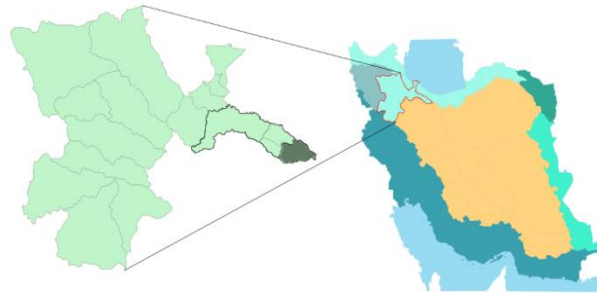


Figure 3.3: Taleghan Upper Basin Location [200]–[202], [223].

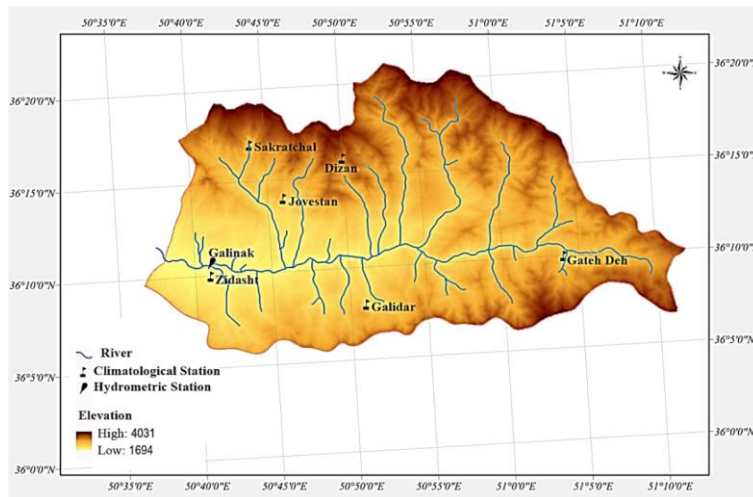


Figure 3.4: The Climatological and Hydrometric Stations in the Upstream Basin of Taleghan [200]–[202], [223].

Over 40 years of hydrometry and climatology records were used for this study. The original records were provided by Iran Water Resources Management Company (WRM) and the Committee of Dam and Basin Management (CDBM), IRCOLD. For each station, the period of available records is represented in Table 3.1. Then the records were analyzed and evaluated to be used for developing a long-term dataset. In this dataset, monthly average data of precipitation and temperature were gathered from six climatology stations: Gatch Deh, Dizan, Galidar, Jovestan, Sakratchal, and Zidasht. Discharge data were collected from a hydrometry station named Galinak. The locations of these stations are shown in Figure 3.4.

The distribution of precipitation differs from 250 to 1,000 mm/year in different locations of this basin. Regarding the precipitation amount and catchment height, the Jovestan, Gateh Deh, and Galidar stations have a high impact on average precipitation and on the basin's runoff [202].

Table 3.1: Specifications of stations in the upstream basin of Taleghan [200]–[202], [223].

Station Name	Station Type	Longitude	Latitude	Elevation (m)	Period
Galidar	Rain gage	50°:51'	36°:08'	2150	1966-2008
Gateh deh	Rain gage	51°:04'	36°:10'	2600	1966-2011
Zidasht	Climatology	51°:18'	31°:45'	2000	1969-2011
Dizan	Rain gage	50°:50'	36°:16'	3200	1967-2011
Sakratchal	Rain gage	50°:44'	36°:17'	2200	1966-2011
Jovestan	Rain gage	50°:41'	36°:10'	1850	1966-2011
Galinak	Hydrometry	50°:40'	36°:10'	1783	1958-2011

According to Figure 3.5, the long-term annual average of precipitation of the Taleghan upper basin in this period is 600 mm. The maximum precipitation occurs in April and May with an average of around 126 mm/year and 119 mm/year, respectively. The minimum precipitation occurs from July to September with an average of below 8 mm/year. The precipitation in winter is more than 45 mm/year in all stations.

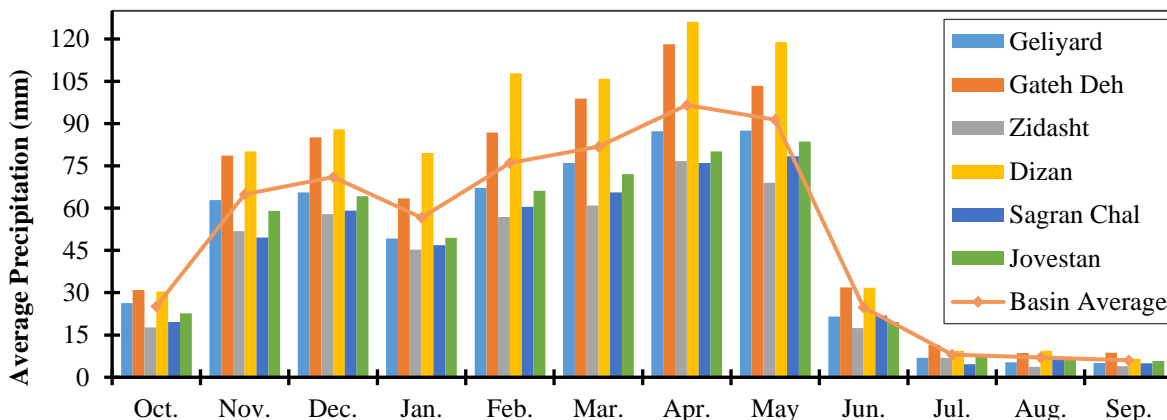


Figure 3.5: The Long-Term Average Precipitation in Each Station and Whole of the Basin [200]–[202], [223].

The average elevation of the basin is 3,722 m. Since the Zidasht station has a similar elevation

(2,000 m), the monthly average data of this station's temperature is considered the basis of calculations. The maximum and minimum temperatures are 37°C in July and 18°C in March. This basin's long-term monthly average temperature is 7.8°C [202]. By using the temperature gradient and height relationship, the long-term average temperature of the basin is calculated and represented in Figure 3.6.

Since the Galinak station is located at the entrance of the Taleghan Dam's reservoir, it could be considered as the outlet of the basin. The data of this point could be considered as the representative of all basin discharges. Therefore, the runoff of this basin can be calculated by subtracting the baseflow from discharge [202]. According to Figure 3.7, the highest runoff occurs from April to June, and from September to February, the runoff is at its lowest. The long-term average runoff of this basin shows that the maximum and minimum runoff of this basin is about 38 m³/s and 2.4 m³/s, which occur in May and September, respectively.

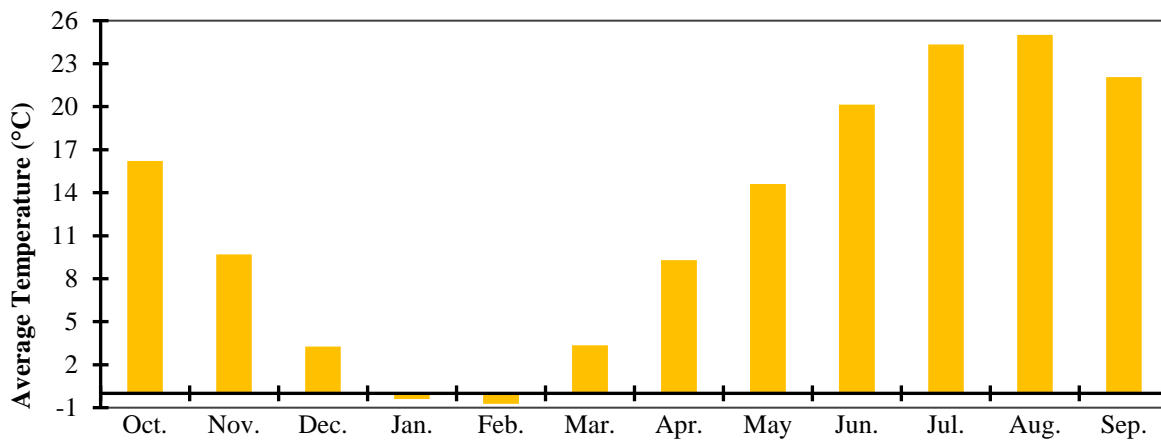


Figure 3.6: Long-term Average Temperature [200]–[202], [223].

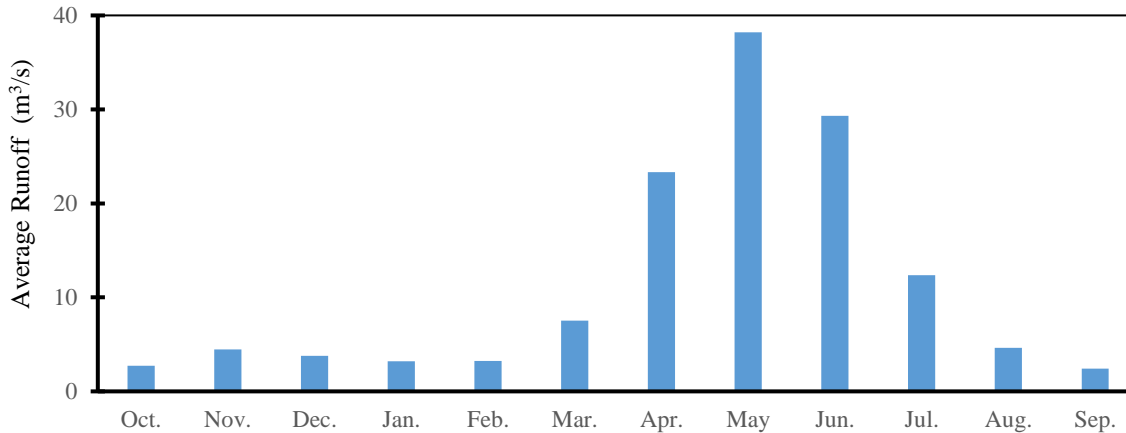


Figure 3.7: Long-term Average Runoff [200]–[202], [223].

3.3 Model Structure

In order to develop an ANN-based runoff estimation model, the temperature and precipitation were considered as inputs and runoff as the output, and the dataset was randomly disturbed. Therefore, the 40 years of monthly observed data were randomized and then divided into three datasets: 60% for training, 20% for cross-validation (C.V.), and 20% for test. These datasets were saved separately to ensure the training, C.V., and test data were the same for all developed models.

A feedforward MLP neural network was used as the base model. Two sub-models were developed: one using EKF for training and one using GD for training. All experiments were completed with a single-layer MLP with 1 to 10 neurons and 1,000 training epochs. For evaluation of the training and model's performance, three evaluation criteria were used: correlation (R), mean absolute error (MAE) and mean square error (MSE).

The weights were updated by either the EKF or GD algorithms during each training process. After each training epoch, cross-validation was completed to check the model performance. New

weights were saved based on an increase of R^2 or decrease in error (MAE). The corresponding epoch number and evaluation criteria values were saved and considered the 'best epoch.' A unique 'minimum epoch of the best' (MEB) was recorded for each evaluation criteria, and the related weights were used for testing. The following three approaches were considered for the training process.

3.3.1 Approach 1: Single Dataset

In this approach, all training was completed with a randomized but single dataset. Therefore, the order of inputs and desired outputs would be the same in the training queue.

3.3.2 Approach 2: Single, Randomized Dataset in Case of No Improvement

In this approach, initial training was completed with a training dataset as per the first approach. After each cross-validation, in case of no improvement in the model results, the next training was completed using a new randomized version of the training dataset. The randomized datasets were the same for all models. Therefore, the results of this approach could be compared with similar models.

3.3.3 Approach 3: Randomized Dataset for Each Training

In this approach, each training process was completed using a new randomized version of the training dataset. To ensure all models were trained in a comparable manner, the number of randomized training datasets was equal to the maximum number of training epochs.

The combination of the three approaches and evaluation using up to ten neurons in the hidden layer resulted in a total of 60 models.

3.4 Results and Analysis

An ideal model has a maximum correlation and minimum error between the predicted and observed data. The higher values of R^2 and lower values of RMSE and MAE were considered to compare and rank the developed models. Also, the number of neurons and computational complexity is considered. The comparison of R^2 , MAE, and RMSE of the best models are represented in Figure 3.8 to Figure 3.10, respectively.

For Approach 1, an EKF-based ANN with eight neurons and an epoch of the best (EB) equal to 1,000 was considered the best model. For Approach 2, the best model was EKF-based with ten neurons and an EB equal to 116. This was 8.62 times (862%) less than the same EB for the GD-based model. Finally, for Approach 3, an EKF-based model with nine neurons and an EB equal to 886 was considered the best model. In addition, this model was considered the best among all of the 60 different developed models used to estimate runoff.

As shown in Figure 3.8, the comparison of the R^2 of the best models demonstrates that for one neuron, GD performs better than the EKF method. However, for one neuron, the value of R^2 is quite low that no model could be considered effective. For models with three neurons or more, the results are nearly the same. However, the EKF demonstrates minor improvements over the GD method. Interestingly, for this case, it appears that using more than three neurons does not yield substantial improvements in model accuracy. In order to lower computational demand, ANNs

could be designed with only three neurons as there appears to be a diminishing return (less than 4% improvement when using ten neurons).

According to Figure 3.9, although the differences are small, the MAE of nearly all EKF-based ANNs were less than GD-based ANNs. According to the MAE evaluation criteria, this case's optimum model could be considered an EKF-based ANN with four neurons.

As shown in Figure 3.10, the RMSE of EKF-based ANNs were less than GD-based ones for 1 to 10 neurons for Approaches 1 and 2. The opposite is true for Approach 3. For more than three neurons, the difference between the highest and lowest RMSE is less than 5%, and the RMSE of all EKF-based ANNs is less than 0.2. Therefore, according to the RMSE evaluation criteria, the optimum model was an EKF-based ANN with three neurons.

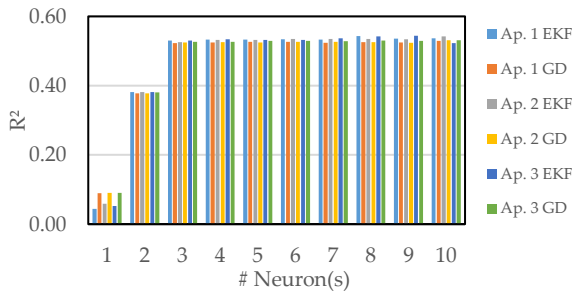


Figure 3.8: R² of the Best Models.

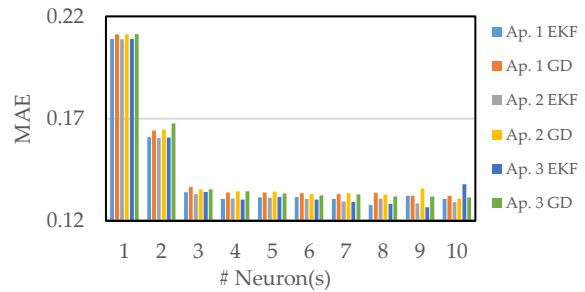


Figure 3.9: MAE of the Best Models.

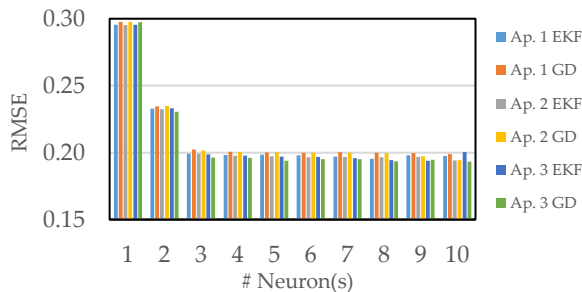


Figure 3.10: RMSE of the Best Models.

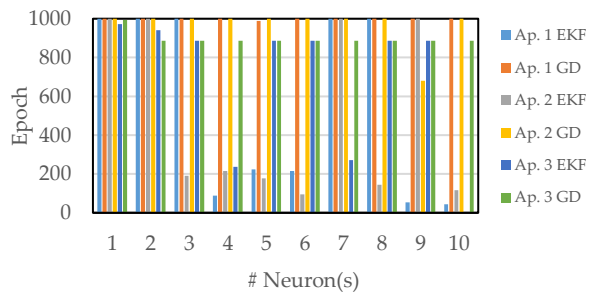


Figure 3.11: EB of the Best Models.

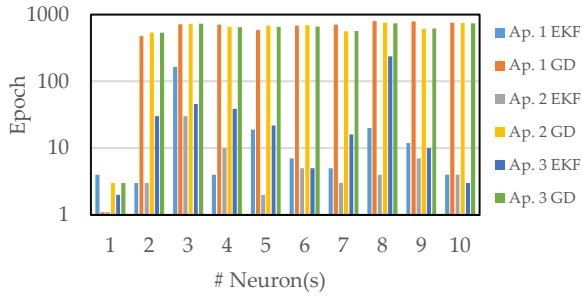


Figure 3.12:MEB Among All Models.

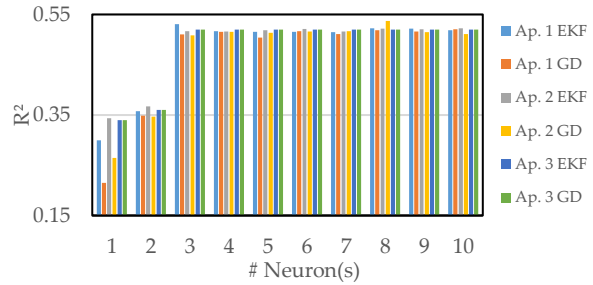


Figure 3.13: R² of the Models with MEB.

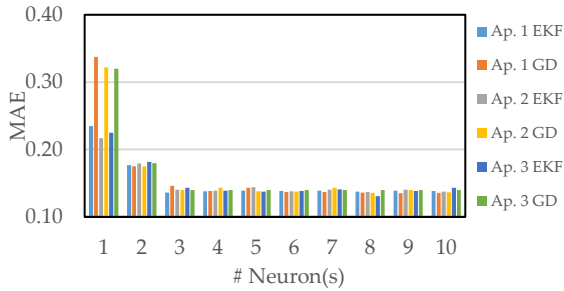


Figure 3.14: MAE of the Models with MEB.

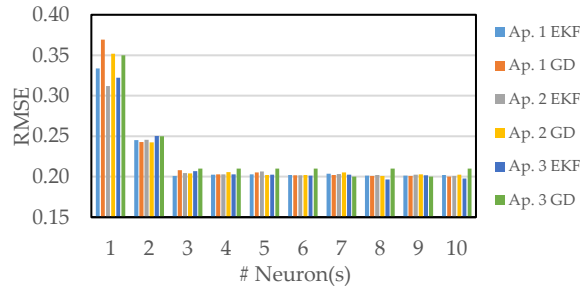


Figure 3.15: RMSE of the Models with MEB.

According to Figure 3.11, for Approach 1, EKF-based ANNs required 4.48 to 22.72 times (448% to 2,272%) fewer training epochs than GD-based ANNs for 4-6, 9, and 10 neurons. For Approach 2, EKF-based ANNs required 4.65 to 10.52 times (465% to 1,052%) fewer training epochs than GD-based ANNs for 3-6, 8, and 10 neurons. For Approach 3, EKF-based ANNs required 3.74 to 177.2 times (374% to 17,720%) fewer training epochs than GD-based ANNs for 4, 7, and 10 neurons. Therefore, Approach 2 was the most effective in reducing the number of training epochs for the EKF-Based ANNs training process.

According to Figure 3.12, the minimum epoch of the best (MEB) for the EKF-based ANN models were so small that a logarithmic graph is needed. The MEB of EKF-based ANNs was smaller than the GD-based ANNs. On average, the MEB of the EKF was 29.37 or 24.44 times (2,444%) fewer than GD for Approach 1. For Approach 2, the MEB of the EKF was 8.12 or 83.45 times (8,345%)

fewer than GD. Finally, for Approach 3, the MEB of the EKF was 47.37 or 12.43 times (1,243%) fewer than GD. Therefore, Approach 2 was considered the best approach for training the EKF-based ANNs in the fewest number of epochs. In addition, these results indicate that the EKF yielded better results in all of the approaches.

According to Figure 3.13, for the R^2 evaluation criteria, the results for one and two neurons are substantially poor and can be dismissed. For three neurons or more, the values are very similar and vary between 0.50 and 0.52. However, on average, the EKF has a better performance than GD by 5.06% and 3.98% in Approaches 1 and 2, respectively. For Approach 3, the results of the EKF and GD were nearly identical. In this case, Approach 1 is considered the best approach for training EKF-based ANNs when considering R^2 as a validation criterion.

The results shown in Figure 3.14 for MAE indicate that the use of 3 or more neurons yields similar errors (less than 0.15 MAE). Although the overall differences between EKF and GD are minimal, on average, the EKF method works better by 3.14% in Approach 1, 2.84% in Approach 2, and 3.53% in Approach 3. According to the MAE evaluation criteria, the performance of EKF-based Approach 3 may be a slightly better choice to train ANNs.

Furthermore, the results presented in Figure 3.15 show the RMSE for both methods to be about 0.20 for more than three neurons. The differences between the EKF and GD methods are nearly insignificant for Approaches 1 and 2, at about 1% better for EKF. In Approach 3, the EKF works slightly better than the GD method by about 3.1%.

As shown in Figure 3.13 to Figure 3.15, the results of ANNs with three or more neurons are so similar that the RMSE, MAE, and R^2 differences are nearly negligible. In this case, an EKF-based

ANN with 3 or 4 neurons is considered as the MEB optimum model. Table 3.3: summarizes the evaluation criteria for the best, optimum, and MEB optimum models. These results indicate that the EKF-based ANN model required a considerably smaller neural network size and fewer training epochs, with a reduction of performance by 2% to 4%.

Table 3.2: The Minimum Epoch of the Best Among All Models.

#Neurons	Approach 1		Approach 2		Approach 3	
	GD - EKF	GD/EKF (%)	GD - EKF	GD/EKF (%)	GD - EKF	GD/EKF (%)
1	3	25	2	300	1	150
2	474	15,900	533	17,867	505	1,783
3	551	436	695	2,417	683	1,585
4	707	17,775	641	6,510	609	1,662
5	569	3,095	681	34,150	632	2,973
6	674	9,729	683	13,760	658	13,260
7	706	14,220	556	18,633	553	3,556
8	778	3,990	749	18,825	498	309
9	776	6,567	607	8,771	607	6,170
10	749	18,825	747	18,775	733	24,533

Table 3.3: The Best, Optimum and MEB Optimum Models Specifications.

Model	Approach	Training Algorithm	#Neurons	EB	R ²	MAE	RMSE
Best	3	EKF	9	886	0.544	0.127	0.194
Optimum	3	EKF	4	237	0.534	0.130	0.198
MEB Optimum	1	EKF	4	4	0.516	0.138	0.203

According to Table 3.3, the best, optimum, and MEB optimum ANN-based models are using the EKF training algorithm. The validation criteria indicate a slight difference between the accuracy of all models in this list. The accuracy of the best and optimum models is very close. However, comparing the required training epochs to achieve such an accuracy (epoch of the best, EB) indicates that a reasonable accuracy was achieved in the optimum model using 3.74 times (373.78%) fewer training epochs. Moreover, the optimum model could achieve such accuracy using 2.25 times (225%) fewer neurons, which makes this network smaller than the best model.

Based on these results, the optimum model offers the most reasonable balance between the training epochs, network size and accuracy.

3.5 Conclusions

This study provides an easy to understand and implement method to develop ANN-based estimation models using MLP and EKF or GD as the training algorithm. To study these models and the three approaches for feeding training data in optimizing the developed feedforward neural networks in reducing the training epochs and size of the network, a runoff estimation problem was considered, which is an important and challenging issue in water resources management and engineering. Two groups of one-layered feedforward ANNs were developed with 1 to 10 neurons, and three approaches for handling the training data were applied, which resulted in 60 models. Model estimations were evaluated by R^2 , RMSE and MAE. For this study, results indicate that the GD method required 11 to 67 percent more neurons than the EKF for a relatively similar performance. In terms of training time, the ANNs applied EKF as the training algorithm required 300 to 34,200 percent fewer training epochs than GD. Based on the results, in comparison to GD, using EKF as a learning algorithm improved estimation models by reducing the number of training epochs and size of ANNs. Further studies are recommended.

3.6 Nomenclature

B	:	Bias
B^L	:	Biases matrix of the layer L
D_n	:	Desired outputs (observations/measurements)
E	:	Error function
EB	:	The epoch of the best

<i>EKF</i>	: Extended Kalman filter
<i>f, F</i>	: Nonlinear, linear state function/ matrix
<i>GD</i>	: Gradient Descent
<i>h, H</i>	: Nonlinear, linear measurement function/matrix
<i>K</i>	: Kalman gain matrix (i.e., EKF)
<i>k+1 k</i>	: A priori time step (i.e., before applied gain)
<i>k+1 k+1</i>	: A posteriori time step (i.e., after update)
<i>L</i>	: Layer number
<i>m</i>	: The number of the neuron connected to the current neuron (<i>n</i>)
<i>MEB</i>	: The minimum epoch of the best
<i>MSE</i>	: Mean square error
<i>n</i>	: Number of Samples/Neuron
<i>N(0, Q)</i>	: The noise of the process with the covariance of <i>Q</i>
<i>N(0, R)</i>	: The noise of the measurement with the covariance of <i>R</i>
<i>O_i</i>	: observed data
\bar{O}	: average of observational data
<i>P</i>	: State error covariance matrix
<i>P_i</i>	: Estimated value
\bar{P}	: Average of estimated data
<i>Q</i>	: System noise covariance matrix
<i>R</i>	: Measurement noise covariance matrix
<i>RMSE</i>	: Root mean square error
<i>S</i>	: Innovation covariance matrix
<i>T</i>	: Transpose of vector or matrix
<i>U</i>	: Input to the system
<i>w</i>	: Weight
<i>W^L</i>	: weight's matrix of the layer L
<i>x</i>	: State vector
<i>X⁰</i>	: Inputs' matrix
<i>X^L</i>	: Inputs' matrix of the layer L
<i>x_m</i>	: Neuron's inputs
<i>Z</i>	: Measurement (system output) vector
Γ	: Hard-limit (unit step) function
Σ	: Neuron's sum function output
Σ^L	: Sigma function matrix of the layer L
Ψ_n	: Model's outputs (estimations/predictions)
\aleph	: Neuron's ultimate output $f(\Sigma)$
\aleph^L	: Neuron output
$\hat{}$: Estimated vector or values

4 Sluice Gates Design and Calibration: Simplified models to Distinguish Flow Conditions, Estimate Discharge Coefficient and Flow Rate

Adapted from:

A. Yoosefdoost, W. D. Lubitz, and W. D. Lubitz, “Sluice Gate Design and Calibration: Simplified Models to Distinguish Flow Conditions and Estimate Discharge Coefficient and Flow Rate,” *Water (Switzerland)*, vol. 14, no. 8, p. 1215, 2022, doi: 10.3390/w14081215.

Thesis Author’s Contribution:

This is an original research article that was written by Arash YoosefDoost [5]. The figures are all original, or from explicitly referenced sources.

4.1 Introduction

Sluice gates are essential hydraulic structures in measuring and regulating flow in Archimedes screw hydropower plants. At most ASG installations, water is supplied by an inlet channel that is controlled using sluice gates.

Sluice is a Dutch word for a channel controlled at its head by a movable gate which is called a sluice gate. A sluice gate can be considered as a bottom opening in a wall [227] or an undershot gate that passes the flow through the bottom, similar to an orifice [228] or a sort of nozzle. The simplicity of sluice gate design, construction, and operation, plus good safety and low maintenance costs [228], result in them being among the most common hydraulic structures to control or measure flow [229].

The volumetric flow rate passing through a sluice gate can be estimated if the opening of the sluice gate (Y_G) and water depths upstream (Y_U) and downstream (Y_D) [228], [229] are known. Low head loss and no need for new equipment make sluice gates preferable for measuring the flow rate where a device is installed [229]. However, the accuracy of flow rates calculated based on sluice gate flows is typically less than weirs, and a complex calibration is needed to account for cases of free or submerged hydraulic jumps downstream of the gate [228]–[231]. The flow under sluice gates can be categorized as a free hydraulic jump (F), partially submerged hydraulic jump (PS), or submerged hydraulic jump (S) [232], [233].

Figure 1 shows a sluice gate when a free hydraulic jump occurs. Here, Y_U is the upstream depth, Y_G is the opening of the gate, Y_m is the minimum depth of flow after the sluice gate, Y_{J1} and Y_{J2} are the initial and secondary depths of the hydraulic jump, respectively, and Y_D is the downstream depth.

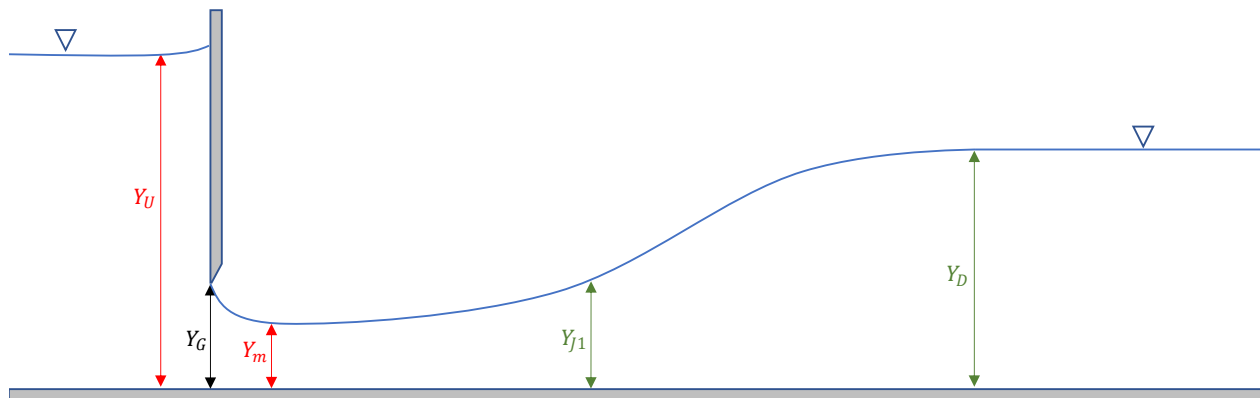


Figure 4.1:Free Hydraulic Jump

Many studies focused on characterizing the free (classic) hydraulic jump [234]–[238]. The flow after the sluice gate behaves like a stream coming out of an orifice (nozzle) [227]. White (2011) proposed that a free discharge is expected for $Y_U/Y_G > 2$ (or $Y_U > 2 Y_G$) [227]. However, the

literature indicates studies that relate the upstream flow depth to the maximum tailwater (downstream) depth to define flow regime distinguishing condition curves [239]. To estimate the volume of flow, many studies focused on determining the coefficient of discharge (C_d). An early, significant study is Henry's 1950 experiment to estimate the C_d for free and submerged flows [240]. Henry developed a relationship between the C_d and Y_U/Y_G by neglecting energy losses and assuming a uniform velocity and a hydrostatic pressure distribution both upstream and at the vena contracta, providing a practical, widely used graph of this relationship represented in Figure 2 [240]. Swamee (1992) indicated that for free flow C_d gradually increases until it reaches the saturation value of 0.611 [241].

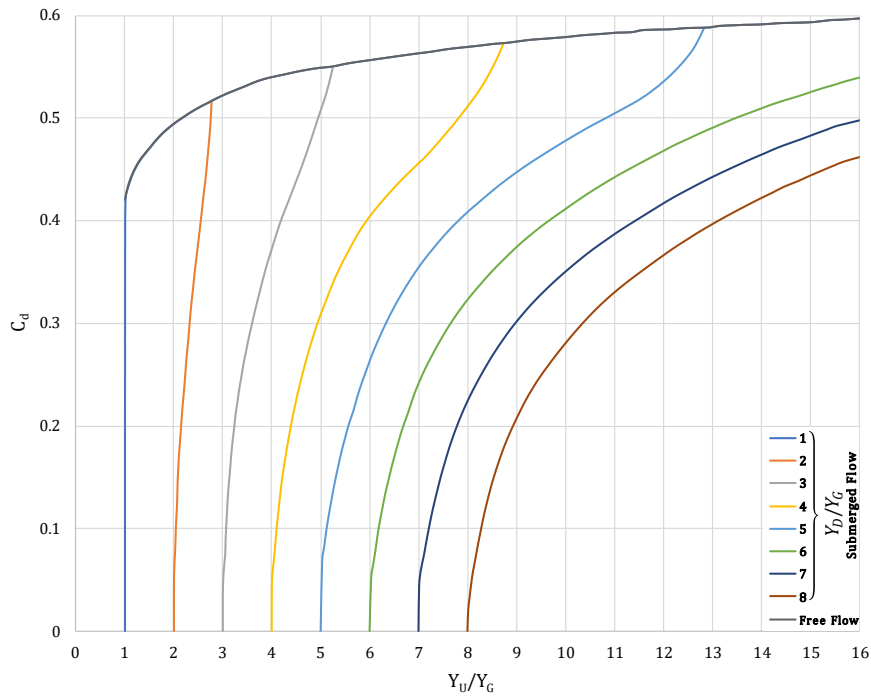


Figure 4.2: Henry's 1950 nomograph for the range of C_d for free and submerged flow regimes in sluice gates [241].

In 1967, Rajaratnam and Subramanya used the energy-momentum (EM) method to prove Henry's

(1950) results [236]. In 1992, Swamee developed several relationships for free and submerged flows based on Henry's (1950) graph [241] to help prevent interpretation errors when interpolating discharge coefficient curves and to provide an analytical or numerical method for determining the discharge coefficient for sluice gates. Lozano et al., Roth and Hager (in 1999) experimentally studied the effects of viscosity and surface tension on scaling sluice gate operations in free-flow conditions. Their research included studies on the contraction coefficient as well as other parameters such as the distribution of velocity and pressure on the gate and the channel bottom [242].

Lozano et al. (2009) performed field studies on four rectangular sluice gates by measuring the water depth and gate opening values [243]. They reported that the EM model resulted in reasonable discharge estimations for three of the studied gates by calibrating the contraction coefficient. For the case where the EM method estimations were not accurate, the sluice gate had a unique nonsymmetric flow condition and was located at the channel's head [243].

Habibzadeh et al., 2011, applied a theoretical method based on the EM method to find an equation for the discharge coefficient of sluice gates in rectangular channels based on orifice-flow conditions, applicable in both free and submerged flow conditions [244]. In most sluice gate models, the energy losses are assumed negligible; however, Habibzadeh et al. reported that turbulence-related phenomena cause significant energy losses in the submerged-flow condition. Additionally, the recirculating region below the gate induces turbulence that results in energy loss in the upstream pool. They considered the magnitude of an additional energy-loss factor as a function of the sluice gate geometry and proposed that it could affect the discharge coefficient [244].

Some studies divided submerged flow regime into two subcategories: 1. low and 2. high submerged regimes [239]. In 2011, Habibzadeh et al. proposed an equation to calculate a parameter called “transitional value of tailwater depth” based on several factors, including the contraction coefficient, upstream flow depth, gate opening, and an energy loss factor which was considered to be 0.062 [244]. The free-flow regime is expected for downstream water depths less than this value, while a submerged flow regime is expected for higher downstream depths. They also proposed a measure to distinguish the submergence ratio of the flow as a function of the maximum downstream depth for free flow. According to this measure, the flow is considered low submerged for submergence ratios between 0 and 20 and considered high submerged for values higher than this range [239], [244]. Castro-Orgaz et al., in 2010, proposed that for high submergence situations, the common EM method is not accurate. They proposed a new equation for submerged flow based on the energy-momentum method principles by applying correction factors on velocity and momentum [245]. However, in 2012, Bijankhan et al. showed that this method has significant errors when the submergence is not significant [239]. The analysis of the EM method indicates that the roller momentum flux and the energy loss could be significant. Therefore, in 2013, Castro-Orgaz et al. published a revised version of their 2010 research for estimating sluice gate discharge in submerged conditions. The new method introduces rationality in the EM equations for submerged gate flow. However, the results of this method were similar to the former one [246].

Gumus et al. (2016) studied the velocity field and surface profile of the submerged hydraulic jump of a vertical sluice gate using 2D CFD modelling. The results of this numerical study were compared with experimental data, and they concluded that the accuracy of the Reynolds Stress

Model (RSM) is more than other studied turbulence models in predicting horizontal velocities and computing the free-surface profile of the hydraulic jump characteristics [247].

Rady (2016) applied developed multilayer perceptron (MLP) artificial neural networks (ANNs) to predict C_d of vertical and inclined sluice gates. This study applies the MLP using the steepest descent back-propagation training algorithm and one hidden layer. For free flow, ANNs used Y_U/G , the sluice gate's inclination angle, Froude number and Reynolds number. For submerged flow, Y_D/G was used in addition to the former inputs. Rady reported that using this method led to reasonable accuracy [248].

Silva and Rijo (2017) studied several methods to determine C_d including EM-bases models, orifice flow rate relationships, and dimensional analysis using Buckingham's Π -theorem. They concluded that the EM-based method led to better results for all free, submerged, and partially submerged flows. Additionally, they reported that there were no improvements in discharge estimation results of the methods that divide the partially and fully submerged flows for the studied sluice gate openings [229].

Kubrak et al. (2020) investigated measuring the volumetric flow rate using sluice gates under submerged flow conditions. A laboratory experiment on a model made on a 1:2 scale of an irrigation sluice gate was conducted to collect the experimental data. This study utilized Swamee's (1992) model as a basis for the determination of C_d . Using this experimental data and empirical methods to adopt corrections, they achieved a reasonable accuracy for estimated discharge coefficients of Swamee's (1992) model for this case study. Based on this and as stated by Boiten

(1992) [249], they concluded that this method is useful in estimating flow through the sluice gate [250].

Nasrabadi et al. (2021) compared the Group Method Data Handling (GMDH) and Developed Group Method of Data Handling (DGMDH) machine learning methods to predict the characteristics of a submerged hydraulic jump of a sluice gate. Their study indicated a reasonable accuracy for both models in estimating relative submergence depth, jump length, and relative energy loss [251].

Based on the literature, the flow under the sluice gate is a classic problem that has been extensively studied experimentally and numerically. Hence, the literature indicates that in recent years the advancements in new measurement methods, such as using a laser Doppler anemometer to measure velocity fields [247], etc., improved the accuracy and domain of experimental measurements on this topic. Beside the classic studies, modern methods such as machine learning techniques, AI, and CFD opened new avenues for investigations on this topic. However, in practice, modern methods are not easy to implement or cost-effective: the new measurement methods are technology-based and require new instruments to be installed, and the application of modern techniques is still highly dependent on the operator's skills and experience.

It is worth mentioning that in practice, some sluice gate models are available in software packages such as SIC and HEC-RAS. The Simulation of Irrigation Canals (SIC) is a one-dimensional hydrodynamic model for river and irrigation canal modelling and regulation [232]. This commercial software has been released by Cemagref since 1989. SIC utilizes empirical relationships [232] based on orifice flow equations [229] to estimate the flow rate under sluice

gates. The Hydrologic Engineering Center's River Analysis System (HEC-RAS) has been released since 1995 and supports 1-D steady flow, 1-D and 2-D unsteady flow calculations [233]. However, these software packages do not estimate C_d . For SIC, some literature suggests considering C_d as 0.6 [252], and the HEC-RAS manual suggests that typically $0.5 \leq C_d \leq 0.7$ [233]. Such a drawback makes the accuracy of results depend on choosing an appropriate value for C_d and the experience of the operators and makes this software not desirable for the design of sluice gates.

In practice, for existing sluice gates, calibration and determination of the optimum C_d is performed using field or experimental measurements. However, models and tools used to characterize flow under sluice gates are essential, especially where the experimental data is not available for calibration, such as for design purposes. On top of that, in system optimization, non-iterative and fast analytical calculations for a component are important for maintaining the overall efficiency of optimizing the whole system of many components. Hence, many available models in the literature still require further investigations, require adequate knowledge to apply, and are not simplified enough or represented in a standard method for such purposes. The essence of developing standard and simple analytical methods is even more significant when sluice gates need to be modelled as a component in a complex hydraulic system, especially when there are many scenarios to be studied, managed, or optimized.

As a result, this study focused on analyzing, evaluating, and simplifying models to improve their application in the design of sluice gates. Five models were reviewed, analyzed, represented in a standard and easy to use form, and their performance was evaluated in distinguishing conditions of flow regimes, estimating the C_d and flow rate. For this purpose, a series of lab experiments were

conducted at the University of Guelph to study the flow on different sluice gate openings, flow rates, and upstream and downstream conditions. The effects of physical scale on models were investigated, and recommendations were provided. Moreover, new analytical equations are proposed to improve the accuracy or applicability of some models. The unscalable initial studies' costs are a large burden on small projects [2], [3]. The presented new equations and simplified models could facilitate their applicability in the design of sluice gates and initial studies of small projects such as the irrigation channels or pico- and micro-hydropower plants. In addition, this study contributes to simplifying these models in a standard form to facilitate the application of models, particularly for modelling sluice gates as a component in complex hydraulic systems such as hydropower plants. The contributions of the analytical equations and models proposed in this study facilitate the development of models for such complex hydraulic systems for optimization purposes, development of management or operation plans, etc.

4.2 Methods and Materials

In order to meet the research goals and to facilitate the application of models for the purposes mentioned above, they were modified and represented in a simplified and standard form.

4.2.1 Hydraulic Background

This section provides the necessary hydraulic background and fundamental equations used in this study. Figure 4.1 represents a classic (free) hydraulic jump. For a specific discharge Q , energy is ideally conserved between sections U and m, and momentum is conserved between sections J1 and J2. The parameters Y_U and Y_m are called alternate depths and Y_{J1} and Y_{J2} are called conjugate

depths. Theoretically, these depths can be estimated using specific energy and momentum methods, respectively. The specific energy at cross-section i is defined as [253]:

$$E_i = Y_i + \frac{Q^2}{2gA_i^2} \quad (4-1)$$

where Y_i is the depth of flow, A is the cross-sectional area, and g is the gravitational constant (usually taken as 9.81 m/s²).

In a free hydraulic jump, the jet exiting after the sluice gate rapidly converges until it reaches the “vena contracta,” a point with the minimum cross-sectional area; here, the minimum flow depth Y_m and, as a result, the maximum velocity. This is a region of Rapidly Varied Flow (RVF). For a specific flow rate, if friction can be neglected, the energy between the U and m cross-sections is conserved ($E_U = E_m$) [227], and Y_U and Y_m will be alternative depths, one above the critical depth (Y_U) and the other below it (Y_m). Therefore, for a specific flow rate, Y_U or Y_m could be estimated using Eq.(4-1) by knowing the other. For rectangular channels with the width b and specific discharge $q = Q/b$ this equation can be simplified as:

$$Y_U + \frac{q^2}{2gY_U^2} = Y_m + \frac{q^2}{2gY_m^2} \quad (4-2)$$

In free flow, solving Eq.(4-2) for q enables calculating the volumetric flow rate using Y_U and Y_m :

$$Q = bY_UY_m \sqrt{\frac{2g}{Y_U + Y_m}} \quad (4-3)$$

In sluice gates, the subcritical upstream flow gradually accelerates to critical near the gate opening and goes to supercritical; then, it comes back to subcritical further downstream after a hydraulic

jump is formed [227]. A hydraulic jump is defined as a jump or standing wave that forms when the flow regime rapidly changes from a supercritical to a subcritical state. During this rapid transition, the supercritical upstream flow depth rises quickly to a subcritical depth downstream. The jump may be distinguished by surface rollers, mixing or air entrainment, leading to significant energy dissipation.

For any cross-sectional shape, at cross-section i , the momentum function M_i is defined as [253]:

$$M_i = A_i \bar{Y}_i + \frac{Q^2}{gA_i} \quad (4-4)$$

The momentum function (M_i) is conserved at cross-sections $J1$ and $J2$ ($M_{J1} = M_{J2}$). The pair of depths before (Y_{J1}) and after the hydraulic jump (Y_{J2}) are known as conjugate depths [253]. Theoretically, a hydraulic jump forms where the initial and secondary depths satisfy the condition $M_{J1} = M_{J2}$ [254]. For rectangular channels the centroid of a flow at depth Y is located at $\bar{Y} = Y/2$, and Eq. (4-4) can be simplified to:

$$\frac{Y_{J1}^2}{2} + \frac{q^2}{Y_{J1}g} = \frac{Y_{J2}^2}{2} + \frac{q^2}{Y_{J2}g} \quad (4-5)$$

For a specific flow rate, solving Eq. (4-5) for either Y_{J1} or Y_{J2} results in the following equation that enables finding the conjugate depths by knowing either of them.

$$Y_a = \frac{Y_b}{2} \left(\sqrt{1 + 8 \frac{q^2}{gY_b^3}} - 1 \right) = \frac{Y_b}{2} \left(\sqrt{1 + 8Fr_b^2} - 1 \right) \quad (4-6)$$

where a and b are $J1$ and $J2$, or vice versa. In practice, the type of hydraulic jump in sluice gates is conditioned by the depth of flow downstream, which depends on the channel slope and

roughness as well as obstacles [255].

The flow under sluice gates can be described analytically using energy-momentum concepts. Theoretically, the presence of a sluice gate leads to a hydraulic jump if its opening (Y_G) is less than the critical depth of the flow passing under the gate (Y_{Cr}). The critical depth occurs where the Froude number ($Fr = V/\sqrt{gD}$, where $D = A/T$) is equal to 1. Solving $Fr = 1$ for any cross-section area A and wetted perimeter T leads to the following equation. Therefore, the flow depth is critical if it satisfies the following equation:

$$\frac{Q^2}{g} = \frac{A^3}{T} \quad (4-7)$$

For rectangular channels, critical flow depth can be calculated by a simplified form of this equation:

$$Y_{Cr} = \sqrt[3]{q^2/g} \quad (4-8)$$

4.2.2 Sluice Gate Models

4.2.2.1 Energy-Momentum Model

Eq.(4-3) enables calculating the volumetric flow rate Q using Y_U and Y_m . This equation can be written as:

$$Q = C_d b Y_G \sqrt{2g Y_U} \quad (4-9)$$

where b is the channel width, g is the gravitational acceleration (9.807 m/s^2), C_d is the sluice gate's coefficient of discharge, and for free flow:

$$C_d = \frac{C_c}{\sqrt{1 + \Delta}} \quad (4-10)$$

where C_c is the contraction coefficient, which is the ratio of the jet width to the orifice opening width [256] or the ratio of the cross-sectional area of the jet at its contraction point (vena contracta) to the opening area [257]. Therefore, in rectangular channels:

$$C_c = Y_m/Y_G \quad (4-11)$$

In this study, Δ is defined as the ratio of the alternate depths ($\Delta = Y_m/Y_U$) and using Equation (3), it could be represented as follows:

$$\Delta = C_c Y_G/Y_U \quad (4-12)$$

A free hydraulic jump (Figure 4.1) could be expected after the sluice gate if the downstream's conjugate depth is equal to or more than the sluice gate's upstream supercritical alternate depth (i.e., $Y_m \leq Y_{J1}$). In a free hydraulic jump, the jet after the sluice gate rapidly converges to Y_m at the contraction point (the vena contracta), which is the minimum possible flow depth. For $Y_m < Y_{J1}$, the flow velocity decreases due to frictional resistance in a Gradually Varied Flow (GVF) regime, leading to a gradual increase in flow depth until it reaches the depth where the hydraulic jump initiates, which is the conjugated depth of downstream depth [254]. For the case where $Y_m = Y_{J1}$, the hydraulic jump forms at cross-section m . Considering the fact that the vena contracta is the minimum possible flow depth, applying Eq. (4-6) to calculate the conjugate depth of $Y_m = Y_{J1}$, and by substituting Y_m from Eq. (4-11) and q from Eq. (4-3) the maximum downstream depth for which free flow could be expected (Y_{DMF}) can be calculated as follows:

$$Y_{D_{MF}} = 0.5Y_U\Delta \left(\sqrt{1 + \frac{16}{\Delta(1 + \Delta)}} - 1 \right) \quad (4-13)$$

Eq. (4-13) could be considered as the distinguishing condition for free and submerged flows [258].

Physically, $Y_m > Y_{J1}$ is not possible, and in practice, a submerged hydraulic jump (SHJ) occurs in such a situation. In such a situation, the jump would ordinarily be pushed further upstream, but the sluice gate prevents this, so the upstream conjugate depth cannot be reached, and a submerged (drowned) hydraulic jump forms [254] (Figure 4.3).

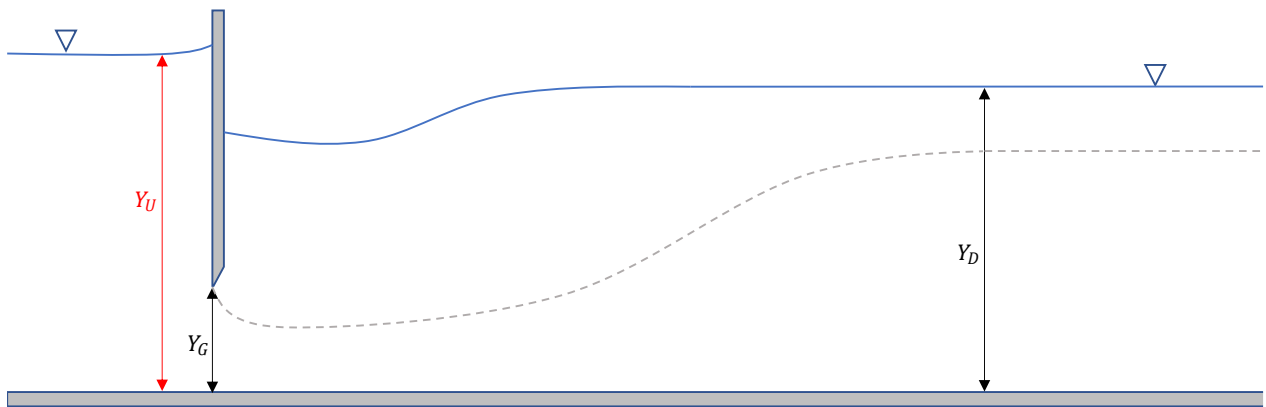


Figure 4.3: Submerged (drowned) hydraulic jump.

For submerged flow, the energy and momentum equations can be re-written by defining the piezometric head Y_P as [229], [244]:

$$Y_U + \frac{q^2}{2gY_U^2} = Y_P + \frac{q^2}{2gY_m^2} \quad (4-14)$$

$$\frac{Y_P^2}{2} + \frac{q^2}{Y_{J1}g} = \frac{Y_{J2}^2}{2} + \frac{q^2}{Y_{J2}g} \quad (4-15)$$

Then, C_d can be found by solving Eq. (4-14) and Eq. (4-15) interactively [259] and eliminating Y_p [258]. Therefore, it can be shown that for submerged flow [258]:

$$C_d = C_c \frac{\Delta}{1 - \Delta^2} \sqrt{\sigma - \sqrt{\sigma^2 - \left(\frac{1}{\Delta^2} - 1\right)^2 \left(1 - \frac{1}{\delta^2}\right)}} \quad (4-16)$$

where

$$\delta = Y_U/Y_D \quad (4-17)$$

$$\sigma = \left(\frac{1}{\Delta} - 1\right)^2 + 2(\delta - 1) \quad (4-18)$$

4.2.2.2 Energy-Momentum Model with Loss

The classic Energy–Momentum (EM) method considers the losses between the upstream and vena contracta negligible. Habibzadeh et al. (2011) proposed that the energy losses between these sections should be considered by adding the loss term $kV_m^2/2g$ to Eq. (4-2):

$$Y_U + \frac{q^2}{2gY_U^2} = Y + K \frac{q^2}{2gY_m^2} \quad (4-19)$$

where k is the energy loss factor, V_m is the average velocity in the vena contracta, and:

$$K = k + 1 \quad (4-20)$$

Based on the experimental data of Rajaratnam and Subramanya (1967) [260], Habibzadeh et al. (2011) determined the value of k as:

$$k = \begin{cases} 0.062, & \text{Free flow} \\ 0.088, & \text{Submerged flow} \end{cases} \quad (4-21)$$

For free flow $Y = Y_m$. Therefore, C_d could be calculated by substituting Eq. (4-9) in Eq. (4-19) to get:

$$C_d = C_c \sqrt{\frac{1 - \Delta}{K - \Delta^2}} \quad (4-22)$$

For submerged flow $Y = Y_p$ and C_d could be obtained by simultaneously solving Eq.(4-15) and Eq.(4-19). Habibzadeh et al. (2011) reported the physically possible root of the resulting equation [244]. In the current study, we offer a simpler equation with an emphasis on its considerable similarity to Eq.(4-16), which is the result of the EM-based analytical nature of this method:

$$C_d = C_c \frac{\Delta}{K - \Delta^2} \sqrt{\lambda - \sqrt{\lambda^2 - \left(\frac{K}{\Delta^2} - 1\right)^2 \left(1 - \frac{1}{\delta^2}\right)}} \quad (4-23)$$

where:

$$\lambda = \sigma + k/\Delta^2 \quad (4-24)$$

Similar to the EM method, substituting Eq. (4-20) in Eq. (4-9), then in Eq. (4-6), leads to finding the maximum tailwater depth for which a free flow could be expected after the sluice gate (Y_{DMF}) that could be used to distinguish free and submerged flow:

$$Y_{DMF} = \frac{\Delta}{2Y_U} \left(\sqrt{1 + \frac{16(1 - \Delta)}{\Delta(K - \Delta^2)}} - 1 \right) \quad (4-25)$$

Finally, Eq. (4-9) is applied to calculate the volumetric flow rate predicted by the EM with the loss model.

In this study, this model, which is proposed by Habibzadeh et al. (2011), is referred to as EML.

4.2.2.3 Henry's Model

Henry (1950) proposed the well-known nomograph based on experimental data to estimate C_d for different flow regimes. Additionally, based on the EM model, Henry proposed that for free flow:

$$C_d = \alpha C_c \sqrt{1 - \beta} \quad (4-26)$$

where Henry assumed $C_c = 0.6$ and [229], [240]:

$$\alpha = \frac{1}{\sqrt{1 - \Delta^2}} \quad (4-27)$$

$$\beta = \begin{cases} \Delta, & \text{Free flow} \\ Y_P/Y_U, & \text{Submerged flow} \end{cases} \quad (4-28)$$

$$Y_P = C_c Y_G \frac{\alpha^2 + \sqrt{\alpha^4 + 4\eta(\eta(Y_D/Y_G)^2 - \alpha^2(Y_U/Y_G))}}{2\eta} \quad (4-29)$$

$$\eta = (4C_c(1 - C_c Y_G/Y_D))^{-1} \quad (4-30)$$

Henry's (1950) model applies Eq.(4-9) to calculate the volumetric flow rate.

4.2.2.4 Swamee's Model

Swamee (1992) applied a nonlinear regression to Henry's (1950) nomograph and proposed the

following range for free flow [241]:

$$Y_U \geq 0.81Y_D \left(\frac{Y_D}{Y_G} \right)^{0.72} \quad (4-31)$$

Therefore, the following equation was proposed as the distinguishing condition for free and submerged flows in Swamee's model based on the maximum downstream depth at which free flow could be expected (Y_{DMF}):

$$Y_{DMF} \leq \sqrt[1.72]{\frac{Y_U Y_G^{0.72}}{0.81}} \quad (4-32)$$

Swamee (1992) considered $C_c = 0.611$ and defined C_d as [241]:

$$C_d = \theta C_c \left(\frac{Y_U - Y_G}{Y_U + 15Y_G} \right)^{0.072} \quad (4-33)$$

where $\theta = 1$ for free flow, and for submerged flow:

$$\theta = \frac{(Y_U - Y_D)^{0.7}}{0.32(0.81Y_D(Y_D/Y_G)^{0.72} - Y_U)^{0.7} + (Y_U - Y_G)^{0.7}} \quad (4-34)$$

To calculate the volumetric flow rate, the Swamee (1992) model applies Eq. (4-9).

4.2.2.5 HEC-RAS Model

The U.S. Army Corps of Engineers' River Analysis System (HEC-RAS) software is developed for open channel flow computation under steady and unsteady conditions [233]. HEC-RAS does not provide a method to calculate C_d for sluice gates and this coefficient needs to be supplied by the user. The HEC-RAS manual suggests that typically $0.5 \leq C_d \leq 0.7$ [233]. In HEC-RAS, the flow

regimes of the sluice gates are categorized based on the ratio of Y_D/Y_U . These ranges are represented in Table 4.1.

Table 4.1: HEC-RAS distinguishing range for sluice gate flow regimes [233]

Flow Regime	Free Flow	Partially submerged flow	Submerged flow
Condition	$Y_D/Y_U \leq 0.67$	$0.67 < Y_D/Y_U < 0.80$	$Y_D/Y_U \geq 0.80$

Therefore, the following equation could be proposed as the distinguishing condition based on the maximum downstream depth at which free flow could be expected ($Y_{D_{MF}}$) based on the HEC-RAS model's definition:

$$Y_{D_{MF}} \leq 0.67 Y_U \quad (4-35)$$

Similarly, the following equation could be proposed as the distinguishing condition based on the minimum downstream depth at which a submerged flow could be expected ($Y_{D_{mS}}$) based on the HEC-RAS model's definition:

$$Y_{D_{mS}} \geq 0.8 Y_U \quad (4-36)$$

For other situations ($0.67 Y_U < Y_D < 0.8 Y_U$) partially submerged flow would be expected based on the HEC-RAS model definition.

To calculate the flow rate, HEC-RAS utilizes Eq. (4-9) for free flow, Eq. (4-37) for partially submerged flow and Eq. (4-38) for submerged flow [229], [233]:

$$Q = C_d b Y_G \sqrt{2g3(Y_U - Y_D)} \quad (4-37)$$

$$Q = C_d b Y_G \sqrt{2g(Y_U - Y_D)} \quad (4-38)$$

4.2.3 Laboratory Flume and Experiment

Experiments were conducted in the Water Resources (Flume) lab of the University of Guelph. The steady-state flow through a sluice gate in a laboratory flume was characterized as a function of various upstream and downstream water depths. Figure 4.4 shows a schematic view of this laboratory experiment setup. Water is pumped from the main reservoir to a header tank connected to a sluice gate that controls the flow that enters the flume. This laboratory flume is a rectangular channel 0.15 m wide and 0.3 m deep, with a length of 6.12 m. It is made of plexiglass to enable flow visualization. The flume was carefully levelled to produce a channel with zero slope, and an adjustable sharp-edged sluice gate was installed near a point 1/3 of flume length downstream of the flume inlet. The downstream flow depth was controlled by an adjustable weir installed at the outlet of the flume. Water passing over the end weir returns to the main reservoir by gravity through a vertical pipe. A valve is installed in this return pipe to allow diversion of the return flow to a gauged tank calibrated volumetrically to measure the volumetric flow rate.

The experiments were performed for target flow rates from 0.5×10^{-3} to 3.0×10^{-3} m³/s. For each flow rate, experiments were performed for a set of sluice gate openings from 5 to 100 mm. For each flow rate and sluice gate opening, tests were conducted for the weir elevations from 0 up to 150 mm. Table 4.2 summarizes the ranges of flow rates, sluice gate openings and weir heights tested.

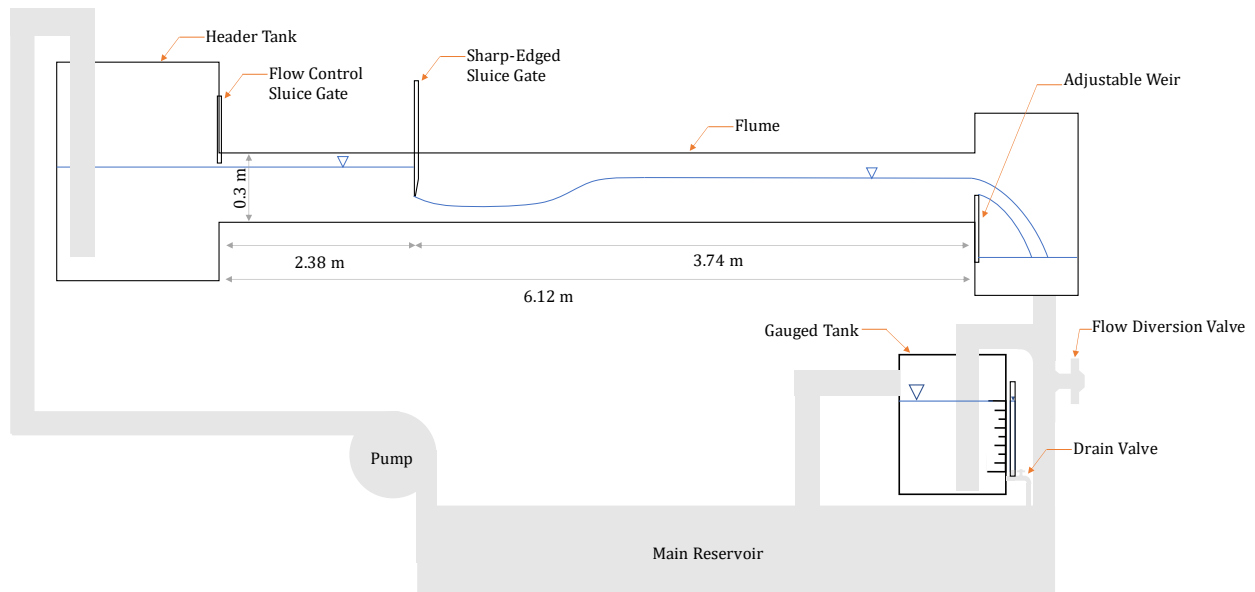


Figure 4.4: Schematic of the lab experiment configuration (not to scale)

Table 4.2: The range of target flow rates, sluice gate openings, and weir heights tested in the experiments

Flow rate ($10^{-3} \text{ m}^3/\text{s}$)	Sluice gate opening (10^{-3} m)	Weir height (10^{-3} m)
0.5	5	0
1.0	10	10
1.5	15	25
2.0	25	50
2.5	50	100
3.0	100	150

These ranges lead to 216 initial combinations of the three variables, which include a wide range of flow conditions based on the flume capacity. To avoid overflow of the flume, a maximum flow depth of 0.2 m in the channel was considered as a limit to halt and exclude a combination during the experiment. Variable combinations that resulted in excessive water depths in the flume were labelled as “overflow” in the records and excluded from testing. Combinations of variables that resulted in the sluice gate having no interactions with the flow (i.e., sluice gate opening is more than flow depth) were measured and recorded in the main dataset to ensure it includes the full

range of the flume capacity, but they were excluded from the final dataset used for testing models and study on flow under sluice gates. All other possible combinations in which the sluice gate affects the flow were studied and measured. To study flow under sluice gates, excluding the combinations that the sluice gate had no effect on flow resulted in a dataset of 54 samples.

Measurements were collected only once the upstream depth became constant to ensure that the system had achieved steady-state flow. The upstream water level was marked periodically to ensure that the upstream depth became constant. Upstream depths were measured at the same distance before the slice gate. The depths measurements were recorded with a precision of 0.01 mm. The average of three measurements was recorded to reduce the measurement uncertainties. Note that due to the scale of the experiment, water surface interactions, particularly in small depths, could be subject to uncertainty in this experiment. For free flow, oscillating jumps and gradually variable jump locations could cause uncertainties in the measurements. Such conditions were reported and tagged in the dataset. For submerged flows, a floater was utilized to determine the location where the recurrent flow of flow surface ended, and the flow direction changed to the downstream after an approximate stagnation point. This point was considered for downstream depth measurement. During the experiments, fluctuations in the volume of flow were observed and noted. The observed fluctuations in the pumped volume of water were more significant in long runs and could be considered as an impossible to control uncertainty of this experiment. For each experiment, the average of at least three volumetric flow rate measurements was recorded. The flows resulting from all the possible variable combinations contains 54 samples of a wide range of sluice gate operating conditions, including free and submerged hydraulic jumps.

4.3 Results

4.3.1 Flow Regimes' Distinguishing Conditions

Figure 4.5 shows the experiment results, with each point representing a measurement. This figure also compares regions of predicted flow regime for each method by providing the distinguishing conditions of each method plotted by dotted lines. For example, all points that fall below the $Y_{D_{MF}}$ curve of the EM model are considered as free flow by this model.

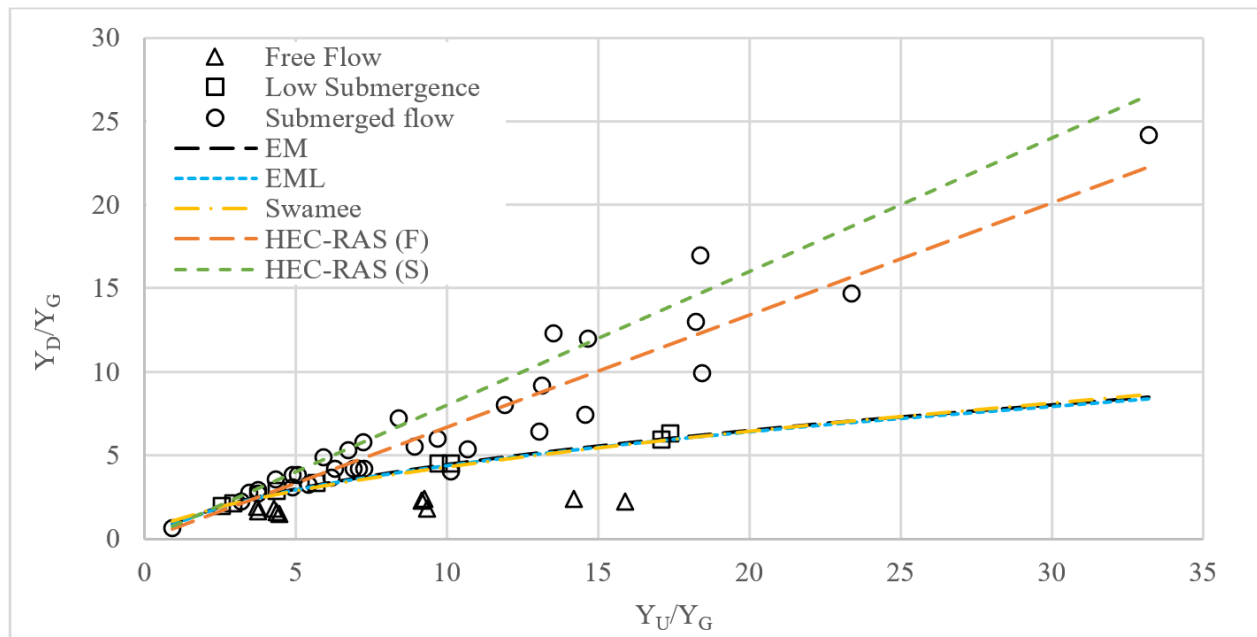


Figure 4.5: Lab experiment results (markers) categorized by observed flow regime, compared with predicted flow regimes by each model (lines).

4.3.2 Discharge Coefficient and Flow Rate

The coefficients of discharge (C_d) and volumetric flow rates for the EM, EML, Henry, and Swamee models were estimated using the equations provided in section 4.2.2. In order to examine scaling

effects on the energy loss factor k , this study applied the loss factor values in Eq.(4-21) reported by Habibzadeh et al. (2011) for the EML. The estimated volumetric flow rate of these models is represented in Figure 4.6. The summary of evaluation models in estimating the flow rate in each sluice gate operation range is represented in Table 4.3.

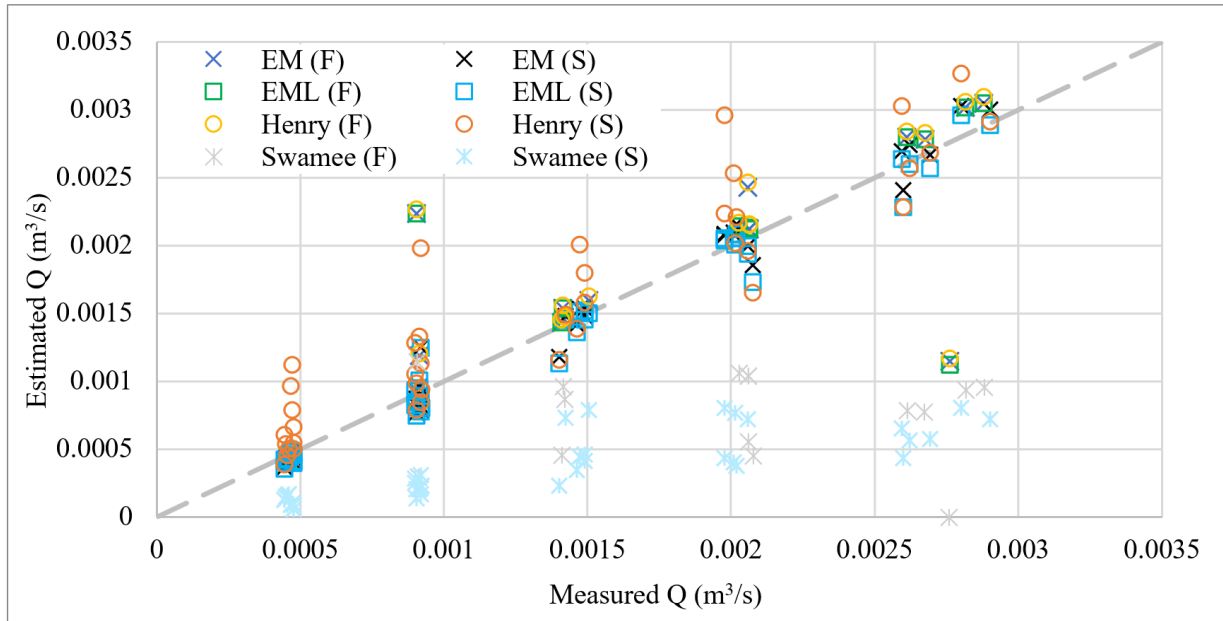


Figure 4.6: The estimated volumetric flow rate of methods for free and submerged flows

Table 4.3: The evaluation criteria for estimated flow rates.

Model	Flow	ME (m ³ /s)	MAE (m ³ /s)	MPE (%)	MAPE (%)
EM	F	1.00×10^{-4}	3.15×10^{-4}	12.59	20.38
	S	7.19×10^{-7}	8.32×10^{-5}	-1.65	7.01
EML	F	6.39×10^{-5}	3.38×10^{-4}	11.30	21.23
	S	-3.39×10^{-5}	8.18×10^{-5}	-3.54	7.25
Henry	F	1.31×10^{-4}	3.44×10^{-4}	14.28	21.99
	S	1.72×10^{-4}	2.48×10^{-4}	20.19	25.20
Swamee	F	-1.15×10^{-3}	1.18×10^{-3}	-53.94	57.70
	S	-9.72×10^{-4}	9.72×10^{-4}	-73.59	73.59

4.4 Discussion

4.4.1 Flow Regimes' Distinguishing Conditions

Based on Figure 4.5, EM, EML and Swamee's model produced almost identical curves to distinguish free and submerged flows. Uniquely, the HEC-RAS model identifies three zones to distinguish free flow, partially submerged flow, and submerged flows.

Comparing the number of cases that a method succeeds in distinguishing a flow regime to the cases that it fails could help measure each method's accuracy in distinguishing the flow regimes. The EM, EML, Swamee, and HEC-RAS models accurately predicted the observed flow regime 83%, 81%, 86%, and 48%, respectively. Note that these results may underestimate the accuracy of models that do not distinguish partially submerged flow conditions, and the cases that could not be clearly categorized as free flow or submerged flow were considered erroneous predictions.

These results also suggest that, at least for this laboratory-scale experiment, the HEC-RAS estimations for distinguishing the flow regime are not accurate. According to Eq. (4-12), Eq.(4-13), Eq. (4-25) and Eq. (4-32), the distinguishing measure of the EM, EML and Swamee's models are represented as a function of Y_U and Y_G . However, the HEC-RAS model distinguishing flow regime is only based on Y_U .

4.4.2 Discharge Coefficient and Flow Rate

Analysis of the experimental results indicates that the contraction coefficient (C_c) in this experiment ranged from 0.576 to 0.623 with an average of 0.591. This range is in good agreement with the 0.58–0.63 range reported by Rajaratnam and Subramanya (1967) [236]. Additionally, this

average is very close to the suggested value of 0.6 by Henry (1950) [240] and 0.61 by Henderson (1966) [259] and Rajaratnam and Subramanya (1967) [236], and the value of 0.611 assumed by Swamee (1992) [241].

The evaluation results of studied models in estimating volumetric flow rate represented in Figure 4.6 and Table 4.3 indicate a reasonable performance for EM, EML, and Henry's models in free flow. For submerged flow, the performance of EM and EML models were reasonable. The performance of Henry's model was significantly lower than EM-based models for submerged flow. Swamee's model performance was not acceptable for free and submerged flows.

According to Figure 4.6, Swamee's model flow rate estimates were significantly lower than other models. The poor results of Swamee's (1992) model with the experimental data in this study were consistent with results reported by Sepulveda et al. (2009), Belaud et al. (2009), and Habibzadeh et al. (2011) [244], [261], [262]. Since EM, EML, Henry, and Swamee models use the same equation to calculate the volumetric flow rate, C_d is the only differing factor in these methods' estimations of volumetric flow rate. Therefore, the volumetric flow rates could be used to evaluate the efficiency of each method in estimating the coefficient of discharge. Results indicate that the Swamee method's estimated coefficients of discharge for this experiment are significantly lower than the other methods. Additionally, in a few cases Swamee's method estimates some imaginary numbers for C_d that are not reasonable. Similar results were reported by Habibzadeh et al. (2011) [244]. Based on these results and considering that the nonlinear regression of Swamee's (1992) model is based on Henry's (1950) nomogram could raise concerns about the generality of this method and the effects of scale on its accuracy.

4.4.3 New Analytical Equations and Methods for Design Purposes

4.4.3.1 Determination of Loss Factor for the EML Model

Studies such as Silva and Rojo's (2017) applied the loss factor values in Eq. (4-21) reported by Habibzadeh et al. (2011) [229], [244] for the EML model. However, calibrating k using this experimental data showed that for this study, the value of k is 0.184 for free flow and 0.0662 for submerged flow. These results indicate the importance of determining the loss factor k for different scales and cases.

For submerged flow, k could be determined by substituting Eq. (4-23) into Eq. (4-9) and applying numerical methods. For free flow, k could be found by substituting Eq. (4-22) into Eq. (4-9) or using Eq. (4-19), which results in the following equation for the determination of k :

$$k = \Delta^2 \left(1 + 2 \frac{Y_U^3}{Y_{Cr}^3} (1 - \Delta) \right) - 1 \quad (4-39)$$

4.4.3.2 Determination of C_d for the HEC-RAS Model

The HEC-RAS model only offers a recommended range for C_d and does not offer any analytical methods to calculate C_d . When experimental data is available, C_d could be estimated by calibrating the model using the experimental data. However, for design purposes, the application and accuracy of this model, and the HEC-RAS software for sluice gates, will be highly dependent on the operator's experience and choice. This study offers and evaluates the application of an analytical model based on the EM method to estimate the C_d dynamically for HEC-RAS since it applies the same flow rate equation to the EM method for free flow and relatively similar equations for other

conditions.

In this study, three methods were proposed and evaluated and compared for the estimation of C_d for the HEC-RAS model: 1. Calibration, 2. Dynamic method, and 3. Adjusted dynamic method. For the calibration (first) method, there is one C_d for each flow regime range which is calculated using the experimental data. For both dynamic methods, a separate C_d is estimated for each calculation based on the EM equations: Eq. (4-10) for free flow, Eq. (4-16) for submerged flow and the average of free and submerged flow for partially submerged flow.

For the adjusted method, the estimated C_d is adjusted to the closest minimum or maximum value of the HEC-RAS recommended range if the calculated value is outside this range. Table 4.4 represents the calibrated and the average C_d of dynamic and adjusted dynamic models for the flow ranges defined by HEC-RAS. The estimated volumetric flow rate of each method is represented in Figure 4.7. The evaluation criteria of these estimations are represented in Table 4.4.

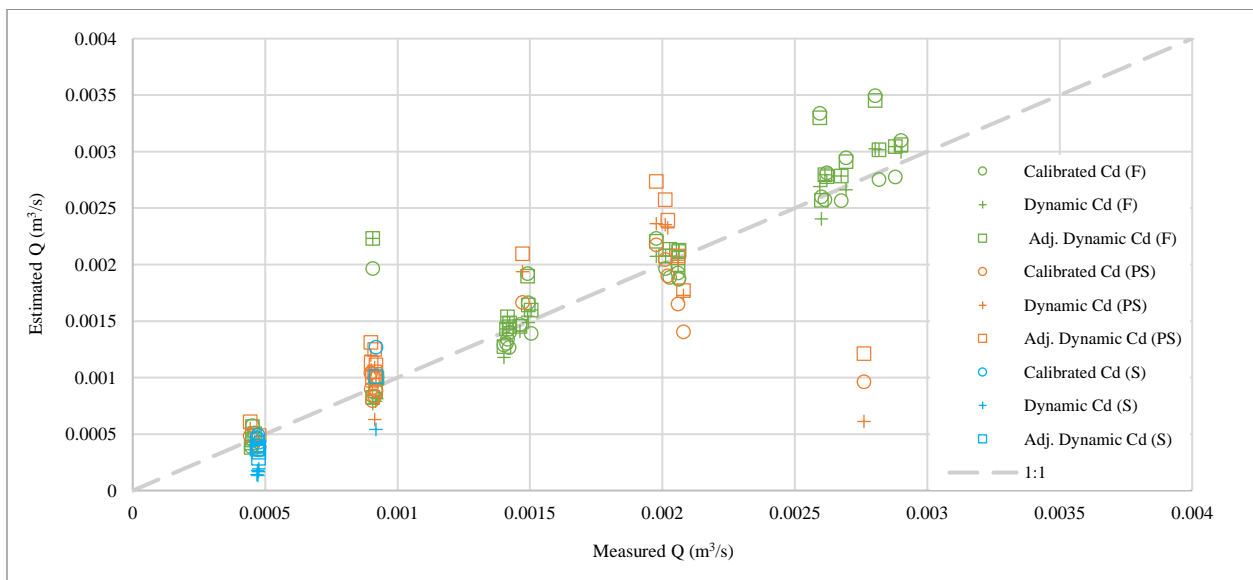


Figure 4.7: The estimated volumetric flow rate of methods to estimate C_d for HEC-RAS

Table 4.4: The estimated C_d for HEC-RAS and the evaluation criteria for estimated flow rates

Flow regime	Free			Partially Submerged			Submerged		
Method	C_d	MPE (%)	MAPE (%)	C_d	MPE (%)	MAPE (%)	C_d	MPE (%)	MAPE (%)
Calibration	0.506	5.6	12.26	0.688	-7.18	15.04	0.363	0.97	13.30
Dynamic	0.499	3.74	10.53	0.435	3.50	21.59	0.241	-61.49	61.49
Dynamic (Adj.)	0.527	9.95	12.44	0.5	16.84	26.30	0.50	-19.69	23.00

4.4.3.3 Analysis of Improvements

The newly proposed equations and methods were applied to calibrate values of k for the EML model. For the HEC-RAS model, C_d is calculated using the dynamic model for free flow, and partially submerged flow and the adjusted dynamic method is used for the submerged flow.

Results from using the calibrated loss factor k are represented in Table 4.5. The comparison of the evaluation criteria results represented in Table 4.3 and Table 4.5 indicates that calibration of loss factor k led to reasonable improvements in the EML model's accuracy for both free and submerged flow regimes.

HEC-RAS applies Eq. (4-9) for estimating the volumetric flow rate, which is the same as the EM-based models. Therefore, Eq. (4-10) seems to be a reasonable analytical method for determining C_d for free flow in HEC-RAS model. These results support this hypothesis since, according to Table 4.4, the dynamic method outperformed other methods with a lower MAPE = 10.53% for free flow. The calibrated C_d led to better performance in estimating the flow rate for partially submerged and submerged flows, resulting in MAPEs of 15.04% and 13.30%, respectively. However, the experimental data are required for calibration. Therefore, for the HEC-RAS model, it may be reasonable to use the dynamic method to estimate C_d for partially submerged flow and

the adjusted dynamic method for submerged flow.

Although HEC-RAS applies a similar equation to estimate flow rate in free flow, results could not be compared with other models since the flow regime distinguishing conditions of HEC-RAS mistakenly considered many submerged flow cases as free flow. It is worth mentioning that for submerged flow, in this experiment, the calibrated $C_d = 0.363$ is significantly lower than the minimum recommended range of C_d suggested by HEC-RAS. Based on these results, the HEC-RAS recommended range for C_d was not practical for this experiment.

Table 4.5 and Figure 4.8 summarize these results and compare them with the results of other studied models.

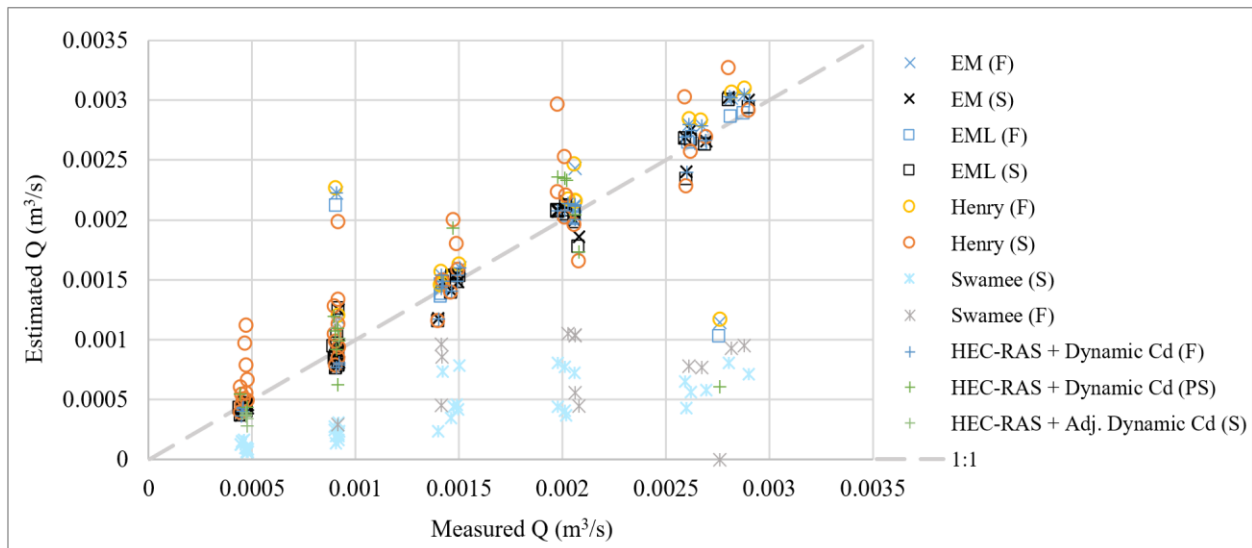


Figure 4.8: The estimated volumetric flow rate of all models compared to corresponding measured flow rates.

Table 4.5: Evaluation of models in estimating the flow rate in the full sluice gate operation range

Model	Flow	ME (m ³ /s)	MAE (m ³ /s)	MPE (%)	MAPE (%)
EM	F	1.00×10 ⁻⁴	3.15×10 ⁻⁴	12.59	20.38
	S	7.19×10 ⁻⁷	8.32×10 ⁻⁵	-1.65	7.01
EML	F	5.45×10 ⁻⁵	2.76×10 ⁻⁴	5.24	18.00
	S	-1.11×10 ⁻⁵	8.13×10 ⁻⁵	-2.00	7.03
Henry	F	1.31×10 ⁻⁴	3.44×10 ⁻⁴	14.28	21.99
	S	1.72×10 ⁻⁴	2.48×10 ⁻⁴	20.19	25.20
Swamee	F	-1.15×10 ⁻³	1.18×10 ⁻³	-53.94	57.70
	S	-9.72×10 ⁻⁴	9.72×10 ⁻⁴	-73.59	73.59
HEC-RAS	F	6.60×10 ⁻⁵	1.3×10 ⁻⁴	3.74	10.53
	PS	-1.54×10 ⁻⁵	1.57×10 ⁻⁴	3.50	21.59
	S	-8.59×10 ⁻⁵	1.16×10 ⁻⁴	19.69	23.00

4.5 Conclusion

Sluice gates are important components in designing, operating, and maintaining water delivery systems and hydropower plants, which are essential elements in the sustainable development of water resources and power generation. This study investigated five models' performances in distinguishing conditions and estimating the coefficient of discharge (C_d) and flow rate in sluice gates for free flow and submerged flows. Experiments in a laboratory flume at the University of Guelph were used to characterize steady-state flow through a sluice gate for different flow rates, gate openings, and upstream and downstream depths. New equations were proposed to make them easier to analyze and compare and facilitate the application of the studied models.

For this experiment, analysis of the EM, EML, and Swamee methods indicated relatively similar curves and performance in distinguishing the sluice gate flow regimes. However, the HEC-RAS model's estimations of the flow regime were not accurate.

Estimating the flow rate results of this experiment indicated a reasonable performance of EM, EML, and Henry's models in free flow. For submerged flow, the performances of EM and EML models were reasonable. The performance of Henry's model was significantly lower than EM-based models for submerged flow. Swamee's models' performance was not acceptable for free and submerged flows. Several other studies report the same issue for this model. The results of this experiment, the fact that the nonlinear regression of Swamee's (1992) method is based on Henry's (1950) nomogram, and similar reports in several studies could raise concerns about the generality of this model and the scaling effects on this method's accuracy. Therefore, it seems that Swamee's (1992) method should be used with extra caution.

This study results also indicated that the scaling effects on loss factor k in the EML model need to be considered for different cases. Investigations showed that calibration k using this experiment data increases the EML accuracy. In practice, most of the losses will be captured through the calibration of C_d using real field or experiment measurements. For design purposes, the EML model could be considered as a model with reasonable accuracy. Further investigations on this model are recommended.

An analytical equation and method were proposed to determine the loss factor k due to the importance of k in the EML model, which makes it easier to use and improved its performance. Additionally, a new equation form was proposed for the EML model to determine the discharge coefficient in submerged flow.

In addition, a solution was proposed for the HEC-RAS model drawback in not providing any analytical methods to estimate the coefficient of discharge C_d . Technically, C_d could be calibrated

when the experimental data is available. However, for design purposes, or when the experimental measurements are not available, such a drawback makes the application and accuracy of HEC-RAS highly dependent on the operator's experience. To address this issue, a method is offered to estimate C_d for HEC-RAS, which enables utilizing this model for design purposes where the experimental data is not available for calibration. Further studies could reveal more facts about this method.

In system optimization, non-iterative and fast analytical calculations for a component are important to maintain the overall efficiency of optimizing the whole system of many components. The new analytical equations, methods, and simplified models presented in this study could assist with modelling sluice gates as a component of complex hydraulic systems, especially when there are many scenarios to be studied, managed, or optimized. Moreover, they could assist where the experimental data is not available for calibration, such as for design purposes or where the flow in open channels needs to be controlled or measured using the sluice gates. This study could benefit the design, optimization, development of management or operation plans, etc., of sluice gates in complex hydraulic systems such as water delivery systems and hydropower plants, which are essential components in the sustainable development of water resources and power generation. Further studies are recommended.

4.6 Nomenclature

A	: Area of cross-section	(m ²)
A_i	: Area of cross-section i	(m ²)
b	: Width of the channel/sluice gate	(m)
C_c	: Coefficient of contraction (Y_m/Y_G)	(-)
C_d	: Coefficient of discharge	(-)

E_i	: Specific energy of the cross-section i	
EM	: Energy-Momentum method	
EML	: Energy-Momentum method by considering losses	
F	: Free flow	
GVF	: Gradually varied flow	
g	: Gravitational constant	(9.81 m/s ²)
k	: Loss factor	
M_i	: Momentum function of the cross-section i	
$MAPE$: Mean absolute percentage error	(%)
MPE	: Mean percentage error	(%)
Q	: Volume flow rate (discharge)	(m ³ /s)
q	: Unit discharge ($q = Q/b$)	(m ² /s)
P	: Wetted perimeter	(m)
PS	: Partially submerged flow	
R	: Pearson correlation	
S	: Submerged flow	
SHJ	: Submerged hydraulic jump	
Y_{Cr}	: Critical depth of flow ($\sqrt[3]{q^2/g}$)	(m)
Y_D	: Downstream depth	(m)
Y_{DMF}	: The maximum downstream depth that a free flow could be expected; the conjugated depth of $Y_m = Y_{J1}$	(m)
Y_G	: Gate's opening	(m)
Y_i	: Depth of flow at the cross-section i	(m)
\bar{Y}_i	: Depth of the centroid of the cross-sectional area from the top of the water surface for the cross-section i	(m)
Y_{J1}	: Initial depth of hydraulic jump	(m)
Y_{J2}	: Secondary depth of hydraulic jump	(m)
Y_m	: The minimum depth of flow after the sluiceway	(m)
Y_P	: The piezometric head	(m)
Y_U	: Upstream depth	(m)
δ	: The upstream to downstream depth ratio (Y_U/Y_D)	(-)
Δ	: The ratio of contraction point depth to the upstream depth ($C_c Y_G/Y_U$)	(-)

5 Development of an Equation for the Volume of Flow Passing through an Archimedes Screw Generator

Adapted from:

A. YoosefDoost and W. D. Lubitz, “Development of an Equation for the Volume of Flow Passing Through an Archimedes Screw Turbine,” in *Sustaining Tomorrow*, D. S.-K. Ting and A. Vassel-Be-Hagh, Eds. Cham, Switzerland: Springer, Cham, 2021, pp. 17–37. doi: 10.1007/978-3-030-64715-5_2.

Thesis Author’s Contribution:

This is an original research article that was written by Arash YoosefDoost [6]. The figures are all original, or from explicitly referenced sources.

5.1 Introduction

In order to design an ASG power plant, it is very important to estimate the volume of flow that can pass through the Archimedes screw. In addition, such information is very important for developing operation plans and management of the powerplant as well as estimating the generated power and power loss. There is no general theory to estimate the volume of water enters to an Archimedes screw [69]. In 1932 Muysken proposed the required equations and design parameters for Archimedes screw pumps (ASPs) [263]. However, ASGs and ASPs operate differently, especially in terms of the direction of flow. Therefore, many of these equations may require further studies or are not applicable to ASGs. In 2013, Nuernbergk and Rorres proposed an analytical model for the water inflow of an ASG [69]. Khan et al. (2018) proposed that the screw rotation speed and

volume flow rate would be the dominant dependent variables in inlet depth. They proposed an equation for the screw's inlet depth [264]. They indicate that this equation works for lab-scale screws similar to the one that is tested. In fact, changing entrance Reynolds and Froude numbers will change with the ASG scale, and effects such as the criticality of the entrance flow are not included in their simple model. So, they proposed that their proposed equation should be used with caution in differing situations [264]. Later, initial investigations for this research proved their prediction: For full-scale screws, the Khan et al. (2018) equation error is considerable and makes it impractical. Kozyn and Lubitz identified scaling between lab-scale and full-scale ASGs as an issue that requires further studies [146].

Therefore, developing a general relationship for all screw sizes to estimate the volume of flow passes through an ASG considering its inlet water level is important but challenging: In ASGs, water flows through a helical array of blades that are wrapped around a central cylinder while there is a small gap between the trough and screw which could be considered as free flow. The existence of this small gap is necessary for allowing free rotation of the screw. This leakage is not considerable in full-scale screws, but it is not negligible in lab-scale ASGs. The screw geometry and rotation speed are two other important factors that intensify the scaling difficulties. This study aimed to address this problem by developing an equation to estimate the volume of water passing through ASGs based on the inlet depth.

5.2 Methodology

5.2.1 Genetic Algorithm

The Genetic Algorithm (GA) is a metaheuristic and evolutionary algorithm which was introduced by John Holland introduced in 1960 and extended by David E. Goldberg in 1989. The GA is based on the concept of Darwin's theory of evolution [265] and inspired by the process of natural selection. It includes bio-inspired operators such as mutation, crossover and selection [266]. In this study, the Genetic Algorithm is used as a tool to find the most optimum coefficients for the developed equation.

5.2.2 Principle Component Analysis

The relationship between two variables could be represented and studied using 2-D graphs. In order to consider the relationship between three variables, a 3-D graph or contour plot could be practical. However, it is not easy to plot or analyze more than three variables since representing each variable requires one dimension (axis) in a plot. Since the same number of dimensions are required to plot the observations, large datasets with more than three variables are hard to plot, interpret and understand. Also, it is not easy to discover which dimensions capture the essence of the observations or the system as a whole. Using a data reduction technique such as Principal Component Analysis (PCA) reduces the dimensionality of the dataset whilst retaining as much of the variability in the data as possible [267].

PCA is a mathematical technique that reduces dimensionality by creating a new set of variables called Principal Components [268]. PCA can uncover facts around data and help to understand

trends [269]. In addition, removes the noise and redundancy from data. The Principal Component is a linear combination of the original variables and explains as much variation as possible in the original data. The first few Principal Components retain most of the variation in the original variables to make interpretation simpler, so they can be used to describe the relationships between the original variables and similarities between observations. PCA It is useful to visualize the relationships between the variables to display the most important variables that explain the variations in a dataset. PCA method identifies correlated variables. The correlation mono plot shows vectors pointing away from the origin to represent the original variables. The angle between the vectors is an approximation of the correlation between the variables.

5.2.3 Base Model

Flow rate (Q) is the volume of fluid per unit time passing through a certain area (A). For a uniform state flow with the velocity V, the volumetric flow rate of incompressible fluids could be calculated using the continuity equation:

$$Q = AV \quad (5-1)$$

In an ASG, a water bucket is a volume of entrapped water between two adjacent helical plane surfaces. For an ideal screw operating under steady-state conditions (steady flow, constant rotational speed), all the buckets will have the same shape and volumetric size [49]. Also, it could be assumed that the flow has a speed equal to the screw's axial transition speed (V_T), which is equal to:

$$V_T = \frac{S\omega}{2\pi} \quad (5-2)$$

The entrance area of the Archimedes screw changes nonlinearly for different inlet water levels.

Therefore, a new concept is developed for the maximum available area of the screw entrance for any inlet water levels, which has called the Effective Area (A_E). Therefore, Eq. (5-1) could be modified by applying A_E and V_T and be represented as follows, which is the base volume flow rate equation:

$$Q = A_E V_T \quad (5-3)$$

This equation represents a basic model for the volume flow rate entering the screw. It is only a function of the rotation speed and effective area and does not include any minor entrance losses, effects due to the ends of the screw flights interacting with the incoming flow, etc. The total cross-sectional area of the screw available for flow is

$$A_{Max} = \frac{\pi(D_o^2 - D_i^2)}{4} \quad (5-4)$$

If the screw were able to operate totally full, A_E will be equal to A_{Max} . It is obvious that A_E will be equal to $\frac{1}{2}A_{Max}$ if the screw is half full. Figure 2.20 suggests that the ASG's inlet water level (h_u) could be projected on the screw's entrance surface based on the inclination angle of the screw.

This new parameter is called the effective water level (h_E):

$$h_E = h_u / \cos(\beta) \quad (5-5)$$

For a known screw geometry defining h_E enables to relate the ASG inlet water level to A_E . The screw's effective inlet area is not constant and varies with different inlet water levels. So, it would be considered as $A_E = f(D_o, D_i, h_E)$. Calculations show that A_E and h_E follow the trends shown in Figure 5.1, which shows this relationship for a range of different D_i/D_o ratios.

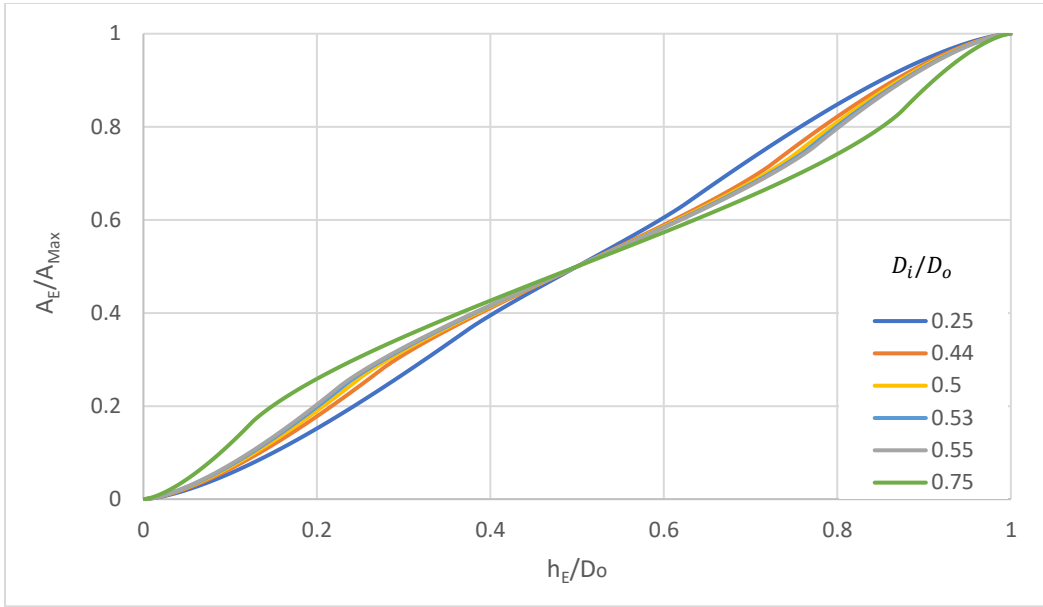


Figure 5.1: Dimensionless effective inlet area (A_E/A_{Max}) as a function of dimensionless effective inlet depth (h_E/D_o) for different D_i/D_o ratios.

Muysken proposed a maximum recommended rotation speed (ω_M) for Archimedes screws as follows [83]:

$$\omega_M = \frac{5\pi}{3D_o^{2/3}} \quad (5-6)$$

Applying the A_{Max} and ω_M into Eq. (5-1) leads to defining the maximum possible practical volume flow rate:

$$Q_{Max} = (D_o^2 - D_i^2) \frac{S\omega_m}{8} \quad (5-7)$$

This is the flow that would be transported by an imaginary turning screw with the entire screw volume completely filled with fluid. Physically, actual Archimedes screws cannot operate with this much fluid because water would spill out of the tops of the bucket volumes, and a screw must have a defined free surface in each bucket to operate. Therefore, the actual flow that passes through the screw is always less than Q_{Max} . In this study, the dimensionless volume flow rate is defined as

the ratio of measured or estimated volume flow rate over Q_{Max} :

$$Q_{ND} = Q/Q_{Max} \quad (5-8)$$

For optimal design of industrial full-scale Archimedes screws running at a fixed speed near Muysken's maximum recommended rotation speed (ω_M) [83], Nuernbergk and Rorres proposed an analytical method based on the screw's water-inflow conditions [33]. This method can be simplified to an equation which is a function of the inlet depth, rotation speed and geometry of the screw using the concept of the effective cross-sectional area within the screw (A_E), and the axial transport velocity of Archimedes screws (V_T) [6]:

$$\frac{Q}{Q_O} = \frac{A_E}{A_O} \quad (5-9)$$

where $A_O = \pi D_O^2/4$ and $Q_O = A_O V_T$.

Using the similar idea of developing a dimensionless form of parameters could lead to more flexible models. Therefore, the base equation (Eq. (5-3)) could be represented in a dimensionless form as follows:

$$\frac{Q}{Q_{Max}} = \frac{A_E}{A_{Max}} \frac{\omega}{\omega_M} \quad (5-10)$$

5.2.4 Experimental Data

The experimental data which will be used to validate and optimize the developed equations were measured at the Fletchers hydropower ASG (7.2 kW design capacity), called "101" in Table 5.1. Data from five lab-scale screws previously examined at the University of Guelph are also used. Table 5.1 summarizes the measured volume flow rate data as well as the geometry details of these Archimedes screws. This table represents the ranges of all parameters introduced before. In this

table, Q_{\min} , Q_{\max} , ω_{\min} and ω_{\max} are the minimum and maximum of the flow rates and rotation speeds in the measured data for each screw. More information can be found in [146].

Table 5.1: Operating Details of the Archimedes screws studied in this experiment

Screw	No. of Samples	D_o (m)	D_i (m)	L (m)	S (m)	N (-)	β ($^\circ$)	D_i/D_o (-)	A_{\max} (m^2)	ω_M (rad/s)	Q_{\max} (m^3/s)	Q_{\min} (m^3/s)	Q_{\max} (m^3/s)	ω_{\min} (rad/s)	ω_{\max} (rad/s)
2	80	0.32	0.17	1.22	0.32	3	24.5	0.53	0.23	11.28	0.032	0.005	0.01	2.06	8.90
3	84	0.32	0.17	1.22	0.25	3	24.5	0.53	0.23	11.27	0.026	0.006	0.014	2.09	8.41
14	22	0.38	0.17	0.48	0.38	4	33.8	0.44	0.36	9.96	0.055	0.01	0.01	1.57	6.29
15	51	0.38	0.17	0.62	0.38	4	24.4	0.44	0.36	9.96	0.055	0.009	0.011	1.57	6.29
16	64	0.38	0.17	0.95	0.38	4	24.5	0.44	0.36	9.96	0.055	0.001	0.014	1.05	5.25
101	37	1.39	0.76	4.54	1.39	3	22.0	0.55	4.26	4.204	0.987	0.348	0.552	4.262	4.262

Table 5.1 shows that the dataset includes Archimedes screws with dimensions in the range of D_i/D_o from 0.44 to 0.55, volume flow rates from 0.001 to 0.552 m^3/s and rotation speeds from 1.045 to 8.9 rad/s. However, the focus of this study is to estimate the volume flow rate passing through ASGs using knowledge of the rotation speed and inlet water level when each bucket is optimally filled. ASGs can handle extra flow rates, up to 20 percent more than their optimal filling, without a significant loss in efficiency [270]. At fill levels above the optimum, some water overflows from the top of the bucket over the central cylinder into the lower bucket, which is called overflow leakage. The overflow leakage does not result in power generation, so it reduces the overall efficiency [69]. In addition, such conditions may lead to unknown phenomena, which are outside the scope of this study. In practice, due to the physical design of screws, the effective water levels (h_E) more than half of the screws' outer diameter are uncommon and is also not the subject of this study. Future experiments are recommended for non-optimum operating conditions.

5.2.5 Evaluation of the Base Equation

Evaluating the dimensionless form of Eq. (5-3) (the base equation) represented as Eq.(5-10) with

the available experimental data and the validation criteria indicates a reasonable accuracy, especially for the full-scale ASG. These results are represented in Figure 5.2. In this figure and all similar figures, the “Ideal” line refers to the ideal line in which the estimations are equal to the corresponding measured value. Therefore, being closer to this line means better estimations.

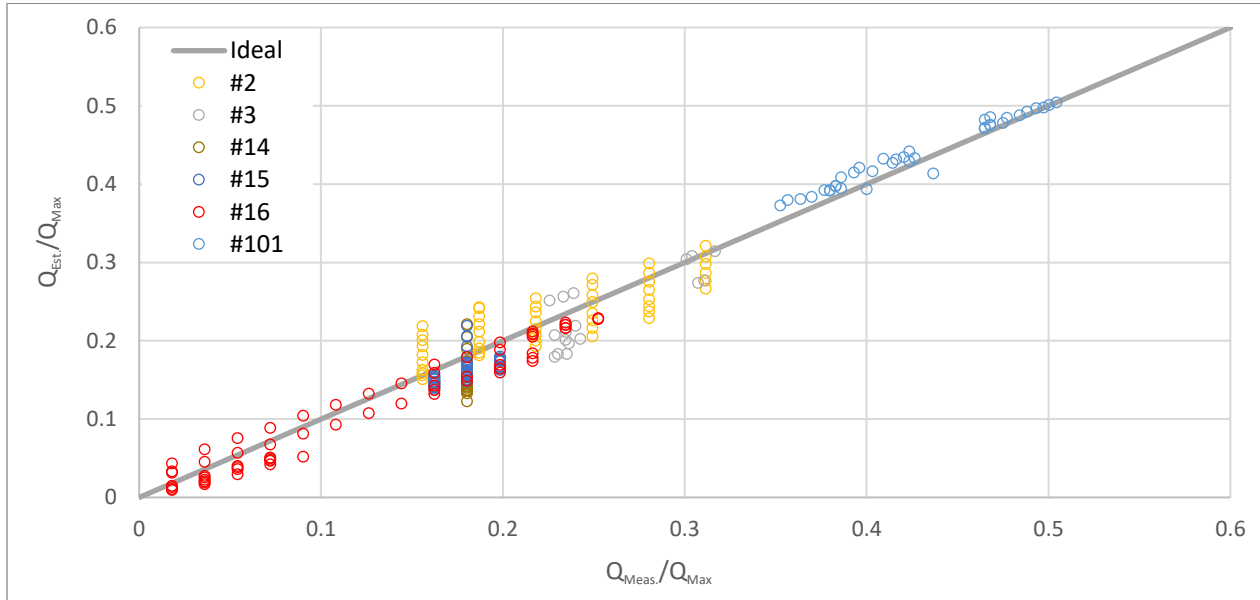


Figure 5.2: Predicted flow from Equation (5-3) versus measured flow for all ASG sizes

5.2.6 Development of the Extended Equation

Figure 5.2 indicates the base equation offers acceptable estimations, especially for the full-size screw. The main goal of this study is to develop an equation that is accurate across the full range of screw scales (i.e., for both lab and full-size screws). In order to increase the accuracy of the model for lab-scale screws and make it more general for all screw sizes, the potential non-dimensional form of relevant variables were developed and investigated. Table 5.2 represents the list of these dimensionless numbers:

Table 5.2: Investigated dimensionless groups

Description	Dimensionless Variable
N.D. Effective Inlet Water Level	$\zeta = h_E/D_o$
N.D. Wetted perimeter	$P_{ND} = P_E/P_{Max}$
N.D. Hydraulic Radius	$R_{hND} = R_h/R_{hMax}$
N.D. Effective Area	$A_{END} = A_E/A_{EMax}$
N.D. Rotation Speed	$\omega_{ND} = \omega/\omega_M$
Pitch Ratio	$PR = S/D_o$
Reynolds Number	$R_e = V_t R_h/\nu$
Froud Number	$F_r = V_t^2/gR_h$

The initial method of expanding the base equation was focused on numerical experiments in applying the dimensionless groups in Table 5.2 to the base equation. Several combinations were developed and evaluated using the validation criteria. Then they analyzed and compared in order to find similarities, governing rules or general terms.

The effect of the most effective dimensionless variables was evaluated by developing various equations based on Eq. (5-3) and as a function of rotation speed, geometry, and fill level of the Archimedes screws, such as:

$$Q = A_E \frac{S\omega}{2\pi} \times a \times \left(\frac{S}{D_o}\right)^b \times \left(\frac{\omega}{\omega_M}\right)^c \quad (5-11)$$

Here, a , b and c are dimensionless constants that must be determined. Values for these constants were found by applying Genetic Algorithm methods to minimize the difference between the predicted values and the experimental data. This process was first done for each screw individually. Optimization results indicate that the range of these constants is very similar for all studied screws. The resulting native optimum constant values for each screw are shown in Table 5.3. The results of Eq. (5-11) for all ASG sizes with native optimum constants for each screw are compared to the measured values in Figure 5.3.

Table 5.3: Optimum native constants for each individual screw in Eq. (5-11)

	a	b	c
#2	0.852	0.119	-0.292
#3	0.873	0.100	-0.421
#14	0.612	0.100	-0.702
#15	0.689	0.100	-0.489
#16	0.878	0.100	-0.274
#101	0.825	0.097	-0.099

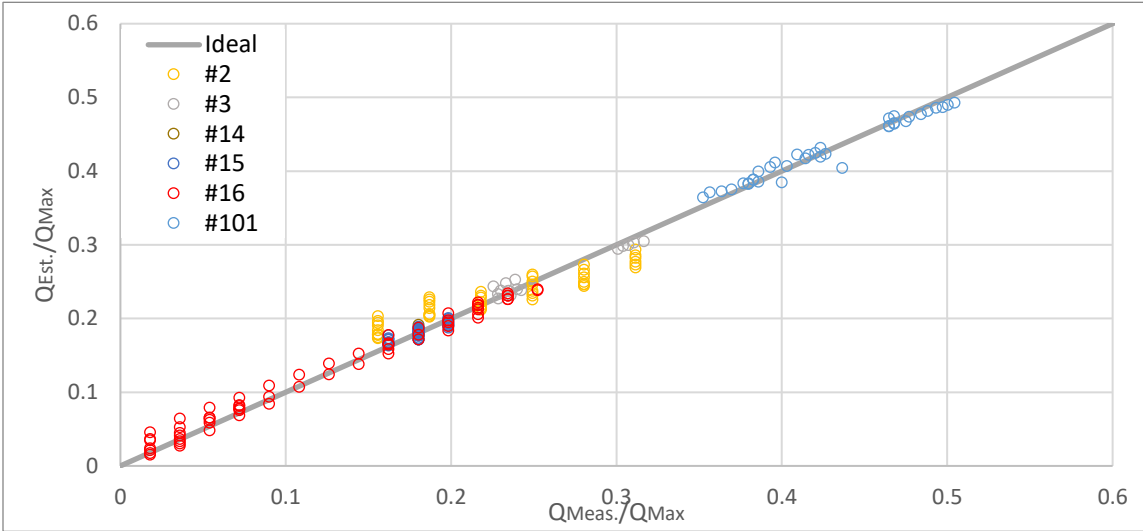


Figure 5.3: Estimations of Eq. (5-11) for all ASG sizes with native optimum constants

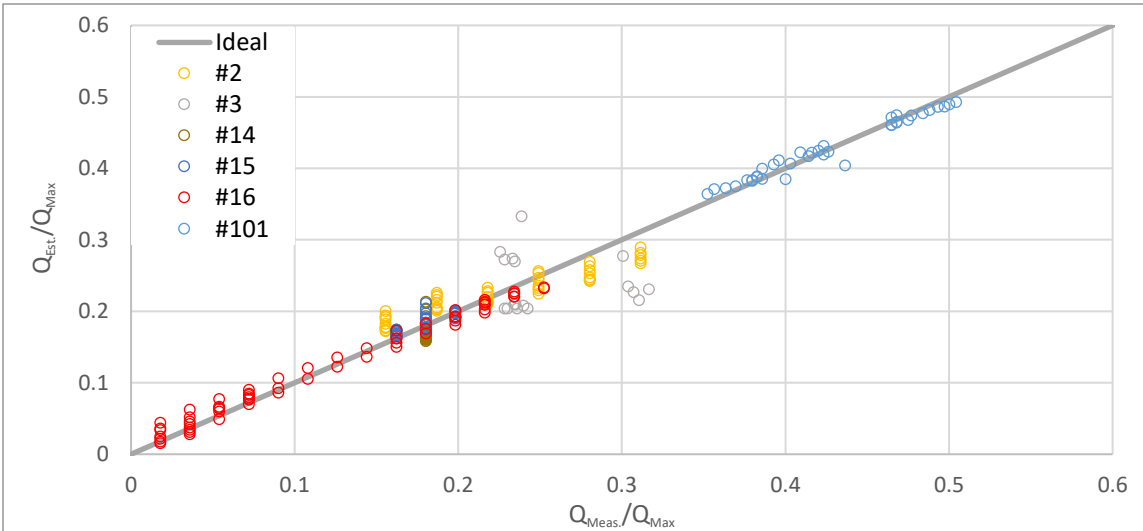


Figure 5.4: Non-dimensional results of estimations using Eq. (5-11) with general coefficients for all ASG sizes ($a = 0.839$, $b = 0.09$ and $c = -0.306$).

In the next step, the dataset of all screw sizes and the genetic algorithm were applied to find the more general values for constants a , b and c . According to Figure 5.4, $a = 0.839$, $b = 0.09$ and $c = -0.306$ reasonably improved the accuracy of Eq. (5-11) for all tested screw sizes.

5.3 Results and Discussion

Figure 5.2 and Figure 5.3 suggest that the extended equation (Eq. (5-11)) improved the results of the Eq. (5-3) for both lab-scale and full-size screws. The native (screw-specific) constants provided the best accuracy for each screw, and the general constants made the equation practical for all screw sizes. Based on the results, Eq. (5-11) using the general constants could be useful as a base for developing a general equation to predict the volume flow rate for all size screws. It would suggest that there would be some concerns about the validity of this three constant equation for screw #101 based on the fitting data as well as because of the number of samples. There are many combinations of a and c that could give equally accurate results. It could either be very accurate or completely inaccurate at other rotation speeds. However, similar to many full-scale ASG, screw 101 rotates at a constant speed near the Muysken proposed a maximum recommended theoretical rotation speed (Eq. (5-6)). Since there is no (and maybe cannot be) any data about the different rotation speeds of this screw, the validation of this equation for this screw in different rotation speeds remains a recommended subject for future studies.

Figure 5.4 does show that some error remains in the predictions, and it indicates that using global constants didn't lead to the best accuracy for screw 3. In addition, although the dimensionless group of S/D_o is an important parameter that reflects the screw properties, this ratio is almost the same for most modern screws, so it could be assumed as just a constant. Therefore, a deeper

analysis was performed to provide a better understanding of the governing phenomenon and the relationship between parameters, equation results and errors.

5.3.1 Error Analysis

According to Figure 5.5, an analysis of the relationship between each dimensionless variable and the error of the base and extended equations (Eq. (5-3) and Eq. (5-11)) indicates that the errors of these equations could not be considered a function of these variables.

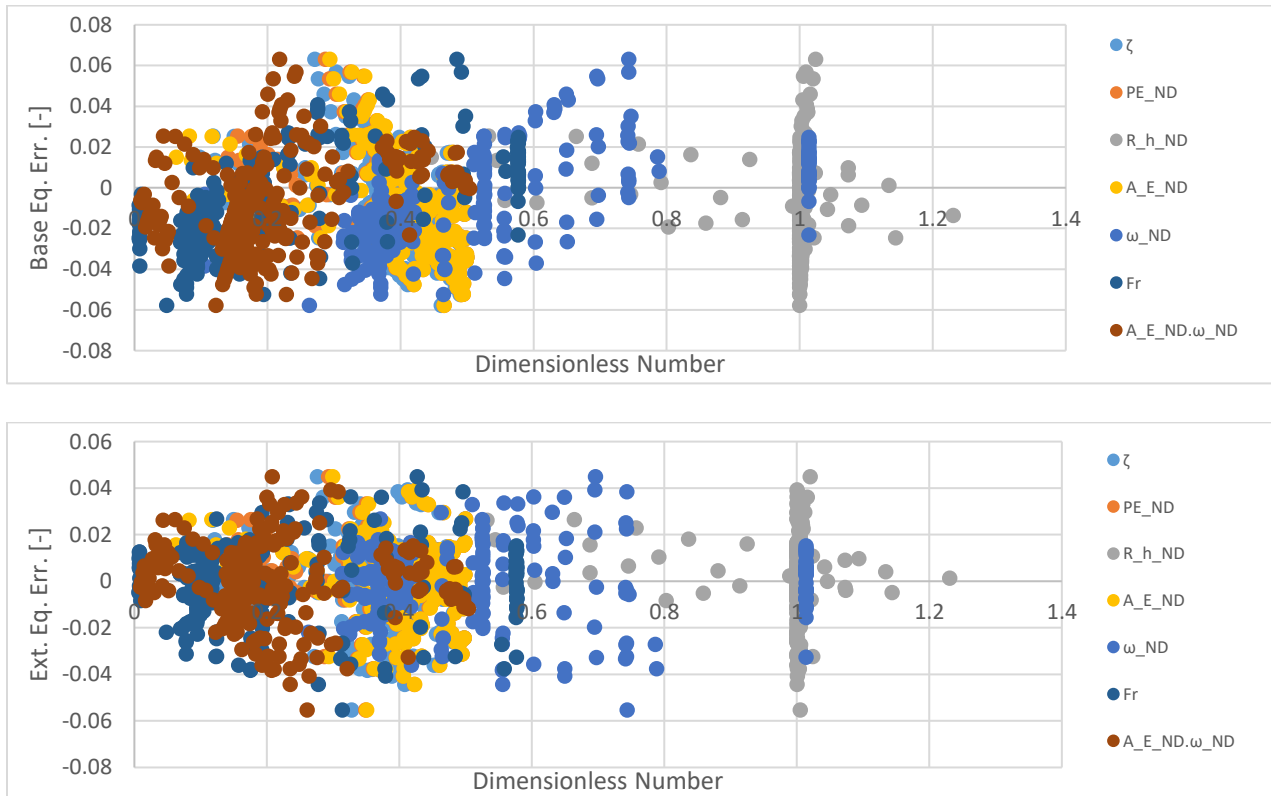


Figure 5.5: Analysis of the relationship between dimensionless variables vs. equations' errors for predictions using the base equation (Eq. (5-3)) (top) and using the extended equation (Eq. (5-11)) (bottom).

Table 5.4 indicates there is a considerable correlation between most of the variables and error for Eq. (5-3). This correlation is reduced significantly for rotation speed-related variables (ω_{ND} , Re ,

Fr) in the extended equation (Eq. (5-11)). It seems there is a meaningful relationship between the ω_{ND} and this significant change in the extended equation. According to this assumption, it seems to apply a A_{END} into the base equation (Eq. (5-3)) can have the same effect for area-based errors.

Table 5.4: The Pearson correlation of dimensionless variables and each equation error

	Eq. No.	ζ	P_{END}	R_{hND}	A_{END}	ω_{ND}	Re	Fr
Base Eq.	(5-3)	-0.45	-0.41	-0.13	-0.39	0.56	0.36	0.62
Ext. Eq.	(5-11)	-0.17	-0.18	-0.15	-0.18	-0.01	0.03	0.04

5.3.2 Application of the Principal Component Analysis

Due to the number of variables in this study, it is hard to comprehend all of the relationships between the variables using the scatter plot or correlation matrix. In order to provide a better understanding of the relationship between parameters and the ASG's flow rate and because of the number of variables in the dataset, Principal Components Analysis was used in this study. PCA help to visualize the relationship between the formerly studied variables and the new dimensionless group of $A_{END} \omega_{ND}$. Also, PCA is used to determine the hidden pattern of the dataset. PCA was applied to the dataset firstly to reduce the dimension. Secondly, a two-dimensional correlation mono plot of the coefficients of the first two principal components was used to visualize the relationships between the variables to display the most important variables that explain the variations in a dataset. For computing PCA, R software is used. The results of PCA analysis are represented in Figure 5.6 and Table 5.5. The influence of each parameter on Q_{ND} is visualized in Figure 5.6. The correlation matrix of the PCA result is represented in Table 5.5.

Table 5.5: The correlation matrix of the PCA results

	ζ	P_{END}	R_{hND}	A_{END}	ω_{ND}	Re	Fr	$A_{END}\omega_{ND}$	Q
ζ	1	0.99	0.57	0.99	0.12	0.18	0.03	0.41	0.53
P_{END}	0.99	1	0.52	0.99	0.16	0.2	0.07	0.44	0.55
R_{hND}	0.57	0.52	1	0.63	0.13	0.09	0.04	0.28	0.33
A_{END}	0.99	0.99	0.63	1	0.17	0.19	0.08	0.45	0.55
ω_{ND}	0.12	0.16	0.13	0.17	1	0.84	0.97	0.94	0.87
Re	0.18	0.2	0.09	0.19	0.84	1	0.81	0.85	0.82
Fr	0.03	0.07	0.04	0.08	0.97	0.81	1	0.89	0.8
$A_{END}\omega_{ND}$	0.41	0.44	0.28	0.45	0.94	0.85	0.89	1	0.98
Q	0.53	0.55	0.33	0.55	0.87	0.82	0.8	0.98	1

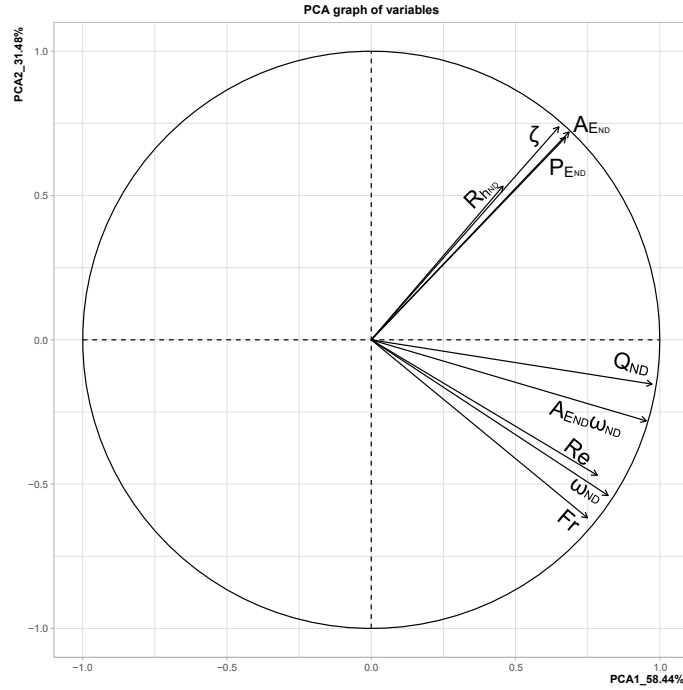


Figure 5.6: Principal component analysis of dimensionless groups

Figure 5.6 represents the correlation mono plot of the PCA analysis, which describes the relationships between the non-dimensional volume flow rate Q_{ND} and the dimensionless parameters for all screws. Component one and component two (the first and second dimensions) are a reflection of 58.44 percent and 31.48 percent of the variations in the data, respectively. Since they collectively describe up to around 90 percent variance of data that would imply that instead

of the initial dataset, they provide a useful approximation of the relationship between the variables [271]. Therefore, only the two first Principal Components were used. The PCA plot in Figure 5.7: shows vectors pointing away from the origin to represent the original variables. The angle between the vectors is an approximation of the correlation between the variables. According to this figure, $R_{h_{ND}}$, ζ then $A_{E_{ND}}$ and $P_{E_{ND}}$ vectors create a larger angle with the vector Q_{ND} which indicates that these parameters are much less correlated with Q_{ND} .

Table 5.5 confirms this conclusion numerically and indicates that variables are not related to the rotation speed of the screw are not strongly correlated to the flow rate since the correlations of $R_{h_{ND}}$, ζ , $A_{E_{ND}}$ and $P_{E_{ND}}$ with Q are 0.33, 0.53, 0.55 and 0.55, respectively.

Table 5.5 indicates that the variables that are related to the rotation speed of the screw have the highest correlations with the flow rate. In terms of correlation, $Fr < Re < \omega_{ND} < A_{E_{ND}}\omega_{ND}$ with the correlations of 0.8, 0.82, 0.87 and 0.98, respectively. Figure 5.6 indicates that despite the relatively good correlation of Re , it could not be considered a very practical representation of Q_{ND} . It is worth mentioning that the numerical experiments for developing the equations supported this conclusion as well.

The high correlation of 0.87 between Q_{ND} and ω_{ND} suggests that, as was expected, ω_{ND} is an effective variable in this phenomenon. However, the high correlation of 0.98 suggests that $A_{E_{ND}}\omega_{ND}$ is the most important and correlated parameter to Q_{ND} . Due to this significant correlation, development of the extended equation was focused on the application of this combination.

5.3.3 Modified Extended Equation

Based on the error analysis and principal component analysis, the extended equation is modified in a way that reflects the importance of the most effective parameters as:

$$Q = A_E \frac{S\omega}{2\pi} \times a \times \left(\frac{A_E}{A_{Max}} \right)^b \times \left(\frac{\omega}{\omega_M} \right)^c \quad (5-12)$$

In order to find constants a , b and c genetic algorithm is applied. Results indicate that $a = 1.266$, $b = 0.335$ and $c = -0.179$ are practical values for these constants to provide enough accuracy for Eq. (5-13) to be used as a general equation for all studied screw sizes.

Eq. (5-12) could be represented in a non-dimensional form if it is divided by the maximum possible volume of flow rate (Q_{Max}). The screw pitch is a constant number for each screw which is usually a ratio of the outer diameter. Analysis of the results of considering $S/2\pi$ as a constant shows a very slight increase of error for the studied screws. Therefore, the simplified non-dimensional form of this equation could be represented as:

$$\frac{Q}{Q_{Max}} = a \times \left(\frac{A_E}{A_{Max}} \right)^b \times \left(\frac{\omega}{\omega_M} \right)^c \quad (5-13)$$

The same application of genetic algorithms indicates that $a = 1.242$, $b = 1.311$ and $c = 0.822$ are practical values for these constants to provide enough accuracy for Eq. (5-13) to be used as a general equation for all studied screw sizes. Figure 5.7 represents the non-dimensional results of this equation's estimations for all ASG sizes.

Analysis of the correlation of dimensionless variables and the developed equation errors indicates that in the modified extended equation (Eq. (5-12)) and Eq. (5-13), the correlation between variables and error is reduced to 3 percent and less for all dimensionless numbers (but Re) so that it could be considered as negligible. Further studies are recommended about the effect of the Reynolds number on this phenomenon. In addition, it seems that ω_{ND} and A_{END} are two important variables in the volume of flow passes through an ASG. These results are represented in Table 5.6.

Table 5.6: The Pearson correlation of dimensionless variables and prediction error using each equation

Eq. Name	Eq. No.	ζ	P_{END}	R_{hND}	A_{END}	ω_{ND}	Re	Fr
Base Eq.	(5-3)	-0.45	-0.41	-0.13	-0.39	0.56	0.36	0.62
Ext. Eq.	(5-11)	-0.17	-0.18	-0.15	-0.18	-0.01	0.03	0.04
Mod. Ext. Eq.	(5-12)	0.01	0.02	0.02	0.03	-0.02	-0.21	0.01
Mod. Ext. Eq. N.D.	(5-13)	0.01	0.02	0.02	0.03	-0.02	-0.22	0.01

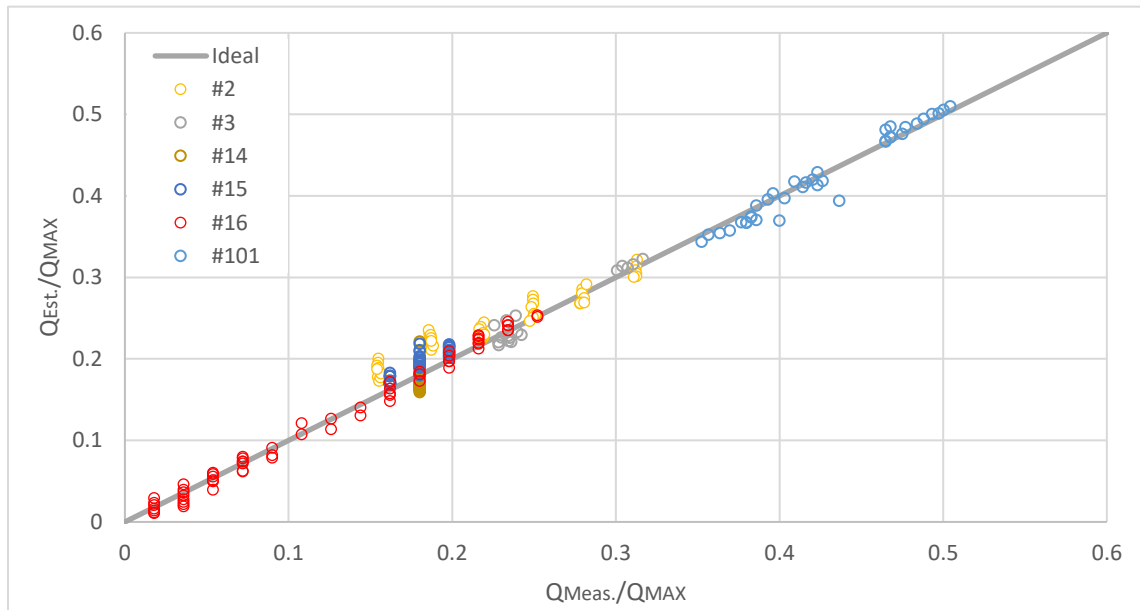


Figure 5.7: Non-dimensional results of Eq. (5-13)'s estimations with general coefficients for all ASG sizes.

Table 5.7 and Table 5.8 compare the accuracy of each equation based on MPE and MAPE, respectively. Although developed equations show an acceptable accuracy for almost all studied

screw sizes, MAPE suggests that for single or short-term estimations, Eq. (5-11) showed a slightly better performance for the full-size screw. However, the modifications of the extended equation (Eq. (5-12) and Eq.(5-13)) showed a bit more precision for lab-scale screws.

According to MPE validation criteria, Eq. (5-12) and Eq. (5-13) could be considered as the most practical equations for long-term estimations, especially when the water level and even rotation speed of ASGs varies through the operation, just like the real hydropower plans. Therefore, it seems that these equations are practical for designing operation plans for full-size ASG-based power plants. Most of the full-scale ASGs are operating at a constant rotation speed near the Muysken rotation speed. Therefore, further investigations may require using these equations for full-scale varying rotation speed ASGs.

Table 5.7: Comparison of the MPE (%) of developed equations with optimum global constants for each ASG

Eq. AST	Base Eq. (5-3)	Ext. Eq. (5-11)	Mod. Ext. Eq. (5-12)	Mod. Ext. Eq. N.D. (5-13)
#2	3.499 %	2.651 %	0.008 %	0.008 %
#3	-7.655 %	-4.989 %	-0.008 %	-0.008 %
#14	-14.299 %	-4.310 %	-0.013 %	-0.013 %
#15	-9.441 %	2.065 %	0.005 %	0.005 %
#16	-8.546 %	9.527 %	0.019 %	0.019 %
#101	2.556 %	0.239 %	-0.006 %	-0.006 %

Table 5.8: Comparison of the MAPE (%) of developed equations with optimum global constants for each ASG

Eq. AST	Base Eq. (5-3)	Ext. Eq. (5-11)	Mod. Ext. Eq. (5-12)	Mod. Ext. Eq. N.D. (5-13)
#2	11.007%	10.385 %	8.031 %	8.270 %
#3	11.476 %	18.662 %	4.540 %	4.712 %
#14	18.322 %	8.022 %	10.346 %	10.302 %
#15	11.110 %	3.439 %	3.527 %	3.498 %
#16	24.040 %	15.468 %	11.428 %	11.584 %
#101	2.939 %	1.877 %	2.633 %	2.452 %

Finding a practical and simple equation that works well for both studied lab-scale and full-scale screws is very promising and important for the design, making operation plans and operation of Archimedes screw hydropower plants. The proposed equation showed acceptable flexibility and performance for almost a wide range of rotation speeds for lab-scale screws. However, it is recommended to use it with caution. Also, although most of the full-scale ASGs are operating in the same rotation speed, which is near to the Muysken rotation speed, further studies are recommended for the ASG powerplants utilizing variable rotation speed Archimedes screws.

5.4 Conclusions

The Archimedes screw is an ancient but effective technology which recently modified to be utilized for power generation. ASGs are safer for aquatic life and a more sustainable solution that offers clean and renewable energy. Although ASGs are using widely in Europe, there is only one operating ASG in North America. This study investigated the development of a model to estimate the volume of flow passing through ASGs, considering their inlet water level and rotation speed. The experimental measurements of five lab-scale and the only operating ASG power plant in Canada are used to find a general equation for all studied screw sizes. The size of investigated ASGs in this study has a variety of 0.17 m to 1.8 m and 0.32 m to 3.6 m for the inner and outer diameters, respectively. In this study, the new concept of the Archimedes screw's effective area (A_E) is proposed, which is a function of the inlet water level and geometry of the Archimedes screw. Investigations proved that there is a strong relationship between the screw's effective area, rotation speed and the volume of flow passing through the screw. Although the base proposed equation (Eq. (5-3)) and its dimensionless form (Eq. (5-10)) showed a reasonable accuracy for the

full-scale screw, investigations continued to develop a general relationship that could be broadly applicable to all studied Archimedes screw sizes. Therefore, new related dimensionless groups were developed and combined with the base equation (Eq. (5-3)). These equations are optimized by the Genetic Algorithm and the experimental measurements to find the optimum value for the constants. Although it is obvious optimizing the equation's coefficients for each screw could lead to the highest accuracy, general constants have been represented for the proposed equation in a way that the final model could be broadly applicable for both studied lab-scale and full-scale screws. Results indicate that modifying the base equation (Eq. (5-3)) with a combination of ω_{ND} and A_{END} leads to achieve reasonable accuracy for all studied screw sizes. According to MPE validation criteria, Eq. (5-12) and Eq. (5-13) could be considered as the most practical equations for long-term estimations, especially when the water level and even rotation speed of ASGs varies through the operation time, just like the real hydropower plans. Therefore, it seems that these equations are practical for developing operation plans for full-size ASG-based power plants. Most of the full-scale ASGs are operating at a constant rotation speed near the Muysken rotation speed. Therefore, further investigations may require using these equations for full-scale varying rotation speed ASGs. Also, it is recommended to evaluate the developed equation's accuracy and applicability for Archimedes screws with different sizes, which may lead to determinate even more general coefficients. Finding a practical equation that works well for both studied lab-scale and full-scale screws is very promising and important for the design, development of the operation plans and operation of Archimedes screw hydropower plants. The proposed equation showed acceptable flexibility and performance for almost a wide range of rotation speeds for lab-scale screws. However, it is recommended to use it with caution. Finally, although most of the full-scale

ASGs are operating at the same rotation speed, which is near to the Muysken rotation speed, further studies are recommended for variable rotation speed Archimedes screws.

6 Archimedes Screw Design: An Analytical Model for Rapid Estimation of Archimedes Screw Geometry

Adapted from:

A. YoosefDoost and W. D. Lubitz, “Archimedes Screw Design: An Analytical Model for Rapid Estimation of Archimedes Screw Geometry,” *Energies*, vol. 14, no. 22, p. 7812, Nov. 2021, doi: 10.3390/en14227812.

Thesis Author’s Contribution:

This is an original research article that were written by Arash YoosefDoost [2]. The figures are all original, or from explicitly referenced sources.

6.1 Introduction

Estimation of the Archimedes screw geometry is a fundamental necessity in designing ASG hydropower plants. The screw geometry affects many aspects of an Archimedes screw powerplant design. Each site has different specifications and limitations, including head, flow and available locations for the power plant installation. Most ASG installations are run-of-river, with small or no reservoirs, and plant performance is directly dependent on the local flow duration curve, which varies from river to river. The lack of active water storage in run-of-river (ROR) powerplants makes the importance of the temporal distribution of volumetric flow rate an important design parameter. This means that ASG designs must be highly site-specific, requiring different designs to account for site-specific characteristics.

Recently there has been an emerging interest in utilizing computational fluid dynamics (CFD) for modelling Archimedes screw generators to measure and visualize the fluid and forces within the screw. Simmons [272], [273] and Shahverdi have completed CFD studies modelling several case studies to study ASG performance [94], optimize screw performance [274], or assess and predict the design parameters of the Archimedes screw generator [275]. However, these studies demonstrate that successful CFD modelling requires significant time, resources and, experienced practitioners, software and hardware infrastructures. Proper CFD models must be carefully developed, validated and analyzed for each case.

Archimedes screw pumps (ASP) could be considered among the well-studied hydraulic machines, and some analytical methods have been developed for ASPs [276]. However, in practice, even some design aspects of ASPs still remain in experience. In designing Archimedes screw generators (ASG), the lack of analytical guidelines is so serious that usually listed among the important ASGs disadvantage [1]. The literature shows that there are still no general analytical standards for designing ASGs [1], and the designs are still highly dependent on the designer's experience [33]. Important non-English language ASG design literature includes the works of Brada (1996) [78], Aigner (2008) [79], Schmalz (2010) [80], Lashofer et al. (2011) [81], and Nuernbergk's (2020) book [82]. The papers by Rorres [34] and Nuernbergk and Rorres [33] are among the well-known studies in English literature. However, the proposed methods in these works require considerable computation costs [1], even for the initial estimations and the early stages of designing the ASG hydropower plants.

Dragomirescu (2021) proposed a method to estimate the required screw outer diameter based on the volume of filled buckets [276]. However, there was no analytical equation to calculate this

volume. To deal with this issue, Dragomirescu used regression to estimate correction factors based on a list of ASGs that were all designed by the same manufacturer (Rehart Power) [277] and selected based on their high overall plant efficiencies (more than 60%) [276]. Using regression analysis for such limited case studies may affect the generality of the model and limit it to these case studies. However, in comparison to the former studies, this method could speed up estimating the required screw size and is easier to understand and implement.

Currently, there is no generally accepted and easy to understand and implement method to rapidly determine the preliminary size and operating characteristics of ASG designs. Obviously, each design requires deep studies, evaluation, modelling and optimization, which is costly and time-consuming. However, the first step of optimizing a design is to develop realistic estimates of the primary variables for the initial designs. Therefore, a model is needed for the purpose of rapidly estimating initial design parameters. This study focused on developing an analytical method to estimate site-specific Archimedes screw geometry properties that offers the remarkable advantage of significantly low computational costs.

6.2 Materials and Methods

6.2.1 Theoretical Basis

The most important dimensions and parameters required to define the Archimedes screws are represented in Figure 2.20 and described in Table 2.2. Archimedes screw design parameters can be categorized as external (D_o , L , and β) and internal (D_i , N , and S) parameters. Generally, the screw installation site location properties and the passing volumetric flow rate determine the

external parameters, and the screw performance can then be optimized by adjusting the internal parameters [34].

The installation level (position) of the screw(s) relative to the dam crest or expected level of poundage (reservoir) should be defined considering the determined geometry and optimum inlet level of the Archimedes screw(s). The inlet depth of the Archimedes screw can be represented in a dimensionless form as:

$$\Xi = h_u(D_o \cos \beta)^{-1} \quad (6-1)$$

The available head (H) and volumetric flow rate (Q) and are two important parameters in ASG hydropower plants. In Archimedes screws, the flow always has a free surface (exposed to atmospheric pressure). In addition, the cross-sectional areas at the inlet and outlet of a screw are equal. Applying continuity and the Bernoulli equation, it can be shown that ideally, the available head at an ASG is the difference of free surface elevations at the upstream (Z_U) and downstream (Z_L) of the ASG, where Z_U and Z_L are both measured from the same datum:

$$H = Z_U - Z_L \quad (6-2)$$

The inclination angle of the Archimedes screw (β) is sometimes restricted based on slope or geometry. Considering Figure 2.20, for a known head (H), the screw length (L) is:

$$L = H / \sin \beta \quad (6-3)$$

For developing the current predictive model, the application of the continuity equation suggests that the flow rate passing through the screw (Q) is dependent on the flow depth at the entrance (h_u), overall (outer) diameter (D_o) and the rotation speed (ω) of the screw. This assumption has

been applied and evaluated formerly in studies such as Nuernbergk and Rorres [33] and YoosefDoost and Lubitz [6].

In Archimedes screws, a water bucket is a volume of entrapped water between two adjacent helical plane surfaces. For an ideal screw operating under steady-state conditions (steady flow, constant rotational speed), all buckets will have the same shape and volumetric size [49]. Moreover, it could be assumed that the flow has a speed equal to the screw axial translation speed (V_T) which is equal to:

$$V_T = \frac{S\omega}{2\pi} \quad (6-4)$$

In 1932 Muysken proposed the required equations and design parameters for Archimedes screws used as pumps [83]. Muysken proposed a maximum recommended rotation speed (ω_M) for Archimedes screws [83], and Lashofer et al. [36] confirmed that many current industrial ASGs are designed with this rotation speed which is close to:

$$\omega_M = \frac{5\pi}{3D_o^{2/3}} \quad (6-5)$$

Based on the concept of the effective cross-sectional area within the screw (A_E), and using the axial transport velocity of Archimedes screws (V_T) [6] the volume of flow passing through the Archimedes screws could be expressed as an equation which is a function of the inlet depth, rotation speed and geometry of the screw:

$$Q = A_E V_T \quad (6-6)$$

The effective area (A_E) is calculated using the following equations, with the definitions of additional variables defined in Figure 6.1.

$$A_E = \frac{1}{8} [D_o^2(2\theta_o - \sin 2\theta_o) - D_i^2(2\theta_i - \sin 2\theta_i)] \quad (6-7)$$

$$\theta_o = \pi - \arccos\left(\frac{y_o}{r_o} - 1\right) \quad (6-8)$$

$$\theta_i = \pi - \arccos\left(\frac{y_i}{r_i} - 1\right) \quad (6-9)$$

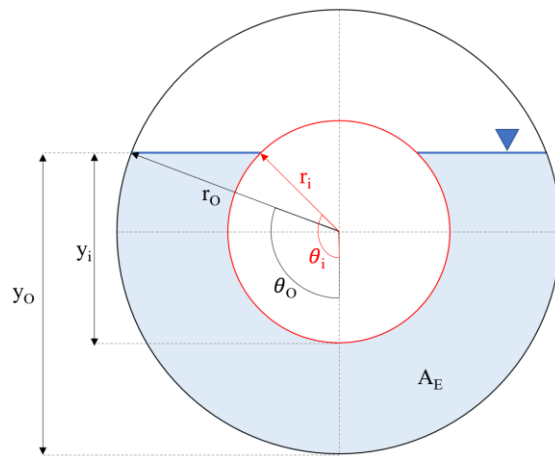


Figure 6.1: Required parameters to define the effective area.

Using the concept of effective area (A_E) with Eq. (6-4) and Eq. (6-6) and defining $\delta = D_i/D_o$ and $\sigma = S/D_o$ results in the following analytical equation for the volume of flow passing through the Archimedes screw:

$$Q = D_o^3 \frac{\sigma \omega}{16\pi} (2\theta_o - \sin 2\theta_o - \delta^2(2\theta_i - \sin 2\theta_i)) \quad (6-10)$$

The overall (outer) diameter of the screw (D_o) can then be determined based on the flow rate passing through the screw. Solving for the outer diameters results in the following equation that enables estimation of the required Archimedes screw outer diameter to accommodate the specified

flow rate passing through the screw:

$$D_o = \sqrt[3]{\frac{16\pi}{\sigma\omega(2\theta_o - \sin 2\theta_o - \delta^2(2\theta_i - \sin 2\theta_i))} Q} \quad (6-11)$$

These equations could be simplified for industrial full-scale Archimedes screws running at a fixed speed near to the Muysken's maximum recommended rotation speed (ω_M) as:

$$Q = \frac{5}{48} \sigma D_o^{7/3} (2\theta_o - \sin 2\theta_o - \delta^2(2\theta_i - \sin 2\theta_i)) \quad (6-12)$$

$$D_o = \left(\frac{48}{5\sigma(2\theta_o - \sin 2\theta_o - \delta^2(2\theta_i - \sin 2\theta_i))} Q \right)^{3/7} \quad (6-13)$$

It is notable that for a specific screw at a specific fill level, the variables other than Q are constant. Therefore, Eq. (6-13) could be represented as a power function with two constants of η and ψ :

$$D_o = \eta Q^\psi \quad (6-14)$$

The inner diameter of the screw (D_i) has an important effect in A_E and the flow rate passing through the screw. In smaller screws, it is possible to deal with technical constraints such as permissible deflection by increasing the thickness of the shaft tube wall. However, to maximize the shaft length, it may be necessary to increase the outer diameter. Nagel in 1968 indicated that reasonable filling of ASPs would be achieved for $\delta = D_i/D_o$ between 0.4 and 0.6 [31]. Theoretical studies and experimental investigations on models and full-scale ASPs indicate that maximizing the water volume in the screw occurs with δ between 0.45 and 0.55. This ratio is reported as the economically optimum ratio as well, due to optimum the usage of material [31]. Lashofer et al. [36] confirmed that for most ASG powerplants, δ is usually very close to 0.5.

Nagel in 1968 indicated the ratio of $\sigma = S/D_o$ is related directly to the number of blades (N) and reversely to the inclination angle (β) of the ASPs (higher β or lower N results in lower δ , and vice versa). From the hydraulic point of view, Nagel recommends [36]:

$$\sigma = \begin{cases} 1.2, & \beta < 30^\circ \\ 1, & \beta = 30^\circ \\ 0.8, & \beta > 30^\circ \end{cases} \quad (6-15)$$

Figure 6.2 visualizes Eq. (6-14) results for these σ values across the full range of dimensionless fill heights (Ξ) of screws with $\delta = 0.5$. An analysis of this result indicates that $\eta_{\sigma=0.8}/\eta_{\sigma=1} \approx 1.1$ and $\eta_{\sigma=1.2}/\eta_{\sigma=1} \approx 0.925$. Due to manufacturing considerations, Nagel proposed to consider $\sigma = 1$ as a fixed ratio (constant) and the inclination angle as a parameter to optimize [36]. The $\sigma = 1$ is proven as a correct ratio for ASPs with three blades and inclination angles up to 35° [31]. Lashofer et al. confirmed that two-thirds of ASG installations follow this ratio and the rest utilized larger variations, most likely as a result of the installation conditions [36].

As a general analytical method to estimate the Archimedes screw outer diameter based on the volumetric flow rate for all ASG inlet depths, Eq. (6-14) could be applied for $\delta = 0.5$, $\sigma = 1$, $\theta = 3/7$ and the corresponding η value of each dimensionless inlet depth.

The observations above can be used to determine an overall relationship between volume flow rate and outer diameter for a screw. The general form of Eq. (6-15) is:

$$D_o = \eta Q^{3/7} \quad (6-16)$$

where η is a constant accounting for screw geometry and fill level. Assuming the commonly used values of $\delta = 0.5$ and $\sigma = 1$, a value of η can be determined for each dimensionless inlet depth,

which is turn is related to volume flow rate.

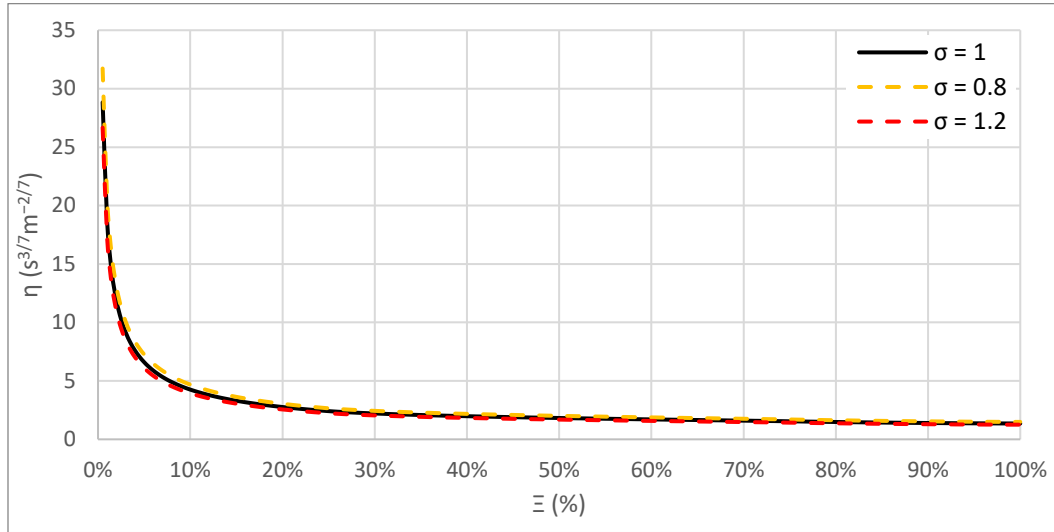


Figure 6.2: Comparison of Eq. (6-14) results for $\delta = 0.5$ and different σ values.

The resulting analytical equation eliminates a considerable amount of design steps, required calculations and iterative processes, which results in significantly lower computational costs for designing Archimedes screws. For example, for the desired flow rate Q , Eq. (6-16) could be used for Archimedes screws with $\delta = 0.5$, and Figure 6.2 could be used to determine the corresponding η value of each dimensionless inlet depths.

For the common Archimedes screw designs ($\delta = 0.5$ and $\sigma = 1$), Eq. (6-12) and Eq. (6-13) could be simplified even more and represented as:

$$Q = \frac{5}{192} (8\theta_o - 4 \sin 2\theta_o - 2\theta_i + \sin 2\theta_i) D_o^{7/3} \quad (6-17)$$

$$D_o = \left(\frac{192}{5 (8\theta_o - 4 \sin 2\theta_o - 2\theta_i + \sin 2\theta_i)} \right)^{3/7} Q^{3/7} \quad (6-18)$$

Solving the same problem for different ASG inlet fill heights leads to results that are in complete agreement with Eq. (6-16). As an analytical test, using Eq. (6-18) for $\Xi = 50\%$ and $\Xi = 75\%$ leads to the following results, respectively:

$$D_{o_{50\%}} = \left(\frac{64}{5\pi} Q\right)^{3/7} \approx 1.8258 Q^{3/7} \quad (6-19)$$

$$D_{o_{75\%}} = \left(\frac{288}{5(3\sqrt{3} + 5\pi)} Q\right)^{3/7} \approx 1.5440 Q^{3/7} \quad (6-20)$$

6.2.2 Case studies

The evaluation criteria are presented in appendix. Table 6.1 provides a detailed list of the Archimedes screw hydro powerplant installations that are used for evaluation purposes in this paper. Table 6.1 is a compilation of published data from multiple sources. References for each plant are listed in this table.

Table 6.1: Details of Archimedes screw hydropower plants used for model evaluation.

ID	Name	D _o (m)	H (m)	Q (m ³ /s)	P (kW)	Note	Ref.
1	Haddo	1.4	5	0.5	15.9	*	[276], [277]
2	Indore	1.4	5.3	0.6	19	*	[276], [277]
3	Mühlen	1.5	3	1	21	*	[276], [277]
4	Bischofsmais	1.6	3.16	1	21	*	[276], [277]
5	Gennkikungou	1.6	1.05	0.99	7.3	*	[276], [277]
6	Herrenhof	1.6	2.1	0.9	13.9	*	[276], [277]
7	Schnaittach	1.6	1.35	0.8	7.5	*	[276], [277]
8	Vierhöfen	1.6	1	1.2	8	*	[276], [277]
9	St. Michael	1.7	3.2	1.2	26.92	*	[276], [277]
10	Vadodara	1.7	5	1	33	*	[276], [277]
11	Eitting	1.8	3.57	1.2	29	*	[276], [277]
12	Erding	1.8	1.75	1.2	13.9	*	[276], [277]
13	Flatford Mill	1.9	1.1	1.6	12.6	*	[276], [277]
14	Niedermühle	1.9	3.17	1.5	33	*	[276], [277]
15	Gescher	2	3.45	1.8	46	*	[276], [277]
16	Yvoir	2.1	1.8	2	26	*	[276], [277]

17	Colditz	2.2	3	1.5	33	*	[276], [277]
18	Ahornweg	2.3	1.45	2	21		[278]
19	Solvay	2.3	2	2.5	35		[138]
20	Stimpfach	2.3	2.55	2.3	44	*	[276], [277]
21	Linton Falls	2.4	2.7	2.6	50		[135]
22	Untermünkheim	2.4	1.8	2.5	31	*	[276], [277]
23	Turbury Mill	2.5	2.1	2.8	43	*	[276], [277]
24	Dautphetal	2.6	2.55	2.5	45.8	*	[276], [277]
25	Hannoversch-Münden	2.8	2.6	2	35.455		[279]
26	Wiener Neustadt	2.8	4.05	3.5	98	*	[276], [277]
27	Pilsing	2.9	3.6	3.2	8	*	[276], [277]
28	Linton Plant	3	3.2	4.5	110	☆	[1], [65]
29	Low Wood	3	7.2	4	200		[135]
30	Marengo	3	1.6	3.7	51		[139], [140]
31	Baiersdorff	3.2	1.5	4.5	48.1	*	[276], [277]
32	Crescenzago	3.2	2.1	5	75		[278]
33	Hausen	3.4	5.8	6	250	*	[276], [277]
34	Hausen III Neumatt	3.4	5.8	5.5	235		[278]
35	Kirchberg	3.4	2.97	6	130	*	[276], [277]
36	Shanes Castle	3.4	5	5.5	192	*	[276], [277]
37	Radyr	3.5	3.5	11	200		[134]
38	Maple Durham	3.6	1.73	8	99	*	[276], [277]
39	Wien	3.6	1.7	7.1	84	*	[276], [277]
40	Totnes	3.7	3.45	6.5	160		[280]
41	Künzelsau	4.1	1.72	8.95	132		[278]
42	Plana	4.1	3.5	8.73	220		[278]
43	Gunthorpe Weir	4.3	2.03	14.15	165		[281]
44	Ham	4.3	10	5	360		[278], [282]
45	Höllthal	4.3	2.22	10.5	220		[278], [283]
46	Olen	4.3	10	5	360		[278], [282]
47	Hasselt	5	10	5	400		[45], [70]
48	Widdington Plant	5	3	14.5	335	☆	[1], [65]

Notes: * Used in Dragomirescu [276]; ☆. Two different Archimedes screws installed in Linton Lock hydropower plant.

6.3 Results and Analysis

To find the most representative dimensionless fill height for the current Archimedes screw installations (Table 6.1), Eq. (6-16) was used to compute all η values for the full range of

dimensionless fill heights (Ξ). Then a numerical experiment was performed to estimate the overall diameter of the Archimedes screw hydro powerplant installations that are represented in Table 6.1 by using Eq. (6-16). Technically, the highest agreement of the studied cases with the equation results where there is the minimum difference between the estimations and the actual observations. As shown in Figure 6.3, the minimum relative difference of MAPE = 2.31% occurs when $\Xi = 69\%$, with a resulting value of η of 1.61. Therefore, this η value was used for the rest of the investigation.

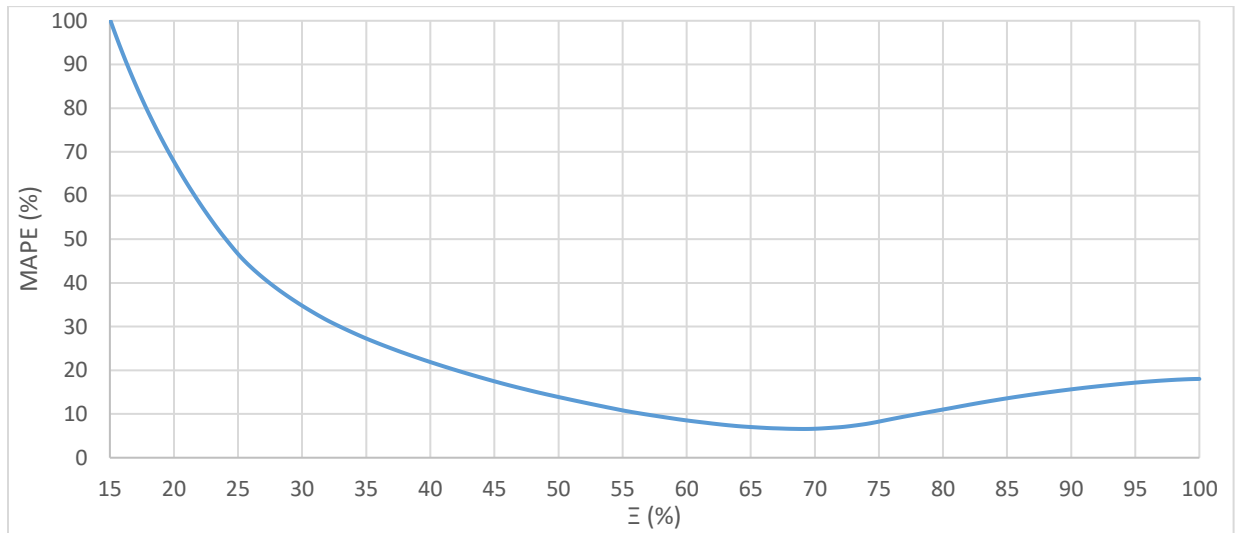


Figure 6.3: Results of Eq. (6-16) for the whole range of the dimensionless inlet depth of the screw (Ξ) values in comparison with the currently installed ASG designs of Table 6.1.

Figure 6.4 shows the outer diameter for each plant in Table 6.1 compared to the corresponding outer diameter predicted using Eq. (6-16) with $\eta = 1.61$. The evaluation of the proposed analytical equation indicates a reasonable accuracy for the developed equation by a correlation high as high as $R = 91.80\%$ and a relative difference as low as $MAPE = 6.58\%$ on average. In these results, the point with highest relative difference is the Hannoversch Münden multi-ASG hydropower plant which has a unique design allowing 0° to 28° adjustable inclination angle for

(6-16), the slightly better performance in term of some evaluation criteria, as well as its significant ease of use may make Eq. (6-16) more practical. Eq. (6-16) is developed based on a strong theoretical basis that makes it a general equation. Moreover, evaluation of Eq. (6-16) with a wide range of different cases indicates a reasonable accuracy. Finally, using the Dragomirescu method requires predefining the number of blades (N) and length (L) or the inclination angle (β) of screw even for initial estimations while Eq. (6-16) may be used without requiring these variables as outlined below.

6.4 Analytical Method for Designing Archimedes Screws

This section proposes a rapid and simple method to estimate the design properties of Archimedes screw generators based on the analytical equations that are proposed in this study. The step-by-step design process for the Archimedes screw is:

- (1) Determine the site properties: available volumetric flow rate (Q), head (H) and the inclination angle of the Archimedes screw (β). Lashofer et al. [36] confirmed that many current industrial ASGs are installed at $\beta = 22^\circ$ [36].
- (2) Use Eq. (6-3) to determine the Archimedes screw's length.
- (3) Use Eq. (6-11) to determinate the overall (outer) diameter D_o of the Archimedes screw based on the desired ω , δ , σ and Ξ values. Or,

Use Eq. (6-16) to design Archimedes screw similar to the current installed ASGs in hydropower plants ($\delta = 0.5$, $\sigma = 1$, $\Xi = 69\%$, $\eta \approx 1.61$ and $\psi = 3/7$). For example, for

$Q = 9 \text{ m}^3/\text{s}$ using Eq. (6-16) results $D_o = 1.61 \times 9^{3/7} \approx 4.128 \text{ m}$. Comparison of the calculated D_o with Table 6.1 indicates that this is a very close outer diameter to the Künzelsau hydropower plant Archimedes screw ($D_o = 4.1 \text{ m}$) which is designed for almost the same flow rate. Or, for $Q = 1 \text{ m}^3/\text{s}$, Eq. (6-18) gives $D_o = 1.61 \text{ m}$ which is almost the same as the average of Bischofsmais, Mühlen and Vadodara ASGs' outer diameters (1.6 m, 1.5 m and 1.7 m respectively).

- (4) Determine the inner diameter (D_i) and screw pitch (S) based on the estimated D_o using the following equations:

$$D_i = \delta D_o \quad (6-21)$$

$$S = \sigma D_o \quad (6-22)$$

This method is summarized in the represented flow chart in Figure 6.5.

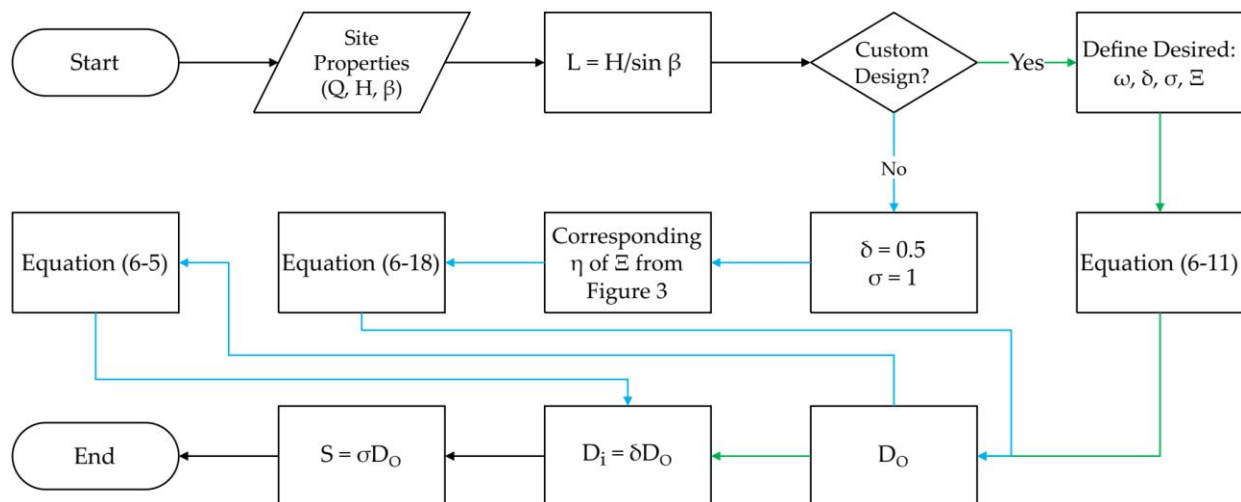


Figure 6.5: The analytical method for designing Archimedes screws.

6.5 Conclusions

This study developed an analytical method to produce a rapid initial estimate of the geometry of an Archimedes screw power plant. Analytical equations were developed based on mathematical, physical and hydraulic facts from the literature. Finally, a general analytical equation is proposed to estimate the overall diameter of the ASG, and a method is proposed to estimate the other design properties of the geometry of the Archimedes screws.

The developed analytical equation has been evaluated by 48 industrial Archimedes screws designed by different manufacturers and currently installed and operating in hydropower plants. For this process, the values of parameters were chosen based on the accepted, proved, reported or observed common aspects of Archimedes screws ($\delta = 0.5$, $\sigma = 1$, $\Xi = 69\%$ and $\psi = 3/7$). This process also led to simplifying the general analytical equation (Eq. (6-12)) into a much simpler form, resulting in a considerably easier and faster to use equation (Eq. (6-16)) that could be used to design Archimedes screw generators in a similar basis of current Archimedes screw installations in hydro powerplants.

The evaluation of the proposed analytical equation indicates a reasonable accuracy for the developed equation with a correlation as high as 91.80% and a MAPE as low as 6.61%.

Moreover, results using this equation were compared with Dragomirescu's method results. Both methods are arguably good given the assumptions and small number of variables used in both methods. However, considering the slightly better performance in terms of the evaluation criteria besides the single-equation nature of Eq. (6-16) as well as its significant ease of use, it seems that

Eq. (6-16) is more practical. The strong theoretical basis of Eq. (6-16) results in a general and potentially more reliable method. Moreover, evaluation of Eq. (6-16) with a wide range of different cases indicates a reasonable accuracy. Eq. (6-16) does not require to predefining of the number of blades (N) and length (L) or the inclination angle (β) of screw for initial estimations, which makes it easier to use for initial estimates.

The proposed analytical equation not only showed a reasonable accuracy based on the evaluations but also simplifies and could eliminate several design steps and loops and accelerate the design of Archimedes screws.

6.6 Nomenclature

A_E	: Effective cross-sectional area at the screw's inlet	(m ²)
A_{Max}	: Maximum cross-sectional water area at the screw's inlet	(m ²)
A_O	: The outer diameter's cross-sectional area	(m ²)
a	: Coefficient of dimensionless flow rate	(-)
b	: Coefficient of dimensionless area constant	(-)
c	: Coefficient of dimensionless rotation speed constant	(-)
D_i	: The inner diameter of the Archimedes screw	(m)
D_O	: The outer diameter of the Archimedes screw	(m)
E_i	: The estimated value	
\bar{E}	: The average of the estimations	
f	: Fill height of water in a bucket of screw	(-)
G_w	: Gap width (The gap between the trough and screw)	(m)
h_u	: Upper (inlet) water level of the screw	(m)
h_L	: Lower (outlet) water level of the screw	(m)
H	: The available head	(m)
L	: The total length of the screw	(m)
$MAPE$: The mean absolute percentage error	(%)
n	: The number of data points in the dataset	
N	: Number of helical plane surfaces	(-)
O_i	: The observed value	
\bar{O}	: The average of the observed data	
PE	: The percentage (percent) error	(%)
Q	: Total flow rate passing through the screw	(m ³ /s)

Q_{Max}	: The maximum flow rate that could pass through a screw when $\omega = \omega_M$ and $A_E = A_{Max}$	(m^3/s)
Q_O	: The volumetric flow rate that passes through the cross-sectional area of A_O at the speed of V_T .	(m^3/s)
r	: Radios	(m)
R	: Pearson correlation	(%)
S	: Pitch of the screw (Distance along the screw axis for one complete helical plane turn)	(m)
V_T	: Axial transport velocity	(m/s)
y	: The cross section fill height	(rad)
Z_U	: The free surface elevations at the upstream	(m)
Z_L	: The free surface elevations at the downstream	(m)
β	: The inclination angle of the screw	(rad)
δ	: The screw's inner to outer diameter ratio (D_i/D_o)	(-)
η	: The constant accounting for screw geometry, rotation speed and fill level in the power function form of the diameter equation	($s^{3/7}m^{-2/7}$)
θ	: Angle of sector	(rad)
σ	: The screw's pitch to outer diameter ratio (S/D_o)	(-)
Ξ	: The dimensionless inlet depth of the screw	(-)
ψ	: The value of power in the power function form of diameter equation	(-)
ω	: The rotation speed of the screw	(rad/s)
ω_M	: The maximum rotation speed of the screw (Muysken limit)	(rad/s)

Subscripts

i	: inner
min	: minimum
Max	: Maximum
O	: Outer

7 Design Guideline for Hydropower Plants Using One or Multiple Archimedes Screws

Adapted from:

A. YoosefDoost and W. D. Lubitz, “Design Guideline for Hydropower Plants Using One or Multiple Archimedes Screws,” *Processes*, vol. 9, no. 12, p. 2128, 2021, doi: 10.3390/pr9122128.

Thesis Author’s Contribution:

This article is an original research article that were written by Arash YoosefDoost [3]. Some parts of this chapter are adapted from an original literature review article that was written by Arash YoosefDoost [1]. The figures are all original, or from explicitly referenced sources.

7.1 Introduction

Operating ASGs at their most mechanically efficient operating condition is not necessarily the most financially efficient solution since it may not essentially lead to generating the highest amount of overall energy [49]. When there are large fluctuations in flow rate, or when the conditions are not perfect for a single fixed speed screw, using variable-speed ASGs or installing more than one screw are ways to potentially better utilize available flow at a wider range of sites. Using more than one ASG may lead to easier maintenance, more flexible operation plans and utilize the available volume of flow more efficiently. However, there are still no general guidelines

with minimal computational costs for designing Archimedes screw power plants utilizing one or more than one Archimedes screws.

This study focuses on addressing this important concern by offering a simple method for quick, rough estimations of the number and geometry of Archimedes screws in considering the installation site properties, river flow characteristics, and technical considerations. It provides an update to the YoosefDoost and Lubitz (2021) analytical method for designing ASGs by introducing slightly different equations based on the same concept to offer a simpler graphical approach that accelerates and eases the design of single and multi-ASG hydropower plants' initial design estimations. The new graph offers three times more ASG design combinations that not only cover standard designs but also simplifies custom designs. Then a simple method for quick rough estimations of the number and geometry of Archimedes screws is proposed considering the installation site properties, river flow characteristics, and technical considerations. This study also provides an update to the new ASG records to provide a better understanding of the advancements and the current possibilities in this technology. A list of currently operating industrial multi-Archimedes screw hydropower plants is compiled to support the exploration of the common design properties that are used by different manufacturers. This study helps us to improve one of the biggest burdens of small projects, the unscalable initial investigation costs, by enabling everyone to evaluate the possibilities of green and renewable Archimedes screw hydropower generation where a flow is available.

7.2 Methods and Materials

7.2.1 Design Parameters of Archimedes Screws

For Archimedes screw generators, it can be shown that the head (H) is the difference of free surface elevations upstream (Z_U) and downstream (Z_L) of the screw relative to the same datum ($H = Z_U - Z_L$) [2]. Therefore, the screw length (L) will be:

$$L = H / \sin \beta \quad (7-1)$$

The inclination angle of the Archimedes screw (β) may be limited by the geometry or slope of the installation site. However, Lashofer et al. [36] confirmed that many current industrial ASGs are installed at $\beta = 22^\circ$ [36]. Inclination angles less than about 20° increase the length of screw and more than 30° considerably decrease the capacity of the screw [1].

Increasing the inclination angle also leads to a faster occurrence of the overflow leakage and increasing gap leakage. These issues could be managed by increasing the number of blades [284]. Based on CFD simulations in conjunction with laboratory-scale experiments, Dellinger et al. proposed that for their particular setup, the optimal inclination angle for $N = 3$ is about 15.5° . The maximum efficiency of the four- and five-bladed screws occur in inclination angles between 20° and 24.5° , and the highest power was achieved for $N = 5$, although it was only marginally higher than $N = 4$ [284]. However, due to the thickness of the blades, more blades come at the cost of reducing the bucket sizes as well as increasing manufacturing costs and challenges. Modern ASGs usually utilize three or four helical blades ($N=3$ or 4). A survey of operating ASG power plants in the UK found that $N = 4$ was the most common configuration [285]. Lashofer (2012) observations

indicate that for most of Archimedes screw installations $N = 3$ [36]. Based on Lyons (2014) experimental observations, there is a considerable reduction in ASGs' performance for $N = 2$ [286]. Rosly et al. (2016) based on CFD simulations of non-rotating screws reported that the number of helix turns (lower is better) are more important than the number of blades so that, the screws with three helix-turns and $N = 3$ showed the highest efficiency [287]. Lyons (2014) and Songin (2017) reported that experimental observations showed no significant increase in the Archimedes screw generators' efficiency for $N > 3$ [286], [288]. Based on these observations, Dragomirescu (2021) concluded $N = 3$ as the optimal number of blades [276].

7.2.2 Archimedes Screws Configurations in Hydropower Plants

It is most common to have only one Archimedean screw installed in a power plant. However, two or more Archimedes screws can be installed in series or parallel to deal with technical limitations, increase the overall energy generation, easier maintenance, or more flexible operation plans. Multiple screws can be configured in series or parallel.

7.2.2.1 Archimedes Screws in Series Configuration

The idea of installing Archimedes screw pumps (ASPs) in series to pump the fluids into higher levels has been used in practice for a long time (e.g., [31, p. 18]). However, installing ASGs in series to take advantage of low flow rate but high heads is not very usual. For higher heads, it is most common to utilize other hydropower technologies, often in combination with a long penstock. However, most hydropower turbines cannot safely pass sediment or larger objects such as living organisms, especially fish. Therefore, one can see Archimedes screws as long as 30 m [70] that are currently installed and in operation (Table 7.1). However, technical limitations such as bending

of long shafts, weight limits of bearings, etc., can limit the maximum length of Archimedes screws. For example, for the two 19 m-long Archimedes screws in the Low Wood project, there is a significant engineering challenge supporting the considerable length and weight of the screw (40 tons) just with bearings at two contact points, one at the top and one at the bottom of the screw [135]. To deal with such limitations, theoretically, several ASGs could be installed in series instead of a very long screw, potentially as a chain of hydropower plants alongside a river or channel [1]. Such a configuration allows utilization of Archimedes screws at locations with an available high head when the available volume of flow rate is low.

Table 7.1: Hydropower plants using several parallel Archimedes screw generators. All screws at a plant are identical unless otherwise noted. Power and flow values are for a single screw at the plant: multiply by the number of screws for total plant flow and power.

Name	No. of ASGs	D_o (m)	H (m)	Q (m ³ /s)	P (kW)	Location (River)	Ref.
Totnes	2	3.7	3.45	6.5	160	Dart, UK	[280]
Hannoversch-Münden	2	2.8	2.6	2	35.455	Werra, DE	[289]
Low Wood	2	3	7.2	4	200	Leven, UK	[135]
Radyr	2	3.5	3.5	11	200	Taff, UK	[134]
Künzelsau	2	4.1	1.72	8.95	132	Kocher, DE	[278]
Ahornweg	2	2.3	1.45	2	21	Mühlbach, DE	[278]
Linton Falls	2	2.4	2.7	2.6	50	Trent, UK	[135]
Niklasdorf/Birgl and Bergmeister	2		3.9	3.6	106	Mur, AT	[278]
Hausen III Neumatt	2	3.4	5.8	5.5	235	Wiese, DE	[278]
Höllthal	2	4.3	2.22	10.5	220	Alz, DE	[283]
Gunthorpe Weir	2	4.3	2.03	14.15	165	Trent, UK	[281]
Solvay	2	2.3	2	2.5	35	Saja, ES	[138]
Linton Lock	Linton Plant	2	3	3.2	4.5	Ouse, UK	[1], [65]
	Widdington Plant	5	3	14.5	335		
Plana	3	4.1	3.5	8.73	220	Vltava, CZ	[278]
Crescenzago	3	3.2	2.1	5	75	Lambro, IT	[278]
Olen	3	4.3	10	5	360	Albert Canal, BE	[278], [282]
Ham	3	4.3	10	5	360	Albert Canal, BE	[278], [282]
Hasselt	3	5	10	5	400	Albert Canal, BE	[45], [70]
Rosko	6		1.7	4.5	60	Noteć, PL	[278], [290]
Steinsau	6		1.4	3	30	Ill, FR	[278]
Marengo	6	3	1.6	3.7	51	Goito, IT	[139], [140]

7.2.2.2 Archimedes Screws in Parallel Configuration

The parallel installation of ASGs is the most common configuration in multi-ASG hydropower plants, especially where the volume of flow in a river is so high that a large ASG is required to make use of that amount of water or when the fluctuations in river volumetric of flow rate are considerable. Using several screws in parallel could lead to preventing the technical limitations of a large screw and offers easier maintenance, as well as more flexible operation plans besides taking advantage of a wider range of flow rates that could lead to an increase in the overall energy generation.

7.2.3 Case Studies

Analysis of current ASG power plants could help in finding common patterns, governing rules and important design points to make guidelines. Table 7.1 details current hydro power plants using more than one Archimedes screw installed in parallel. Based on the available data of the operating industrial screws, the relationships between the overall diameter of the screws, flow rate, available hydraulic power and the claimed power by the manufactures were analyzed and the results represented graphically and as empirical equations.

7.3 Results and Discussion

7.3.1 Volumetric Flow Rate and Diameter of Archimedes Screws

According to Table 7.1, current multi-ASG hydropower plants were identified that are designed for the minimum, maximum, and average total flow rates of 4, 28.3 and 14.5 (m³/s), respectively, for a wide range of hydraulic heads between 1.4 m to 10 m. Also, the minimum, maximum and

average diameter of installed Archimedes screws in these plants ranges from 2.3 m to 5 m, with an average of about 3.58 m. This is a wide range of diameters per cubic meter of flow rate (between 0.3 m/m³/s to 1.4 m/m³/s and 0.71 m/m³/s on average). Studies showed that in addition to the screw diameter, the inlet depth and rotation speed are also important factors in the volumetric flow rate of ASGs [6].

Figure 7.1 compares the volumetric flow rate and diameter of installed screws in hydropower plants listed in Table 7.1. The same size screws are installed in all these hydropower plants except at Linton Lock, where the two screws are different sizes. It is worth mentioning that, as discussed, ASGs could be used to upgrade or retrofit the current developments. The Linton Lock power plant is an example of a second ASG installed later as an upgrade.

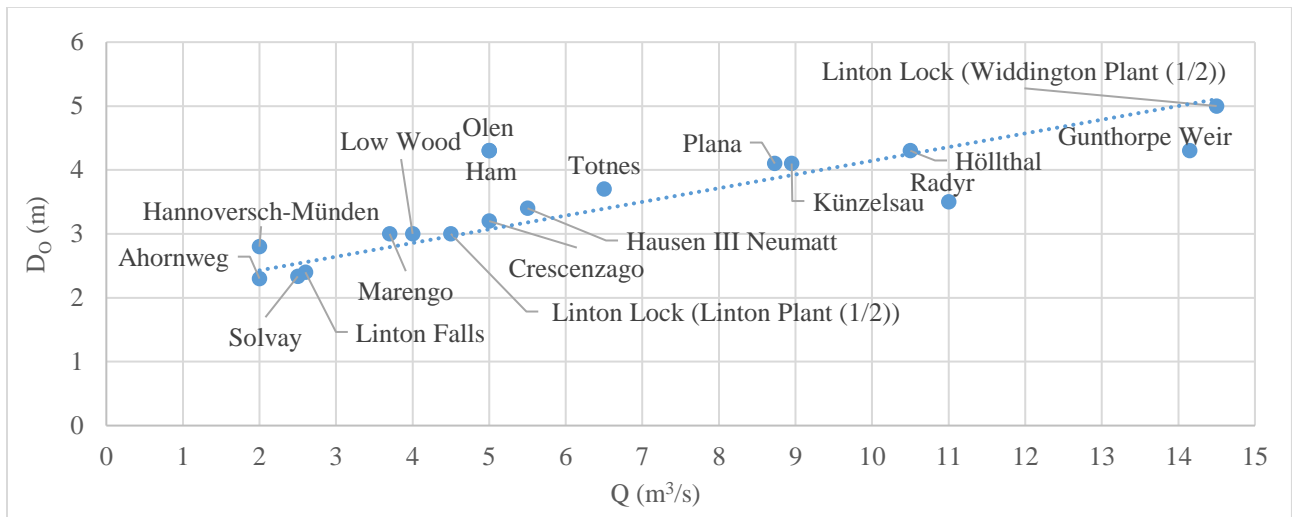


Figure 7.1: Comparison of the volumetric flow rate and diameter of installed screws in hydropower plants listed in Table 7.1. All values above are for a single screw.

According to Figure 7.1, many multi-ASG designs follow a relatively similar trend. For the current multi-ASG hydropower designs, the relationship between the flow rate (Q) and diameter of the

screw (D_o) can be described linearly as follows. In this relationship, the coefficients are optimized using genetic algorithm and the represented case studies in Table 7.1:

$$D_o = 0.2 Q + 2.2 \quad (7-2)$$

where D_o must be in meters, and Q must be in m^3/s . This equation relates the Archimedes screw outer diameter (D_o) and passing volumetric flow rate (Q) with reasonable accuracy ($R = 69.81\%$, $MAPE = 10.59\%$).

The relationship between the flow rate (Q) and diameter of the screw (D_o) can also be described as the following power function. In this relationship, the constants are optimized using Generalized Reduced Gradient (GRG) algorithm [291], [292] and the represented case studies in Table 7.1:

$$D_o = 1.76 Q^{0.386} \quad (7-3)$$

This equation relates the Archimedes screw outer diameter (D_o) and passing volumetric flow rate (Q) with reasonable accuracy ($R = 74.68\%$, $MAPE = 7.52\%$).

7.3.2 Power and Diameter of Archimedes Screws

The available hydraulic power could be calculated by the following equation:

$$P_H = \gamma H Q \quad (7-4)$$

Figure 7.2 compares the potential available hydraulic power that is calculated using equations with the power that manufacturers estimated that their Archimedes screw designs could generate (Table 7.1). In this figure, all values are for a single screw, which are determined by dividing plant power by the number of screws, except at Linton Lock, where the two screws are different sizes.

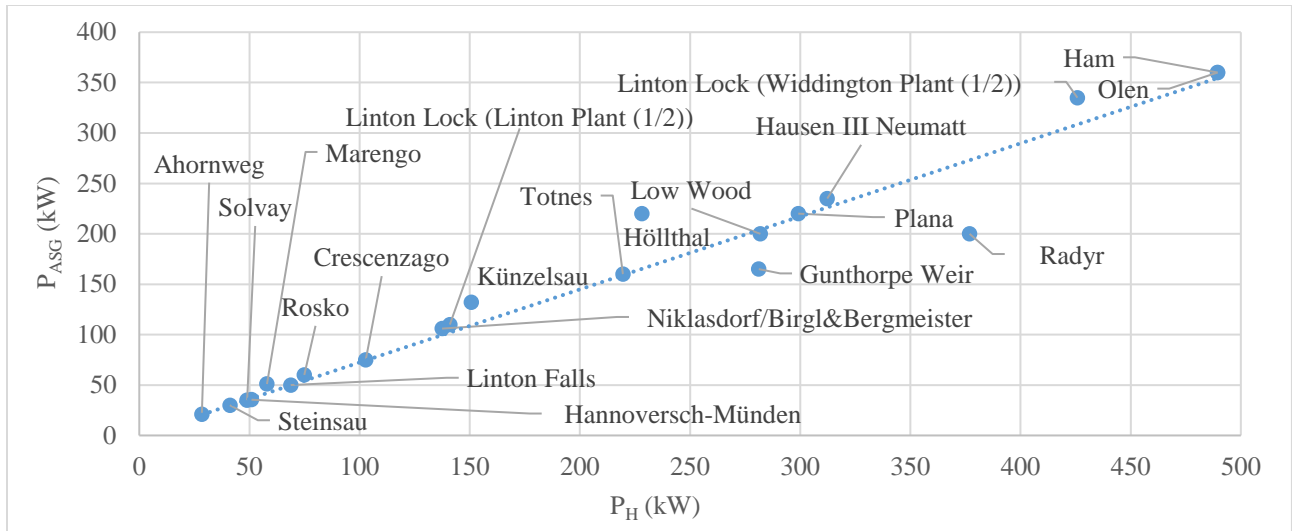


Figure 7.2: The theoretical available power vs. the power of installed screws published by manufacturers in current Archimedes screws hydropower plants represented in Table 7.1.

The efficiency of ASGs depends on many variables, including but not limited to the screw’s design, installation, operation condition, fill height, rotation speed, etc. [1]. Typically, ASG water-to-wire efficiency is reported between 60% to 80% [52]. However, some studies reported hydraulic efficiencies of more than 80% in full-load and as high as 94% in partial-load situations [53]. Nonetheless, with reference to Figure 7.2, many of the studied designs follow a relatively similar trend that could be described as:

$$P = \eta\gamma HQ \quad (7-5)$$

where γ is the specific weight of water and H is the available hydraulic head. Using GRG algorithm and the represented case studies in Table 7.1 to optimize the η as a coefficient indicates that for $\eta = 0.736$ the Eq. (7-5) results are in good agreement with the case studies ($R = 97.78\%$, $MAPE = 7.90\%$). Since the available hydraulic power at a site is the product of head and flow (Eq. (7-4)), the coefficient $\eta = 0.736$ in Eq. (7-5) suggests that the average efficiency of the plants based on the manufacturer’s specifications in Table 7.1 is 73.6%, which is consistent with expectations from

the literature. These results of estimated power by Eq. (7-5) in comparison with the reported power by the manufacture that also visualized in Figure 7.3. In this figure, all estimated values are computed for a single screw, and the actual power is determined by dividing plant power by the number of screws except at Linton Lock, where the two screws are in different sizes.

Figure 7.4 compares the theoretical available hydraulic power (P_H) and the diameter of the Archimedes screw designs represented in Table 7.1. Since the size of screws is the same in almost all power plants, each point represents an ASG hydropower plant, and the number of installed screws is represented in the parentheses in front of each power plant. The only exception is for Linton Lock, where the size of two installed screws is different. Therefore, these screws are distinguished by marking them as (1 of 2).

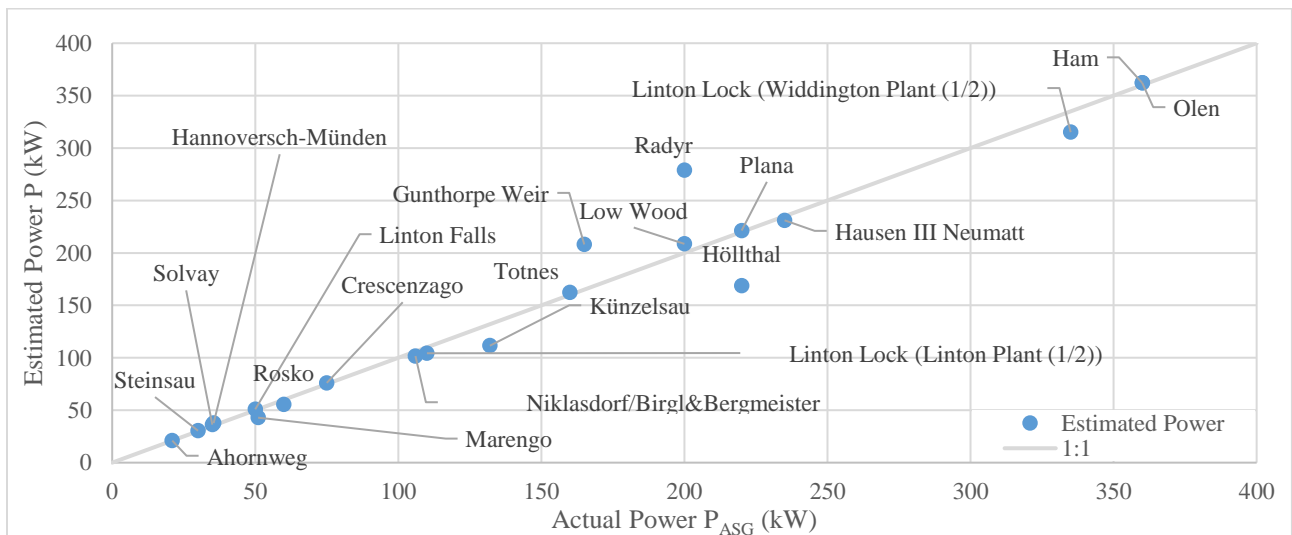


Figure 7.3: Comparison of the estimated power of each screw vs. the power of each installed screws in ASG hydropower plants.

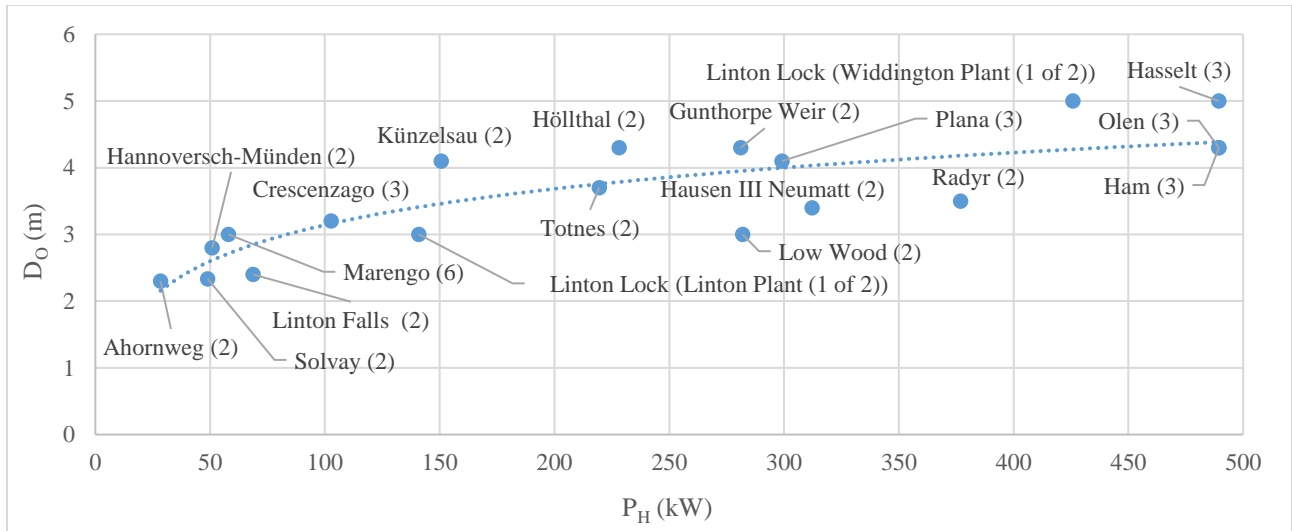


Figure 7.4: The theoretical available power vs. the diameter and number of installed screws in current hydropower plants represented in Table 7.1.

According to Figure 7.4, the relationship between the available power and diameter of these Archimedes screws could be defined in the form:

$$D_o = \lambda(\gamma HQ)^\psi \quad (7-6)$$

By using the genetic algorithm (GA) and Table 7.1 to optimize the constants λ and ψ results in values of $\lambda = 0.213$ and $\psi = 0.232$ providing reasonable accuracy for these cases ($R = 83.28\%$, $MAPE = 10.64\%$ and $MPE = 1.52\%$).

7.3.3 Analytical Equation

YoosefDoost and Lubitz (2021) developed a concept to define the maximum available area of the screw entrance for any inlet water level, which was called the effective area (A_E) [6]. The required parameters to define A_E are represented in Figure 6.2.

Using the concept of effective inlet cross-section area [6], YoosefDoost and Lubitz (2021) offered an analytical equation to estimate the overall (outer) diameter of the screw (D_o) based on the volumetric flow rate (Q) for the desired rotation speed (ω) [2]:

$$D_o = \sqrt[3]{\frac{16\pi}{\sigma\omega(2\theta_o - \sin 2\theta_o - \delta^2(2\theta_i - \sin 2\theta_i))}} Q \quad (7-7)$$

The simplicity, efficiency and lower cost per watt of single-speed screws make them advantageous in a steady flow [1]. Single-speed Archimedes screws can operate in a partially full condition even if the flow rate is not sufficient to fill the screw at its operation speed [49]. The variable-speed screws are recommended to increase the power generation when the flow varies, as well as if hydropower is the sole source of electricity or for off-grid power plants [1]. Lashofer et al. studies [36] showed that many current industrial ASGs are designed with a rotation speed close to the maximum rotation speed recommended by Muysken (ω_M) [83]:

$$\omega_M = \frac{5\pi}{3D_o^{2/3}} \quad (7-8)$$

Therefore, for full-scale Archimedes screws running at a fixed rotation speed near ω_M , Eq. (7-7) could be simplified as:

$$D_o = \left(\frac{48}{5\sigma(2\theta_o - \sin 2\theta_o - \delta^2(2\theta_i - \sin 2\theta_i))} Q \right)^{3/7} \quad (7-9)$$

Eq. (7-9) could be represented in the form of a power function such as $D_o = \lambda Q^\psi$. Studies showed that for most ASG power plants $\delta = 0.5$ and $\sigma = 1$ [2], [31], [36]. By defining $\Theta =$

$5\sigma(2\theta_0 - \sin 2\theta_0 - \delta^2(2\theta_i - \sin 2\theta_i))/48$ the values of λ and ψ will be equal to $\theta^{-3/7}$ and $3/7$ respectively and Eq. (7-9) could be represented in a much simpler form:

$$D_o = \theta^{-3/7} Q^{3/7} \quad (7-10)$$

$$Q = \theta D_o^{7/3} \quad (7-11)$$

The θ values for different δ and σ for a full range of dimensionless inlet depths (Ξ) could be determined by using Figure 7.5. Studies indicates that Eq.(7-10) has the minimum relative difference with the current operating industrial ASG installations ($\delta = 0.5$ and $\sigma = 1$ [2], [31], [36]) for $\Xi = 69\%$ [2] where $\theta = 0.32918$.

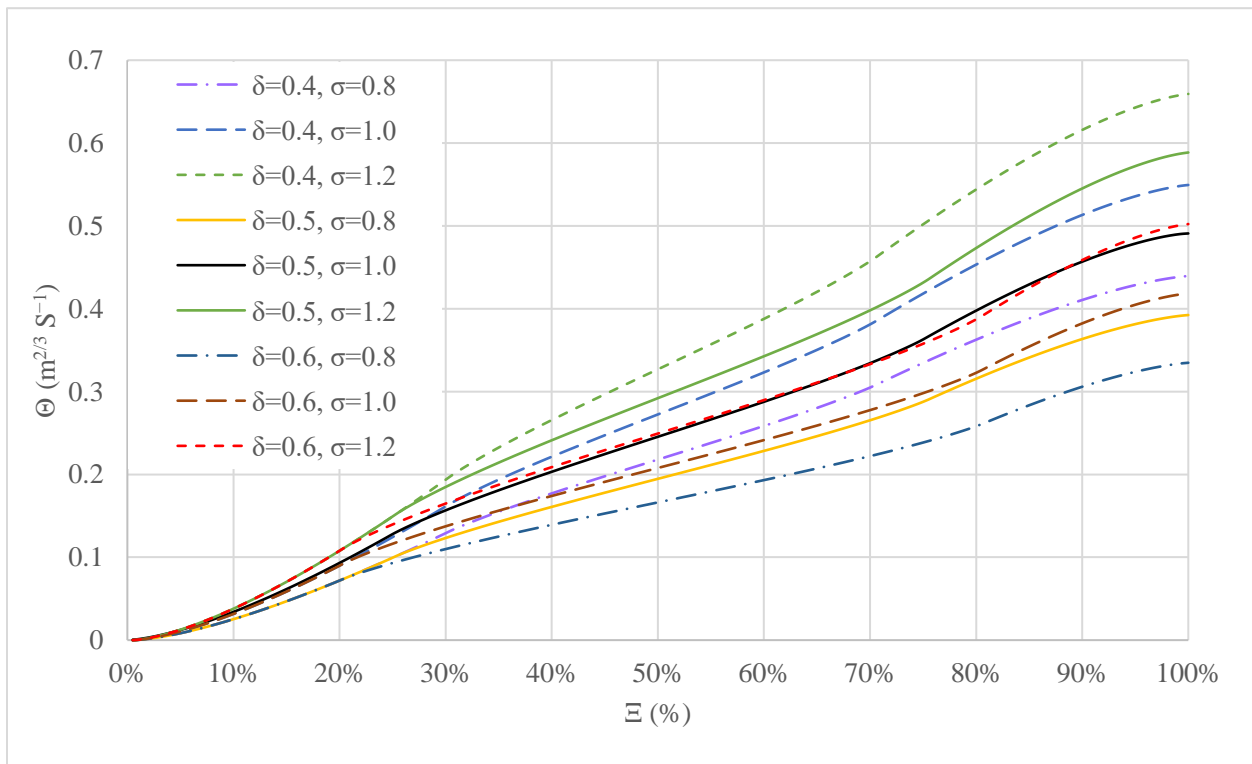


Figure 7.5: The corresponding θ of different δ and σ for a full range of Ξ .

7.3.4 Evaluation of the Developed Equations

Eq. (7-6) and Eq. (7-10) could be represented in a simplified form by applying the represented values of λ and ψ constants in Equation (8) and Θ in the analytical Eq. (7-10). The simplified version of the developed empirical Eq. (7-2) and Eq. (7-6), as well as the analytical Eq. (7-10), besides the evaluation results for Archimedes screws based on the evaluation criteria, are summarized in Table 7.2. Results of each equation for these cases are also visualized in Figure 7.6.

Table 7.2: Evaluation of equations based on the evaluation criteria.

Equation No.	Equation	R (%)	MAPE (%)
(7-12)	$D_o = 0.2 Q + 2.2$	69.81	10.59
(7-13)	$D_o = 1.76 Q^{0.386}$	74.68	7.52
(7-14)	$D_o \approx 1.796(HQ)^{0.232}$	83.28	10.64
(7-15)	$D_o \approx 1.61 Q^{3/7}$	74.38	9.69

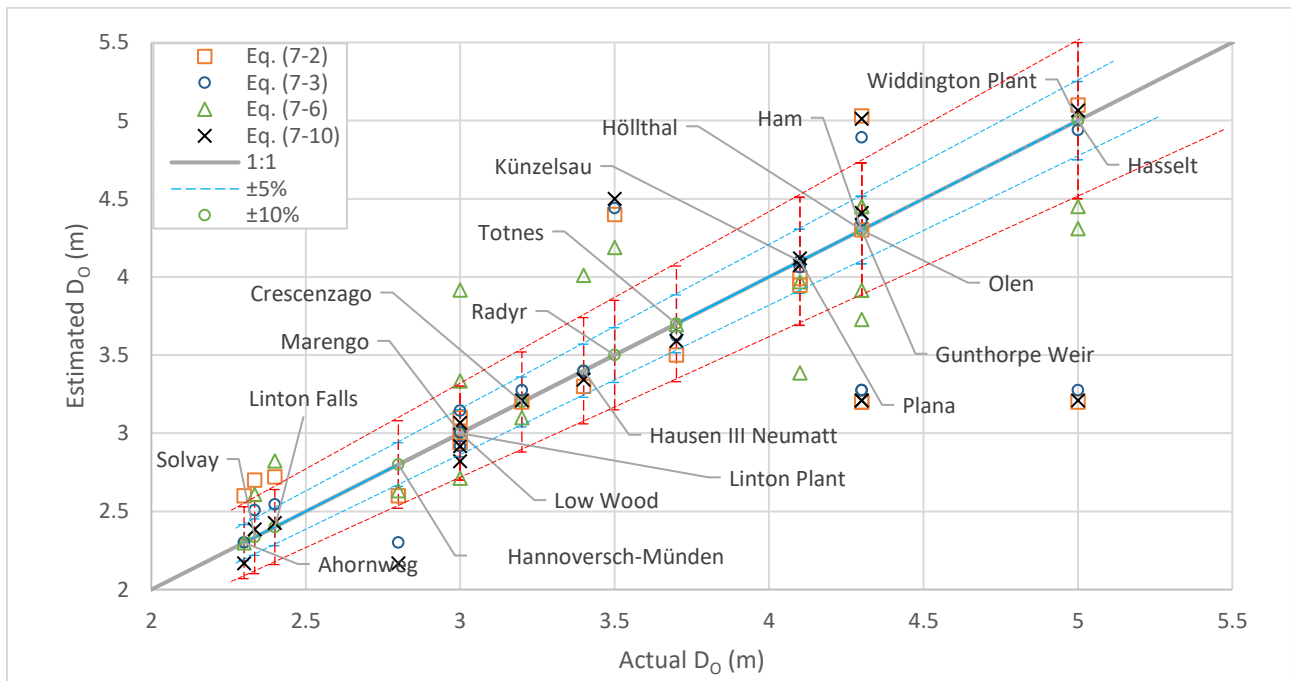


Figure 7.6: Graphical comparison of Eq. (7-2), Eq. (7-6) and Eq. (7-10) estimations vs. actual overall diameter of ASG installations.

According to Table 7.2, Considering the small number of variables required for these equations, all of them indicate arguably reasonable results. The empirical Eq. (7-6) shows the highest correlation with the case studies. In term of relative difference, empirical Eq. (7-16), then analytical Eq. (7-10) shows the highest agreement with the current ASG installations. However, empirical Eq. (7-2), Eq. (7-17) and Eq. (7-6) are optimized for the case studies and it may affect the generality of these equations and limit them to these case studies. In contrast, the analytical Eq. (7-10)'s strong theoretical basis makes it presumably more reliable and also general.

According to Table 7.2, Eq. (7-10) estimations have the lowest relative difference with the case studies represented in Table 7.1. In addition, Figure 7.6 indicates many of these estimations are in the range of $\pm 5\%$ of the relative difference. However, in several cases, the estimations fall beyond $\pm 10\%$ of the relative difference: according to this figure, the relative difference of Eq. (7-10)'s estimation for Hannoversch Münden multi-ASG hydropower plant seems considerable. More investigations indicate that this ASG has a unique flood protection design that enables it to have a 0° to 28° adjustable inclination angle to operate under variable tailwater levels. Therefore, it is probable that the published data for this ASG is not under a conventional operation condition [2], [289]. For the Radyr, the manufacturer published details are roughly [134]. For Gunthorpe Weir Hydro Scheme, Q_{95} is reported as 28.33, which is according to the published data used in Table 7.1. However, reviewing the Fisheries and Geomorphology Assessment documents indicates that each screw is designed for $10 \text{ m}^3/\text{s}$ [281]. Using this flow rate and Eq. (7-5) results in much less relative difference for this power plant ($PE = 0.44\%$).

The unique design could be considered as one of the important reasons for the high relative differences between Eq. (7-10) estimations for the Ham and Olen hydropower plants. These screws

are installed on the Albert Channel in Ham and Olen in Belgium. These screw designs are unique not only because of their length (21.6 m) but also because they are compact, switchable Archimedes screws. These screws have a unique design to operate as ASPs (780 kW pumping operation) and ASGs (360 kW power generating operation) [282].

The highest relative difference of Eq. (7-10) estimations is for the longest hybrid Archimedean screws in the world, installed on the Albert Canal in the Hasselt hydropower plant. With the remarkable length of 30 m, these ASGs have the most unique designs in the case studies. A hydraulically operated jacket valve is used to switch from pump and turbine mode. In ASP mode, each of these hybrid Archimedes screws can pump $5 \text{ m}^3/\text{s}$ over a head of more than 11 m (installed power 800 MW) during dry seasons and drain $5 \text{ m}^3/\text{s}$ over a head of 10 m to generate 400 MW of energy in wet seasons [70].

7.4 A Quick Design Guideline for Archimedes Screw Power Plants

In developing hydropower plants, the site and connection assessment expenses, geotechnical, electrical, and civil engineering costs, as well as licensing or approval fees, are among the fixed or semi-fixed soft costs. Many of these activities are carried out just as larger projects. Therefore, regardless of the amount of power that could be generated, these costs are almost the same and so become disproportionate for small projects. For example, these costs are almost the same for 7.2 kW and 150 kW ASG hydropower power plants [293]. However, there are situations that some or several costs could be reduced, at least for initial investigations. For example, when a small dam or weir exists (i.e., upgrade retrofit). Moreover, the results of the analysis of the current multi-ASG

hydropower plants help to make some rough estimations. Here are some guidelines for rough estimations of Archimedes screw hydropower plants:

7.4.1 Design Assessments of Archimedes Screw Hydro Powerplants

In order to design an Archimedes screw hydro powerplant, three important assessments should be done: (1) electricity needs assessment and (2) site assessments. Then, the type of screw (fixed/variable speed) should be determined in (3) plant design assessment.

For the electricity needs assessment, it is recommended to:

- Estimate the required power as well as predict the possible future changes in demand.
- Determine whether the powerplant will be connected to the grid or will be off-grid.
- If the ASG powerplant is designed to be off-grid, it would be important to:
 - Consider the comparison of the value of reliable baseload power versus maximizing the annual production of the powerplant in making decisions for the design.
 - Define and consider the needed voltages and/or currents.

For the site assessment:

- Permitting requirements, restrictions on access or water use should be determined.
- The flow duration curve of the river should be used to determine the baseload and other options for the operation of the powerplant. This information also helps to make decisions in the plant design step.

- Ecological assessments should be done, and the water needs of other users or ecological functions should be determined. For example, the required flow for fish passage or installing a fish ladder should be determined.
- The potential plant location should be selected based on the following considerations:
 - Accessibility for construction, operation, and maintenance. This is important for civil works and installation of the screw, especially for larger powerplants that have big and bulky screw(s) that need cranes for installation
 - Geotechnical concerns, particularly stability and suitability for plant foundations
 - Supply channel and outlet channel routing
 - Conflicts with other site use considerations.

In plant design assessment, the type of plant should be selected based on previous assessments:

- For steady flow, a single-speed plant could be considered as a simpler and more efficient option. On average, the cost per watt of these systems is less than the variable-speed ones. Even if the available flow is not sufficient to fill the screw at its operating speed, fixed speed screws can still generate power in a partially full condition [49].
- For large surplus flow, variable-speed screws could be recommended to generate partial power at low flow times. It would be particularly important if the powerplant will be off-grid, or other power sources (like diesel generators) are not available or are expensive. Generally, variable-speed screws are recommended when there is an excess flow that could be used to generate more power from an available flow of when the flow varies. The main reason is that although operating ASGs at the full capacity may be the most mechanically efficient operating

condition, it will not definitely lead to the highest overall energy generation. Therefore, it may not be the most economically efficient operating condition [49].

For all plant designs:

- A sluice gate to control flow to the plant, and trash racks to prevent large debris from entering the plant, must be planned upstream of the screw. Ease of trash rack cleaning is important.
- Provision to dry out the top and bottom of the screw for bearing inspection, maintenance should be included in the plant design. The sluice gate should be able to shut off all flow. At the outlet, build vertical grooves to hold stop logs to allow drying out of the screw outlet.
- Be sure to plan for flooding water levels, and be sure to protect electrical components from water damage. This could be done by elevating the generator, sealing the powerhouse, and/or putting control equipment on the bank at a higher level.

7.4.2 Determination of the ASG Configuration

- For the known available average flow rate and head, Eq. (7-5) could be used for rough estimations about the possible amount of power that could be generated.
- If the estimated power is less than the requirements, site properties could be checked to evaluate the possibilities of the series configuration of ASGs. e.g., to take advantage of low flow rates but reasonable available heads, ASGs could be installed in series to deal with technical considerations of a very long ASG.

- To take advantage of high flow rates, instead of a very large (in diameter) and heavy ASG, it is possible to install ASGs in parallel. This approach could help to reduce the challenges of technical limitations and offers several advantages.
- For very low flow rates and heads, using industrial pico-ASGs available in the market may facilitate the process or even save some costs. For example, currently, pico-ASGs can generate up to 500 W with a flow rate as low as 0.1 m³/s and 0.7 m of the head (more information is available in [1]). Obviously, several units of such screws could be used in parallel or in series to take advantage of higher flow rates or available heads. For higher flow rates and heads, custom ASGs designs could be more efficient options. For example, Fletcher's Horse World Archimedes Screw can generate up to 7.2 kW using a design flow rate, head and outer diameter of 0.536 m³/s, 1.7 m [294], [295] and 1.39 m [145], respectively.

7.4.3 Estimation of Archimedes Screws Design Properties

1. Determine the site properties: the river's historical data or hydrograph for the volumetric flow rate (Q) and the site geometry to find the appropriate head (H) and the Archimedes screw inclination angle (β). Studies show that many ASGs are installed at $\beta = 22^\circ$ [36].
2. Determine the maximum and minimum overall diameter of the screw (D_{Max} , D_{min}) based on the site properties and the Archimedes screw hydro power plants design assessments proposed in Section 5-1 of [1].
3. Use Eq. (7-1) to determine the screw(s) length.

4. Use the historical dataset of the river's flow rate to determine the flow duration curve (FDC).

The probability that a system will take on a particular value or collection of values could be described by a mathematical expression which is known as a distribution function. The cumulative distribution function (CDF) of a variable for a value is the probability that this variable will take values less than or equal to this value [296]. Therefore, for a time series with n items, for item i with m items equal or bigger than it:

$$p_i = \frac{m}{n} \times 100 \quad (7-18)$$

In an FDC, the horizontal axis p_i represents the percentage of the period that the flow rate is more than or equal to its corresponding flow rate represented in the vertical axis. Usually, the flow exceeding for 95% of the period (Q_{95}) is considered as minimum river flow rate. It is important to note that considering the regulations, hydropower plants may need to bypass a portion of flow for aesthetic, ecological, environmental, or other purposes. This flow is called reserved, residual, compensation, prescribed or hands-off flow and should be deducted from the available flow rates.

5. Use the volume of flow rate that is provided on the flow duration curve (e.g., Q_{95}) and use Eq. (7-10) to estimate the corresponding diameter of the screw for this flow rate (D_o).
6. Check the estimated diameter:
 - If $D_{min} \leq D_o \leq D_{MAX}$, go to step 7.
 - If $D_o < D_{min}$, use a higher volume of flow rate (e.g., Q_{90}) and repeat step 6.
 - If $D_o > D_{Max}$, several approaches could be considered:

- **Identical screws:** divide the volume of flow rate by $i = 2$ and follow the process from step 6. If it ends to $D_O > D_{MAX}$ again, repeat it for $i = i + 1$ until the condition passes. Then use the analytical Archimedes screw design method that is offered in [2] to design the screw. In this approach, “ i ” Archimedes screw generators with the same geometry will be designed to handle this flow rate. The advantage of this approach is that similar screws are easier to build, operate and maintain.
 - **Design based on the maximum diameter:** design the screw for $D_O = D_{Max}$ and use the analytical Archimedes screw design method that is offered in [2] to design the Archimedes screw generator. Then use Eq. (7-11) to estimate the volumetric flow that passes through this screw and design the next Archimedes screw by following the process from step 6 for the remaining volume of flow rate. This approach could lead to reducing the number of Archimedes screws.
 - **Trial and error:** consider a higher probability that means a lower flow rate (e.g., $Q_{97.5}$ instead of Q_{95}) and do and follow the process from step 6 and perform a trial and error. This approach could lead to an increase in the design of Archimedes screw generators with higher reliability in generating power.
7. To utilize the remaining available volumetric flow rate, more Archimedes screws could be designed (parallel ASG power plants). The next flow rate to design the screw could be selected from the FDC based on the desired step size (Δ). For example, for the previous design flow rate of Q_n choose the next flow rate $Q_{n-\Delta}$ which is the flow exceeding for $n - \Delta$ % of the period and continue the design starting from step 5.

8. The design process should be halted based on logical constraints. For example, for economic reasons designing screws for volumetric flow rates less than the certain probability (e.g., Q_{Limit}) is not reasonable. Or, due to site limitations, there may be some restrictions such as the total area of the power plant (the minimum required area to install the Archimedes screw generators is equal to the sum of the diameter times to the length of each screw. If it goes beyond the installation site limitations, some of the screws designed for flow rates with lower probabilities could be cancelled. In such conditions, an optimized larger screw for the flow rates with the highest probabilities or using variable speed screws could be considered as alternative solutions to utilize more flow rate).
9. Use Eq. (7-5) to estimate the possible amount of power that each ASG can generate. Then, estimate the ideal overall power that the Archimedes screw hydropower plant could generate.

$$P_{Overall} = \sum p_i P_i \quad (7-19)$$

Figure 7.7 summarizes this guideline as a flow chart.

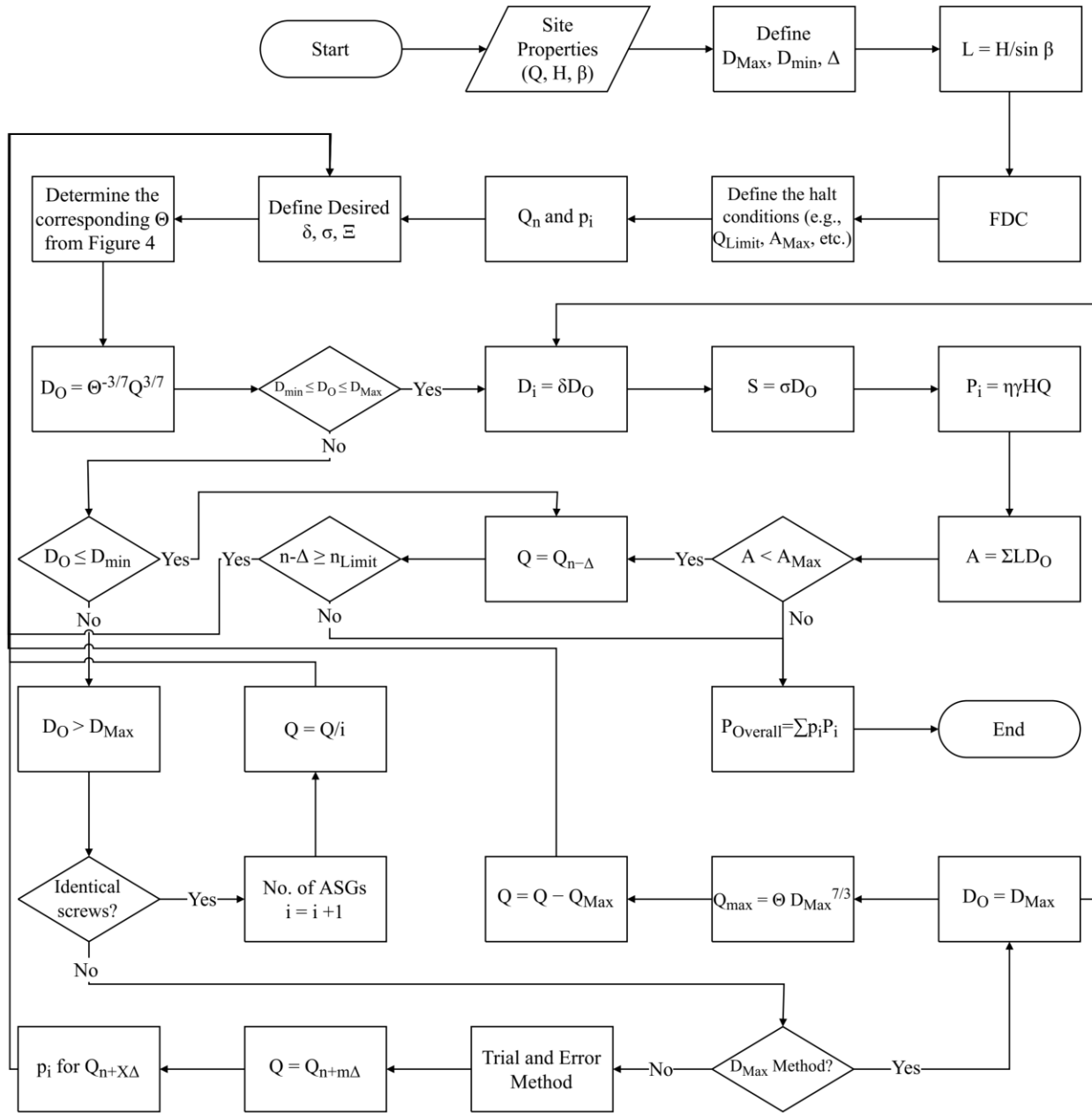


Figure 7.7: The guideline for quick estimations of Archimedes screw power plants design.

7.5 Conclusions

This study focuses on offering a simple method to address the important lack of a general and easy-to-use guideline for designing Archimedes screw power plants using more than one ASG. Then, a detailed design study should be undertaken on the ASGs suggested by this process's estimations. In addition, this study helps to address one of the significant burdens of small projects, the unscalable initial investigation costs.

Moreover, this study updates the records of the currently installed Archimedes screw generators and provides a better understanding of the advancements and the current possibilities in this technology. It also provides a list of currently installed and operating industrial multi-Archimedes screw hydropower plants in order to review and explore the common design properties between different manufacturers. Therefore, several empirical equations are proposed and optimized using the genetic algorithm and generalized reduced gradient. Moreover, this study provides an updated version of a new analytical method for designing Archimedes screws and offers a new graph that not only supports standard designs but also accelerates and simplifies custom designs. The evaluation of these equations with the list of industrial ASG installations provided indicates they have reasonable accuracy.

The proposed method enables everyone to evaluate the possibilities of green and renewable Archimedes screw hydropower generation where a flow is available and helps to make many potential sites feasible to study for this.

7.6 Nomenclature

A_E	: Effective cross-sectional area at the screw's inlet	(m ²)
D_i	: The inner diameter of the Archimedes screw	(m)
D_O	: The outer diameter of the Archimedes screw	(m)
h_u	: Upper (inlet) water level of the screw	(m)
h_L	: Lower (outlet) water level of the screw	(m)
H	: The available head	(m)
G_w	: Gap width (The gap between the trough and screw)	(m)
L	: The total length of the screw	(m)
$MAPE$: The mean absolute percentage error	(%)
n	: The number of data points in the dataset	
N	: Number of helical plane surfaces	(-)
O_i	: The observed value	
\bar{O}	: The average of the observed data	
P_i	: The estimated value	
\bar{P}	: The average of the estimations	
PE	: The percentage (percent) error	(%)
Q	: Total flow rate passing through the screw	(m ³ /s)
r	: Radius	(m)
R	: Pearson correlation	(%)
S	: Pitch of the screw (Distance along the screw axis for one complete helical plane turn)	(m)
y_i	: The fill height of the inner diameter of the screw at the inlet	(m)
y_O	: The fill height of the screw at the inlet	(m)
Z_U	: The free surface elevations at the upstream	(m)
Z_L	: The free surface elevations at the downstream	(m)
β	: The inclination angle of the screw	(rad)
γ	: The specific weight of water	(N/m ³)
δ	: The screw's inner to outer diameter ratio (D_i/D_O)	(-)
η	: The average efficiency of the ASGs based on manufacturer's specifications in Table 7.1 ($\eta = 73.6\%$)	
Δ	: Step size	(%)
Θ	: A constant accounting for screw geometry and fill level	(m ^{2/3} s ⁻¹)
θ	: Angle of sector	(rad)
λ	: The constant value in the power function form	
σ	: The screw's pitch to outer diameter ratio (S/D_O)	(-)
Ξ	: The dimensionless inlet depth of the screw	(-)
ψ	: A constant in the power function form of diameter equation	(-)
ω	: The rotation speed of the screw	(rad/s)
ω_M	: The maximum rotation speed of the screw (Muysken limit)	(rad/s)

Subscripts

i : inner
min : minimum
Max : Maximum
O : Outer

8 Conclusion

The lack of analytical models and methods to design Archimedes screws and guidelines to support the design of Archimedean screw hydropower plants were major unsolved problems for about three decades. The presented thesis outlined the analytical and experimental research that led to solving this important problem by introducing analytical equations, models, and a guideline to support the design or operation of ASGs and ASG hydropower plants. In addition, it outlines the process of developing new models for estimating the volume of flow passing through the Archimedes screw generators. Moreover, it presents new equations and methods to facilitate the design, calibration and modelling of such as sluice gates as an essential component of ASG hydropower plants. The presented analytical equations and models are remarkably efficient due to significantly low computational costs. The non-iterative and fast analytical calculations for each component are essential to maintain the overall efficiency of the multi-component systems, and it makes these equations significantly important for modelling the complex hydraulic system of ASG hydropower plants, studying in different scenarios such as climate change, development of management plans and operation plans, etc.

The characteristics of ASGs were investigated, and their pros and cons were analyzed to learn the potentials of ASGs in the sustainability of hydropower development and determine what is required to facilitate the use of this technology.

Investigations of potential tools to support initial water resource studies of hydropower sites led to the discovery of the potential of EKF and the importance of methods to feed training data in

improving ANN-based estimation models to solve an estimation problem with the minimum number of available parameters.

The geometry, rotation speed and inlet depth of the Archimedes screw were confirmed as the most important factors of supply flow into ASGs during investigations on experimental measurements of a grid-connected Archimedes screw generator and five lab screws at the University of Guelph. The concept of the effective inlet area, and the required analytical equations, were developed based on these findings, which later became the foundation of developing the ASG design analytical equation. Moreover, it led to the development of equations that, despite the complexities of flow through the ASGs, can estimate the volume of flow passing through the screw easily using the minimum number of variables: the inlet depth and rotation speed for variable speed screws and the inlet depth for fixed speed screws.

In addition, studying the governing factors of supply flow into ASGs showed the importance of measuring and regulating flow to ASGs using sluice gates. The laboratory experiment to study sluice gate models resulted in improving the understanding of these models' performance, similarities, advantages and disadvantages. Learning the concepts and general governing factors in these models enabled the development and proposition of new equation forms that made them simpler to implement and easier to compare and analyze. Scaling effects were observed in the loss factor in the modified energy-momentum model that considers losses. Therefore, new equations and methods were developed to reflect the scaling effects on this factor, which improved the generality and performance of this model. Furthermore, lessons learned about the sluice gate models aided in developing a method to estimate the discharge coefficient for the HEC-RAS

model, which enables utilization of the HEC-RAS model for design purposes or when experimental measurements for calibrating discharge coefficient are not available.

General trends and rules in ASG designs were discovered, characterized, and utilized by surveying and analyzing worldwide currently operating ASGs in hydropower plants that are designed and installed by different manufacturers. These findings were utilized to develop empirical equations to estimate several aspects of Archimedes screw hydropower plants. These discoveries, besides the results of the development of ASGs' flow rate concepts and models, facilitated research that led to developing an analytical equation to design site-specific Archimedes screws. This analytical equation requires a minimum number of variables and does not require complex mathematics like iterative methods to estimate the Archimedes screws' geometry.

Investigation of some ASGs that are not in good agreement with this analytical model led to learning about ASGs with unique designs, such as extra-long ASGs using new materials, switchable pump-generator Archimedes screws, and ASGs with adjustable inclination angles. Investigations on such screws led to learning about advancements in manufacturing ASGs to overcome technical concerns led to expanding the feasible operation range of ASGs.

Some manufacturing design considerations were identified for determining the geometry of screws. Observations indicated that some ASP manufacturing recommendations are common in ASG designs. For ASPs, δ values between 0.4 to 0.6 are recommended to optimize the fill of screws and use of materials. Also, the screw's inner to outer diameter ratio (σ) is related directly to the number of blades (N) and reversely to the inclination angle (β); higher β or lower N results in lower σ , and vice versa. Three σ values are offered based on the range of β (Eq. (6–15)). For

ASPs with $N = 3$ and inclination angles up to 35° , the literature recommended considering $\sigma = 1$ and adjusting β for optimizing the screw. [31]. Reviewing the literature and studies on currently operating ASG designs led to results similar to such recommendations. Also, it suggests $N = 3$ as a reasonable number of blades [36], [276], [286]–[288]. For the majority of ASGs $\delta = 0.5$, $\beta \simeq 22^\circ$, and $\sigma = 1$ is common and larger variations of σ are most likely due to the installation conditions [36]. The developed analytical method for estimating the ASG geometry, represented in chapter 6, is flexible to support different δ and σ values for custom designs or optimization purposes. Based on what is learned, pre-computed data is represented in the form of graphs to support and facilitate custom ASG designs based on various σ and δ , which are represented in chapter 7 (section 7.3.3).

Guidelines were developed to support the design of Archimedes screw hydropower plants using one or multiple Archimedean screw generators. Methods were proposed to estimate the number and geometry of ASGs in hydropower plants considering that many ASG power plants are run-of-river, which makes them highly dependent on local flow duration curves, that vary from river to river. These methods significantly reduce the computational costs of the initial design of the site-specific Archimedes screws and facilitate the design and optimization of ASG powerplants. This guideline provides several important factors that allow more accurate predictions than just looking at similar examples of existing installations, require a minimum of input data, and do not require mathematical complexity such as iterative methods. A detailed ASG design study could be undertaken using the results of this process as the design starting point.

Using Archimedes screws as generators is relatively new, and in comparison with other hydropower technologies, there are many not well-known aspects about ASGs, from the phenomenon at the inlet, through, and outlet of ASGs and their effect on the screws' performance to manufacturing details and considerations. Also, the author believes further studies may be required even on some of the widely evaluated and applied information. For example, a large portion of current Archimedes screws literature, including this study, and the majority of full-scale ASGs designs are based on a constant speed close to Muysken's maximum rotation speed. Observations showed that this speed is too fast for small-scale screws, and it is also not constant in variable speed screws. Further studies are recommended to characterize effective parameters in determining the maximum rotation speed of screws and find an analytical alternative for Muysken's empirical equation that is not subjected to scaling effects. In addition, considering the emerging interest in small ASGs and the potentials of variable speed screws, further investigations of this study's models and equations are suggested for such screws.

There are some optimization recommendations that are adopted from ASPs. For example, literature proposes that reasonable filling of ASPs would be achieved for δ between 0.4 to 0.6, and theoretical studies and experimental investigations narrowed this range down to 0.45 and 0.55 [1]. Also, due to manufacturing considerations and optimum use of materials, it is proposed to consider $\sigma = 1$ as a fixed ratio (constant) and the inclination angle as a parameter to optimize [1]. Increasing inclination angle leads to higher overflow and gap leakages that could be managed by increasing N [41]. However, due to the thickness of the blades, more blades come at the cost of reducing the bucket sizes as well as increasing manufacturing costs and challenges. Modern ASGs usually utilize three or four helical blades ($N = 3$ or 4). These recommendations are considered in designs

suggested by the methods offered in this thesis. These designs are in reasonable agreement with the currently operating industrial ASGs that are probably optimized by the manufacturers. They can be used as a basis for the optimization process, especially in studies that use methods that could be accelerated or improved by better initial guesses, such as heuristic or metaheuristic algorithms. Dedicated investigations are recommended to develop analytical models to determine the optimum values of δ , σ , β and N and other effective parameters in optimizing ASGs. There are few analytical studies and methods for optimizing the ASG designs. For example, some studies focused on optimizing D_i and S to maximize the volume of flow passes per screw turn [34]. However, this study showed that the passing flow rate through the screws is not just a function of the screw's geometry. Moreover, due to the concepts discussed in chapter 5, for a specific discharge, the flow depth could be different in open channels and based on the Lubitz et al. (2012) power model, it could be concluded the higher volume of flow passing through a screw does not essentially lead to more power. There are experimental studies about the effects on inclination angle and the generated power of screws that reinforce this hypothesis by indicating shallower inclination angles led to generating more power [297], [298]. Therefore, this author recommends studies to study optimizing ASGs considering such effective factors. Moreover, ASGs could operate in a wide range of flow rates and optimizing the screw for the design flow rate does not essentially lead to optimally supporting all operation conditions. Therefore, optimization studies could focus on topics such as the optimum range of operating screws or optimizing ASGs to operate near optimum for a wider range of operating conditions. Many optimization studies are focused on the application of CFD, which is highly dependent on the knowledge and skills of the user. At any rate, case optimizations may limit the results to specific cases or scales. Therefore,

further studies are recommended to characterize the effective parameters and general rules in optimizing ASGs and develop general analytical methods or guidelines to optimize ASG designs.

Determination of the optimum or most effective size and combination screws in multi-ASG powerplants is recommended to take advantage of the available flow rate in high flow sites. This study proposed three methods for determining the size of screws based on the flow duration curve. The identical screws method could be advantageous for remote locations, mass production of screws, and ease the maintenance, while the trial-and-error method could result in higher reliability in generating power. Further investigations on the proposed methods are recommended to understand their pros and cons better and find the optimum methods for this purpose. Such investigations may help find general rules or recommendations that benefit the development of analytical methods or algorithms to develop guidelines, models or supporting tools for this purpose.

Optimizing operation plans require defining constraints for upper and lower limits. The maximum filling of screws could be estimated using physical constraints, and there are methods to determine the optimum filling of screws. Some studies reported that ASGs could utilize up to 20% more flow than their optimal filling without considerable loss in their efficiency [2]. However, there are no analytical measures to define the minimum reasonable flow to operate ASGs (MRFO). It is important to note that this theoretical construct is not associated just with the flow. In real plants, the MFRO depends on bearings, generators and electrical aspects of the plant. For single screw powerplants, MRFO could help more realistic and reliable operation plans and estimations of overall power generation. Determination of MRFO is even more important in optimizing operation plans of powerplants using more than one ASG since deciding between overloading the operating

ASGs or running the next ASG based on available flow could affect the overall power generation. Observation of experimental measurements showed that the efficiency of an ASG varies at different rotation speeds or flow rates. Even for constant rotation speeds, observations showed that the efficiency of ASGs varies at different flow rates. More efficiency does not essentially mean more overall power generation, and it needs to be considered in optimizing operation plans. For example, based on the available flow and MRFO, the optimization models should be able to estimate whether overfilling ASGs or running an extra ASG will lead to more power generation. To define MRFO, further research is recommended to identify and characterize effective factors which running a screw is feasible and efficient enough mechanically and reasonable economically, then develop proper measures to determine this condition.

This thesis outlined the author's laboratory experiments, analytical research, numerical investigations, and studies on Archimedes screw generators and ASG hydropower plants' components to develop new equations, models, and guidelines to support ASG hydropower plants' design and operation. The developed equations, tools and design guidelines enable the estimation of design aspects of ASG hydropower plants rapidly and easily, using the minimum number of required parameters. The author hopes that the outlined research in this thesis facilitates the design and operation of green and renewable Archimedes screw hydropower plants and serves future research.

REFERENCES

- [1] A. YoosefDoost and W. D. Lubitz, “Archimedes screw turbines: A sustainable development solution for green and renewable energy generation-a review of potential and design procedures,” *Sustain.*, vol. 12, no. 18, p. 7352, Sep. 2020, doi: 10.3390/SU12187352.
- [2] A. YoosefDoost and W. D. Lubitz, “Archimedes Screw Design: An Analytical Model for Rapid Estimation of Archimedes Screw Geometry,” *Energies*, vol. 14, no. 22, p. 7812, Nov. 2021, doi: 10.3390/en14227812.
- [3] A. YoosefDoost and W. D. Lubitz, “Design Guideline for Hydropower Plants Using One or Multiple Archimedes Screws,” *Processes*, vol. 9, no. 12, p. 2128, 2021, doi: 10.3390/pr9122128.
- [4] A. Yoosefdoost, S. M. Tahsien, S. A. Gadsden, W. D. Lubitz, and M. Kaviani, “Artificial Neural Networks and Extended Kalman Filter for Easy-to-Implement Runoff Estimation Models,” 2022.
- [5] A. Yoosefdoost, W. D. Lubitz, and W. D. Lubitz, “Sluice Gate Design and Calibration: Simplified Models to Distinguish Flow Conditions and Estimate Discharge Coefficient and Flow Rate,” *Water (Switzerland)*, vol. 14, no. 8, p. 1215, 2022, doi: 10.3390/w14081215.
- [6] A. YoosefDoost and W. D. Lubitz, “Development of an Equation for the Volume of Flow Passing Through an Archimedes Screw Turbine,” in *Sustaining Tomorrow*, D. S.-K. Ting and A. Vasel-Be-Hagh, Eds. Cham, Switzerland: Springer, Cham, 2021, pp. 17–37. doi: 10.1007/978-3-030-64715-5_2.
- [7] J. Mensah and S. Ricart Casadevall, “Sustainable development: Meaning, history, principles, pillars, and implications for human action: Literature review,” *Cogent Soc. Sci.*, vol. 5, no. 1, Aug. 2019, doi: 10.1080/23311886.2019.1653531.
- [8] UN, *Our Common Future: Report of the World Commission on Environment and Development*. New York, NY, USA, 1987. Accessed: May 10, 2020. [Online]. Available: https://netzwerk-n.org/wp-content/uploads/2017/04/0_Brundtland_Report-1987-Our_Common_Future.pdf
- [9] UNICEF and FN-SAMBANDENT, “What is sustainable development?,” 2017. <https://www.youtube.com/watch?v=7V8oFI4GYMY&t> (accessed Jan. 29, 2020).
- [10] R. Passet, *The Economic and the living (L'Économique et Le Vivant)*. Paris, France: FeniXX réédition numérique, 1996. doi: 10.3917/econo.passe.1996.01.
- [11] United Nations, *Prototype Global Sustainable Development Report*, Online une. New York: United Nations Department of Economic and Social Affairs, Division for Sustainable

- Development, 2014. Accessed: Dec. 03, 2018. [Online]. Available: <http://sustainabledevelopment.un.org/globalsdreport/>
- [12] P. James, L. with Magee, A. Scerri, and M. B. Steger, *Urban Sustainability in Theory and Practice: Circles of Sustainability*. London: Routledge, 2015. Accessed: Dec. 03, 2018. [Online]. Available: https://www.academia.edu/9294719/Urban_Sustainability_in_Theory_and_Practice_Circles_of_Sustainability_2015_
- [13] R. R. Shaker, “The spatial distribution of development in Europe and its underlying sustainability correlations,” *Appl. Geogr.*, vol. 63, pp. 304–314, Sep. 2015, doi: 10.1016/j.apgeog.2015.07.009.
- [14] J. Dréo, “Sustainable development.svg,” *Wikipedia*, 2007. https://en.wikipedia.org/wiki/File:Sustainable_development.svg (accessed Dec. 03, 2018).
- [15] O. Ellabban, H. Abu-Rub, and F. Blaabjerg, “Renewable energy resources: Current status, future prospects and their enabling technology,” *Renewable and Sustainable Energy Reviews*, vol. 39. Elsevier Ltd, pp. 748–764, 2014. doi: 10.1016/j.rser.2014.07.113.
- [16] F. Appavou *et al.*, *Renewables 2019 Global Status Report*. Paris, France: REN21 Secretariat, 2019. [Online]. Available: <https://wedocs.unep.org/bitstream/handle/20.500.11822/28496/REN2019.pdf?sequence=1&isAllowed=y%0Ahttp://www.ren21.net/cities/wp-content/uploads/2019/05/REC-GSR-Low-Res.pdf>
- [17] A. McNally, D. Magee, and A. T. Wolf, “Hydropower and sustainability: Resilience and vulnerability in China’s powersheds,” *J. Environ. Manage.*, vol. 90, no. SUPPL. 3, Jul. 2009, doi: 10.1016/j.jenvman.2008.07.029.
- [18] S. J. J. Williamson, B. H. H. Stark, and J. D. D. Booker, “Low head pico hydro turbine selection using a multi-criteria analysis,” *RENE*, vol. 61, pp. 43–50, Jan. 2014, doi: 10.1016/j.renene.2012.06.020.
- [19] A. Date and A. Akbarzadeh, “Design and cost analysis of low head simple reaction hydro turbine for remote area power supply,” *Renew. Energy*, vol. 34, no. 2, pp. 409–415, 2009, doi: 10.1016/j.renene.2008.05.012.
- [20] R. Lafitte, *Survey of Energy Resources*. London, United Kingdom: World Energy Council, 2001. Accessed: Jul. 29, 2020. [Online]. Available: www.worldenergy.org
- [21] C. J. Cleveland and C. G. Morris, *Handbook of Energy: Chronologies, Top Ten Lists, and Word Clouds*, vol. 2. Waltham, Amsterdam, Oxford: Elsevier, 2013. Accessed: Jul. 29, 2020. [Online]. Available: <https://books.google.ca/books?hl=en&lr=&id=ScL77rOCZn0C&oi=fnd&pg=PP1&dq=Cleveland+Handbook+of+Energy&ots=niiTlk2mtb&sig=mSO-coW->

m05YVGwT7ScIWmFq5oc&redir_esc=y#v=onepage&q=Cleveland Handbook of Energy&f=false

- [22] Icold, “Role of Dams,” *International Commission on Large Dams*, 2014. http://www.icold-cigb.org/GB/Dams/role_of_dams.asp (accessed Jul. 07, 2020).
- [23] S. Born, K. Field, D. Lander, and M. Bendewald, “Water Resources: Why Do We Build Dams?,” *Teach Engineering*, 2007. https://www.teachengineering.org/lessons/view/cub_dams_lesson01 (accessed May 03, 2020).
- [24] M. Casini, “Harvesting energy from in-pipe hydro systems at urban and building scale,” *Int. J. Smart Grid Clean Energy*, vol. 4, no. 4, pp. 316–27, 2015, doi: 10.12720/sgce.4.4.316-327.
- [25] IRENA, *Renewable Energy Techlogies: Cost Analysis Series, Hydropower*, vol. 1, no. 3/5. Bonn, Germany: IRENA Innovation and Technology Centrer, 2012. Accessed: Jun. 23, 2019. [Online]. Available: www.irena.org/Publications
- [26] S. H. Suh *et al.*, *Theory and Applications of Hydraulic Turbines*, 1st ed. Paju, Gyeonggi-do, South Korea: Dong Myeong Publishers, 2014.
- [27] G. Muller and J. Senior, “Simplified theory of Archimedean screws,” *J. Hydraul. Res.*, vol. 47, no. 5, pp. 666–669, 2009, doi: 10.3826/jhr.2009.3475.
- [28] S. Simmons and W. Lubitz, “Archimedes screw generators for sustainable energy development,” in *Proceedings of the 2017 IEEE Canada International Humanitarian Technology Conference (IHTC), Toronto, ON, Canada, 21–22 July 2017*, 2017, pp. 144–148. doi: 10.1109/IHTC.2017.8058176.
- [29] T. Koetsier and H. Blauwendraat, “The Archimedean Screw-Pump: A Note on Its Invention and the Development of the Theory,” in *International Symposium on History of Machines and Mechanisms*, Dordrecht: Springer Netherlands, 2004, pp. 181–194. doi: 10.1007/1-4020-2204-2_15.
- [30] S. Dalley and J. P. Oleson, “Sennacherib, Archimedes, and the Water Screw: The Context of Invention in the Ancient The Context of Invention in the Ancient World,” *Technol. Cult.*, vol. 44, no. 1, pp. 1–26, 2003, doi: 10.1353/tech.2003.0011.
- [31] G. Nagel, *Archimedean Screw Pump Handbook*. Schwabisch Gmund: RITZ-Pumpenfabrik OHG, 1968.
- [32] K. Brada, “Wasserkraftschnecke ermöglicht Stromerzeugung über Kleinkraftwerke [Hydraulic screw generates electricity from micro hydropower stations],” *Maschinenmarkt, Würzbg.*, vol. 105, no. 14, pp. 52–56, 1999, doi: ISSN: 0341-5775.

- [33] D. M. Nuernbergk and C. Rorres, “Analytical Model for Water Inflow of an Archimedes Screw Used in Hydropower Generation,” *J. Hydraul. Eng.*, vol. 139, no. 2, pp. 213–220, Feb. 2013, doi: 10.1061/(ASCE)HY.1943-7900.0000661.
- [34] C. Rorres, “The Turn of the Screw: Optimal Design of an Archimedes Screw,” *J. Hydraul. Eng.*, vol. 126, no. January, pp. 72–80, Jan. 2000, doi: 10.1061/(ASCE)0733-9429(2000)126:1(72).
- [35] A. Kozyn, “Power Loss Model for Archimedes Screw Turbines,” University of Guelph, Guelph, ON, Canada, 2016.
- [36] A. Lashofer, W. Hawle, and B. Pelikan, “State of technology and design guidelines for the Archimedes screw turbine,” in *Hydro 2012 - Innovative Approaches to Global Challenges*, 2012, no. October, pp. 1–8. [Online]. Available: <https://bit.ly/3pC7Vah>
- [37] P. Kibel, “Fish Monitoring and Live Fish Trials. Archimedes Screw Turbine, River Dart. Phase 1 Report: Live fish trials, smolts, leading edge assessment, disorientation study, outflow monitoring.,” Moretonhampstead, Devon, England, 2007.
- [38] C. A. Boys, B. D. Pflugrath, M. Mueller, J. Pander, Z. D. Deng, and J. Geist, “Physical and hydraulic forces experienced by fish passing through three different low-head hydropower turbines,” *Mar. Freshw. Res.*, vol. 69, no. Special Issue, pp. 1934–1944, 2018, doi: 10.1071/MF18100.
- [39] C. D. McNabb, C. R. Liston, and S. M. Borthwick, “Passage of Juvenile Chinook Salmon and other Fish Species through Archimedes Lifts and a Hidrostral Pump at Red Bluff, California,” *Trans. Am. Fish. Soc.*, vol. 132, no. 2, pp. 326–334, Mar. 2003, doi: 10.1577/1548-8659(2003)132<0326:POJCSA>2.0.CO;2.
- [40] P. Kibel, R. Pike, and T. Coe, “Archimedes Screw Turbine Fisheries Assessment. Phase II: Eels and Kelts.,” Moretonhampstead, Devon, England, 2008.
- [41] P. Kibel, R. Pike, and T. Coe, “The Archimedes screw turbine: Assessment of three leading edge profiles.,” Moretonhampstead, 2009.
- [42] United Kingdom Environment Agency, “Hydropower Good Practice Guidelines Screening requirements,” *J. Hydraul. Res.*, vol. 4, pp. 1–16, Dec. 2012.
- [43] A. T. Piper, P. J. Rosewarne, R. M. Wright, and P. S. Kemp, “The impact of an Archimedes screw hydropower turbine on fish migration in a lowland river,” *Ecol. Eng.*, vol. 118, no. March 2018, pp. 31–42, 2018, doi: 10.1016/j.ecoleng.2018.04.009.
- [44] I. S. Pauwels *et al.*, “Multi-species assessment of injury, mortality, and physical conditions during downstream passage through a large archimedes hydrodynamic screw (Albert canal, Belgium),” *Sustain.*, vol. 12, no. 20, pp. 1–25, 2020, doi: 10.3390/su12208722.

- [45] VANDEZANDE BVBA, “Lock of Hasselt - Hybrid hydropower screw/ screw pump,” *Youtube*, Jul. 05, 2018. <https://youtu.be/FUIYjkzAIs8> (accessed Aug. 08, 2021).
- [46] M. Rühlmann, *Allgemeinen Maschinenlehre*, 1 st. Braunschweig: Verlag von C.A. Schwetschke und Sohn, 1862.
- [47] IFICPS, “DE4139134A1 - Hydrodynamic screw for energy conversion - uses changes in water supply to regulate energy output - Google Patents,” *IFI CLAIMS Patent Services*, 2020. <https://patents.google.com/patent/DE4139134A1/en> (accessed Feb. 15, 2020).
- [48] W. Moerscher, “Water-power system ,” US1434138A, Oct. 31, 1922 Accessed: Oct. 02, 2021. [Online]. Available: <https://patents.google.com/patent/US1434138A/en?inventor=Moerscher>
- [49] W. D. Lubitz, M. Lyons, and S. Simmons, “Performance Model of Archimedes Screw Hydro Turbines with Variable Fill Level,” *J. Hydraul. Eng.*, vol. 140, no. 10, p. 04014050, 2014, doi: 10.1061/(ASCE)HY.1943-7900.0000922.
- [50] A. J. Lynch and C. A. Rowland, *The history of grinding*. Littleton, CO, USA: Society for Mining, Metallurgy, and Exploration, 2005.
- [51] Siyavula, “Water-wheels,” *Openstax CNX*, Sep. 10, 2009. <https://cnx.org/contents/IRxiIGmY@1/Water-wheels> (accessed May 13, 2020).
- [52] W. Hawle, A. Lashofer, and B. Pelikan, “Lab Testing of the Archimedean Screw,” 2012.
- [53] C. Rorres, *Archimedes in the 21st Century: Proceedings of a World Conference at the Courant Institute of Mathematical Sciences*. Cham: Springer Basel AG, 2017. doi: 10.1007/978-3-319-58059-3.
- [54] Voith-Siemens, “Plan view of a Pelton turbine installation,” *Voith Siemens Hydro Power Generation*, Dec. 16, 2005. https://en.wikipedia.org/wiki/File:S_vs_pelton_schnitt_1_zoom.png (accessed Aug. 23, 2020).
- [55] J. Schwizer, “Map of Hydro Turbines,” *WikiMedia*, Feb. 16, 2018. https://commons.wikimedia.org/wiki/File:Kennfeld_Wasserturbinen.svg (accessed Aug. 23, 2020).
- [56] P. A. Breeze, *Power generation technologies*, 3rd ed. Amsterdam, The Netherlands: Elsevier, 2019.
- [57] Bermiego, “Turgo turbine,” *WikiPedia*, Apr. 29, 2005. https://en.wikipedia.org/wiki/File:Turgo_turbine.png (accessed Aug. 23, 2020).
- [58] K. Subramanya, *Hydraulic Machines*. New Delhi, India: McGraw Hill Education (India)

- Private, 2013. [Online]. Available: https://books.google.ca/books?id=RhB_AgAAQBAJ
- [59] A. H. Elbatran, O. B. Yaakob, Y. M. Ahmed, and H. M. Shabara, "Operation, performance and economic analysis of low head micro-hydropower turbines for rural and remote areas: A review," *Renew. Sustain. Energy Rev.*, vol. 43, pp. 40–50, Mar. 2015, doi: 10.1016/J.RSER.2014.11.045.
- [60] Voith-Siemens, "Sectional drawing of a Francis turbine for the Xingu power plant , Brazil ,"
WikiMedia, Dec. 16, 2005.
https://commons.wikimedia.org/wiki/File:M_vs_francis_schnitt_1_zoom.jpg (accessed Aug. 23, 2020).
- [61] M. Schweiss, "Sectional drawing of a Kaplan turbine with a diameter of 9.5 m for Yacyretá, Argentina,"
WikiMedia, Dec. 31, 2005.
https://commons.wikimedia.org/wiki/File:S_vs_kaplan_schnitt_1_zoom.jpg (accessed Aug. 23, 2020).
- [62] D. R. Durgaiyah, *Fluid mechanics and machinery*. New Delhi, India: New Age International, 2007.
- [63] E. Quaranta and R. Revelli, "Gravity water wheels as a micro hydropower energy source: A review based on historic data, design methods, efficiencies and modern optimizations," *Renewable and Sustainable Energy Reviews*, vol. 97. Elsevier Ltd, pp. 414–427, Dec. 01, 2018. doi: 10.1016/j.rser.2018.08.033.
- [64] UNIDO, "Renewable energy: Micro Hydraulic Power Unit (Spiral Type Pico-Hydro Unit 'PicoPica10', 'PicoPica500')," *United Nations Industrial Development Organization, Tokyo, Japan*, 2020. http://www.unido.or.jp/en/technology_db/5276/ (accessed Jul. 07, 2020).
- [65] Landustrie, "Linton Lock," *Landustrie Sneek BV*, 2017.
<https://web.archive.org/web/20210804020631/https://www.landustrie.nl/en/products/hydropower/projects/linton-lock.html> (accessed Jul. 29, 2020).
- [66] ANDRITZ (formerly Ritz-Atro), "Hydrodynamic screws: Energy extraction-efficient and fish-friendly," Nuremberg, Germany, 2006. Accessed: May 12, 2020. [Online]. Available: www.schleich-burckhardt.de
- [67] J. A. Senior, "Hydrostatic Pressure Converters for the Exploitation of Very Low Head Hydropower Potential," University of Southampton, Southampton, UK, 2009. Accessed: May 12, 2020. [Online]. Available: https://eprints.soton.ac.uk/73702/1/James_Senior_-_Hydrostatic_Pressure_Converters_thesis.pdf
- [68] J. Kleemann and D. H. Hellmann, "Gutachten zur Wirkungsgrad- bestimmung an einer Wasserkraftschnecke Fabrikat RITZ-ATRO," 2003.

- [69] D. M. Nuernbergk and C. Rorres, “Analytical Model for Water Inflow of an Archimedes Screw Used in Hydropower Generation,” *J. Hydraul. Eng.*, vol. 139, no. 2, pp. 213–220, Feb. 2013, doi: 10.1061/(ASCE)HY.1943-7900.0000661.
- [70] Vandezande Diksmuide, “PS/ WKC lock Hasselt,” *Vandezande*. <https://web.archive.org/web/20210405220637/https://www.vandezande.com/en/projects/p-s-wkc-lock-hasselt> (accessed Aug. 09, 2021).
- [71] J. Adlard, “Archimedes screw: Copley Hydropower Generator,” Leeds, UK, 2011.
- [72] D. Bennion, “Maintaining Archimedes Screw Pumps,” *ECS Engineering Services*, 2013. <http://www.ecsengineeringservices.com/maintaining-archimedes-screw-pumps/> (accessed Jun. 26, 2018).
- [73] ECS, “Archimedes Screw Pumps,” *ECS Engineering Services*, 2018. <http://www.ecsengineeringservices.com/archimedes-screw-pumps/> (accessed Jun. 26, 2018).
- [74] SBH, “Archimedean Screw Turbine,” *Spaans Babcock bv*, Spaans Babcock Hydro Power, Balk, Netherlands, 2012.
- [75] O. M. Dada, I. A. Daniyan, and O. . Adaramola, “Optimal Design of Micro Hydro Turbine (Archimedes Screw Turbine) in Arinta Waterfall in Ekiti State, Nigeria,” *Res. J. Eng. Appl. Sci.*, vol. 4, no. 2, pp. 34–38, 2014.
- [76] C. M. Pringle, M. C. Freeman, and B. J. Freeman, “Regional Effects of Hydrologic Alterations on Riverine Macrobiota in the New World: Tropical-Temperate ComparisonsThe massive scope of large dams and other hydrologic modifications in the temperate New World has resulted in distinct regional trends of biotic impoverishment. While neotropical rivers have fewer dams and limited data upon which to make regional generalizations, they are ecologically vulnerable to increasing hydropower development and biotic patterns are emerging,” *Bioscience*, vol. 50, no. 9, pp. 807–823, Sep. 2000, doi: 10.1641/0006-3568(2000)050[0807:reohao]2.0.co;2.
- [77] R. J. Neves, A. E. Bogan, J. D. Williams, S. A. Ahlstedt, and P. W. Hartfield, *Status of Aquatic Mollusks in the Southeastern United States: A Downward Spiral of Diversity. In: Aquatic Fauna in Peril: The Southeastern Perspective*, 1th ed., no. January. Decatur, GA, USA: Decatur: Southeast Aquatic Research Institute Special Publication, 1997. [Online]. Available: <https://pubs.er.usgs.gov/publication/85779>
- [78] K. Brada and K.-A. Radlik, “Wasserkraftschnecke: Eigenschaften und Verwendung,” in *Heat exchange and renewable energy sources International symposium, 1996 Szczecin, Poland*, 1996, pp. 43–52.
- [79] D. Aigner, *Current research in hydraulic engineering 1993-2008*. Dresden, Germany: Institut für Wasserbau und Technisch Hydromechanik der TU. Association, 2008.

- [80] W. Schmalz, “Studies on fish migration and control of possible fish loss caused by the hydrodynamic screw and hydropower plant,” *Fischo- kologische und Limnol. Untersuchungsstelle Sudthurign, Rep., Thüringer Landesanstalt für Umwelt und Geol. Jena (in Ger., 2010.*
- [81] A. Lashofer, F. Kaltenberger, and B. Pelikan, “Does the archimedean screw turbine stand the test? (Wie gut bewährt sich die Wasserkraftschnecke in der Praxis?),” *WasserWirtschaft*, vol. 101, no. 7–8, pp. 76–81, 2011, doi: 10.1365/s35147-011-0109-5.
- [82] D. M. Nuernbergk, *Wasserkraftschnecken - Berechnung und optimaler Entwurf von archimedischen Schnecken als Wasserkraftmaschine (Hydro-power screws - Calculation and Design of Archimedes Screws)*, 2nd ed. Detmold: Verlag Moritz Schäfer, 2020. Accessed: Aug. 24, 2020. [Online]. Available: https://www.researchgate.net/publication/342173423_Wasserkraftschnecken_-_Berechnung_und_optimaler_Entwurf_von_archimedischen_Schnecken_als_Wasserkraftmaschine_Hydro-power_screws_-_Calculation_and_Design_of_Archimedes_Screws_2_Auflage_2020_Verlag_Mori
- [83] J. Muysken, “Calculation of the Effectiveness of the Auger,” *De Ingenieur*, vol. 21, pp. 77–91, 1932.
- [84] P. Fraenkel, O. Paish, A. Harvey, R. Brown, A. Edwards, and V. Bokalders, *Micro-hydro power: a guide for development workers*. London, UK: Intermediate Technology Publications, 1999. [Online]. Available: <https://www.osti.gov/etdeweb/biblio/5564378>
- [85] NationalTrust, “Hydropower returns to Cragside | National Trust,” 2020. <https://www.nationaltrust.org.uk/features/hydropower-returns-to-cragside> (accessed Jul. 01, 2020).
- [86] M. Sumino, “Ultra-Small Water Power Generator,” May 14, 2019. <https://youtu.be/XjEgFIngZ04> (accessed Jun. 23, 2020).
- [87] Rosser, “The Cragside Estate Archimedes screw water turbine and generator, Rothbury, England.,” *Wikimedia Commons*, Oct. 14, 2016. https://commons.wikimedia.org/wiki/File:The_Cragside_Estate_Archimedes_screw_water_turbine_and_generator,_Rothbury,_England.jpg (accessed Jul. 05, 2020).
- [88] C. Down, “Cragside Archimedes’ screw from bottom,” *Wikimedia Commons*, May 17, 2017. https://commons.wikimedia.org/wiki/File:Cragside_Archimedes%27_screw_from_bottom.jpg (accessed Jul. 05, 2020).
- [89] Spaans Babcock Ltd., “Hydro Power using Waste Water at Esholt WwTW,” *Spaans Babcock Ltd.*, 2009. https://cms.esi.info/Media/documents/54053_1316689157666.pdf (accessed Jul. 29, 2020).

- [90] M. K. Padhy and R. P. Saini, “A review on silt erosion in hydro turbines,” *Renew. Sustain. Energy Rev.*, vol. 12, no. 7, pp. 1974–1987, 2008, doi: 10.1016/j.rser.2007.01.025.
- [91] A. K. Awasthi, “Design for Small hydro-An Innovative Approach,” in *Proceedings of 2nd International Conference on Silting Problems in Hydropower Plants, 26–28 September 2001*, 2002, pp. 83–89. [Online]. Available: <https://books.google.ca/books?id=iKXDcAAUP5wC&lpq=PP1&pg=PR1#v=onepage&q&f=false>
- [92] M. W. Kang, N. Park, and S. H. Suh, “Numerical Study on Sediment Erosion of Francis Turbine with Different Operating Conditions and Sediment Inflow Rates,” in *Procedia Engineering*, 2016, vol. 157, pp. 457–464. doi: 10.1016/j.proeng.2016.08.389.
- [93] M. Rinaldi *et al.*, “Final report on methods, models, tools to assess the hydromorphology of rivers,” European Union’s Seventh Programme for Research, Technological Development, 2015. [Online]. Available: [https://reformrivers.eu/system/files/6.2 Methods to assess hydromorphology of rivers part I.pdf](https://reformrivers.eu/system/files/6.2%20Methods%20to%20assess%20hydromorphology%20of%20rivers%20part%20I.pdf)
- [94] K. Shahverdi, R. Loni, J. M. Maestre, and G. Najafi, “CFD numerical simulation of Archimedes screw turbine with power output analysis,” *Ocean Eng.*, vol. 231, no. February, p. 108718, 2021, doi: 10.1016/j.oceaneng.2021.108718.
- [95] A. M. Durrani and M. Uzair, “Micro Hydro Power Plant using Sewage Water of Hayatabad Peshawar,” 2019.
- [96] A. Kozyn, S. Ash, and W. D. Lubitz, “Assessment of Archimedes Screw Power Generation Potential in Ontario,” in *4th Climate Change Technology Conference, 25-27 May 2015*, 2015, no. 1570095585, pp. 1–11. Accessed: Jun. 03, 2019. [Online]. Available: [https://www.cctc2015.ca/TECHNICAL PAPERS/1570095585.pdf](https://www.cctc2015.ca/TECHNICAL%20PAPERS/1570095585.pdf)
- [97] IWPDC, “A quiet revolution,” *International Water Power & Dam Construction*, Nov. 29, 2010. <https://www.waterpowermagazine.com/features/featurea-quiet-revolution/> (accessed Jul. 06, 2020).
- [98] Yorkshire Water, “Words Of Water: UK’s First Energy Self-Sufficient Large Sewage Works,” *Yorkshire Water*, 2014. <http://wordsofwater.blogspot.com/2012/01/uks-first-energy-self-sufficient-large.html> (accessed Jul. 29, 2020).
- [99] U.S. Department of the Interior, “Obsolete Dams are a Hazard to People and Wildlife. We’re Working Together to Remove Them.,” *U.S. Department of the Interior*, 2016. <https://web.archive.org/web/20220213082301/https://www.doi.gov/blog/obsolete-dams-are-hazard-people-and-wildlife-were-working-together-remove-them> (accessed Feb. 13, 2022).
- [100] S. M. Born, K. D. Genskow, T. L. Filbert, N. Hernandez-Mora, M. L. Keeper, and K. A. White, “Socioeconomic and institutional dimensions of dam removals: The Wisconsin

- experience,” *Environ. Manage.*, vol. 22, no. 3, pp. 359–370, 1998, doi: 10.1007/s002679900111.
- [101] B. Babbit, “What Goes Up, May Come Down,” *New Sci.*, vol. 52, no. 8, pp. 656–658, 2002, doi: 10.1641/0006-3568(2002)052[0656:WGUMCD]2.0.CO;2.
- [102] A. G. C. Lejon, *Ecosystem response to dam removal*. Umeå, Sweden: Department of Ecology and Environmental Science, Umeå University, 2012. Accessed: Jul. 07, 2020. [Online]. Available: <https://www.diva-portal.org/smash/get/diva2:527655/FULLTEXT01.pdf>
- [103] M. S. Tahmiscioğlu and N. Durmuş, “POSITIVE AND NEGATIVE IMPACTS OF DAMS ON THE ENVIRONMENT,” in *Proceedings of the International Congress On River Basin Management, 8 March 2007*, 2007, pp. 759–769. Accessed: Jul. 07, 2020. [Online]. Available: <https://cvc.ca/wp-content/uploads/2011/02/60.pdf>
- [104] C. D’Antonio and L. A. Meyerson, “Exotic plant species as problems and solutions in ecological restoration: A synthesis,” *Restor. Ecol.*, vol. 10, no. 4, pp. 703–713, Dec. 2002, doi: 10.1046/j.1526-100X.2002.01051.x.
- [105] P. B. Shafroth, J. M. Friedman, G. T. Auble, M. L. Scott, and J. H. Braatne, “Potential Responses of Riparian Vegetation to Dam Removal,” *Bioscience*, vol. 52, no. 6, pp. 703–712, 2002, doi: 10.1641/0006-3568(2002)052.
- [106] C. H. Orr and E. H. Stanley, “Vegetation development and restoration potential of drained reservoirs following dam removal in Wisconsin,” *River Res. Appl.*, vol. 22, no. 3, pp. 281–295, 2006, doi: 10.1002/rra.891.
- [107] G. Grant, “Dam removal: Panacea or Pandora for rivers?,” *Hydrol. Process.*, vol. 15, no. 8, pp. 1531–1532, 2001, doi: 10.1002/hyp.473.
- [108] J. T. F. Ashley, K. Bushaw-Newton, W. Matt, A. Boettner, G. Drames, and D. J. Velinsky, “The Effects of Small Dam Removal on the Distribution of Sedimentary Contaminants,” *Environ. Monit. Assess.*, vol. 114, pp. 287–312, 2006, doi: 10.1007/s10661-006-4781-3.
- [109] L. Hetling, E. Horn, and J. Tofflemire, “Summary of Hudson River PCB Study Results,” New York, NY, USA, Apr. 1978. Accessed: Jul. 04, 2020. [Online]. Available: <https://semspub.epa.gov/work/02/67559.pdf>
- [110] S. Waters and G. A. Aggidis, “Over 2000 years in review: Revival of the Archimedes Screw from Pump to Turbine,” *Renew. Sustain. Energy Rev.*, vol. 51, pp. 497–505, Nov. 2015, doi: 10.1016/J.RSER.2015.06.028.
- [111] J. Keyes and O. Pastinak, “MNR’s Role in Public Safety Around Dams – An Overview,” *Ministry of Natural Resources, Biodiversity Branch Policy Division. Ontario Waterpower Association.*, 2011. <https://slideplayer.com/slide/6376193/> (accessed May 09, 2020).

- [112] L. Demal, “Dam Safety in Ontario New Dam Safety Technical Guidelines – What do they mean for Ontario?,” 2012. [Online]. Available: [http://owa.ca/assets/files/conferences/New Dam Safety Technical Guidelines.pdf](http://owa.ca/assets/files/conferences/New_Dam_Safety_Technical_Guidelines.pdf)
- [113] ASDSO, *The Cost of Rehabilitating Our Nation’s Dams: A Methodology, Estimate & Proposed Funding Mechanisms*. Lexington, USA: Association of State Dam Safety Officials, 2016.
- [114] Ontario Energy Board, “Ontario’s System-Wide Electricity Supply Mix: 2013 Data,” Toronto, ON, Canada, 2014. [Online]. Available: https://www.oeb.ca/oeb/_Documents/Regulatory/2013_Supply_Mix_Data.pdf
- [115] Ontario Ministry of Energy, *Ontario’s Long-Term Energy Plan*. Toronto, ON, Canada: Queen’s Printer for Ontario, 2010. [Online]. Available: https://files.ontario.ca/books/final_mei_ltep_en_acc.pdf
- [116] Hatch Acres, “Evaluation and Assessment of Ontario’s Waterpower Potential Ministry of Natural Resources Final Report,” Peterborough, ON, Canada, 2005. Accessed: Jun. 03, 2019. [Online]. Available: <https://owa.ca/wp-content/uploads/2017/01/Evaluation-and-Assessment-of-Ontarios-Waterpower-Potential-Final-Report-.pdf>
- [117] OMNR, “Potential waterpower generation sites (WPPOTSTE),” *Ontario Ministry of Natural Resources*, 2004. <https://www.ontario.ca/data/potential-waterpower-generation-sites-wppotste> (accessed Jan. 10, 2015).
- [118] C. Hart and S. Saling, “To cut poverty in Asia and the Pacific, ‘Energy Plus’ package a must, says UN report | UNDP,” *United Nations Development Programme*, Jan. 19, 2012. <https://www.undp.org/content/undp/en/home/presscenter/pressreleases/2012/01/19/to-cut-poverty-in-asia-and-the-pacific-energy-plus-package-a-must-says-un-report.html> (accessed Jul. 29, 2020).
- [119] M. J. Khan, M. T. Iqbal, and J. E. Quaicoe, “River current energy conversion systems: Progress, prospects and challenges,” *Renewable and Sustainable Energy Reviews*, vol. 12, no. 8. Pergamon, pp. 2177–2193, Oct. 01, 2008. doi: 10.1016/j.rser.2007.04.016.
- [120] U. Muhammad, “Rural solar electrification in Nigeria: Renewable energy potentials and distribution for rural development,” in *World Renewable Energy Forum, WREF 2012, Including World Renewable Energy Congress XII and Colorado Renewable Energy Society (CRES) Annual Conference*, 2012, vol. 4, pp. 2674–2681. Accessed: Jul. 09, 2020. [Online]. Available: <https://www.semanticscholar.org/paper/RURAL-SOLAR-ELECTRIFICATION-IN-NIGERIA-%3A-RENEWABLE-Muhammad/34d8927ef0c09a96437a08b2818c984da8fd7e03>
- [121] A. Eberhard, O. Rosnes, M. Shkaratan, and H. Vennemo, “Africa’s Power Infrastructure Investment, Integration, Efficiency Infrastructure,” Washington DC, USA, 2011. doi:

10.1596/978-0-8213-8455-8.

- [122] Helmizar, A. Nuramal, N. Daratha, and A. Setiawan, “The Effect of the Ratio of the Hub Diameter (d) to the Diameter of the Screw (D) to the Performance of the Archimedes Screw,” in *IOP Conference Series: Materials Science and Engineering*, 2020, vol. 874, no. 1, pp. 1–8. doi: 10.1088/1757-899X/874/1/012032.
- [123] A. I. Siswantara, H. M. S. Gumelar, Budiarmo, R. Harmadi, Warjito, and D. Adanta, “Analysis of the Effects of Overflow Leakage Phenomenon on Archimedes Turbine Efficiency,” *Proc. - 2018 4th Int. Conf. Sci. Technol. (ICST)*, , Yogyakarta, Indones. 7–8 August 2018, vol. 1, pp. 1–6, 2018, doi: 10.1109/ICSTC.2018.8528687.
- [124] Erinofiardi *et al.*, “Experimental Study of Screw Turbine Performance based on Different Angle of Inclination,” in *Energy Procedia*, 2017, vol. 110, pp. 8–13. doi: 10.1016/j.egypro.2017.03.094.
- [125] I. Syam, M. I. Maulana, and A. Syuhada, “Design and Performance of Archimedes Single Screw Turbine as Micro Hydro Power Plant with Flow Rate Debit Variations (Case Study in Air Dingin, Samadua - South Aceh),” *J. Inotera*, vol. 4, no. 1, p. 13, 2019, doi: 10.31572/inotera.vol4.iss1.2019.id71.
- [126] UNIDO, “Technologies from Japan,” *Sustainable Technology Promotion Platform (STePP)*, vol. 1, no. May, p. 18, 2019. [Online]. Available: <https://docplayer.net/150446464-Technologies-from-japan.html>
- [127] Kakuno Seisakusho Co. Ltd., “Small hydro,” *Suminoseisakusho*. <http://suminoseisakusho.jp/saisei.html> (accessed Jul. 21, 2020).
- [128] Kakuno Manufacturing Co., “The ecological Arita River town in the Sankei Shimbun; Ena, Gifu, Japan,” *Kakuno Manufacturing Co., Ltd.*, Sep. 13, 2017. <https://www.fb.com/YouXianHuiSheJiaoYeZhiZuoSuo/posts/1900744169952506> (accessed Jul. 21, 2020).
- [129] SuminoSeisakusho, “Multi-AST two Pico Pika units running since 2012 in ibi-Cho, Gifu,” *Kakuno Manufacturing Co., Ltd.*, Jun. 07, 2018. <https://www.fb.com/YouXianHuiSheJiaoYeZhiZuoSuo/posts/2201719083188345> (accessed Aug. 05, 2020).
- [130] Kakuno Manufacturing Co., “Reniks project in suginami tree park in Nikko City, Tochigi, Japan,” *Kakuno Manufacturing Co., Ltd.*, Nov. 18, 2016. <https://www.fb.com/YouXianHuiSheJiaoYeZhiZuoSuo/posts/1535798529780407> (accessed Jul. 21, 2020).
- [131] A. Lashofer, “Project hydropower screw location - Ingenieurbüro Lashofer!,” *Lashofer Ingenieurbüro für Wasserwirtschaft*. <https://www.lashofer.at/deutsch/wasserkraftschnecke/projekt-wasserkraftschnecken->

verortung/ (accessed Jul. 04, 2020).

- [132] AberdareOnline, “Weir – d What Ronald Kear knows about Archimedes, the Royal Family and a successful fish pass | AberdareOnline,” *AberdareOnline*, Sep. 23, 2009. <https://web.archive.org/web/20110416143406/http://www.aberdareonline.co.uk/content/weir—d-what-ronald-kear-knows-about-archimedes-royal-family-and-successful-fish-pass> (accessed Jul. 05, 2020).
- [133] R. JONES, “Monmouth New Hydro Scheme,” *Wikimedia Commons*, Mar. 20, 2009. https://commons.wikimedia.org/wiki/File:Monmouth_New_Hydro_Scheme_-_geograph.org.uk_-_1538784.jpg (accessed Jul. 05, 2020).
- [134] RenewablesFirst, “Radyr Weir hydro turbines,” *Renewables First*, Oct. 28, 2015. <https://web.archive.org/web/20210804003006/https://www.renewablesfirst.co.uk/project-blog/radyr-weir-hydro-scheme/> (accessed Jul. 05, 2020).
- [135] R. Rose, “Linton Falls and Low Wood Hydropower Schemes,” *River Coast.*, no. UK Water Projects 2011, pp. 197–202, 2011, [Online]. Available: https://web.archive.org/web/20190621110557/http://www.waterprojectsonline.com/case_studies/2011/Hydropower_Linton_Fall_2011s.pdf
- [136] G. James, “Radyr weir hydro scheme,” *Geograph.org.uk*, Sep. 11, 2016. [https://commons.wikimedia.org/wiki/File:Radyr_weir_hydro_scheme_\(geograph_5112329\).jpg](https://commons.wikimedia.org/wiki/File:Radyr_weir_hydro_scheme_(geograph_5112329).jpg) (accessed Jul. 05, 2020).
- [137] P. James, “Linton Falls Hydroelectric Power Station,” *Wikimedia Commons*, Jul. 07, 2018. https://commons.wikimedia.org/wiki/File:Linton_Falls_Hydroelectric_Power_Station.jpg (accessed Jul. 05, 2020).
- [138] SinFin, “Solvay industrial plant,” *SinFin Energy*, 2019. <http://www.sinfinenergy.com/en/projects/solvay/> (accessed Jul. 08, 2020).
- [139] N. Fergnani, “Hydroelectric plants Energy efficiency,” *Hydrosmart Srl.*, 2020. <https://www.hydrosmart.it/energia-rinnovabile> (accessed Aug. 02, 2020).
- [140] Sto98, “Marengo hydropower plant-Goito [Centrale idroelettrica Marengo - Goito],” *YouTube*, Feb. 19, 2015. <https://youtu.be/19px1EKa--4> (accessed Jul. 19, 2020).
- [141] G. Nagel and K. A. Radlik, *Wasserröderschnecken: Planung, Bau und Betrieb von Wasserhebeanlagen [Water lifting screws: planning, construction and operation of water lifting systems]*. Berlin [in German]: Pfiemer, 1988. [Online]. Available: <https://books.google.ca/books?id=6xySAAAACAAJ>
- [142] G. Nagel, *Archimedian screw pump handbook: fundamental aspects of the design and operation of water pumping installations using Archimedian screw pumps*. Schwäbisch Gmünd: RITZ-Pumpenfabrik OHG, 1968. Accessed: Dec. 08, 2018. [Online]. Available:

<http://www.worldcat.org/title/archimedian-screw-pump-handbook-fundamental-aspects-of-the-design-and-operation-of-water-pumping-installations-using-archimedian-screw-pumps/oclc/8702853>

- [143] W. D. Lubitz, “Gap Flow in Archimedes Screws,” in *Proceedings of the Canadian Society for Mechanical Engineering International Congress 2014 CSME International Congress 2014; June 1-4, 2014, Toronto, ON, Canada*, 2014, pp. 1–6.
- [144] B. P. Tullis and S. C. Robinson, “Quantifying Culvert Exit Loss,” *J. Irrig. Drain. Eng.*, vol. 134, no. 2, pp. 263–266, Apr. 2008, doi: 10.1061/(ASCE)0733-9437(2008)134:2(263).
- [145] A. Passamonti, “Investigation of energy losses in laboratory and full-scale Archimedes screw generators,” Politecnico Di Milano: Milan, Italy, 2017.
- [146] A. Kozyn and W. D. Lubitz, “A power loss model for Archimedes screw generators,” *Renew. Energy*, vol. 108, pp. 260–273, Aug. 2017, doi: 10.1016/j.renene.2017.02.062.
- [147] S. J. Russell and P. Norvig, *Artificial Intelligence: A Modern Approach*. Prentice Hall. [[Prentice Hall]], 2009. Accessed: Feb. 27, 2019. [Online]. Available: https://www.researchgate.net/publication/235890207_Artificial_Intelligence_A_Modern_Approach_Prentice_Hall
- [148] M. J. Apter and P. McCorduck, “Machines Who Think: A Personal Inquiry into the History and Prospects of Artificial Intelligence,” *Leonardo*, vol. 15, no. 3, p. 242, 2006, doi: 10.2307/1574702.
- [149] N. J. Nilsson and N. J., *Artificial Intelligence: a new synthesis*. Morgan Kaufmann Publishers, 1998. Accessed: Feb. 27, 2019. [Online]. Available: <https://dl.acm.org/citation.cfm?id=280491>
- [150] D. L. Poole, A. K. Mackworth, and R. Goebel, *Computational intelligence: a logical approach*. Oxford University Press, 1998.
- [151] A. Ligeza, “Artificial Intelligence: A Modern Approach,” *Neurocomputing*, vol. 9, no. 2, pp. 215–218, 1995, doi: 10.1016/0925-2312(95)90020-9.
- [152] R. Kohavi and F. Provost, “Glossary of Terms,” *Mach. Learn.*, vol. 30, no. 2/3, pp. 271–274, 1998, doi: 10.1023/A:1017181826899.
- [153] A. Sarve, S. S. Sonawane, and M. N. Varma, “Ultrasound assisted biodiesel production from sesame (*Sesamum indicum* L.) oil using barium hydroxide as a heterogeneous catalyst: Comparative assessment of prediction abilities between response surface methodology (RSM) and artificial neural network (ANN),” *Ultrason. Sonochem.*, vol. 26, pp. 218–228, Sep. 2015, doi: 10.1016/J.ULTSONCH.2015.01.013.
- [154] W. S. McCulloch and W. Pitts, “A logical calculus of the ideas immanent in nervous

- activity,” *Bull. Math. Biophys.*, vol. 5, no. 4, pp. 115–133, Dec. 1943, doi: 10.1007/BF02478259.
- [155] R. Rojas, “Neural Networks: A Systematic Introduction,” in *Springer*, Berlin: Springer, 1996, p. 29. doi: 10.7312/zuri90466-007.
- [156] D. O. Hebb, *The Organization of Behavior: A Neuropsychological Theory*. Oxfordshire, United Kingdom: Taylor & Francis, 2009.
- [157] B. Farley and W. Clark, “Simulation of self-organizing systems by digital computer,” *Trans. IRE Prof. Gr. Inf. Theory*, vol. 4, no. 4, pp. 76–84, Sep. 1954, doi: 10.1109/TIT.1954.1057468.
- [158] F. Rosenblatt, “The Perceptron: A Probabilistic Model for Information Storage and Organization in The Brain,” *Psychol. Rev.*, pp. 65--386, 1958, Accessed: Feb. 22, 2019. [Online]. Available: <https://citeseerx.ist.psu.edu/viewdoc/summary?doi=10.1.1.588.3775>
- [159] J. Schmidhuber, “Deep learning in neural networks: An overview,” *Neural Networks*, vol. 61, pp. 85–117, Jan. 2015, doi: 10.1016/J.NEUNET.2014.09.003.
- [160] A. Ivakhnenko, *Cybernetic predicting devices*. N.Y.: CCM Information Corp., 1973. Accessed: Feb. 23, 2019. [Online]. Available: <https://www.worldcat.org/title/cybernetic-predicting-devices/oclc/219866001?referer=di&ht=edition>
- [161] A. Ivakhnenko, *Cybernetics and forecasting techniques*,. New York: American Elsevier Pub. Co., 1967. Accessed: Feb. 23, 2019. [Online]. Available: <https://www.worldcat.org/title/cybernetics-and-forecasting-techniques/oclc/537162>
- [162] M. Minsky and S. Papert, *Perceptrons: An Introduction to Computational Geometry*. Cambridge, MA, USA: MIT Press, 1969.
- [163] P. J. Werbos, “Beyond Regression: New Tools for Prediction and Analysis in the Behavioral Sciences,” Harvard University, Cambridge, MA, 1975.
- [164] M. Riedmiller and H. Braun, “Direct adaptive method for faster backpropagation learning: The RPROP algorithm,” in *1993 IEEE International Conference on Neural Networks*, 1993, pp. 586–591. doi: 10.1109/icnn.1993.298623.
- [165] A. Gadsden, S. Habibi, D. Dunne, and T. Kirubarajan, “Nonlinear Estimation Techniques Applied on Target Tracking Problems,” *J. Dyn. Syst. Meas. Control*, vol. 134, no. 5, p. 054501, 2012, doi: 10.1115/1.4006374.
- [166] H. H. Afshari, S. A. Gadsden, and S. Habibi, “Gaussian filters for parameter and state estimation: A general review of theory and recent trends,” *Signal Processing*, vol. 135, pp. 218–238, Jun. 2017, doi: 10.1016/J.SIGPRO.2017.01.001.

- [167] S. S. Haykin, *Neural networks : a comprehensive foundation*. New York City, United States: Macmillan, 1994.
- [168] K. J. Astrom and B. Wittenmark, *Adaptive Control*, 2nd ed. Boston, Massachusetts, United States: Addison-Wesley, 1994.
- [169] L. Ljung and T. Söderström, *Theory and practice of recursive identification*. MIT Press, 1983.
- [170] B. D. O. Anderson and J. B. Moore, “Optimal Filtering,” in *Random Processes for Image and Signal Processing*, New Jersey: Englewood Cliffs, 1979, pp. 307–482. doi: 10.1117/3.268105.ch4.
- [171] T. Söderström, *Discrete-time Stochastic Systems*. London: Springer London, 2002. doi: 10.1007/978-1-4471-0101-7.
- [172] M. B. Matthews, “Neural network nonlinear adaptive filtering using the extended Kalman filter algorithm,” in *Proceedings of the International Neural Networks Conference*, 1990, vol. 1, pp. 115–119. Accessed: Mar. 09, 2019. [Online]. Available: <https://ci.nii.ac.jp/naid/10004332129/>
- [173] S. Shah, F. Palmieri, and M. Datum, “Optimal filtering algorithms for fast learning in feedforward neural networks,” *Neural Networks*, vol. 5, no. 5, pp. 779–787, Sep. 1992, doi: 10.1016/S0893-6080(05)80139-X.
- [174] S. Singhal and L. Wu, “TRAINING MULTILAYER PERCEPTRONS WITH THE EXTENDED KALMAN ALGORITHM,” 1989. Accessed: Mar. 09, 2019. [Online]. Available: <http://papers.nips.cc/paper/101-training-multilayer-perceptrons-with-the-extended-kalman-algorithm.pdf>
- [175] Y. Iiguni, H. Sakai, and H. Tokumaru, “A real-time learning algorithm for a multilayered neural network based on the extended Kalman filter,” *IEEE Trans. Signal Process.*, vol. 40, no. 4, pp. 959–966, Apr. 1992, doi: 10.1109/78.127966.
- [176] D. W. Ruck, S. K. Rogers, M. Kabrisky, P. S. Maybeck, and M. E. Oxley, “Comparative analysis of backpropagation and the extended Kalman filter for training multilayer perceptrons,” *IEEE Trans. Pattern Anal. Mach. Intell.*, vol. 14, no. 6, pp. 686–691, Jun. 1992, doi: 10.1109/34.141559.
- [177] G. V. Puskorius and L. A. Feldkamp, “Neurocontrol of nonlinear dynamical systems with Kalman filter trained recurrent networks,” *IEEE Trans. Neural Networks*, vol. 5, no. 2, pp. 279–297, Mar. 1994, doi: 10.1109/72.279191.
- [178] E. S. Plumer, “Training neural networks using sequential extended Kalman filtering,” *1995 world Congr. neural networks, Washington, DC (United States), Jul 1995*, Mar. 1995, Accessed: Mar. 01, 2019. [Online]. Available:

<https://digital.library.unt.edu/ark:/67531/metadc678272/>

- [179] J. Pui-Fai SUM, “Extended Kalman Filter Based Pruning Algorithms and Several Aspects of Neural Network Learning,” The Chinese University of Hong Hong, 1998.
- [180] J. Sum, Chi-Sing Leung, G. H. Young, and Wing-Kay Kan, “On the Kalman filtering method in neural network training and pruning,” *IEEE Trans. Neural Networks*, vol. 10, no. 1, pp. 161–166, 1999, doi: 10.1109/72.737502.
- [181] R. J. Williams, “Training recurrent networks using the extended Kalman filter,” in *[Proceedings 1992] IJCNN International Joint Conference on Neural Networks*, 1992, vol. 4, pp. 241–246. doi: 10.1109/ijcnn.1992.227335.
- [182] J. A. K. Suykens, B. L. R. De Moor, and J. Vandewalle, “Nonlinear system identification using neural state space models, applicable to robust control design,” *Int. J. Control*, vol. 62, no. 1, pp. 129–152, Jul. 1995, doi: 10.1080/00207179508921536.
- [183] G. V. Puskorius and L. A. Feldkamp, “Decoupled extended Kalman filter training of feedforward layered networks,” in *IJCNN-91-Seattle International Joint Conference on Neural Networks*, 2002, vol. i, pp. 771–777. doi: 10.1109/ijcnn.1991.155276.
- [184] F. Caliskan, R. Aykan, and C. Hajiyev, “Aircraft Icing Detection, Identification, and Reconfigurable Control Based on Kalman Filtering and Neural Networks,” 2008, doi: 10.1061/ASCE0893-1321200821:251.
- [185] S. Leung Chi and W. Chan Lai, “Dual extended Kalman filtering in recurrent neural networks,” *Neural Networks*, vol. 16, no. 2, pp. 223–239, 2003, Accessed: Mar. 01, 2019. [Online]. Available: www.elsevier.com/locate/neunet
- [186] W. Pietruszkiewicz, “A comparison of nonlinear Kalman filtering applied to feed-forward neural networks as learning algorithms,” in *2010 IEEE 9th International Conference on Cybernetic Intelligent Systems*, Sep. 2010, pp. 1–6. doi: 10.1109/UKRICIS.2010.5898137.
- [187] Y. Kurylyak, K. Barbe, F. Lamonaca, D. Grimaldi, and W. Van Moer, “Photoplethysmogram-based Blood pressure evaluation using Kalman filtering and Neural Networks,” in *2013 IEEE International Symposium on Medical Measurements and Applications (MeMeA)*, May 2013, pp. 170–174. doi: 10.1109/MeMeA.2013.6549729.
- [188] A. Krok, “The development of Kalman Filter learning technique for Artificial Neural Networks,” *J. Telecommun. Inf. Technol.*, vol. 2013, no. 4, pp. 16–21, 2013.
- [189] S. R. Jondhale and R. S. Deshpande, “Kalman Filtering Framework-Based Real Time Target Tracking in Wireless Sensor Networks Using Generalized Regression Neural Networks,” *IEEE Sens. J.*, vol. 19, no. 1, pp. 224–233, Jan. 2019, doi: 10.1109/JSEN.2018.2873357.

- [190] F. Ahmat Ruslan, R. Adnan, A. Manan Samad, and Z. Md Zain, "Flood Prediction Modeling Using Hybrid BPN-EKF And Hybrid ENN-EKF: A Comparative Study," *Zainazlan Md Zain / Int. J. Eng. Res. Appl. www.ijera.com*, vol. 3, no. 4, pp. 290–297, 2013.
- [191] N. J. de Vos Kamerlingh, "Hydrology and Earth System Sciences Echo state networks as an alternative to traditional artificial neural networks in rainfall-runoff modelling," *Hydrol. Earth Syst. Sci.*, vol. 17, pp. 253–267, 2013, doi: 10.5194/hess-17-253-2013.
- [192] F. A. Ruslan, A. M. Samad, and R. Adnan, "Modelling of flood prediction system using hybrid NNARX and Extended Kalman Filter," in *Proceedings - 2017 IEEE 13th International Colloquium on Signal Processing and its Applications, CSPA 2017*, 2017, no. March, pp. 149–152. doi: 10.1109/CSPA.2017.8064941.
- [193] D. Santhusitha, K. Karunasingha, and S.-Y. Liong, "Enhancement of chaotic hydrological time series prediction with real-time noise reduction using Extended Kalman Filter," 2018, doi: 10.1016/j.jhydrol.2018.08.044.
- [194] D. S. K. Karunasinghe and S. Y. Liong, "Chaotic time series prediction with a global model: Artificial neural network," *J. Hydrol.*, vol. 323, no. 1–4, pp. 92–105, May 2006, doi: 10.1016/J.JHYDROL.2005.07.048.
- [195] A. Hosseini, M. R. Golabi, S. Marofi, N. Khalediyan, and M. Solatani, "Evaluation of Extended Kalman Filter-based Neural Network (EKFNN) model and Gene Expression Planning in Rainfall-Runoff Modelin," *Watershed Eng. Manag.*, vol. 12, no. 3, pp. 771–784, Sep. 2020, doi: 10.22092/IJWMSE.2019.121031.1457.
- [196] J. J. Wang, J. Wang, D. Sinclair, and L. Watts, "A Neural Network and Kalman Filter Hybrid Approach for GPS/INS Integration," *12th IAIN Congr. 2006 Int. Symp.*, vol. 3, p. 3, 2006.
- [197] J. E. Moody, "Note on generalization, regularization, and architecture selection in nonlinear learning systems," in *Neural Networks for Signal Processing*, 1991, pp. 1–10. doi: 10.1109/nnsf.1991.239541.
- [198] R. Reed, "Pruning algorithms-a survey," *IEEE Trans. Neural Networks*, vol. 4, no. 5, pp. 740–747, 1993, doi: 10.1109/72.248452.
- [199] N. Chen *et al.*, "Automatic Detection of Pearlite Spheroidization Grade of Steel Using Optical Metallography," *Microsc. Microanal.*, vol. 22, no. 01, pp. 208–218, Feb. 2016, doi: 10.1017/S1431927615015706.
- [200] A. YoosefDoost, M. S. Sadeghian, and M. R. Bazargan Lari, "Analysis and Evaluation of Using Artificial Parameters Generated by Data Mining in Runoff Estimation by Neural Networks considering to the climate change," 2014. [Online]. Available: <https://civilica.com/doc/319125/>

- [201] A. YoosefDoost, M. S. Sadeghian, and M. R. Bazargan Lari, "Analysis and Evaluation the Inputs which Provided from Data Mining and RPROP Learning Algorithm in Optimization FTDNN and FGam Artificial Neural Networks," 2014. [Online]. Available: <https://civilica.com/doc/319126/>
- [202] A. YoosefDoost, M. S. Sadeghian, and M. R. Bazargan Lari, "Data Mining and Optimization of Runoff Estimation by Artificial Neural Networks," 2014. [Online]. Available: <https://en.civilica.com/doc/319126/>
- [203] S. Cash and R. Yuste, "Linear summation of excitatory inputs by CA1 pyramidal neurons.," *Neuron*, vol. 22, no. 2, pp. 383–94, Feb. 1999, doi: 10.1016/S0896-6273(00)81098-3.
- [204] D. Morel, C. Singh, and W. B. Levy, "Linearization of excitatory synaptic integration at no extra cost," *J. Comput. Neurosci.*, vol. 44, no. 2, pp. 173–188, Apr. 2018, doi: 10.1007/s10827-017-0673-5.
- [205] D.-R. Liou, J.-W. Liou, and C.-Y. Liou, *Learning Behaviors of Perceptron*. Hong Kong: iConcept Press, 2013.
- [206] M. H. Yousofi, "Utilizing Automatic Recognition and Classification of Images for Pattern Recognition," *Int. J. Intell. Inf. Syst.*, vol. 3, no. 6, p. 80, Nov. 2014, doi: 10.11648/j.ijis.s.2014030601.25.
- [207] A. J. Novikoff, "On convergence proofs for perceptrons," WASHINGTON, D.C., 1963. Accessed: May 05, 2021. [Online]. Available: <http://classes.engr.oregonstate.edu/eecs/fall2017/cs534/extra/novikoff-1963.pdf>
- [208] G. Cybenko, "Approximation by superpositions of a sigmoidal function," *Math. Control. Signals, Syst.*, vol. 2, no. 4, pp. 303–314, Dec. 1989, doi: 10.1007/BF02551274.
- [209] F. Rosenblatt, *Principles of Neurodynamics: Perceptrons and the Theory of Brain Mechanisms*. Spartan Books (1962), 1961.
- [210] D. E. Rumelhart, J. L. McClelland, and S. D. P. R. G. University of California, "Learning internal representations by error propagation," in *Parallel distributed processing: explorations in the microstructure of cognition, vol. 1*, MIT Press, 1986, pp. 318–362. Accessed: Apr. 24, 2019. [Online]. Available: <https://dl.acm.org/citation.cfm?id=104279.104293>
- [211] I. Goodfellow, Y. Bengio, and A. Courville, *Deep Learning*. MIT Press, 2016. Accessed: May 06, 2021. [Online]. Available: <https://www.deeplearningbook.org/contents/mlp.html#pf25>
- [212] J. L. McClelland, D. E. Rumelhart, P. D. P. R. Group, and others, *Parallel distributed processing*. MIT press Cambridge, MA, 1986.

- [213] K. Judd, “Nonlinear state estimation, indistinguishable states, and the extended Kalman filter,” *Phys. D Nonlinear Phenom.*, vol. 183, no. 3–4, pp. 273–281, Sep. 2003, doi: 10.1016/S0167-2789(03)00180-5.
- [214] I. Russell, “The Delta Rule,” *University of Hartford*, Nov. 05, 2012. <https://web.archive.org/web/20160304032228/http://uhavax.hartford.edu/compsci/neural-networks-delta-rule.html> (accessed May 05, 2021).
- [215] I. Dabbura, “Gradient Descent Algorithm and Its Variants,” *Towards Data Science*, 2017. <https://towardsdatascience.com/gradient-descent-algorithm-and-its-variants-10f652806a3> (accessed Dec. 21, 2017).
- [216] S. Ruder, “An overview of gradient descent optimization algorithms,” *Insight Cent. Data Anal. NUI Galw.*, Sep. 2016.
- [217] N. S. Nise, *Control systems engineering*, 6th ed. Hoboken, New Jersey, United States: John Wiley & Sons, Inc., 2011.
- [218] R. E. Kalman, “A New Approach to Linear Filtering and Prediction Problems,” *J. Basic Eng.*, 2011, doi: 10.1115/1.3662552.
- [219] M. S. Grewal and A. P. Andrews, *Kalman Filtering: Theory and Practice Using MATLAB®: Third Edition*, 3rd Editio. New York: Wiley, 2008. doi: 10.1002/9780470377819.
- [220] Y. Bar-Shalom, X.-R. Li, and T. Kirubarajan, *Estimation with Applications to Tracking and Navigation*. 2003. doi: 10.1002/0471221279.
- [221] B. D. O. Anderson and J. B. (John B. Moore, *Optimal filtering*. Dover Publications, 2005.
- [222] A. YoosefDoost, M. Sadegh Sadeghian, M. Ali Node Farahani, and A. Rasekhi, “Comparison between Performance of Statistical and Low Cost ARIMA Model with GFDL, CM2.1 and CGM 3 Atmosphere-Ocean General Circulation Models in Assessment of the Effects of Climate Change on Temperature and Precipitation in Taleghan Basin,” *Am. J. Water Resour.*, vol. 5, no. 4, pp. 92–99, Sep. 2017, doi: 10.12691/ajwr-5-4-1.
- [223] A. Yoosefdoost, I. Yoosefdoost, H. Asghari, and M. S. Sadeghian, “Comparison of HadCM3 , CSIRO Mk3 and GFDL CM2 . 1 in Prediction the Climate Change in Taleghan River Basin,” *Am. J. Civ. Eng. Archit.*, vol. 6, no. 3, pp. 93–100, 2018, doi: 10.12691/ajcea-6-3-1.
- [224] A. YoosefDoost, H. Asghari, R. Abunuri, and M. Sadegh Sadeghian, “Comparison of CGCM3, CSIRO MK3 and HADCM3 Models in Estimating the Effects of Climate Change on Temperature and Precipitation in Taleghan Basin,” *Am. J. Environ. Prot.*, vol. 6, no. 1, pp. 28–34, 2018, doi: 10.12691/env-6-1-5.

- [225] Regional Water Company of Tehran, “Taleghan Dam’s Structure,” *THRW*, 2015. https://www.thrw.ir/SC.php?type=component_sections&id=229&sid=7 (accessed Apr. 16, 2019).
- [226] MehrNews, “Taleghan Dam’s Overflow has not Finished Yet,” 2017. <https://www.mehrnews.com/news/4001375/> (accessed Apr. 16, 2019).
- [227] F. M. White, *Fluid Mechanics*, 7th ed. New York: McGraw-Hill, 2011.
- [228] P. C. F. Erbsti, *Design of hydraulic gates*, 2nd ed. Boca Raton, Florida, USA: CRC Press/Balkema, 2014.
- [229] C. O. Silva and M. Rijo, “Flow Rate Measurements under Sluice Gates,” *J. Irrig. Drain. Eng.*, vol. 143, no. 6, p. 06017001, 2017, doi: 10.1061/(asce)ir.1943-4774.0001177.
- [230] C. A. Sepúlveda Toepfer, “Instrumentation, model identification and control of an experimental irrigation canal,” Ph.D. Thesis, Technical Univ. of Catalonia, Barcelona, Spain, 2007. [Online]. Available: https://web.archive.org/web/20211214013540/https://www.tdx.cat/bitstream/handle/10803/5951/01_Sepulveda.pdf
- [231] J. Lewin, *Hydraulic gates and valves : in free surface flow and submerged outlets*. Thomas Telford, London, 1995.
- [232] J. P. Baume, P. O. Malaterre, B. Gilles, and L. G. Benoit, “SIC: A 1D hydrodynamic model for river and irrigation canal modelling and regulation,” in *Métodos Numéricos em Recursos Hídricos*, Porto Alegre, Brazil: Associação Brasileira de Recursos Hídricos, 2005.
- [233] G. W. Brunner, “HEC-RAS River Analysis System Hydraulic Reference Manual—Version 5.0,” *US Army Corps of Engineers Hydrologic Engineering Center*, no. February. US Army Corps of Engineers Hydrologic Engineering Center, Davis, California, USA, 2016.
- [234] C. E. Kindsvater, “The Hydraulic Jump in Sloping Channels,” *Trans. Am. Soc. Civ. Eng.*, vol. 109, no. 1, pp. 1107–1120, Jan. 1944, doi: 10.1061/TACEAT.0005733.
- [235] J. N. Bradley and A. J. Peterka, “The hydraulic design of stilling basins: hydraulic jumps on a horizontal apron (basin i),” *J. Hydraul. Div.*, vol. 83, no. 5, pp. 1–24, 1957.
- [236] N. Rajaratnam and K. Subramanya, “Flow equation for the sluice gate,” *J. Irrig. Drain. Div.*, vol. 93, no. 3, pp. 167–186, 1967.
- [237] W. H. Hager, “Classical Hydraulic Jump,” in *Energy Dissipators and Hydraulic Jump*, vol. 8, Dordrecht, Netherlands: Kluwer Academic, 1992, pp. 5–40. doi: 10.1007/978-94-015-8048-9_2.
- [238] G. Mahtabi, B. Chaplot, H. M. Azamathulla, and M. Pal, “Classification of Hydraulic Jump

- in Rough Beds,” *Water* 2020, Vol. 12, Page 2249, vol. 12, no. 8, p. 2249, Aug. 2020, doi: 10.3390/W12082249.
- [239] M. Bijankhan, V. Ferro, and S. Kouchakzadeh, “New stage-discharge relationships for free and submerged sluice gates,” *Flow Meas. Instrum.*, vol. 28, pp. 50–56, Dec. 2012, doi: 10.1016/j.flowmeasinst.2012.07.004.
- [240] R. Henry, “Discussion to ‘On submerged jets,’” *Trans. Am. Soc. Civ. Eng.*, vol. 115, pp. 687–694, 1950, [Online]. Available: <https://books.google.ca/books?id=noJBAQAIAAJ>
- [241] P. K. Swamee, “Sluice-Gate Discharge Equations,” *J. Irrig. Drain. Eng.*, vol. 118, no. 1, pp. 56–60, Jan. 1992, doi: 10.1061/(asce)0733-9437(1992)118:1(56).
- [242] A. Roth and W. H. Hager, “Underflow of standard sluice gate,” *Exp. Fluids*, vol. 27, no. 4, pp. 339–350, Sep. 1999, doi: 10.1007/s003480050358.
- [243] D. Lozano, L. Mateos, G. P. Merkley, and A. J. Clemmens, “Field Calibration of Submerged Sluice Gates in Irrigation Canals,” *J. Irrig. Drain. Eng.*, vol. 135, no. 6, pp. 763–772, Dec. 2009, doi: 10.1061/(asce)ir.1943-4774.0000085.
- [244] A. Habibzadeh, A. R. Vatankhah, and N. Rajaratnam, “Role of Energy Loss on Discharge Characteristics of Sluice Gates,” *J. Hydraul. Eng.*, vol. 137, no. 9, pp. 1079–1084, Sep. 2011, doi: 10.1061/(asce)hy.1943-7900.0000406.
- [245] O. Castro-Orgaz, D. Lozano, and L. Mateos, “Energy and Momentum Velocity Coefficients for Calibrating Submerged Sluice Gates in Irrigation Canals,” *J. Irrig. Drain. Eng.*, vol. 136, no. 9, pp. 610–616, Sep. 2010, doi: 10.1061/(asce)ir.1943-4774.0000233.
- [246] O. Castro-Orgaz, L. Mateos, and S. Dey, “Revisiting the Energy-Momentum Method for Rating Vertical Sluice Gates under Submerged Flow Conditions,” *J. Irrig. Drain. Eng.*, vol. 139, no. 4, pp. 325–335, Apr. 2013, doi: 10.1061/(asce)ir.1943-4774.0000552.
- [247] V. Gumus, O. Simsek, N. G. Soydan, M. S. Akoz, and M. S. Kirkgoz, “Numerical Modeling of Submerged Hydraulic Jump from a Sluice Gate,” *J. Irrig. Drain. Eng.*, vol. 142, no. 1, p. 04015037, Aug. 2016, doi: 10.1061/(ASCE)IR.1943-4774.0000948.
- [248] R. A. E. H. Rady, “Modeling of flow characteristics beneath vertical and inclined sluice gates using artificial neural networks,” *Ain Shams Eng. J.*, vol. 7, no. 2, pp. 917–924, Jun. 2016, doi: 10.1016/j.asej.2016.01.009.
- [249] W. Boiten, “Vertical Gates for Distribution of Irrigation Water,” Delft, Netherlands, 1992.
- [250] E. Kubrak, J. Kubrak, A. Kiczko, and M. Kubrak, “Flow measurements using a sluice gate; Analysis of applicability,” *Water (Switzerland)*, vol. 12, no. 3, p. 819, 2020, doi: 10.3390/w12030819.

- [251] M. Nasrabadi, Y. Mehri, A. Ghassemi, and M. H. Omid, “Predicting submerged hydraulic jump characteristics using machine learning methods,” *Water Supply*, vol. 21, no. 8, pp. 4180–4194, Dec. 2021, doi: 10.2166/ws.2021.168.
- [252] A. Lencastre, *Hidráulica Geral [General hydraulics]*. Lisbon, Portugal (in Portuguese): Edição Luso-Brasileira, 1983.
- [253] G. E. Moglen, *Fundamentals of Open Channel Flow*. Boca Raton, London, New York: CRC Press (Tylor & Francis Group), 2015. doi: 10.1201/b18359.
- [254] M. H. Chaudhry, *Open-Channel Flow*, 2nd ed. Boston, MA: Springer US: Springer, 2008. doi: 10.1007/978-0-387-68648-6.
- [255] K. G. R. Raju, *Flow through open channels*. New Delhi, India: TATA McGraw-Hill Publishing Company Limited, 1981.
- [256] N. D. Katopodes, “Ideal Fluid Flow,” in *Free-Surface Flow*, Oxford, United Kingdom: Elsevier, 2019, pp. 428–515. doi: 10.1016/b978-0-12-815489-2.00006-x.
- [257] AMS, “Contraction coefficient - Glossary of Meteorology,” *American Meteorological Society*, 2012. https://glossary.ametsoc.org/wiki/Contraction_coefficient (accessed Jan. 26, 2021).
- [258] C. H. Lin, J. F. Yen, and C. T. Tsai, “Influence of Sluice Gate Contraction Coefficient on Distinguishing Condition,” *J. Irrig. Drain. Eng.*, vol. 128, no. 4, pp. 249–252, Aug. 2002, doi: 10.1061/(ASCE)0733-9437(2002)128:4(249).
- [259] F. M. Henderson, *Open channel flow*. New York: Macmillan, 1966.
- [260] N. Rajaratnam and K. Subramanya, “Flow immediately below submerged sluice gate,” *J. Hydraul. Div.*, vol. 93, pp. 57–77, 1967, doi: 10.1061/JYCEAJ.0001667.
- [261] C. Sepúlveda, M. Gómez, and J. Rodellar, “Benchmark of Discharge Calibration Methods for Submerged Sluice Gates,” *J. Irrig. Drain. Eng.*, vol. 135, no. 5, pp. 676–682, 2009, doi: 10.1061/(asce)ir.1943-4774.0000013.
- [262] G. Belaud, L. Cassan, and J.-P. Baume, “Calculation of Contraction Coefficient under Sluice Gates and Application to Discharge Measurement,” *J. Hydraul. Eng.*, vol. 135, no. 12, pp. 1086–1091, 2009, doi: 10.1061/(asce)hy.1943-7900.0000122.
- [263] J. Muysken, *Berekening van het nuttig effect van de vijzel*. De Ingenieur, 1932. Accessed: Feb. 27, 2020. [Online]. Available: https://issuu.com/tryissuu?issuu_product=header&issuu_subproduct=document_page&issuu_context=tryissuu&issuu_cta=become_a_publisher
- [264] A. Khan, S. Simmons, M. Lyons, and W. Lubitz, “Inlet Channel Effects On Archimedes

- Screw Generators,” pp. 1–5, 2018, doi: 10.25071/10315/35291.
- [265] J. Sadeghi, S. Sadeghi, and S. T. A. Niaki, “Optimizing a hybrid vendor-managed inventory and transportation problem with fuzzy demand: An improved particle swarm optimization algorithm,” *Inf. Sci. (Ny)*, vol. 272, pp. 126–144, Jul. 2014, doi: 10.1016/j.ins.2014.02.075.
- [266] M. Mitchell, *An introduction to genetic algorithms*. Cambridge, MA: MIT Press, 1996.
- [267] J. Shlens, “A Tutorial on Principal Component Analysis,” in *Google Research*, 2014, vol. Version 3. [Online]. Available: <http://arxiv.org/abs/1404.1100>
- [268] H. Abdi and L. J. Williams, “Principal component analysis,” *Wiley Interdiscip. Rev. Comput. Stat.*, vol. 2, no. 4, pp. 433–459, Jul. 2010, doi: 10.1002/wics.101.
- [269] C. Ding and X. He, “K-means clustering via principal component analysis,” in *Proceedings, Twenty-First International Conference on Machine Learning, ICML 2004*, 2004, pp. 225–232.
- [270] K. Brada, “Wasserkraftschnecke—Eigenschaften und Verwendung,” 1996, pp. 43–52.
- [271] D. Conway and J. M. White, *Machine Learning for Hackers*, 1st ed. Cambridge, Beijing, Farnham, Köln, Sebastopol, Tokyo: O’REILLY, 2012. Accessed: Jun. 16, 2020. [Online]. Available: [https://doc.lagout.org/science/Artificial Intelligence/Machine learning/Machine Learning for Hackers_ Case Studies and Algorithms to Get You Started %5BConway %26 White 2012-02-25%5D.pdf](https://doc.lagout.org/science/Artificial%20Intelligence/Machine%20learning/Machine%20Learning%20for%20Hackers_Case%20Studies%20and%20Algorithms%20to%20Get%20You%20Started%20Conway%20White%202012-02-25.pdf)
- [272] S. Simmons, “A Computational Fluid Dynamic Analysis of Archimedes Screw Generators,” MAsc. Thesis, University of Guelph, 2018. [Online]. Available: https://www.researchgate.net/publication/327474222_A_Computational_Fluid_Dynamic_Analysis_of_Archimedes_Screw_Generators
- [273] S. C. Simmons and W. D. Lubitz, “Analysis of internal fluid motion in an Archimedes screw using computational fluid mechanics,” *J. Hydraul. Res.*, p. 2020, 2020, doi: 10.1080/00221686.2020.1844813.
- [274] K. Shahverdi, R. Loni, B. Ghobadian, S. Gohari, S. Marofi, and E. Bellos, “Numerical Optimization Study of Archimedes Screw Turbine (AST): A case study,” *Renew. Energy*, vol. 145, pp. 2130–2143, 2020, doi: 10.1016/j.renene.2019.07.124.
- [275] K. Shahverdi, “Modeling for prediction of design parameters for micro-hydro Archimedean screw turbines,” *Sustain. Energy Technol. Assessments*, vol. 47, no. May, p. 101554, 2021, doi: 10.1016/j.seta.2021.101554.
- [276] A. Dragomirescu, “Design considerations for an Archimedean screw hydro turbine,” in *IOP Conf. Ser.: Earth Environ. Sci*, 2021, vol. 664, p. 12034. doi: 10.1088/1755-1315/664/1/012034.

- [277] Rehart Power, “Rehart Power 2020 Referenzen.” <https://web.archive.org/web/20211024035002/https://www.rehart-power.de/referenzen/wasserkraftanlagen-typ-sh/hausen-sh.html> (accessed Oct. 23, 2021).
- [278] Ingenieurbüro Lashofer, “Hydropower screws in Europe,” *Google Maps*. efort.info/AST-Map (accessed Aug. 03, 2021).
- [279] Rehart Power, “Hannoversch Münden CS.” <https://web.archive.org/web/20211027000737/https://www.rehart-power.de/en/reference-projects/hydropower-screw-type-cs/hannoversch-muenden-cs.html> (accessed Oct. 26, 2021).
- [280] Landustrie Sneek BV, “Totnes Weir (UK),” *Landustrie Worldwide Water Technology*, Nov. 18, 2015. https://web.archive.org/web/20210803231005/https://www.landustrie.nl/fileadmin/user_upload/Totnes_Times_November_2015.pdf (accessed Aug. 03, 2021).
- [281] P. Gratton, T. Meadows, and T. Brook, “Gunthorpe Weir Hydropower Scheme: Fisheries and Geomorphology assessment,” The Mill, Stroud, UK, 2019. [Online]. Available: [http://web.archive.org/web/20210804003408/https://consult.environment-agency.gov.uk/psc/canal-river-trust-27520-29519/supporting_documents/Fisheries and Geomorphology Assessment Gunthorpe Weir MD0280064047.pdf](http://web.archive.org/web/20210804003408/https://consult.environment-agency.gov.uk/psc/canal-river-trust-27520-29519/supporting_documents/Fisheries_and_Geomorphology_Assessment_Gunthorpe_Weir_MD0280064047.pdf)
- [282] Vandezande BVBA, “Vandezande Specialist in Mechanics.” Vandezande.com, Zeepziederijstraat, Brugge, Belgium. Accessed: Aug. 08, 2021. [Online]. Available: https://web.archive.org/web/20210809031945/https://www.vandezande.com/sites/default/files/vandezande-folder_2017-eng_LR04.pdf
- [283] Vandezande Diksmuide, “Hydropower Screws Höllthal,” *Vandezande*. <https://web.archive.org/web/20210809061648/https://www.vandezande.com/en/projects/hydropower-screws-höllthal> (accessed Aug. 09, 2021).
- [284] G. Dellinger, S. Simmons, W. D. Lubitz, P. A. Garambois, and N. Dellinger, “Effect of slope and number of blades on Archimedes screw generator power output,” *Renew. Energy*, vol. 136, pp. 896–908, 2019, doi: 10.1016/j.renene.2019.01.060.
- [285] S. C. Simmons, C. Elliott, M. Ford, A. Clayton, and W. D. Lubitz, “Archimedes screw generator powerplant assessment and field measurement campaign,” *Energy Sustain. Dev.*, vol. 65, pp. 144–161, Dec. 2021, doi: 10.1016/j.esd.2021.09.007.
- [286] M. Lyons, “Lab Testing and Modeling of Archimedes Screw Turbines,” University of Guelph, Guelph, 2014. Accessed: Oct. 31, 2021. [Online]. Available: <http://atrium.lib.uoguelph.ca/xmlui/handle/10214/8647>
- [287] C. Zafirah Rosly, U. K. Jamaludin, N. Suraya Azahari, M. Ammar Nik Mu’tasim, A. Nurye Oumer, and N. T. Rao, “Parametric study on efficiency of archimedes screw turbine,” *ARNP*

J. Eng. Appl. Sci., vol. 11, no. 18, pp. 10904–10908, 2016.

- [288] K. Songin, “Experimental Analysis of Archimedes Screw Turbines,” MASC. Thesis, University of Guelph, 2017. [Online]. Available: <http://atrium.lib.uoguelph.ca/xmlui/handle/10214/11481>
- [289] Rehart Power, “Hannoversch Münden CS,” *Rehart Power*. <https://web.archive.org/web/20211115031954/https://www.rehart-power.de/en/reference-projects/hydropower-screw-type-cs/hannoversch-muenden-cs.html> (accessed Nov. 14, 2021).
- [290] Melbud S.A., “A Small Hydropower Plant– Rosko,” *Melbud S.A.* <https://web.archive.org/web/20210804011025/http://www.melbud.pl/language/pl/mala-elektrownia-wodna-rosko/> (accessed Aug. 03, 2021).
- [291] L. S. Lasdon, A. D. Waren, A. Jain, and M. Ratner, “Design and Testing of a Generalized Reduced Gradient Code for Nonlinear Programming,” *ACM Trans. Math. Softw.*, vol. 4, no. 1, pp. 34–50, Mar. 1978, doi: 10.1145/355769.355773.
- [292] D. Waleed and H. Alrabadi, “Portfolio optimization using the generalized reduced gradient nonlinear algorithm An application to Amman Stock Exchange,” *Int. J. Islam. Middle East. Financ. Manag.*, vol. 9, no. 4, pp. 570–582, 2016, doi: 10.1108/IMEFM-06-2015-0071.
- [293] GreenBug Energy, “Archimedes Screw Generators ,” *GreenBug Energy*. <https://web.archive.org/web/20210128050704/https://greenbugenergy.com/how-we-do-it/archimedes-screw-generators> (accessed Aug. 06, 2021).
- [294] L. Heron, “Fletcher’s Horse World - Nanticoke Creek - Archimedes Screw - 7.2 kW,” *Ontario Rivers Alliance*, Nov. 20, 2014. <https://web.archive.org/web/20210806171348/https://www.ontarioriversalliance.ca/fletchers-horse-world-nanticoke-creek-archimedes-screw-7-2-kw/> (accessed Aug. 06, 2021).
- [295] GreenBug Energy, “Fletchers Horse World,” *GreenBug Energy Inc.* <https://greenbugenergy.com/projects/fletchers-horse-world> (accessed Aug. 06, 2021).
- [296] M. P. Deisenroth, A. A. Faisal, and C. S. Ong, *Mathematics for Machine Learning*. Cambridge: Cambridge University Press, 2020. [Online]. Available: <https://github.com/mml-book/mml-book.github.io>
- [297] S. Simmons, M. Lyons, W. D. Lubitz, and G. Dellinger, “Effects of varying inclination angle on Archimedes screw generator power production with constant head,” in *Proceedings of The Joint Canadian Society for Mechanical Engineering and CFD Society of Canada International Congress 2019, CSME-CFDSC Congress 2019*, 2019, pp. 451–456. [Online]. Available: <https://www.eng.uwo.ca/csme-cfdsc/files/program-events/proceedings/Proceedings-of-CSME-2019.pdf>

- [298] S. Simmons, G. Dellinger, ; Murray Lyons, A. Terfous, A. Ghenaim, and W. David Lubitz, “Effects of Inclination Angle on Archimedes Screw Generator Power Production with Constant Head,” *J. Hydraul. Eng.*, vol. 147, no. 3, p. 04021001, Jan. 2021, doi: 10.1061/(ASCE)HY.1943-7900.0001854.
- [299] J. Lee Rodgers and W. A. Nicewander, “Thirteen Ways to Look at the Correlation Coefficient,” *Am. Stat.*, vol. 42, no. 1, pp. 59–66, Feb. 1988, doi: 10.1080/00031305.1988.10475524.
- [300] C. Willmott and K. Matsuura, “Advantages of the mean absolute error (MAE) over the root mean square error (RMSE) in assessing average model performance,” *Clim. Res.*, vol. 30, pp. 79–82, Dec. 2005, doi: 10.3354/cr030079.
- [301] E. L. (Erich L. Lehmann and G. Casella, *Theory of point estimation.*, 2nd ed. New York: Springer, 1998.
- [302] J. E. Hanke and D. Wichern, *Business Forecasting*, 9th ed. London, United Kingdom: Prentice Hall, 2009. Accessed: Jun. 15, 2020. [Online]. Available: https://www.google.ca/books/edition/Business_Forecasting/WaiOrL8oct4C?hl=en&gbpv=1&printsec=frontcover
- [303] S. Kim and H. Kim, “A new metric of absolute percentage error for intermittent demand forecasts,” *Int. J. Forecast.*, vol. 32, no. 3, pp. 669–679, Jul. 2016, doi: 10.1016/j.ijforecast.2015.12.003.
- [304] B. L. Bowerman, R. T. O’Connell, and A. B. Koehler, *Forecasting, Time Series, and Regression: An Applied Approach*, 4th ed. Belmont, CA: Thomson Brooks/Cole, 2005. [Online]. Available: https://books.google.ca/books?id=2Yc_AQAAIAAJ

APPENDICES

A. Evaluation Criteria

A correlation refers to any statistically significant relationship between two variables [299]. According to the definition, to compare the results of model outputs (predictions) with observed data (observations or measurements) for a statistical sample with n couples (O_i, P_i) , the correlation could be calculated by the following equation:

$$R = \frac{\sum_{i=1}^n (O_i - \bar{O})(P_i - \bar{P})}{\sqrt{\sum_{i=1}^n (O_i - \bar{O})^2} \sqrt{\sum_{i=1}^n (P_i - \bar{P})^2}} \quad (\text{A-1})$$

Note that O_i is the observed data, P_i is the estimated value, \bar{O} is the average of observational data, \bar{P} is the average of estimated data, and n is the number of data. The correlation coefficient values could be in a range between -1 to $+1$. Correlation close to $+1$ means a good and direct correlation between two datasets. Correlations close to -1 mean a good but reverse relation between datasets. A correlation close to zero implies a lack of correlation. The range of R^2 is between 0 and 1. Therefore, a higher value indicates better relation between datasets.

The mean error (ME) is defined as the average difference between the model estimations and the experimentally measured value:

$$\text{ME} = \frac{1}{n} \sum_{i=1}^n (P_i - O_i) \quad (\text{A-2})$$

The mean absolute error (MAE) is a criterion that compares the predicted results to the desired or

actual results. This criterion is calculated using the following equation [300]:

$$MAE = \frac{1}{n} \sum_{i=1}^n |O_i - P_i| \quad (A-3)$$

The mean squared error (MSE) or mean squared deviation (MSD) of an estimator measures the average of the squares of the errors. It is the average squared difference between the estimated values and desired or actual values. The MSE is a measure of the quality of an estimator. It is always non-negative, and smaller values indicate better performance [301].

$$MSE = \frac{1}{n} \sum_{i=1}^n (O_i - P_i)^2 \quad (A-4)$$

Root mean square deviation (RMSD) or root mean square error (RMSE) is a common measuring criterion calculated from the difference between the predicted values by a model or estimator and the observed data. It indicates the sample standard deviation from the predicted values and the experimental data. These differences are called residual when calculations are estimated from samples and are called forecast error when they are predicted out of sample. RMSE is an acceptable measure to compare the prediction errors of a special variable and is calculated using the following equation [301]:

$$RMSE = \sqrt{\frac{1}{n} \sum_{i=1}^n (O_i - P_i)^2} \quad (A-5)$$

The percentage (percent) error (PE) is a dimensionless error measure defined as the difference between the model estimations and the experimentally measured value:

$$PE = \frac{P_i - O_i}{O_i} \times 100 \quad (\text{A-6})$$

The mean percentage error (MPE) is the average of percentage errors (the difference between predicted and measured values) [302] and represents errors in a dimensionless form which is easier to analyze and compare:

$$MPE = \frac{100}{n} \sum_{i=1}^n \frac{P_i - O_i}{O_i} \quad (\text{A-7})$$

The mean absolute percentage error (MAPE) is the average of absolute percentage errors and one of the most common accuracy measures [303] that is recommended in many textbooks (e.g. [302], [304]). MAPE considers errors regardless of their sign, so positive and negative errors cannot cancel each other. MAPE is calculated as:

$$MAPE = \frac{100}{n} \sum_{i=1}^n \left| \frac{E_i - O_i}{O_i} \right| \quad (\text{A-8})$$